CUTTING TOOL CONDITION MONITORING USING MULTIPLE SENSORS AND ARTIFICIAL INTELLIGENCE TECHNIQUES ON A COMPUTER NUMERICAL CONTROLLED MILLING MACHINE

By
Steven John Wilcox

SUBMITTED FOR THE DEGREE OF
DOCTOR OF PHILOSOPHY
AT HERIOT-WATT UNIVERSITY
ON COMPLETION OF RESEARCH IN THE
DEPARTMENT OF MECHANICAL ENGINEERING,
HERIOT-WATT UNIVERSITY
NOVEMBER 1992.

Contents

List of Tables

List of Figures

Acknowledgements

Firstly, I would like to thank my wife for her support and encouragement over the last few years. Next, I would like to thank both people who have given me help and guidance on this work throughout my time at Heriot-Watt, namely Dr.W.K.D.Borthwick and especially Dr.R.L.Reuben who took over as my supervisor with only a lot of extra work as a reward.

Next I would like to thank all the technicians who have helped me, in particular Mr.J.Ramsay and Mr.E.Morgan in the Electronics Workshop, and Mr.B.Wilson and all in the Advanced Manufacturing Unit for their help in building equipment and performing experiments.

Finally, I would like to thank the CEC under its BRITE EURAM Programme for the funds that have enabled me to complete this work, which formed a small part of project number P2049.

Abstract

This work documents an investigation of the degradation of a variety of different tools whilst conducting milling operations on a computer numerical controlled (CNC) milling machine. The potential of a range of sensors to detect tool degradation has been investigated and the outputs have been incorporated into a monitoring system.

Progressive degradation under nominal rough and finish face milling and rough groove milling has been investigated using a two point grooving tool and four and eight point face milling tools on En8, En24 and En24T workpiece materials. Rapid degradation of the cutting tool has also been observed under rough milling conditions using four and eight point face milling tools, whilst machining En8 and En24T materials in a variety of simulated and actual tool breakage situations.

A limited investigation of the effect of the individual wear geometries associated with both progressive and instantaneous tool degradation has been conducted by simulating these geometries and carrying out rough milling tests using a four point face milling tool on a workpiece of En8 material. Similarly, a limited investigation of the effect of machining on different machines has also been undertaken.

A number of different sensing technologies have been used, including conventional sensors such as spindle current and cutting force but also novel sensing techniques such as Acoustic Emission. These have been combined using artificial intelligence techniques to provide automatic recognition of the tool wear state. Similarly, the feasibility of breakage detection/prediction has also been demonstrated.

Nomenclature

A cross-sectional area of workpiece material removed by one tooth

AE_{rms}^2 square of the rms of the acoustic emission signal

B width of chip

b magnitude of Burger's vector

C constant

C_{av} averaging constant for rms processing unit

c_g group velocity

c_l longitudinal wave velocity

c_t tortional wave velocity

c' phase velocity

c_1 dilatational wave velocity

c_2 distortional wave velocity

D mean distance between obstacles

$do(i)$ desired output of the ith neuron

E thickness of chip

E Young's modulus

F_N normal to shear plane component of cutting force

F_c cutting force

F_s shear plane component of cutting force

F_f feed force

F_p perpendicular force

F_v vertical force

$f'(\epsilon)$ derivative of the excitation function

$f(\epsilon)$ excitation function

H hardness of softer material

h tool-chip contact length

hp horse power

I second moment of area

$i(j)$ input to the ith neuron on the jth input line

K constant

K thermal conductivity

k_{AB} shear flow stress on the shear plane

K_T crater wear

L distance moved in unit time

l length of shear plane

l_1 length of sticking zone

l_2 length of sliding zone

N normal force to insert

n strain hardening index

$o(i)$ output of the ith neuron

P power

R resultant cutting force

R_T thermal number

r machining exponent for different materials

r_c cutter ratio, $\frac{t_1}{t_2}$

S peripheral speed of cutter

S specific heat

T average number of cutter teeth in contact with workpiece

T_W workpiece temperature

T_{ab} shear plane temperature

T_c chip temperature

T_{int} interface temperature

T_{mod} velocity modified temperature

T_{sz} tool-chip shear zone temperature

t_1 undeformed chip thickness

t_2 deformed chip thickness

U cutting speed

V volume of material removed in unit time

V normal chip velocity to shear plane

v dislocation velocity

VB_B non-uniform wear land

VB_C uniform wear land

V_c chip velocity

VB_N notch wear

V_s shear plane velocity

W normal load

$w(j)$ weight of the jth input to the ith neuron

α rake angle

α_1 an elastic constant

γ shear strain

γ_{ab} shear strain at AB

$\dot{\gamma}_{ab}$ shear strain rate at AB

γ_{int} shear strain at interface

$\dot{\gamma}_{int}$ shear strain rate at interafce

$\dot{\gamma}_O$ constant

$\Delta(i)$ error of the ith neuron

Δ_x width of shear zone

δ ratio of average chip thickness of tool-chip interface plastic zone to chip thickness

ϵ_{ab} strain at AB

$\dot{\epsilon}_{ab}$ strain rate at AB

ϵ_{int} strain at interface

$\dot{\epsilon}_{int}$ strain rate at interface

ϵ_w prior cold working of workpiece

θ angle between resultant friction force and the shear plane

λ friction angle for the chip on the rake face

λ one of Lame's constants

λ' friction angle for the shear plane of the chip

μ shear modulus

σ_1 flow stress

ρ medium density

ρ_m mobile dislocation density

τ maximum shear strength of workpiece or time of flight

τ_{int}, k_{chip} interface shear stress

ϕ shear plane angle

w width of cut

Chapter 1

Introduction

1.1 Problem Specification

As the demand for increased productivity in metal cutting rises, methods such as adaptive control applied for example to, flexible manufacturing systems, are looked upon to improve the efficiency of metal removal, reduce the machine down time and determine when it is necessary to change a tool, due to excessive wear or other tool damage such as an insert being broken. It is therefore essential that any adaptive control system can accurately predict tool wear, thus letting the control system determine the most productive time to change the tool. Such a facility would reduce errors in machining accuracy and also reduce the risk of breaking inserts, a common cause of damage to the machine. This latter point is more important when the metal removal rate is high, when a tool approaches the end of its life, or under operator or program error.

Tool wear monitoring for both long-timescale (progressive cutter wear) and short-timescale (insert breakage) degradation has been researched for many decades as will be seen in Chapter 2. However, there has never been a complete solution to the problem and this can be attributed to the extensive nature of the task. Metal cutting, in whatever form, takes place over a large number of cutting conditions, workpiece materials, cutting tools and cutting operations. It is therefore unlikely that a universal description will emerge in the near future or, indeed, whether it is necessary to find one.

This work concentrates on milling, which is one of the more complex metal cutting processes. However, attempts are made, where appropriate to relate the work to other machining processes and this is particularly important when considering the current state of knowledge which is usually specific to a given operation.

The benefits of a system that would be capable of monitoring tool wear on a variety of machines would be great. Edwin and Vlash [1] list the following;

(a) lower annual cutter cost due to optimised tool changing.

(b) lower machine down time.

(c) fewer machine failures.

In a general scheme of tool wear monitoring, a sensor is used to detect some measurand from the cutting process. The signal emitted from the sensor is then processed, either digitally or in analogue form, and some sort of 'intelligence' is used to give an estimated value of tool wear. To be able to detect this tool wear, the sensor should be capable of functioning over a wide variety of machine operating conditions and it is here that some problems are encountered, as no single sensor is necessarily suitable for all conditions.

It would therefore seem to be important to utilise a variety of sensors in order to cover as wide a condition space as possible and also to allow increased confidence in the wear estimation that is made Mathew et al [2]. An ideal wear monitor would be able to sense several different metal cutting parameters, apply the appropriate weighting to each sensor depending on the cutting that was being performed and combine them to produce an accurate expected value for tool wear. Clearly, such performance can only be achieved with a very large knowledge base and this work is confined to a small subset of metal cutting in order to achieve measurable results in a reasonable time.

The background against which this work has been performed will be presented in Chapter 2, with only a brief introduction to the main subject areas of condition monitoring being made here. Before this, the conditions which require to be monitored are described; namely long-timescale and short-timescale cutting tool degradation.

1.1.1 Long Timescale Tool Degradation

In this work long-timescale tool degradation is defined as that which occurs progressively on the cutting edge over minutes or even hours of cutting time. Three main geometries of progressive tool wear can occur on carbide inserted and high speed steel tools and these are identified below:

(a) *Flank Wear*
This type of wear evolves predominantly as a zone of uniform wear on the flank of the insert. Figure 1 shows the various ways in which this condition might be quantified.

As an example of a tool life criterion, ISO 3685-1977, recommends VB_C=0.-3 mm for a uniform wear land and a maximum value of VB_B=0.6 mm if the wear land is non-uniform. However, if the notch value (a second type of tool wear on the flank face), VB_N=1 mm is reached first then this could be used instead. At the present time, flank wear is the main method of determining whether a tool is capable of cutting.

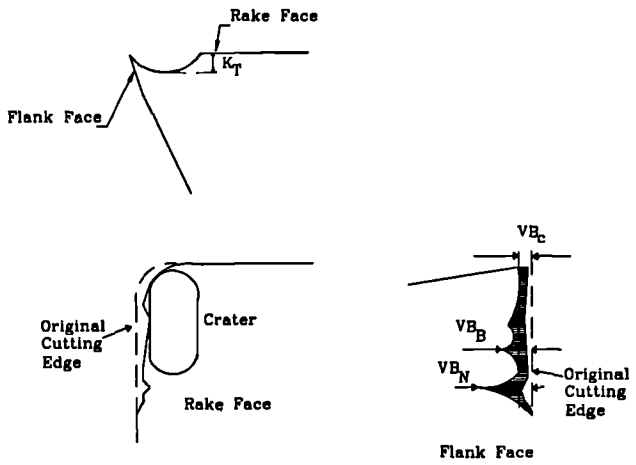

Figure 1: Flank and Crater Wear Definitions

In this work VB_B=0.7 mm is taken as the tool wear-out condition, a little higher than the recommendation of ISO 3685. This was done to allow additional information to be acquired on the variation in sensorial output with tool wear, rather than to suggest an alternative criterion. In this work flank wear evolved in four different ways and these are shown in Figures 2 to 5.

(b) *Crater Wear*
It is common for another type of wear to occur on the rake face of the tool. This takes the form of a pit or 'crater' which is created immediately behind the cutting edge, shown schematically in Figure 1.

For carbide inserts, crater wear is the result of the high interfacial temperatures facilitating diffusion of the carbide matrix into the workpiece material, Trent [3]. This process is normally more prevalent in the later stages of the life of an insert, perhaps due to the fact that the worn tool will generate larger amounts of heat. The maximum depth of the crater, defined as K_T (Figure 1) could be used to determine the tool life but in practice it is difficult to measure this parameter with the cutter mounted in a machine tool. In a similar manner to flank wear craters developed in a different manner for each of the machining operations in this work, with these different forms being shown in Figures 6 to 8.

(c) *Grooves in Relief Face*
Occasionally grooves develop in the relief face of the cutting insert at a

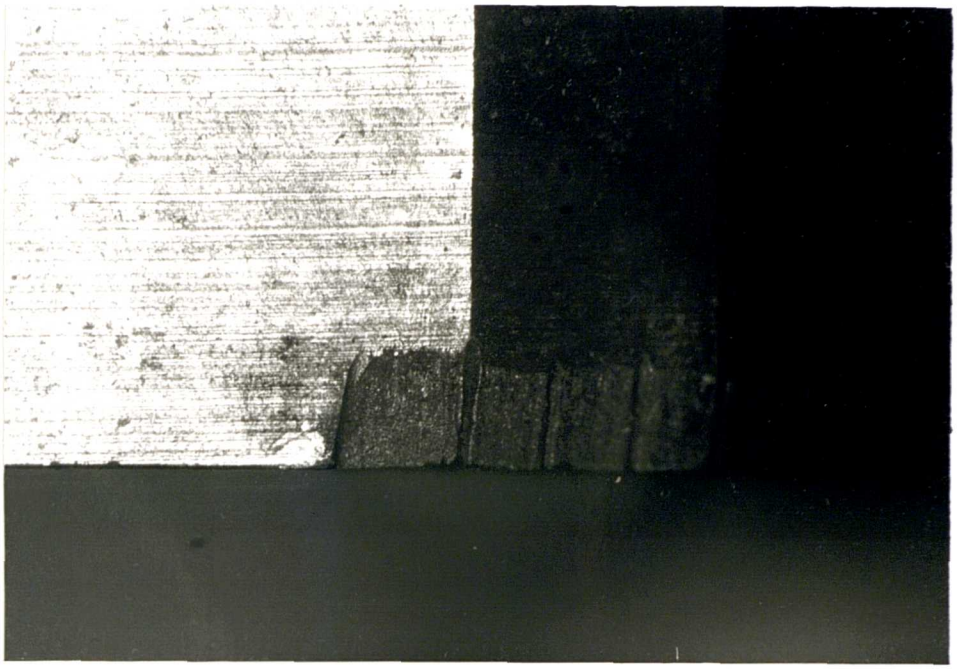

Figure 2: Flank Wear during Roughing Operations on En24(T) (X25)

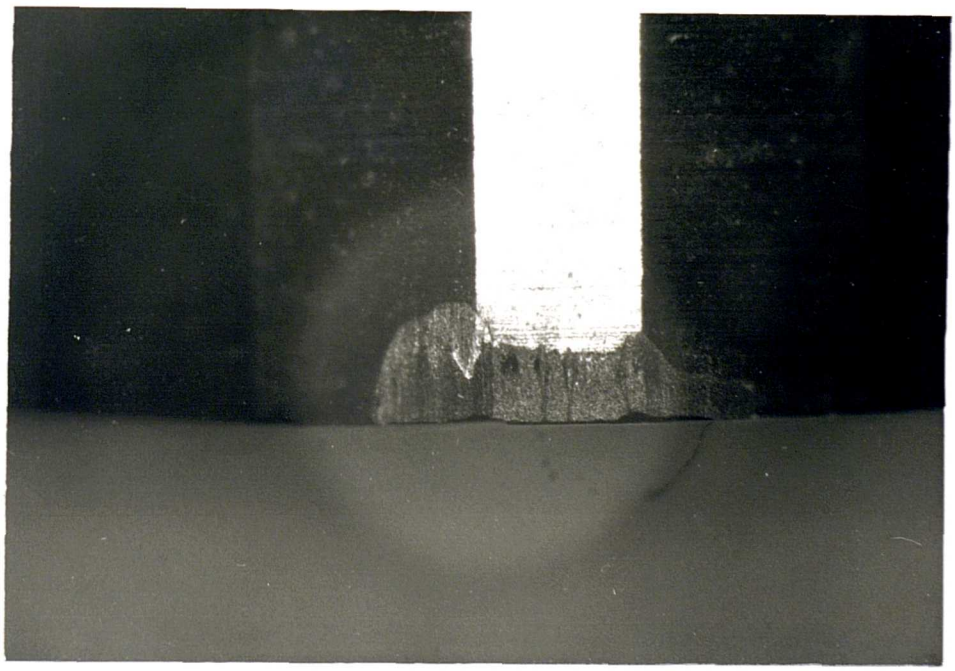

Figure 3: Flank Wear during Finishing Operations on En24(T) (X25)

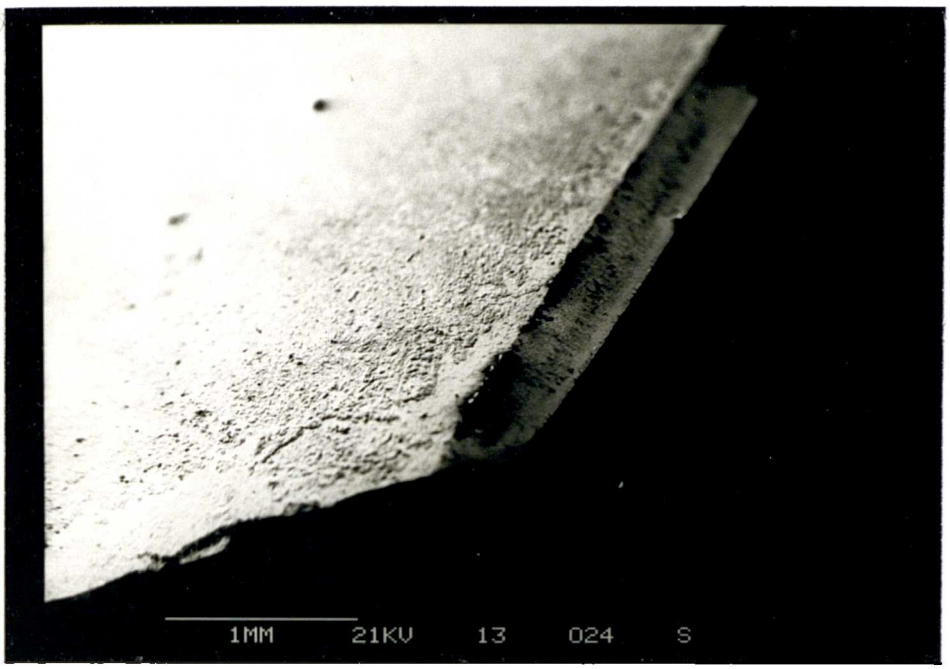

Figure 4: Flank Wear during Roughing Operations on En8

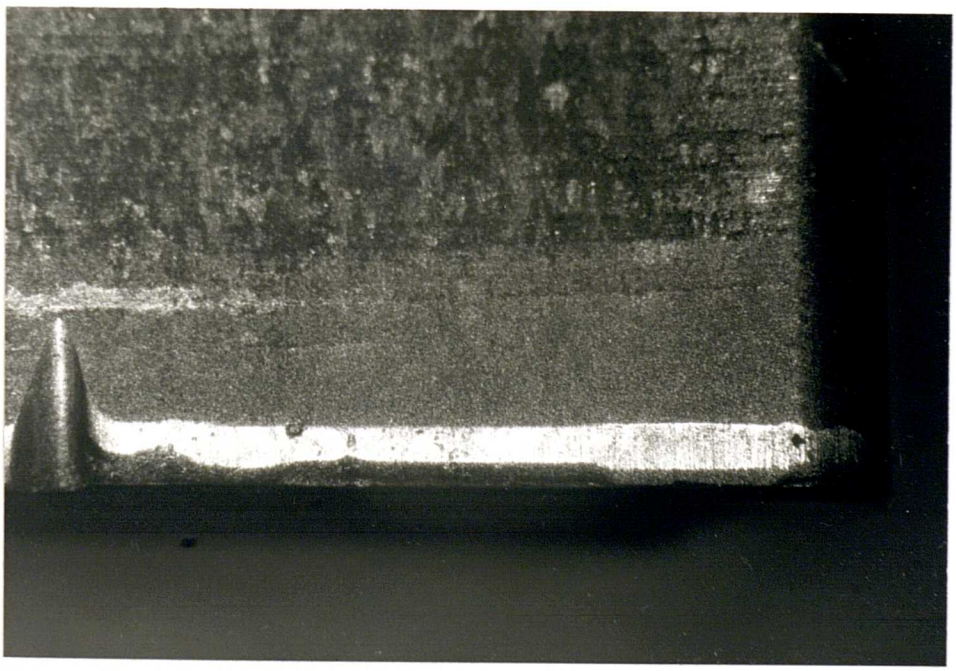

Figure 5: Flank Wear during Grooving Operations on En24(T) (X25)

Figure 6: Crater Wear during Roughing Operations on En24(T) (X25)

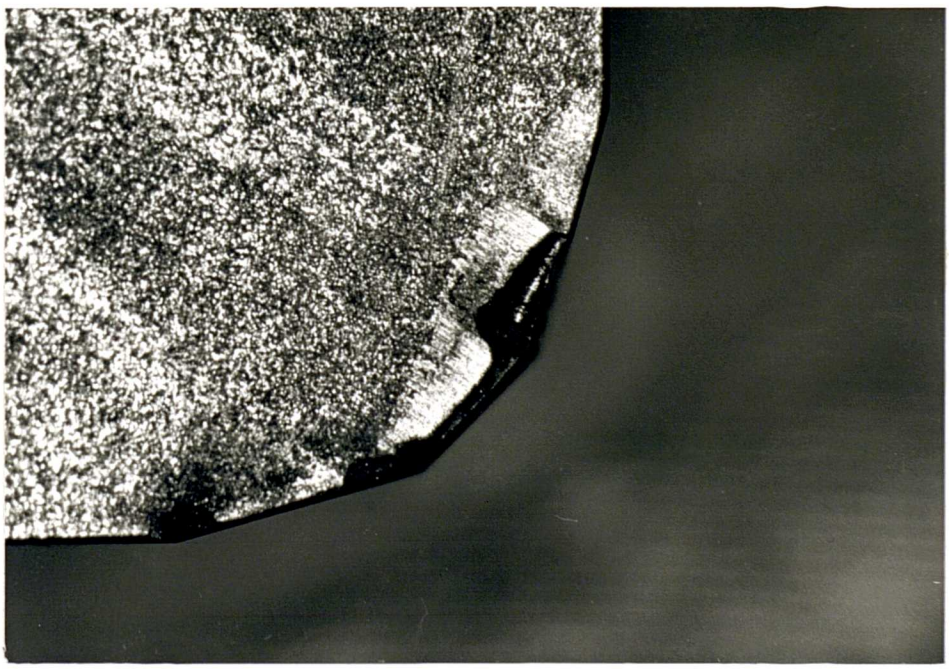

Figure 7: Crater Wear during Finishing Operations on En24(T) (X25)

Figure 8: Crater Wear during Grooving Operations on En24(T) (X25)

distance from the cutting edge corresponding to the feed rate. These grooves can contribute to an increase in the surface roughness of the workpiece, Cook [4].

1.1.2 Short Timescale Degradation

Throughout this work, short-timescale degradation is defined as those events which develop over a few rotations of the tool holder (around 200 ms) as opposed to long-timescale tool wear which occurs over 20 minutes or more.

Short timescale events such as cutting edge breakdown or even insert breakage can result from excessive tool wear. Alternatively, localised hard patches in the workpiece and machining under inappropriate cutting conditions can all cause such degradation to occur on a machine tool.

Another problem that is occasionally encountered in a machine shop is the accidental mistake that can stall the machine tool, break the milling cutter or even cause serious damage to the machine tool, for example scoring of the spindle. When a mistake is made and the cutter jams, there is probably a 10 % chance of a serious problem occuring. This could cause between £5000 and £10000 of damage to the machine, with the machine tool being out of action for anywhere between a few days to a week. (The foregoing figures were obtained from consultation with a large machine shop).

Long timescale events, namely progressive cutter wear, in the form of flank and crater wear pose different problems as regards both the workpiece and machine tool but are rarely catastrophic in effect. However, if the monitoring system is allowed to adaptively control the cutting conditions, in order to optimise the tool wear rate with the metal removal rate, then a breakage due to built up edge or due to large levels of wear on the more modern high metal removal rate inserts is more likely to occur.

1.2 Condition Monitoring

In order to carry out effective condition monitoring it is necessary to consider the three main aspects. Firstly there is the phenomenon(a) to be monitored, in this case short and long-timescale tool degradation. Next come the sensors that are used to monitor the phenomenon(a) and finally there is the 'artificial intelligence' that is required to fuse the sensorial information and infer the required result from the sensor output. The action resulting from such a diagnosis of condition enters the area of adaptive control and this is not pursued in this work.

1.2.1 The Phenomenon - Cutting Tool Degradation

The metal cutting process can be described as one of intense plastic and elastic deformation along with fracture. During this process a large amount of heat is generated due in part to the enormous levels of strain occurring in the material being machined.

The exact form of tool wear will vary somewhat according to the operation that is being performed, and the understanding of tool wear during the machining process, particularly the milling process, is complicated by the fact that several different wear processes may take place concurrently. These include:

(a) Diffusion of the cutting tool material into the workpiece.

(b) Attrition of the cutting tool.

(c) Thermal fracture.

(d) Mechanical fracture.

(e) Abrasion of the cutting tool.

The balance of the above mechanisms is dependent on the workpiece and tool materials, the cutting tool geometry and wear condition, the cutting conditions, the chip and interfacial temperatures, cutting fluid and the rigidity of the machine tool and its age. The difficulty is to isolate from these complex phenomena the information that is actually required, i.e. the condition of the cutting tool.

1.2.2 Monitoring the Phenomenon

It is possible to monitor tool degradation either directly or indirectly. Indirect measurement is normally the prefered method for tool wear monitoring because of the following points:

(a) Direct measurement of the tool wear by imaging the rotating tool could be dangerous and, at best, measurements can only be made intermittently. This would not constitute a problem for small workpieces as the number of measurement opportunities is high leading to an accurate measurement of the wear rate but a substantial time penalty would be added to the machining operation. For large workpieces, the frequency of measurement may not be high enough for the monitoring system to accurately predict tool wear.

(b) Other direct measurements, such as electrical resistance or radioactive impregnation of the inserts require special inserts to be manufactured. This may not be acceptable as the cost would be large and, in the latter case, it is unlikely that popular acceptance would be forthcoming due to obvious safety issues.

Indirect methods of monitoring tool wear, as used in this work, do not have these disadvantages. There is one major drawback, however, as it is necessary to find a (preferably monotonic) relationship between the sensor output and tool wear, through some signal processing scheme. This requires an extensive investigation to determine whether such a relationship exists for a range of candidate sensors and processing schemes.

Spindle current, or machine power, and the feed component of cutting force have already been used to establish relationships with tool wear and this has led to the option of having a monitoring system installed on newly purchased machines provided by a number of manufacturers.

However, spindle current may not be a good sensor to use for small diameter tools, or for small depths of cut, as there might not be enough sensitivity in the signal. Cutting force suffers from the fact that any relationship between it and tool wear tends only to be relevant for a particular set-up due to its dependence on the static and dynamic properties of the machine tool.

Acoustic Emission (AE) has the advantage of occurring in a frequency range remote from that of the vibrations of the machine being monitored and should therefore be independent of it. Because of its relative novelty, the principal difficulty in employing AE is that of finding an analysis technique that isolates the variation of the sensorial information with tool wear if, indeed, such a relationship exists. This needs to be solved taking into account the possible effects of changing such parameters as feed rate, cutting speed, depth of cut, material, tool and sensor specification.

Other measurands, such as workpiece vibration, tool temperature or audio emissions could similarly be used to monitor tool wear but all suffer drawbacks of one form or another. For example, workpiece vibration suffers similar drawbacks to cutting force and tool temperature either requires special inserts or expensive full-field imaging systems.

1.2.3 Artificial Intelligence

Quite recently, researchers in condition monitoring have viewed the sphere of artificial intelligence as a method for achieving the goal of automatic tool wear monitoring, Rangwala and Dornfeld [5] and have started to apply various aspects of this approach to the metal cutting problem. AI techniques have some advantages when attempting to solve the problems associated with monitoring tool wear and these are summarised below:

(a) Using Expert Systems it is possible to utilise conventional knowledge about the machining process along with more machine specific information and sensor information.

(b) Using Neural Networks it is possible to provide an automatic learning capability which would allow the system to adapt to different machines or conditions.

(c) Using either of the above methods it is possible to automatically combine the sensorial information in a convienient way by applying appropriate weighting factors.

(d) Using Expert Systems it is possible to take the inferred value for tool wear and make predictions as to remaining tool life.

1.3 Scope of this Investigation

This work has been aimed at utilising the AE, spindle current, cutting force and workpiece vibration signals emitted during cutting in order to make a diagnosis of tool condition. In order to achieve this it has been necessary to attempt to find a relationship between various features of the different sensor outputs and tool degradation in both the short and long-timescale.

A limited demonstration of the use an Artificial Neural Network (ANN) and Expert System (ES) for use as a monitor of progressive tool degradation using three sensors is also presented. For monitoring short-timescale tool degradation, an ANN has been used to monitor the cutting process using one sensor.

Many further results that could be used in either the ANN or ES are also presented from cutting operations with different tools on different steels whilst using one

CNC milling machine. The effect of using a different machine has been simulated by varying fixture stiffness.

Chapter 2

Background

In order to provide an introduction to the work in this thesis, background material has been selected from a review of the available literature. This background material is divided into three main areas, each covering one of the three areas of condition monitoring outlined in the introduction:

(a) *The Phenomenon - Metal Cutting Theory.*
The section on metal cutting theory traces its development from a quite early date up to the current state of knowledge along with the present thinking on the wear mechanisms that are taking place on sintered carbide inserts.

(b) *Monitoring the Phenomenon*
This section follows the use of various sensors for monitoring the mean tool flank wear level. The sensors covered include:

- Machine Power
- Cutting Force
- Acoustic Emission
- Workpiece Vibration
- Tool Temperature

With the current state of the art being summarised for each sensor.

(c) *Artificial Intelligence*
This section examines the application of two different artificial intelligence techniques to tool wear monitoring; Expert Systems and Neural Networks. Again the current state of the art for the application of each technique to tool wear monitoring is summarised at the end of each section.

2.1 The Phenomenon: Metal Cutting and Tool Wear

The following summary of early work in metal cutting has been extracted from a review paper written by Finnie [6].

Cutting machines have been used since the late 18th century to produce specific components. For example, Witney, in 1792, designed a machine to automate the manufacture of muskets and, in 1806, Brunel designed a machine to manufacture pulley blocks. In addition to this, a number of the machine tools that are used today were, in their basic form, developed in the 1840s to 1850s. For example, wood turning lathes were among the first 'machines' to be designed. The very early analytical studies from the 1840's onwards, kept pace with the rapidly developing processes until about 1900, when empirical work gained greater favour as a method of analysis providing, for example, tool life predictions.

The earliest scientific work that could be found by Finnie is attributable to Cocquilhat who published an experimental analysis of the drilling process in 1851. In this work the drill was held and the workpiece was rotated. Whilst the drill was advanced the cutting torque was measured with a weight balance. Cocquilhat was then able to tabulate the work done per unit volume of material removed and the force per unit area of cut for cast iron, malleable iron, brass, stone, and some other materials. This work was extended by Clarinval who conducted an analysis of cutting fluids giving also a formula for the work required to rotate a drill as a function of its diameter. In 1858 Wiebe published the following formula for power consumption in drilling:

$$P = K.E.B \tag{1}$$

Where:

P is the power required to remove a chip

B is the width of the chip

E is the chip thickness

K is a material constant

Attempts continued from this early work to produce a unified theory that encompassed and adequately predicted all of the variables of the different types of metal cutting processes. The analysis can be broken down into several areas of interest. These are; chip formation during metal cutting, the prediction of cutting forces and tool temperature calculations. This list can then be subdivided into the different machining processes that exist, for example, grinding, milling, turning, drilling and blanking.

2.1.1 Chip Formation

One of the earliest analyses of chip formation, again reviewed by Finnie [6], was conducted by Tresca. In a study on the planing of metals and, later, in 1878, in a general study on the flow of solids Tresca (incorrectly) assumed that the metal ahead of the cutting edge was in compression. It was the work of Time who, in an experimental analysis of the chip formation process, was the first person to correctly describe the process of metal removal. He pointed out that the material ahead of the cutting edge is being sheared, for ductile materials, or fractured, for brittle ones. However, Time visualised the process of chip formation as occurring by fracture on successive shear planes rather than by plastic deformation.

In 1893 Zvorykin produced a very complete analysis of metal removal by a plane. He produced a formula to predict the shear angle, the angle the shear plane makes with the horizontal, by assuming that the force in the direction of the cutting velocity would be a minimum:

$$\phi = \frac{\pi}{4} + \frac{\alpha}{2} - \frac{\lambda}{2} - \frac{\lambda'}{2} \tag{2}$$

Where:

α is the rake angle

λ is the friction angle for the chip on the rake face

λ' is the friction angle for the shear plane of the chip

(λ or λ' are given by $tan^{-1}(F/N)$ with F being the friction force and N being the force normal to the sliding surfaces.)

Similar equations have appeared independently in several later studies, the most notable of these being due to Merchant [7]. In his original study Merchant investigated the formation of chips during orthogonal cutting and proposed a theory that allowed the calculation of the cutting forces, assuming that the system was in equilibrium. Shortly afterwards, Merchant [8] extended his theory to take into account simple plasticity conditions. With these modifications he found that the accuracy of the model was greatly improved, even though such factors as shear strain rate had not been included.

Later, Stabler [9] analysed the relative importance of the different geometrical features found on a machine cutter. From this analysis of geometry he deduced that the rake angle has the largest effect in determining the efficiency of the metal removal process.

Albrecht [10] extended the analysis of the cutting process, by attempting to include the dynamic response of the machine tool in the cutting model. He found

that the dynamic response of the cutting force was related to the surface roughness of the workpiece produced from the previous cut. In his experimental work he found that some, but not all, of his theory was supported and this led to the conclusion that a geometric analysis does not provide a full model of the cutting process and that other factors, such as temperature in the shear plane, need to be taken into account.

It was Fenton and Oxley [11] who first allowed for the effect of strain rate and temperature in the machining process. They analysed this effect for orthogonal cutting, and developed an approximate theory, based on the earlier work of Merchant, that takes into account strain, strain rate, velocity-modified temperature (a temperature calculation that takes account of the strain rate) and the flow stress characteristics of the workpiece material in chip formation. Later, Stevenson and Oxley [12] [13] conducted some experimental work on the zone of intense plastic deformation just in front of the cutting edge and found that, at high strain rates, the flow stress increases with strain rate.

In later studies Oxley and Hastings [14] [15] further extended metal cutting theory. In the first of these extensions [14] the 'frictional conditions' at the tool-chip interface were described in terms of a minimum work criterion and good agreement with the previous experimental work was found. In the later work, Oxley and Hastings extended their theory to eliminate the need for an empirical relationship between the strain rate, temperature and the work material flow stress properties to calculate the maximum shear strain rate. The predicted values agreed closely with the limited experimental data that was available for very high strain rates and temperatures.

A summary of the basic elements of the Oxley and Hastings model along with differences from previous models is given below:

(a) The shear plane model of Merchant is replaced with a shear zone model, incorporating a primary shear zone surrounding the Merchant shear plane and a secondary shear zone at the tool-chip interface (this is in accord with observations made by Trent [3]).

(b) The flow stress of the work material is allowed to vary with strain, strain rate, temperature and sliding conditions at the tool-chip interface.

(c) The sliding conditions at the tool-chip interface are described in terms of the shear flow stress in the layer of chip material adjacent to the tool cutting face.

(d) Plain strain, steady-state conditions are assumed to apply.

(e) The shear plane near the centre of the chip formation zone and the tool-chip interface are assumed to be directions of local maximum shear stress and shear strain rate.

(f) The tool is assumed to be perfectly sharp.

The equation for strain rate is very different from the previous work of Merchant [7,8] and there is considerable difficulty in estimating the value of the shear zone thickness. Stevenson and Oxley [12], using printed grids on the workpiece surface after a series of quick-stop experiments, measured the deformation in the primary shear zone and found that the maximum shear strain rate varied directly with the shear velocity and indirectly with the uncut thickness. Further work by Oxley and Hastings [14] showed that the ratio of the shear plane length to the width of the shear zone was approximately constant over the range of speeds investigated.

Phispanen [16] presented a theoretical analysis of the chip formation mechanism for orthogonal machining at low cutting speeds with continuous and discontinuous chips. He assumed that the chips are formed by thin lamellae of metal moving up the rake face. However, he neglected the lateral expansion of the chip, which can, according to Trent [3], be quite large.

Childs [17] extended the earlier work of, for example, Phispanen to take into account the elastic contact between the chip and tool surface. In order to perform this analysis, Childs considered the elastic contact as an externally applied force and replaced the straight slip line fields with circular arcs. He noted that the chip contact length is of critical importance when theory and experiment are compared. Also, by considering the elastic contact, he accounted for approximately one third of the total cutting force that up until that time had been neglected.

According to Trent [3] a chip forms as the tool shears the work material in the region of a plane extending from the tool edge to the position where the upper surface of the chip leaves the work surface, Figure 9. The chip thickness is a very important parameter, and it is not constrained by the tooling, as might be thought. In fact, the chip may be five or more times as thick as the feed. The shear plane angle is determined from the experimental values of the undeformed chip thickness, t_1, and the mean chip thickness, t_2.

$$cot\phi = \frac{\frac{t_2}{t_1} - sin\alpha}{cos\alpha} \tag{3}$$

Where:

α is the rake angle

ϕ is the shear plane angle

The chip moves away with a velocity V_c, which is related to the cutting speed, U and chip thickness ratio:

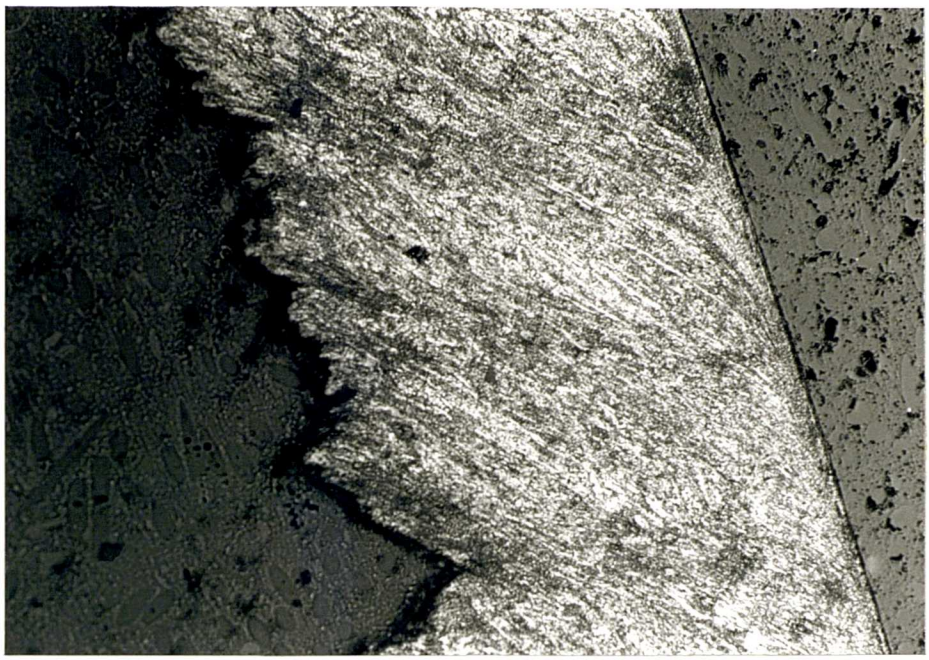

Figure 9: Shear flow in a Cutting Produced During this work (X25)

$$V_c = U\frac{t_1}{t_2} \tag{4}$$

Finally, the amount of plastic deformation (expressed as shear strain) has been shown to be related to the shear plane angle and the rake angle by:

$$\gamma = \frac{cos\alpha}{sin\phi cos(\phi - \alpha)} \tag{5}$$

Lee [18], by machining a relatively strain rate insensitive aluminium alloy and a strain sensitive low alloy steel, AISI 4340, found that the nature of the strain distribution and chip morphology could be rationalised on the basis of material properties, namely strength and fracture ductility, and the parameters of strain rate and strain hardening index, obtained from a tension test.

2.1.2 Chip Seizure

Nearly all metal cutting theory is based on classical frictional models at the tool-workpiece interface, the work of Oxley et al being a notable exception. It has been shown, and is now generally acknowledged, that the chip is bonded to the

tool for part of its contact length and it is important to note that, in the case of metal cutting, the process of seizure does not relative movement of the chip and tool. This is because the area of seizure is relatively small and the available force is large so that shearing in the chip can take place close to the plane of seizure, Trent [3].

The process of metal removal is not a steady one, with transient stresses being built up as chips form and break off. In the case of milling where there is a periodic cutting frequency along with a non-constant chip thickness the force is no longer steady with severe fluctuations in the tool-chip contact stresses during tooth entry and exit. This means that it is quite possible to induce failure by fatigue in the modern brittle cutting tool materials, Chandasekaran [19].

2.1.3 Cutting Forces

It has been found from extensive research that the forces involved in cutting a pure metal are much larger than when cutting an alloy. With these pure materials the contact area is very large and the shear plane angle is very small and the long chips move away at a very slow speed. The large contact area is probably associated with the high ductility of many pure metals, but it is unclear at present as to the precise relationship [3].

Trent [3] notes that it is possible to reduce the cutting forces by altering the tool geometry so that the contact area between the chip and tool rake face is reduced. He quotes a reduction of 50 %, from 1400 N and an increase of 14° in the shear plane angle when a reduced contact area tool is used in preference to a normal cutting tool. The cutting force is also greatly dependent on the tool geometry. For example, reducing the measured rake angle from 30° to 5° increases the measured cutting force by 30 % from 600 N in one typical test.

Obviously the cutting force will be indicative, to some extent, of the stresses involved in shearing the workpiece material. Many reasearchers have investigated the dependence of the cutting force on the shear flow stress.

Jain and Gupta.[20] observed that the shear flow stress is governed by the shear strain acceleration. This is could be of importance in milling where the strain rate is not constant, thus greatly increasing the likelihood of tool breakage at tooth entry and exit. Even for the case of interrupted milling where the chip thickness remains constant the strain rate has to increase very quickly to its constant value on insert entry, and vice versa on exit.

Sarwar and Thompson [21] have observed that, for a blunt tool, there is an increase in the transient forces at the beginning of a cut. This could partly explain why a worn tool is at greater risk of breakage when compared to a new one.

Stephenson and Wu [22,23], in a two-part study provide a numerical model of the

cutting process in turning and drilling. The model that they developed predicts the power requirements and chip form based on rigid plastic material behaviour for the cutting of ductile metals. In the presentation of results they find that their model quite accurately predicts the chip geometry and force for the relatively simple process of turning, whereas for the more complex cutting process of drilling, the cutting force and the chip thickness are consistently underestimated.

Usui and Takeyama [24], in a photoelastic analysis of the stresses in machining, proved that the maximum value of stress on the rake face of a cutting tool occurs at the cutting edge and that it remains relatively constant over most of the tool-chip contact length before reducing sharply towards the exit point of the chip, away from the tool.

Nakayama et al [25] presented an empirical model of cutting force with which the authors obtained an accuracy of better than 10 % and, in some cases better than 5 % in the prediction of force when compared to experimental measurements. They also provide a tabulation of material constants required in the model for prediction of the cutting force in-process. The model is, however, limited to tools of zero rake angle but, for the cases examined, it provides good agreement with the measured values of the three orthogonal components of cutting force.

Summary

For this work, it has been decided to take forward the work of Oxley et al to predict cutting force, temperature and strain rate from the metal cutting process. This is because this model requires the least experimental data in order to obtain estimates of the above parameters and appears from the literature to be the most complete theory available at the present time.

For power calculations it has been decided to use an empirical formula, as shown in the next section, to determine the relationship between spindle current, cutting conditions and wear. This is because the measurement has a low fidelity and will probably not display much sensitivity to strain rate, for example, even though there will be a direct relationship between the power required to perform cutting and the specific cutting force.

2.1.4 Wear Mechanisms in Sintered Carbide Inserts

Trent [3] provides a review of the wear processes that can occur on carbide inserts, and describes the following mechanisms:

(a) *Diffusion Wear*
When cutting steel at high speed and feed with carbide inserts a crater forms on the rake face immediately behind the cutting edge. Sections through the crater show no evidence of deformation by shear as is the case for high

speed steel tools. Trent [3] notes that the carbide grains are smoothly worn through with no evidence of particles large enough to be seen through a microscope being broken away and concludes that the carbide insert wears on the rake face by a process of diffusion.

Cook [4] also observes that both crater and wear land development are primarily functions of temperature under high speed machining. He also notes that the interface temperatures can be in excess of 700 °C whilst machining carbon steel with a tungsten carbide insert on a lathe and proposes the wear mechanism to be one of diffusion of the insert carbides into the workpiece metal, with the harder particles being mechanically removed.

(b) *Attrition Wear*
Trent notes that, when using carbide inserts, attrition wear is common when cutting at lower speeds and feeds when the temperature is not high enough to cause diffusion. The process occurs most commonly when the cutting is intermittent and a built up edge has formed on the insert. As the chip cross-section changes and the built up edge breaks away, it removes a small amount of the insert.

(c) *Abrasive Wear*
Because of the high hardness of tungsten carbide, abrasive wear is not likely and Trent [3] notes that there is little evidence to suggest that sliding contact causes much wear except in cases of cutting very abrasive material, such as sand castings.

Accelerated wear can occur at those positions where the tool and workpiece interface slide relative to each other and, while abrasion may form a part of the wear mechanism in this instance, it seems that the primary wear mechanism of the insert is that of chemical reaction (oxidation) with the atmosphere.

(d) *Mechanical Fracture*
Trent [3] notes that with the proper selection of insert grade it is not common for failure to occur except in the case of intermittent cutting. Milling as a metal removal mechanism, is according to Trent, one of the severest of processes, with even the impact of chips flying away from the cutting site and impacting on inserts that are not cutting being capable of causing fatigue or fracture.

(e) *Thermal Fracture*
Thermal cracking is common on the insert when, as in the case of milling, the cutting is interrupted frequently with short cracks running perpendicular to the cutting edge. Usually, these cracks are initiated on the hottest part of the insert, the location of largest thermal variation, as the insert alternately heats up and cools down. Trent notes that these cracks rarely cause failure of the insert, although sometimes when they join up small fragments of the insert will break away.

Idealised Wear Studies

Boness et al [26,27] have studied the wear of a ball that is sliding in a cup shaped object. In this study the authors confirmed that the wear rate could be expressed as:

$$V = \frac{KW}{HL} \tag{6}$$

Where:

V is the volume of material removed in unit time

L is the distance moved in unit time

K is a constant of proportionality

W is the normal load

H is the hardness of the softer material

These authors also found that by cumulating the rms of the Acoustic Emission Signal (AE) a relationship with the wear on the ball could be found and, further, that the Acoustic Emission signal was severely attenuated if the process was lubricated with heavy parafin. Using the AE along with the rotational speed, the load applied to the ball and the hardness of the softer material it was possible to predict the wear rate coefficient.

2.2 Monitoring the Phenomenon

Monitoring the metal cutting process and, in particular, the degradation of the cutting tool is an activity that has been conducted by many researchers for the last few decades using a variety of sensors. This monitoring work is reviewed in the following sections each of which is devoted to a particular sensor and covers both types of degradation process. The current state of knowledge will be presented firstly for cutting power, followed by force, temperature, surface finish and acoustic emission.

2.2.1 Cutting Power

Although most machine operators and machine tool manufacturers are of the opinion, (and this view is supported by the current work), that the power consumed in machining the material is a good monitoring method for tool wear

detection, it has proved very difficult to find any scientific papers regarding the subject. This is probably due to the obvious nature of the parameter and possibly also because the power is related to the cutting force, Lissaman [28].

One source of an empirical relationship between the power required to perform the cutting operation and the cutting parameters is the 'Tool and Manufacturing Engineers Handbook' [29]. Here it is stated that the machine power is given by the following relationship:

$$hp = KST[0.00549(1000A)^r] \tag{7}$$

Where:

hp is the approximate horse power required at the machine spindle for milling, including a 30 % 'dull tool' allowance and a 20 % 'machine friction' allowance.

K is a machinability factor for milling different materials.

S is the peripheral speed of cutter, sfm.

T is the average number of cutter teeth in contact with the workpiece.

A is the cross-sectional area of workpiece material removed by one cutter tooth, in^2.

r is a machining exponent for different workpiece materials

2.2.2 Cutting Force

The use of cutting force in tool wear monitoring is quite commonplace in the modern CNC or DNC machine. Some manufacturers have incorporated simple tool monitoring systems into the CNC that they have used. For example, Kennametal [30] market a module which links to the CNC controller and allows the user to specify a maximum force level above which the unit will stop the cutting process. They claim that the system is applicable to breakage detection, collision protection, and the detection of a maximum tool wear level on milling machines.

Sandvik [31] have also produced a multi-channel unit that the manufacturers claim, is capable of adapting itself to the force signals it receives in its learn mode. This enables the instrument to be used in different machine tools, recognising the difference between new and worn tools and between stable and unstable cutting conditions. When an error is detected in the cutting process the unit sends an alarm to the controller thus stopping the turning operation for which the unit has been designed.

At a research level, cutting force has been used very convincingly to monitor tool wear, detect tool breakage and detect collisions. For example, Danai [32] has constructed a dynamic state model using the cutting parameters of feed, cutting speed and depth of cut and, with force as the input, tool wear was predicted during the turning process.

Sata et al [33], using linear discriminant functions, found that the power spectrum of the cutting force in turning could be used to discriminate between the different types of cutting in turning, namely continuous and discontinuous chips, chatter and the formation of built up edge. It was observed by these authors that the nature of the power spectrum of the force signal changed for each of these cutting features by the introduction of characteristic spectral peaks for each phenomenon; 50 Hz for properly broken chips (obviously a function of the chip breaking frequency), 100 Hz for chatter (probably a function of the machine stiffness) and a small peak at 150 Hz for the formation of built up edge. It is possible that these higher frequencies correspond to harmonics of the 50 Hz signal.

Konig [34], Kashimura [35], Taraman [36] and Nair et al [37] all found that the cutting force increased linearly with increases in flank and crater wear levels, but that the gradient was dependent upon the material being machined and the cutting conditions used in the turning process. In addition, Kashimura and Taraman found that the force only remained linear to a flank wear level of 0.5 mm, and Nair et al found that it was necessary to remove transient information from the signal before the linear relationship could be observed.

Lan et al [38] and Altintas et al [39,40] have both used the cutting force signature for the detection of short timescale events in the milling process. Lan et al used a model reference adaptive system developed by Landau [41,42] and an autoregressive time series model of the sensorial output. The authors found that the processing scheme gave a good response to both breakage and cracking of the tool, and that the response time was fast enough to allow continuous monitoring of the cutting process. Altintas et al used a similar scheme with similar success.

Rao [43] developed a novel method for monitoring the flank wear level by defining a wear index, for the turning process. This was defined to be a ratio of the measured dynamic force amplitude to the acceleration signal at the first natural frequency of the cantilever formed by the tool holder. He found that the system used was independent of the cutting parameters for the range of cutting conditions investigated but that the wear index was still very much dependent on the material being machined.

Petrie et al [44] identified one of the main problems associated with using force or vibration as a tool wear monitor whilst turning, namely that of variations in the vibrational response of the machine. They found that the tool wear level induced an increase in the measured vibration, but that this increase could be as much as an order of magnitude less than the variations between machines. Such an effect necessitates the use of calibration runs on every machine before a tool wear monitor is capable of working correctly.

Lindström and Lindberg [45] described a new sensor for in-process monitoring of cutting force. The sensor consisted of a small piezoelectric element which was placed behind the cutting insert. With the sensor in place these authors were able to monitor the dynamic cutting forces involved in the shear zone. They also showed results in the frequency domain which appear to be superior to conventional transducers based on strain gauged flexible members and they claimed that the sensor could be used as part of a commercial monitoring system. This would, however, entail considerable work as numerous tool holders would have to be modified, resulting in a considerable increase in the cost of tooling for any machine shop.

Elbestawi et al [46] and Tarng [47] both presented similar approaches to the monitoring of tool wear with cutting force in the milling process. In these methods the authors used the harmonics of the frequency with which inserts come into contact with the workpiece to monitor tool wear. It was found that the relative amplitudes of the harmonics in the power spectrum of the force, were linearly related to the flank wear level. In addition Tarng found that the power spectrum gave a good indication of insert breakage and that there was a certain element of prediction in the signal. This is something that the present author has also observed, although in the current work the signal processing was conducted in the time domain as opposed to the frequency domain.

It is often stated that it is very difficult to measure the cutting force whilst machining. However, further work by Tarng [48] in the milling process has shown that there are novel ways of measuring this information without resorting to flexible members in the feed mechanism and other intrusive methods. In this approach, accelerometers were mounted on a static part of the machine spindle. The signal was then integrated to yield the displacement signal and by using a calibration function, which essentially contains the dynamic and static stiffness of the spindle, the displacement signal could be used to give a value of force. This would again be machine specific.

Oraby and Hayhurst [49] has developed analytical models for the relationships between wear, cutting time and cutting force. With these models it was found that an accurate prediction of tool wear could be made from the force signature in turning. The ratio of the radial to the vertical forces was used as the wear descriptor.

Thangaraj and Wright [50], in a piece of work on drill wear estimation, measured the thrust force primarily to assess the effectiveness of force in the prediction of tool failure. It was found that the main reason for drill failure in smaller drills is excessive wear since, as the wear increases, the temperatures of the drill and chips (Hale and Jones [51]) both increase which in turn increases the wear rate partly due to welding of the slow moving central part of the drill to the workpiece [50]. Thangaraj and Wright also found that the cutting force generally exhibited a linear increase with increasing tool wear with a very sharp rise in the cutting force when a breakage is imminent. These authors went on to discuss what is needed in a general tool wear monitoring scheme, and the view that was expressed

was one of a multi-sensor scheme with intelligent extraction of the tool wear level.

Summary

From the studies of the relationship between tool wear and cutting force discussed above it would appear that the best correlation is obtained when the d.c. level of the cutting force is plotted against flank wear. In the vast majority of published work the d.c. force level rises linearly with the mean flank wear on the cutting tool.

In addition it has been found that the force signal is a reasonable breakage detector and, although it does not really give a direct indication of breakage, it does give an indication of circumstances that could lead to a breakage.

2.2.3 Cutting Temperature

Since diffusion wear and metal cutting properties are both functions of temperature and, furthermore, since it is expected that the cutting temperature will rise as the tool wears, it might be of interest to measure temperature to assist wear monitoring.

One method of doing this, described by Hale et al [51] and by Infrared Monitoring Systems [52], is to use an infra-red camera to observe the cutting tool. This approach does show that the temperature of a tool increases with tool wear but the implementation requires full-field thermography and interpretation may be quite subjective. Furthermore, if coolant is to be used, thermography is probably impracticable. One other disadvantage of infra-red thermography is that the full field systems are extremely expensive. At 1992 costs, a camera and monitor would cost in the region of £20,000 to £40,000 and this would not include any interpretation or tool wear prediction capabilities.

Šolaja et al [53], Redford et al [54] and Colwell [55] have used thermo-couples embedded into a cutting insert to monitor the cutting temperature variations with tool wear in the turning process. They all found that a linear relationship existed between the insert temperature and the level of flank wear on the tool. In addition, Redford et al found that the temperature at a given wear level was dependent on the cutting conditions.

Both the thermocouple and full-field thermographic methods are difficult to incorporate into a tool wear monitoring system and, as such, are unlikely to be developed commercially for any but the most critical of applications.

2.2.4 Surface Finish

In many machining operations it is the degradation of surface finish that leads to the definition of unacceptable tool wear. It is therefore reasonable to expect that surface finish might be used to monitor wear.

Raja et al [56] found that it was possible to use the machined surface profile to monitor tool wear. However, the method was also sensitive to wear in the machine tool itself so that, for example, wear in the slideways was also detectable in the surface profile of the workpiece. As the authors point out, this is not a problem that is specific to this particular sensor but applies to vibration monitoring as well as force and consumed power monitoring of the cutting operation.

Dong et al [57], in an analysis of the parameters responsible for the surface roughness of a machined component, found that it is possible for a tool with a high level of wear to produce a machined surface with a lower surface roughness as defined by the R_a value, a result confirmed by the current work. They found also that the vibration of the machine tool was a major contributor to the surface profile produced by a machining operation.

2.2.5 Acoustic Emission

One of the sensors used in this work for tool condition monitoring is acoustic emission (AE). Since this is a relatively novel sensor a little more space will be devoted to its description than the foregoing sensors.

Definition of the Acoustic Emission Signal.

The European Working Group for Acoustic Emission (EWGAE) [58] defines acoustic emission (AE) as "the transient elastic waves resulting from local internal microdisplacements in a material". The American National Standards Institute [59] defines AE as "the class of phenomena whereby transient elastic waves are generated by a rapid release of energy from a localised source or sources within a material, or the transient elastic waves so generated".

Clearly AE can be generated by a large variety of fundamental processes such as fracture and plastic deformation. In some simple applications, such as tensile test specimens, it has been quite conclusively proven that AE is dependent on the strain rate that the material undergoes. However, in metal cutting, high strain rate plastic deformation, fracture and wear processes all occur simultaneously over a region where the temperature varies very rapidly with position, making the AE generation mechanism rather complex. The key questions, in relation to AE in metal cutting are therefore;

(a) What is the cause of AE in the metal cutting process ?

(b) What is the best method of detecting it ?

Sources of Acoustic Emission

From the above general definitions of AE it is possible to identify a number of micromechanical phenomena where a transient elastic wave results from a rapid release of energy. Researchers such as Lenain [60] and Tatro [61] and others have proposed the following possible sources of AE:

(a) plastic deformation

(b) fracture, fatigue crack initiation and growth

(c) phase transformations

The process of wear will probably not be expected to generate AE per se but will include all, or some, of the above generation mechanisms and so indirectly will generate AE.

It has been normal to divide the AE signals obtained whilst monitoring into two qualitative groups:

(a) continuously occurring emission

(b) burst type emission

Sometimes, however, it is not possible to draw a distinction between these as there is no precisely defined point at which the transition takes place.

Low Strain Rate Plastic deformation :- Plastic deformation in a crystalline material can take place by one of two mechanisms; slip or twinning. During slip, one part of the crystal moves relative to the other, the slippage taking place on certain planes in the crystal, resulting in visible steps on the crystal surface. Each atom is moved by an integer increment, leaving the crystal continuous. In metal cutting, where the strain rates are very large ($10^3 s^{-1}$ - $10^6 s^{-1}$), the major component of plastic deformation is slip, which is caused by dislocation motion, Trent [3].

Chung and Kannatey-Asbu [62], in an analysis of AE resulting from the plastic deformation of a single crystal, found that there are two components of dislocation motion that give rise to AE:

(a) Initial Motion

(b) Steady oscillatory motion

For the initial motion, there is a step change in the dislocation velocity (from zero) due to the high initial static Peierls stress. Following the initial motion the dislocation undergoes a periodic variation in the dislocation velocity.

Gillis [63] in an article on AE generation mechanisms states that as a dislocation passes from one minimum energy level to the next, the level of elastic strain is increased until a critical value is reached. When this value is exceeded the dislocation jumps to the next minimum energy level thus producing a vibrational wave in the lattice which manifests itself as acoustic emission.

Dunegan and Green [64] found that the intensity of the AE signal from tensile test specimens was strain rate sensitive, with higher strain rates generating AE with greater energy levels whereas the AE signal could disappear completely in some materials at very low strain rates. Similarly Friesel and Carpenter [65], in an investigation of AE sources during the deformation of titanium, found that the rms of the AE signal was dependent on the sample orientation, mode of testing, strain rate, test temperature and purity of material but that in all cases the AE generated was caused either by dislocation slip or deformation twinning. Landy and Ono [66] found that when they tested different heat treatments of the same steel the rms AE generated at yield during a tensile test varied markedly, and the authors had some success in relating this to differences in dislocation motion and in the different crystal structures and phases.

Fracture and Crack Initiation and Growth :- The growth of cracks by brittle fracture results in the formation of new surfaces and the release of elastic strain energy which is partly transformed into AE. In many materials (including the steels of interest here) hard, brittle second phase particles are present whose fracture during plastic deformation can give rise to AE events. Heiple et al [67] found that by introducing boron particles into an aluminium alloy (2219) they could account for a large proportion of the AE events when the material was strained plastically by the fracture of boron particles, any remaing AE events being accounted for by decohesion of the particles from the aluminium matrix. In a similar study, Carpenter and Zhu [68] found that the AE generated during a series of compression tests on samples of fully ferritic ductile cast iron was related to the average diameter of graphite nodules in the matrix, and also to the fracture toughness of the material by a power law.

In some cases of macroscopic fracture it has been possible to relate the energy in the measured AE signal to the theoretical energy resulting from fracture, Heiple et al [67] and Carpenter et al [69]. The AE generated from the propagation of such a crack was found to be the burst type, bursts often being generated in rapid succession.

Phase Transformation :- It is generally known that phase transformation can occur by two main processes:

(a) Nucleation and growth

(b) Martensitic

In the first the transformation takes place by the transfer of atoms across the interface. With a martensitic transformation, however, there is a shear-like rearrangement of atoms. In general, once a martensitic transformation has started it will continue at a very high rate. This transformation process is accompanied by the formation of new crystallites, a process that gives rise to sudden energy releases. Heiple and Carpenter [70] and Liu and Kannatey-Asibu [71] both found that in some of the martensitic phase transformations of plutonium and steel, detectable AE was generated, but that in the other types of phase transformations no AE was detected.

AE generation from Metal Cutting

During metal cutting the chip that is formed is the result of large amounts of plastic deformation. In general, the strain rates in metal cutting are many orders of magnitude greater ($> 1000\ s^{-1}$) than in tensile tests ($< 0.1\ s^{-1}$). Under such conditions, the dynamics of dislocation motion can be different and there is no reason to assume that the low strain rate AE source mechanisms are dominant or even present in the case of metal cutting.

Energy Analysis :- A general investigation of AE production due to plastic deformation at high strain rates has been developed since 1979 by Dornfeld [72]. In this work, Dornfeld found that plots of the rms AE against the various parameters of the cutting process were very similar in form to plots of the shear strain rate against the same cutting parameters. Dornfeld thus built a link between the rms AE signal and the shear strain rate by equating the rms AE and the cutting parameters from Merchant's theoretical work:

$$AE_{rms}^2 = C\tau\dot{\gamma}V \tag{8}$$

Where:

C is a constant of proportionality (a function of strain rate and temperature.)

τ is the maximum shear strength of the material

$\dot{\gamma}$ is the strain rate

V is the volume of material participating in the cutting process

Dornfeld concluded by observation that the rms AE signal is sensitive enough to monitor changes in the strain rate when the cutting conditions are altered in orthogonal machining.

A later study of the turning process, also conducted by Dornfeld [73], resulted in a refined model of AE generation from the zone of plastic deformation. This model provided a good correlation with the experimental observations and it was concluded that, for those cutting conditions and materials investigated, the primary AE generation mechanism was that of plastic deformation in the zone of high strain rate immediately in front of the cutting edge:

$$AE_{rms}^2 = C[\tau r_c \frac{\cos\alpha}{\sin\phi}\frac{U}{\Delta_x}V] \tag{9}$$

Where:

C is a constant dependent on material

r_c is the cutting ratio, $\frac{t_1}{t_2}$

t_1 is the undeformed chip thickness

t_2 is the deformed chip thickness

Δ_x is the width of the shear zone

U is the cutting speed

α is the rake angle

ϕ is the shear plane angle

In yet another study along similar lines Kannatey-Asibu and Dornfeld [74] related the energy content of the Acoustic Emission signal to the plastic work of deformation. Here it was found that, for a given rake angle and feed rate, the mean rms AE signal level increased linearly with the cutting speed. Also, if the other cutting parameters remained constant, the rms AE signal level increased with increasing values of the rake angle.

Dornfeld and Kannatey-Asibu [75], made a further analysis of the AE generated during orthogonal metal cutting. Included in this analysis was a study of the relationship of friction between the chip and insert and the AE signal level. The authors also provided more experimental evidence for the dependence of the AE signal on the strain rate.

$$AE_{rms}^2 = C[\tau w U(\frac{\cos\alpha}{\sin\phi\cos(\phi-\alpha)}t_1 + \frac{1}{3}(l_1+l_2)\frac{\sin\phi}{\cos(\phi-\alpha)})] \tag{10}$$

Where;

w is the width of the cut

l_1 is the length of the sticking zone

l_2 is the length of the sliding zone

For the most part, the above equation is defined by machining parameters, but the contact length, $l_1 + l_2$, and ϕ must be determined experimentally.

Using this semi-empirical formula the authors set about analysing its usefulness and found that the correlation between theoretical and experimental results was very good, except at zero rake angle. By determining the total contact length of the chip on the insert they found that the contribution of plastic deformation to the total AE signal is approximately 45 % with the remainder being accounted for by 'friction' at the tool-chip interface.

The assumptions made by these authors in all the above work are summarised below:

(a) The workpiece shear strength is constant both temporally and spatially

However, Oyane [76] has shown that shear flow stress of the material varies with temperature.

(b) The shear strain rate in the shear zone is constant with time

A reasonable assumption for orthogonal cutting, but not for milling.

(c) The tool-chip interface is divided into two zones, the sticking and the sliding zones, the sliding zone obeying classical friction theory

The work of Trent [3] and Oxley et al [11,12,13,14,15,77] has shown that the tool-chip interface does not obey classical friction theory so, according to these authors, this assumption would not be correct.

(d) Linear relationships were assumed between the actual contact area between tool and chip and the apparent area of contact (classical friction theory assuming that there is a very small area of material in actual contact)

Trent and others have demonstrated that the actual area of the chip in contact with the tool is equal to the apparent area of contact, thus supporting the claim that the tool and chip are bonded to each other.

(e) The length of the sticking zone is half of the total tool-chip contact length

This last assumption is not supported at all by the literature. In fact, Oxley et al [11,12,13,14,15,77] have developed a theory of metal cutting which quite accurately predicts the cutting forces, and this theory completely disregards the sliding zone replacing it by a zone of plastic deformation immediately adjacent to the tool-chip interface.

Further, Trent [3] states that this simplistic view of the flow of metal past the rake face is not correct for most metals. In his authoritative work he states that; "The most important conclusion from the observations is that contact between tool and work surfaces is so nearly complete over a large part of the total area of the interface, that sliding at the interface is impossible under most cutting conditions". Thus, with metal cutting there are some processes other than friction at work.

The area of contact is small and the forces present are large enough to allow shearing of the workpiece material. Furthermore, tools are made of very high tensile strength materials so that they do not fracture easily. Under seizure conditions at the tool-chip interface it is not reasonable to assume that the chip slides past the tool rake face because the force required to break the bond between the two contacting surfaces could be much larger than that required to shear the workpiece material adjacent to the rake face. Trent argues that the relative motion of the two bodies involves shearing in the weaker workpiece material. In other words the chip acts as its own lubricant, which is an observation backed up by microscopic examination of chips.

Messaritis and Borthwick [78] took the model of AE generation whilst machining a stage further by attempting to include the effect of temperature on the strain rate induced during cutting by utilising the semi-empirical cutting theory advanced by Oxley and Hastings [11,12,13,14,15,77]. This prediction of the strain rate, the authors found, correlated excellently with the rms AE obtained during turning tests with sharp tools, indicating that, in that work, the predominant factor in the generation of AE was the strain rate.

The 'frictional effects' on the AE signal during metal cutting, have also been analysed by Yaohui and Rongbao [79]. In this work, the authors found that 'friction' between the chip and insert affected the spectral characteristics of the AE signal. As the rake angle was varied, whilst keeping all other conditions constant the relative spectral peak heights changed. The authors claimed that the amount of friction between the chip and insert will be the only variable which changes and so its effect can be isolated. They found that the frictional AE signal produced a peak in the power spectrum at 200 kHz whereas the effect of plastic deformation was to cause a peak at 100 kHz. However, it should be noted that the sensor used was a piezo-electric crystal so that the spectral information is contaminated by resonances of the crystal.

Hutton and Yu [80] have analysed the effect of built up edge on the AE signal. This analysis is important because many researchers have reported variations in the AE signal with changes in the rake angle and built-up edge can be regarded as a local change in the rake angle. They found that the presence of a built-up edge is generally comparable with changes in the rake angle. Hutton and Yu utilised the relationship established between strain rate and AE^2_{rms} proposed by Dornfeld to calculate the increased rms AE signal due to the effective change in local rake angle and the experimental evidence seemed to support this relationship.

Summary :- The process of AE generation in metal cutting is therefore highly dependent on the amount of plastic deformation and the rate at which it takes place. This, in turn, is dependent on the motion of dislocations in the metallic structure, which is dependent on the way in which the metal is removed from the parent material by the tool.

As a tool wears it would be expected that the changes in tool geometry bring about changes in the amounts of plastic deformation that are taking place, a blunt tool perhaps causing larger amounts of plastic deformation than a new one. It might be expected that this would be reflected by changes in the AE signal so that a sensor that is independent of the machine tool dynamics but is related to the cutting process could be employed to monitor the tool condition. The work of Dornfeld and Borthwick goes some way to isolating the manner in which the AE signal is dependent on the process variables in orthogonal and semi-orthogonal cutting in the turning process but milling is generally more complex since the chip thickness does not usually remain constant as the tool rotates. This means the strain rate will be constantly changing and hence that the AE signal will vary in intensity with the position of the insert during its cut.

However, the same broad principles of AE generation should hold in the milling process and, in particular, the relationship between the rms AE signal and the strain rate undergone by the chip should obey the same laws as in turning. Therefore, it is hoped that AE monitoring of the milling process will reveal similar trends to those in more simple processes. The ways in which the foregoing theory might be modified for the more complex process of milling are indicated in Chapter 3.

Frequency Analysis :- The power spectrum of the AE signal reveals the variation in signal power with frequency. Phase information for the AE signal is lost during the transformation but this is not a problem because current sensing technology provides little information about the phase of the signal and it is unlikely that the original phase of the AE signal when generated is preserved during the multiple reflections, refractions and mode changes that the signal must undergo before it can be detected.

Fleischman et al [81] and Malaprade et al [82] have developed a theoretical analysis to explain the spectral characteristics of the AE signal due to dislocation motion. They propose that the motion of a dislocation segment between obstacles produces a stress pulse which is transmitted as an elastic wave to the surface of the medium. This is consistent with the current thinking that it is dislocation motion and not unpinning that is responsible for AE generation. The relevant equations from [81,82] are summarised below.

The time of flight of the dislocation segment between obstacles is given by:

$$\tau = \frac{D}{\nu} \tag{11}$$

Where:

τ is the time of flight in seconds

D is the mean distance between obstacles, or the mean free path of the dislocation (a function of temperature, material and strain rate)

ν is the dislocation velocity

Equation 11 assumes that the acceleration and deceleration of the dislocation are negligible.

Since acceleration and deceleration are neglected the dislocation velocity vs time profile is essentially a rectangular pulse in the time interval $[0,\tau]$ with a fundamental frequency of:

$$f = \frac{1}{2\tau} = \frac{\nu}{2D} \tag{12}$$

In reality, the AE spectrum will also reflect the transmission properties of the propagation medium, sensor-surface coupling characteristics, sensor response and the response of the recording media. However, the general trend is that, as the dislocation velocity increases or the mean free path decreases, a larger proportion of the AE signal power will be concentrated at higher frequencies.

In the context of metal cutting dislocation velocities are related to the plastic strain rate by:

$$\dot{\gamma} = \rho_m b \nu \tag{13}$$

Where:

ρ_m is the mobile dislocation density (a function of γ)

b is the magnitude of the Burger's vector

From the previous two equations it would be expected that process parameters which increase the strain rate would tend to shift the AE signal power towards higher frequencies. Also, the high levels of strain in the primary and secondary

shear zones affect the amount of strain hardening that occurs which in turn will affect the mean free path of dislocations as dislocation forests and sessile dislocations effectively act as obstacles. Thermal softening, on the other hand, will increase the mean free path of dislocations and thus shift the spectral power to lower frequencies.

Rangwala and Dornfeld [83] have presented an experimental investigation of the effect on mean AE frequency with changes in cutting parameters. In this work, the authors found that the mean frequency of the AE signal increased with cutting speed but that a point was reached where no further increase took place and the mean frequency reduced slightly for further increases in cutting speed. Dornfeld attributed this effect to thermal softening, but no quantitative prediction of the turning point was given.

Acoustic Emission Propagation

Acoustic Emission propagates as a stress wave through its host medium. However, it is not possible for a wave to pass through a finite medium and not be affected by that medium so that the recorded signal will not only represent the generating event but also the propagation path to the sensor.

It is possible to construct an approximation to the infinite medium in a laboratory but, on a machine tool, the geometry of the propagation medium is fixed by functional considerations.

In the current application, the workpiece and vice, which are at or near to room temperature, will be dispersive due to their wave guide properties. As it is not very practical to mount the sensor on the workpiece during metal cutting operations, the interface between the workpiece and vice will have an effect on the propagation of the AE. Where it might be possible to estimate the dispersion that will result from the temperature and geometry effects on the AE signal, this would be an enormous amount of computational work for the benefit that would be gained.

It is likely, however, that the propagation path of the AE from source to sensor, will not have a great effect on the frequency content of the AE signal as long as the AE sensor is capable of responding with a large enough amplitude to record. It is, however, inevitable that the amplitude of the signal will be affected by the propagation and this may vary with frequency. Severe attenuations will occur at every interface that obstructs the path of the wave, with different waves being hindered by different types of interface. For example, surface waves will probably have difficulty in propagating around sharp corners and pressure waves will have great difficulty in finding a transmission path through an interface between two media that are not completely in contact.

Detecting Acoustic Emission

AE transducers are capable of detecting surface disturbances of very small amplitude. In machining, these amplitudes are of the order of 10^{-6} m at a maximum and this is approximately six orders of magnitude smaller than the machine vibration which is detectable with more conventional sensing techniques, such as strain gauges. Historically, there are two types of AE transducer, the piezoelectric and the capacitive sensors. Quite recently, work on interferometric techniques has allowed a fibre optic based AE sensor to be used reliably in a workshop environment, McBride et al [84].

Kakino [85] in an experiment that varied the position of the AE sensor found that the position determines the amplitude of signal that is detected but that the frequency content is unaffected. This result is probably influenced by the fact that a piezoelectric sensor relies on the resonances of the crystal in order to detect AE so it is therefore not too surprising that the frequency content is not noticably affected by the position of the sensor. Kakino concluded that the amplitude is affected by the number of interfaces through which the wave has to propagate.

Piezoelectric AE transducers :- This type of sensor relies on the fact that, when a piezoelectric element is compressed, it produces across its faces a voltage proportional to the compression induced. The most popular material in use is lead zirconate titanate (PZT-5) and this is used almost exclusively in commercial sensors, mainly because it is readily available and cheap. However, PZT does have a few other advantages such as a low impedance at reasonance which allows for easy connection on the electronic side and it matches most metals acoustically. Typically, the sensor will respond to an impulse with a sharp rise time but with a much slower decay time i.e. it will 'ring' for a considerable time after initial excitation. The fundamental frequency of this ringing will correspond to the most easily excitable reasonance of the crystal. It is, of course, possible to tune this resonance into the frequency range that is of interest by reducing the diameter and thickness for a high reasonant frequency and vice versa for a low resonant frequency but a trade-off does occur, since smaller crystals produce sensors of a lower sensitivity.

A piezoelectric sensor can be represented as a simple damped spring-mass system attached to a base that is subject to an input displacement. It can be shown that, when such a system is operated at or near its resonance, the relative displacement of the base of the sensor is a measure of the base velocity. Hence most piezoelectric sensors behave as velocity transducers

Some manufacturers have attempted to approach a displacement sensor more closely by arranging the crystals that form the sensing element in concentric cylinders, so that a range of resonances occur in the frequency band of interest. It is one such 'broad band' sensor which was used during this work.

Proctor [86] has built an improved AE sensor that possesses a frequency response that is flat to within 2.5 dB over a megahertz bandwidth and this has been proven to behave as a displacement sensor. The active element consists of a truncated cone of PZT which is attached to a relatively large brass backing. However, this arrangement is not very sensitive and the active element, being very small, is also very fragile.

At a research level (Kerkyras et al [87]) it is possible to build a much more sensitive displacement sensor. To do this, instead of using a crystal as the sensing element, a piezoelectric polymer film can be used. This type of sensor does not resonate and, when mass loaded with the correct backing, it is possible to build a sensor with a frequency response that is flat to within one or two dBs over a megahertz bandwidth (a commercial PZT sensor typically has a frequency response that is flat to within 20 dB over a megahertz bandwidth), and hence a greatly improved decay time.

Capacitive and Interferometric Sensors :- If the capacitance between the metal surface and a fixed plate is recorded whilst an AE wave propagates underneath, then the true displacement of the surface will be recorded by the sensor. There is, however, a problem with the implementation of such a capacitive sensor in a production machine shop environment as the sensing element must be isolated from machine vibrations. In addition to this, the theoretical limits of the technique would suggest that the transducer will be around 100 times lower in sensitivity than a PZT-5 based transducer. Therefore, capacitive transducers have tended to remain as a calibration sensing technique for AE.

An interferometer can be used to measure displacement by allowing one beam of the interferometer to be reflected by the vibrating surface whilst the other is reflected by a static reference surface. When the two beams are then combined an interferometric pattern is generated, the phase difference between the two beams being proportional to the relative displacement between the two surfaces.

Palmer and Green [88] first used an interferometer to measure AE from a tensile test specimen. Their set-up was based on bulk optics and it is as difficult to envisage implementation of this in a machine shop as was the capacitive transducer of the previous section, but for different reasons. Recently, with the use of fibre optic techniques (McBride et al [84]) it has been possible to implement an interferometric sensor in a machine shop and use it to measure AE from a face milling operation, removing low frequency high amplitude effects by means of a PZT-driven path length servo.

Acoustic Emission as a Monitoring Tool

One of the first practical uses to which AE was put was the detection and location of cracks in pressure vessels and critical structures [64]. Traditionally, only the time of flight of a significant AE event generated, for example, by a crack enlarging

in a pressure vessel was of interest. This allowed for the application of simple signal processing to obtain the necessary location information.

The following discussion summarises the findings of researchers using AE to monitor wear during the metal removal processes of blanking, turning, milling and grinding respectively. A final section concerns multi-sensor monitoring and monitoring for non-wear applications.

Blanking :- Mardapitas and Au [89] and Kim [90] have both used AE sensors to monitor progressive wear on a blanking tool. They both found that the amplitude of the AE signal was correlated with the sharpness of the tool and also that the AE signal was dependent on the machining parameters of stock thickness and hardness and also on punch velocity at impact. Additionally, Mardapitas and Au found that the AE signal could be related to the mean plastic shear strain rate. Liang and Dornfeld [91] performed a similar analysis drawing similar conclusions.

Rangwala et al [92] investigated the AE signal in the frequency domain during punch stretching operations. They found that, for the different AE generation mechanisms, such as plastic deformation and fracture of the workpiece, the power spectrum of the AE signal displayed substantial differences, with the signal power in the 50 kHz band centred on 735 kHz exhibiting an amplitude five times greater for plastic deformation than for fracture.

Turning :- Much analysis of the use of Acoustic Emission as a tool wear monitoring sensor has been conducted on the turning process as this is a less complex process than milling.

Iwata and Moriwaki [93] investigated the use of AE in monitoring tool wear during the turning process. In this experiment a piezoelectric AE sensor was mounted on the tool holder and the sensor output was monitored during a systematic wear test on carbon steel. Iwata and Moriwaki concluded that the frequency content of the AE signal does not significantly change with tool wear but that the rms AE increases to a fixed level and then remains almost constant, this constant level varying with the cutting conditions used. The most satisfactory relationship with tool wear found by these workers was that for the total number of AE counts.

Kannatey-Asibu and Dornfeld [94] and Moriwaki and Tobito [95] have undertaken an amplitude distributution analysis of the rms AE signal during turning. Both researchers found that most of the amplitude distribution statistical parameters exhibited a good correlation with tool wear.

Raghunandan et al [96], in a general review article, concluded that the AE signal is independent of the machine tool structure vibration. This provides an important contrast to workpiece vibration monitoring, which is heavily dependent on the machine tool structure. The present author has confirmed this finding, Wilcox et al [97].

Takeshita [98] used the ratio between the rms AE when the tool enters the workpiece and the AE whilst it is cutting steadily to predict flank wear accurately. Also, the surface roughness of the workpiece was found to correlate very well with the same ratio.

Sturgess [99] used the AE signal in the frequency domain to detect workholder failure and certain tool failure conditions. The signal processing scheme was novel in that it used prior information about the workpiece geometry and tool in order to define the AE signal that was to be expected. Then, the AE signal recorded was compared with that expected and an analysis made of the tool condition. With this scheme, the author claimed to be able to make very accurate measurements of the tool edge condition, although the measurements presented were made in the absence of built up edge or burrs.

Vainberg [100] processed the AE signal produced in the turning process to generate nybles of information which he related to the tool wear state. He found that it was possible to distinguish between different wear states; a newly ground tool, a bedded-in tool and a worn tool. This author did not describe how the binary feature vectors were arrived at, but did describe an instrument that appears to process the AE signal in terms of the AE burst.

Lan and Dornfeld [101], in a study of progressive wear whilst turning, found that it was possible to relate the mean rms AE signal to the flank wear on the carbide insert, but that the signal was not a monotonic one.

Diniz et al [102] used AE as a monitor of both tool wear and surface finish in a finish turning process. The authors monitored the variation in the mean rms AE signal in the frequency band of 150 kHz to 250 kHz with variations in the R_a and VB_B values. They found that the surface roughness increased almost linearly with increasing tool wear, and that the amplitude in the frequency band noted also increased linearly with tool wear. This allowed the authors to develop a prototype system for monitoring tool wear and surface finish in a finish turning operation.

Milling :- Osuri et al [103] presented a mathematical model for the production of Acoustic Emission during machining, which included the cutting parameters as inputs to the model. This analysis was verified on a CNC milling machine and a simple control chart type approach to the progressive wear monitoring problem was proposed by utilisation of the monotonic relationship with tool wear.

Diei and Dornfeld [104] found that, for milling with only one insert, it is possible to correlate the rms AE with the specific cutting force, both of which show similar trends to increase with tool wear. They proposed a time domain averaging technique for removing variation in the rms AE due to 'random chip noise'. Blum et al [105], using an AE sensor only, found that the normalised AE-mode mean value exhibited a montonic trend with tool wear, and that events such as insert edge chipping were easily detectable with this signal processing scheme.

Grinding :- Roethel et al [106] undertook a study of the grinding process and found that the Acoustic Emission signal was primarily dependent upon the machining parameters. However, it was found that there was an increase in the amplitude of the AE signal with tool wear (defined by the authors as a wheel that is in need of re-dressing).

Dornfeld and Cai [107] investigated the AE signal emitted from the grinding process and found that it was possible to relate the energy of the rms AE signal, AE^2_{rms}, to both the wheel wear and the wheel loading, as it was found that the AE signal is a function of the undeformed chip thickness. As the rms AE signal was dependent on wheel loading it was shown that the signal accurately detected workpiece-wheel contact and sparkout.

Tool Failure using AE :- One of the first experiments conducted on the problem of insert breakage was that of Kaneeda et al [108]. In this work the authors performed quick-stop experiments on a vertical milling machine, so that they could examine the fracture geometry of the insert and correlate it with the AE generated. They found that the fracture of the insert was easily discernable above the general AE level as did Inasaki and Yonetsu [109], Moriwaki and Tobito [95], Diei and Dornfeld [110], Vajpayee and Sampath [111] and Lan and Dornfeld [112]. These results are similar to a breakage event observed by this author [113] when incorrect cutting conditions were monitored using an AE sensor. Whereas Kakino et al [114] managed to relate the integral of the power spectrum, to the total area of thermal cracks in a cutting tool.

Ramaraj et al [115] and Yen and Wright [116] have both proposed that it would be possible to avoid some breakage situations, either by avoiding certain tool workpiece geometries or by avoiding cutting conditions that are likely to induce breakage. In a similar study, Sampath et al [117] state that in the milling process, it is much more common for an insert to crack at the end of a cut than at the beginning.

Kannatey-Asibu and Emel [118,119] utilised linear discriminant function classification techniques on the power spectrum of the AE signal in the frequency range of 0.1 to 1 MHz generated during turning. It was found that, when plotting the magnitude of the 110 kHz signal against the 990 kHz signal, it was possible to discriminate between normal cutting and insert breakage with a success rate of 90 %, the breakage signal having the higher frequency component.

Blum et al [105] proposed methods for the detection of tool failure in single and multi-point machining operations. It was suggested that, for single point machining with the use of an adapted tool holder, and by using a normalised amplitude distribution of the envelope of the AE signal that it was possible to discriminate tool damage on a generally increasing background level of AE which was caused by progressive tool wear. For multi-point machining, such as milling and drilling, the authors proposed the use of a magnetic coupling device in order to mount the AE sensor close to the cutting tool, rather than the more conventional mounting

on the workpiece. With this type of sensor mounting they found that it is possible to determine a chipping event on the multi-point tool by examining the relative amplitudes of the peaks corresponding to the spindle rotational frequency and the tooth passing frequency, which in this case was four times the spindle rotational frequency.

Wilcox et al [120] have described the reduction in the AE amplitude after an edge chipping event on one of the inserts in a multi-point cutting tool. They suggested that the best method for detecting the damage may be to monitor the power spectrum of the rms AE averaged at 0.5 ms.

Takeshita and Inasaki [98] also used the power spectrum of the rms AE signal to determine the state of the cutting tool. In this work, however, the power in the signal does not reduce but rather a peak corresponding to the frequency of the spindle rotational speed emerges. These authors used the ratio of the peak height at the spindle rotational speed and the tooth passing frequency to describe a power ratio, and with this they proposed to detect multi-point tool damage.

Summary :- Kakino [121] in a review of Acoustic Emission technology in Japan found that at that time AE methods were more appropriate for GO-NO GO situations rather than where a quantitative evaluation was required. For this situation the author cited load current and feed force as more appropriate sensing techniques.

Raghunandan et al [96] in a review of AE and vibration condition monitoring techniques, highlighted the problem of AE signal processing/acquisition that required a solution before AE can be used to its full potential in condition monitoring. On the other hand, Vahaviolos [122] cites AE as an excellent, intelligent sensor that is ideally suited to monitoring of machining operations.

It would appear from the literature that the application of AE to insert breakage is well established, with the AE signal undergoing a step increase at the moment of fracture, but that the variation of AE with progressive tool wear is less clear.

2.2.6 Application of Multiple Sensors, Novel Methods and Current Industrial Methods for Tool Wear Monitoring

Emel and Kannatey-Asibu [123] used a combination of acoustic emission and cutting force in the quest for a reliable and versatile tool wear monitoring station. In this work the authors used pattern recognition techniques based on linear discriminant functions to distinguish between a new tool and an old tool. The system was also applied to the problem of tool breakage detection with considerable success. It was found that the combination of both sensors led to an increase in the confidence with which a breakage or worn tool could be detected. As would be

expected, the force signal exhibited a dramatic rise in level, followed by a greater drop when a cutting insert broke. The signal was much clearer than in the present work, probably due to the fact that the former was conducted on a lathe rather than a milling machine without the effect of the additional inserts.

Gomayel and Bregger [124] proposed a novel approach to the problem of tool wear monitoring, particularly for turning. The method proposed consisted of using an electromagnetic probe to measure accurately the cut thickness on the workpiece and thus indirectly measure the reduction in the cutting tool dimensions. This approach has the advantage of being independent of all cutting conditions, materials and machines and has the distinct disadvantage of having to be accurately set-up for each cut and that some materials (non-conductive) do not lend themselves to probing with this kind of sensor.

Pekelharing and Orelio [125], in a discussion of tool breakage, found that tool breakage is, in some cases, of more economic importance than tool wear, for example in the case of small tools or ceramic tools. The authors cite the most common cause of tool breakage as mistreatment some time before breakage which passes unnoticed. Later, the tool breaks and the prevailing conditions are those that are blamed for the breakage leading to false conclusions. These authors developed a breakage sensor by grinding gullies close to the cutting edge of the insert and filling these with electrically conductive material so that, when a crack propagates, the resistance is increased thereby warning of impending failure. This method has the distinct disadvantage of requiring specially manufactured inserts.

At present it is normal for a CNC machine to be able to track the total machining time that a particular tool has accumulated. This allows the user to set a threshold above which no further cutting will be performed. The CNC machine used in this work had such a facility, although it was rare for it to be used as the number of materials machined on it was quite large as was the number of different tools used.

The reason that this method is not acceptable when accurate results are required is highlighted by Wager [126] who analysed the life of cutting tools in a statistical manner, and found that there was a large distribution in the life of of high speed tools whilst machining mild steel. This problem is also noted by Vajpayee and Sampath [111] who note a 35 % variation in tool life, which results in any method that monitors cutting time being necessarily conservative.

These studies also point to another problem in using an accumulated cutting time approach to tool wear monitoring in that it does not address the problem of a cutter that might be used on a variety of materials and under a variety of different cutting conditions although some more sophisticated tool management systems may have the facility to take this into account.

2.3 Artificial Intelligence

Machine learning (ML) has played a central role in artificial intelligence (AI) from the start of research into this field, although it is true that the main thrust of AI research has deviated from this theme with the advent of such significant developments as problem solving, theorem proving, robotics and expert systems (ES). Recently ML has again started to play a significant and increasing part in the development of AI. For instance, early work on perceptrons (simple neuron like processing unit), Rosenblatt [127] suffered some set-backs in the light of difficulties in solving non-linear functions, as suggested by Minsky and Papert [128]. However, there has been a resurgence of scientific and media interest due in part to the work of Tank and Hopfield [129] and Ballard, Hinton and Sejnowski [130] who have played a large part in the development of connectionist networks with hidden layers that are capable of learning to recognise non-linear functions.

The ability to learn, to adapt and to modify behaviour has been regarded by some as an inalienable property of organic beings and many would question whether an expert system can be regarded as being any more intelligent that the Encyclopedia Brittanica. However, an ES is more than simply a convenient way of representing knowledge in a computer and normally has the ability to search for inconsistencies in its knowledge base and to infer further knowledge from the input it receives.

It is probable that the 'ability to learn' is a prerequisite for any form of intelligence and, in order to check for intelligence, a test has been proposed by Turing [131]. In this test a human being is asked to communicate, through a terminal, with two or more other operators one of which is the artificial system. If the human being cannot tell whether the answers to their questions were from the system or the other human then the artificial system could be regarded as possessing true intelligence.

Early attempts at applying this test have proved how difficult it will be for a machine to achieve intelligence defined in this way. A computer program known as ELISA, Weizenbaum [132] achieved partial success until the person communicating with it realised how it was composing its answers. In reality, the program did not 'understand' the sentence but simply examined it for key words to operate on or, used one of a set of standard replies.

Two of the approaches to AI, as briefly mentioned earlier, are artificial neural networks (ANN) and expert systems (ES). It is not clear whether these approaches are likely to achieve success as defined by Turing, but both approaches have merits of their own where specific solutions are required to specific problems. In view of their use in this work some of the features of both artificial neural networks and expert systems are outlined below.

2.3.1 Artificial Neural Networks

Two of the main components of the brain are the cortex and the cerebral cortex which surrounds it. The cerebral cortex has a surface area of 2000 cm^2, is approximately 3 mm thick, and is composed almost entirely of neurons six layers thick. It contains about 100 billion neurons, and the central nervous system as a whole contains perhaps as many as 1000 billion neurons.

Figure 10 shows a photomicrograph of neurons from the cerebral cortex of a cat (Roberts [133]). The number of neurons shown is only a small fraction of those present as only a small number have taken the stain which was used to highlight them. At the top of the photomicrograph are axons, along which communications are sent to other neurons, these being the triangular-shaped objects in the lower half of the photomicrograph. Neurons can die if they do not make useful connections and in the first few years of a child's life around 15 % of its neurons die because they do not make useful connections with other neurons through these axons.

The neuron communicates through the axon and dendrite with other neurons by emitting electrical pulses (termed 'firing') around 2 ms in duration and 100 mV in amplitude. When the weighted sum of the inputs (pulses from other neurons) received by the neuron exceeds a certain excitation level it will itself 'fire'.

Artificial Neural Networks (ANN) are a simplistic representation of this biological network. Usually they consist of a set of inputs with a series of hidden layers followed by a set of outputs. There are two broad classes of artificial neural network. The first class uses distributed representation, where the total knowledge (for every problem to be solved) of the network is distributed between each processing unit. The second uses localised representation, where single processing units, or small groups of units hold the specific knowledge required to solve a single problem.

A network learns to discriminate between classes of patterns from an input domain in a holistic manner. The network is presented with sets of feature vectors that are representative of the instances of each class, correctly labelled, and the ANN "learns" to recognise these. It does this by readjusting internal weights in a fixed network topology via a learning algorithm, so that the weights are optimised to the entire training set. These algorithms, in essence, calculate the amount of credit each active processing unit deserves by comparing the output of the system with the correct response.

Current ANN's do not accurately represent the biological equivalent, but rather exploit ways in which it is possible to connect a set of simple processing units. The application of the approach to real problems, such as word recognition, has shown that the ANN has the ability to recognise features more accurately from the input domain than has previously been possible using a deterministic approach, Tank and Hopfield [129].

Figure 10: Neurons from the Cerebral Cortex of a Cat, Reproduced with Permission from [133]

2.3.2 Expert Systems

One of the earliest acknowledged examples of an ES was "Dendral" (dating back to 1965, Lindsay et al [134]) which was used for determining the molecular structure of a compound from the molecular formula and its mass spectrum.

The first attempts at using computers to perform real world tasks such as recognition of shapes were largely unsuccessful. This was because the task is actually much more complex than we, as humans, realise. Perhaps this is because we do not remember the amount of learning that we performed in our infancy.

An Expert System can vary considerably in nature from one implementation to another and this is in part due to the fact that the term 'Expert System' has not yet been properly defined. The knowledge that can be implemented into an ES is usually the experience of a 'domain expert' which has built up over several years of work in a limited area. It is therefore unlikely that textbooks would give sufficient detail in the area as, much of the domain expert's skill will be stored as approximate 'rules of thumb', which are seldom if ever recorded.

To encode this knowledge, it is usually necessary for a 'knowledge engineer' to interview the 'domain expert' and break down the knowledge into its constituent pieces and then to encode the knowledge into the Expert System. This is usually not implanted as procedures and functions as in more traditional procedural based programming languages, but as a set of 'rules' in a declarative form contained in what is known as the 'knowledge base'.

It is the function of the knowledge engineer to make each 'rule' correspond to a piece of knowledge meaningful to the domain expert. In principle, it might seem possible to extend the rules so that all eventualities are covered but in practice these conditions may not be known.

In general there are three methods for encoding knowledge into an expert system, Michie [135]:

(a) *Production Systems*
The basic idea of a production system (Newell and Simon [136]) is that a database and a collection of production rules is maintained in the following form:

$$\text{Situation} \Rightarrow \text{Action}$$

The 'situation' part of the rule specifies some condition in the state of the database and at any point is either satisfied or not. The action part of the rule specifies changes that are to be made to the database every time the rule is used. Conceptually, a production system goes through an evolutionary process. At each cycle, one rule is selected and used, thus modifying the database and so altering the way in which rules will act on the next cycle.

(b) *Logic Systems*
In this form of knowledge encoding, some of the flexibility of the previous method is sacrificed in exchange for the well-understood semantics of logic. With this form of knowledge representation there is no distinction between the rules and the database. Information about the problem domain is represented by logic formulæ and augmented by rules of inference.

(c) *Frame Systems*
In this method, frames, which correspond to an entity in the problem domain and contain a number of labelled slots for information pertinent to that entity, are used to represent the entire problem. Usually the collection of frames is linked together in a network, with different frames inheriting the slots of knowledge from other frames. It is possible for frames to represent almost anything the knowledge engineer wants them to represent.

Once the knowledge has been encoded, inferences about solutions to the problem are undertaken by the inference engine. There is again a variety of methods to be used, depending on the problem and these are itemised below:

(a) *Forward Chaining*
The inference engine looks into the database to see which rules are to be used by examining which of them have their situation part satisfied (for example in a production system). It then selects one and carries out the action part of the rule. The rules that get used are thus determined by the information in the database and such systems are called foward-chained or data driven.

(b) *Backward Chaining*
For the case of backward chaining, the inference engine checks to see if the action part of any rule is satisfied (again for production systems). If this is so, then an attempt is made to establish the situation part of the rule.

In this case we are led to a different method for inferring results from the knowledge base. This manner of inferencing the rules that are used in the knowledge base could be different from that used under forward chaining, as the rule which is selected to be used is not determined by what is in the knowledge base but by what we expect or hope to find there.

(c) *Knowledge Organisation*
Finally, the knowledge for all but the smallest models, must be organised into areas of similar relevance. This is because, as the model grows in size, the amount of work that the inference engine has to perform grows enormously as it checks each rule in turn. If, however, the knowledge is organised into similar areas then the inference engine only has to examine those areas it determines to be necessary. This approach to knowledge organisation is termed a 'blackboard system' as each domain expert has access to a particular blackboard so that they can describe and check their particular knowledge.

2.3.3 Artificial Intelligence used in Condition Monitoring

Relatively recently, researchers in the area of condition monitoring have attempted to apply artificial intelligence techniques. In general two AI techniques are applied to condition monitoring problems, namely:

(a) Artificial Neural Networks

(b) Expert Systems

In the following two sections a short review of the work performed in applying these techniques to general condition monitoring problems will be given.

Neural Networks

Witcomb et al [137] has described a method for automatically ordering a reference set of vibrational spectra from an aircraft engine for later diagnosis using an artificial neural network. The network, in this case a Kohonen artificial neural network, was used to automatically order the spectra. It was found that the method was applicable to all such machines as the set-up would automatically adjust itself to the characteristics of, for example, an older machine and, once the referencing was complete, it would be possible to monitor incoming spectra for the development of faults in the engine.

Chow et al [138], have applied neural networks to the condition monitoring of induction motors. They used the network to recognise incipient faults in real time on a laboratory based magnet induction motor. They found that the network was capable of better than a 95 % classification of such faults, a performance which they claimed was better than that attainable by a more traditional fault detection scheme.

Grabec et al [139] proposed neural networks for the detection of discrete AE events and their automatic characterisation. However, the definition that Grabec used for AE is different from that normally understood in that he was interested in the low frequency audible range, and so perhaps was investigating vibration rather than AE. Nevertheless, he found that the network could detect the difference between the signal emitted from a new and worn tool in metal cutting.

Rangwala and Dornfeld [5] used neural networks to integrate the output of two sensors, namely a force and AE sensor, and hence provide a diagnostic capability for turning operations. These authors found it necessary to perform some preliminary signal processing on the sensorial information before inputting the data into the network. This consisted of calculating the power spectrum of both the AE and force signals and combining them to yield a vector of relevant features. Using a perceptron training algorithm the network was capable of correctly classifying

around 90 % of the feature vectors from a new and worn tool after having been trained on a set of 30 feature vectors, 15 from a new tool and 15 from an old tool. The authors also found that using both the cutting force and AE signal enabled the network to make better decisions than those based on the AE or force signal alone.

Choi et al [102] used neural networks in the adaptive control of turning processes. They used a neural network to simulate the turning process, in-as-much as it was used to predict the AE and force signal generated from the cutting operation. The results indicated that it was possible to use a neural network as a control mechanism. As the network required minimal a priori information, it was possible to use it to model the nonlinearities of the system under investigation.

Burke and Rangwala [140] compared two types of neural network for monitoring turning operations; a back propagation supervised system and an unsupervised technique called 'adaptive reasonance theory'. They found that both systems provided excellent recognition of the tool condition in terms of the flank wear and suggested that the adaptive reasonance theory, due to its ability to operate unsupervised, was more suitable for a 'real world' system than the supervised back propagation technique.

Okafor et al [141] used a neural network to integrate AE, force and spindle acceleration signals from a turning operation in order to predict surface roughness and bore tolerance. They found that three sensors gave better prediction than did two when used with the neural network for classification. They also found that the AE signal provided the best correlation with the surface finish and bore tolerance, followed by the force signal and that network errors were consistently below 10 %.

Choi et al [142] used a neural network simulation to monitor a turning operation by combining the output from the cutting force and the rms AE signal. They aimed to provide detection of tool wear whilst removing the effects of process variables from the sensorial information and to this end they claimed a better than 90 % success in determining whether the tool is worn out or not. (The system was not capable of providing any better resolution.)

Sukvittayawong and Inasaki [143] have used an artificial neural network to identify the AE produced during the formation of different types of chips produced during a turning operation. The authors found that the trained neural network (based on the skew and kurtosis of the AE signal) was capable of correctly classifying 97 % of examples after 1000 iterations.

Venkatasubramanian et al [144] used artificial neural networks to monitor faults in steady state processes, in particular in the chemical industry. The authors used a back-propagation algorithm to train the network on the output of various sensors such as flow rate, temperature and reactant concentration, from instances of process failures in and normal running of the plant. They found that the network provided an excellent method for the monitoring of chemical plant. They also

found that the network was capable of correct diagnosis even in the presence of missing sensors and that the performance did not reduce quickly in the presence of such problems, rather the response degraded slowly.

Expert Systems

Ahmed and Pringle [145], have used an expert system approach in the detection of abnormal vibration spectra from different types of machinery. They found that the use of an expert system with knowledge of 'noisy' and 'clean' vibrational spectra allowed for accurate detection of faults that developed on the machinery.

Yuedong and Liangsheng [146] used the 'fuzzy classification' facility of most expert system shells to allow classification of 'noisy' vibrational spectra and concluded that the classification of three different machine faults was possible.

Brown et al [147], have used an expert system approach to the problem of a general manufacturing process control. In this work, the authors developed a model of a manufacturing process and showed that it would be feasible to use the expert system to control the entire process, indicating, for example, faults to the system manager.

As was indicated in the introduction, the background material for this Chapter has been gathered from a variety of different applications, only some of them related to metal cutting and few related to milling. The following Chapter develops this material into a specific strategy for the monitoring of face and groove milling on En8 and En24(T) steel on a CNC milling machine.

Chapter 3

Application of Background to Milling

This chapter covers developments of the background material for the specific application of milling monitoring. In particular, the differences between the particular milling processes of interest and the more idealised conditions of orthogonal cutting are highlighted in order to extend the observations of other authors to this process and predict the likely sensor behaviour with cutting conditions and wear. Also, some aspects of AI are developed and applied to the milling monitoring problem.

3.1 Geometric Comparison between Milling and Orthogonal Cutting

During orthogonal and semi-orthogonal turning, the chip thickness remains constant whereas during milling operations, such as grooving the chip thickness varies as the chip has to taper as the insert breaks out of the workpiece. In this work, the face milling operations are slightly different from this in that there are no side surfaces, and the tool completely spans the surface. This means that the chip thickness must remain constant during steady cutting, as each insert will trace out an arc parallel to that of the previous insert. Figure 11 shows the differences in the geometrical arrangement of tool and workpiece between face milling and orthogonal cutting.

Thus the main difference between the current milling operation and orthogonal turning is that the relative magnitudes of the feed and perpendicular forces will change as the tool rotates. The peak feed force will occur at tooth entry, whilst the peak perpendicular force will occur around the central point of the cut. Figure 12 shows the measured time evolutions of perpendicular and feed force as a four point cutter rotates.

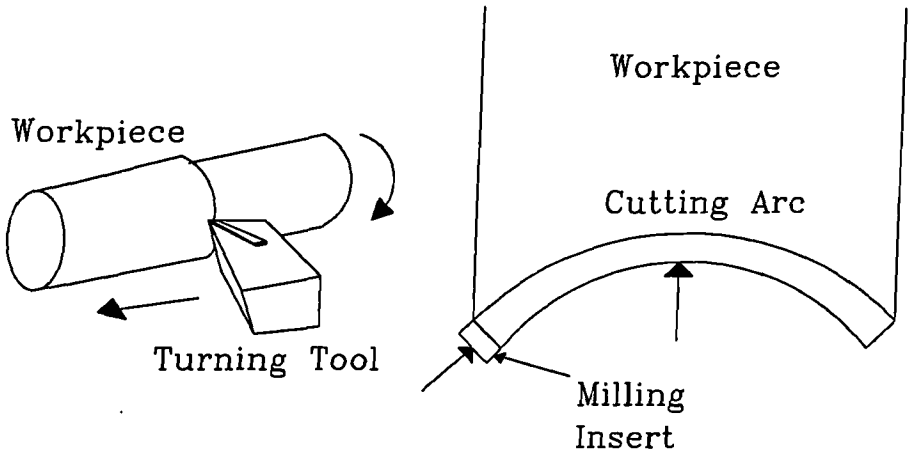

Figure 11: Differences between Orthogonal Cutting and Milling

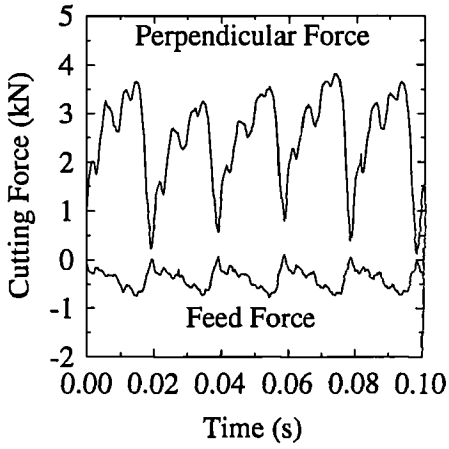

Figure 12: Time Evolutions of Perpendicular and Feed Forces

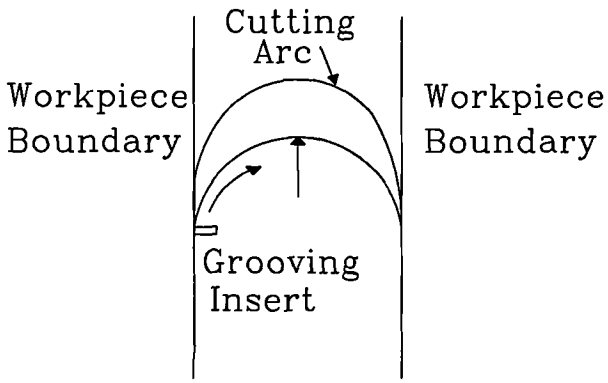

Figure 13: Schematic of the Grooving Operation

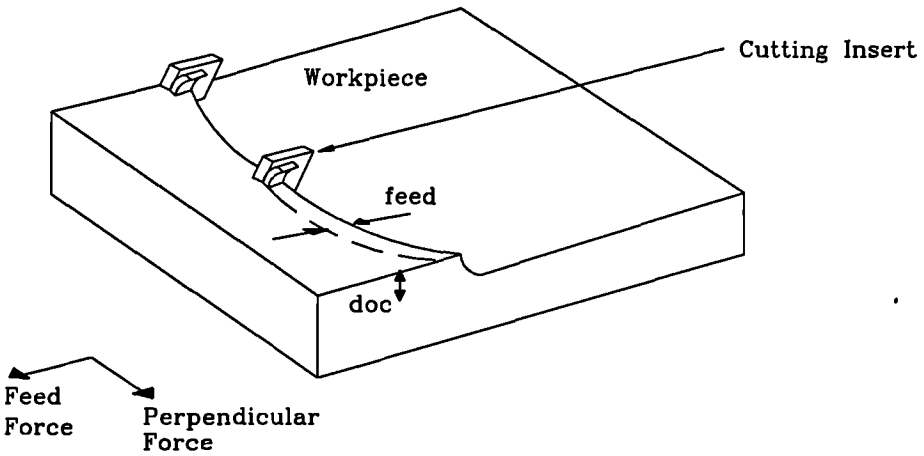

Figure 14: Schematic of the Face Milling Operation with a Large Tool

On the other hand, the grooving operation will have a non-constant chip thickness since the tool is constrained on both sides, thus forcing the inserts to taper into and out of the workpiece as the tool rotates. Figure 13 shows this process schematically.

In addition, cutting with some face milling tools with large numbers of inserts will mean that there may be more than one insert in the workpiece at any one moment in time. Figure 14 shows this in operation schematically.

Dynamically, there will also be differences between the milling process and the turning process, for in both the face milling and grooving operations investigated there will be a discontinuous forcing function that will excite resonances in the machine tool/fixture structure. As the turning operation is a steady-state one there will be a lower tendency for this cutting process to excite these resonances. The dynamic problem will also be exacerbated by tools with more than one insert for, as the tool wears, not all inserts will wear by the same amount thus varying the force with which they impact with the workpiece and introducing a periodic fluctuation of impact forces as the tool rotates.

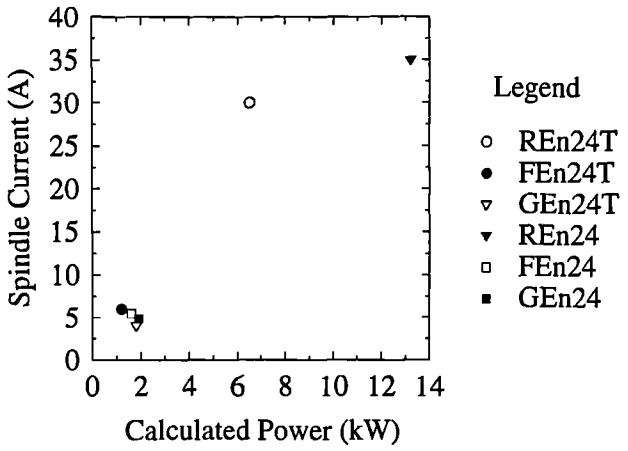

Figure 15: Calculated Power Requirement vs Measured Spindle Current

3.2 Effect of Process on Spindle Current

The power required to perform any particular cutting operation will be affected by several variables and has been related empirically to the material hardness and metal removal rate. Tool wear is not normally included in such relationships other than as a change in the efficiency of the cutting process, usually a decrease of around 40 % (to cater for the worn tool) from the value required to cut with a new tool. The predicted values of power required to perform the cutting operations in Chapter 5 are shown in Figure 15 along with the mean measured spindle current values for cutting with a new tool. The power was calculated from Equation 7 with the appropriate values for the different variables in Equation 7 being obtained from [29].

It is clear from Figure 15 that the variation in spindle current does not match the expected power requirement and so the voltage applied to the motor must be varying. The motor in question is a d.c. one and is controlled by voltage, in this case using 'pulse width modulation'. A servo controls the width of voltage pulses applied to the motor circuit from 0 to 100 % "on" time at a rate of 2 kHz. The rectangular pulses, with an amplitude of 90 V , are applied to the motor and are filtered by the inductance of the armature circuit so that the armature current is related to the average pulse width. This control mechanism explains why more current than would be expected is drawn for rough machining of En24T, where the spindle speed is low (477 RPM) in comparison to rough machining of En24 (800 RPM). Since the power is dependent on both the voltage and current, the current is higher to compensate. It is not possible to use the impedance of the motor armature to calculate the power as this will vary with the pulse width and the current drawn from the supply.

However, for a fixed set of cutting conditions the spindle current is a measure of the power and so during any one wear test it would be expected that the current would vary with the required power. The problem occurs in obtaining

general rules for the variation in current with wear and cutting conditions, as it is necessary to know the power that the machine requires rather than the current. In many machines a.c. motors are used and, in this instance, it would be a simpler matter to calibrate the current in terms of the power that the machine requires.

The effect of a tool breakage on the spindle current will probably be quite small. Only conditions that are likely to cause breakage, due perhaps to removing more material than the machine is capable of are likely to produce detectable current excursions. This is because the breakage of a single insert does not alter the average metal removal rate as the next insert (after the damaged one) to come into contact with the workpiece will remove more metal to compensate. Only when the total power requirement increases will the spindle current or power change to an extent that the low time resolution current signal will be capable of detecting.

3.3 Effect of Process on Cutting Force and Acceleration

The most complete prediction of cutting force for orthogonal and semi-orthogonal turning, has been derived by Oxley et al [11,12,13,14,15,77] and is given by the equation:

$$F_c = \frac{t_1 w k_{AB} \cos(\lambda - \alpha)}{\sqrt{3} \sin\phi \cos\theta} \tag{14}$$

Where:

F_c is the cutting force

t_1 is the undeformed chip thickness

w is the width of cut

k_{AB} is the shear flow stress on the shear plane

λ is the 'friction' angle

α is the cutting rake

ϕ is the shear plane angle

θ is the angle between the resultant friction force and the shear plane

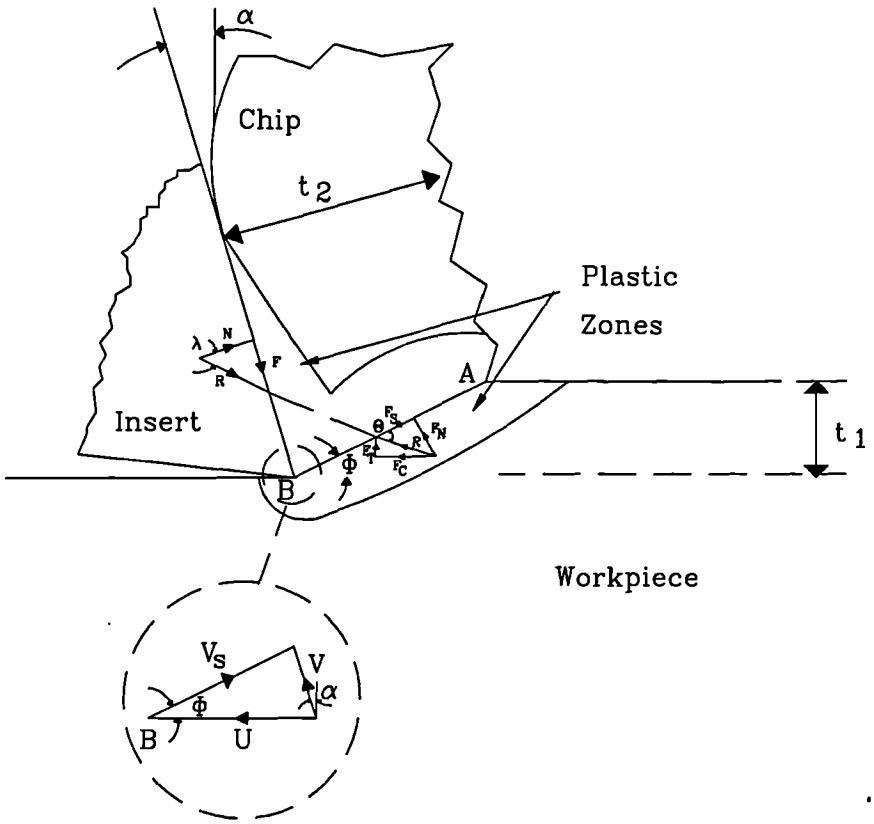

Figure 16: Geometrial Features calcluated and required in the Oxley Model

Figure 16 shows the major geometrical features in a diagrammatical form, along with the location of the zones of plastic deformation that occur in the cutting process.

The application of this equation is complicated by the fact that the shear flow stress on the shear plane, the friction angle and the angle between the resultant friction force and the shear plane and the shear plane angle are all dependent on the tool geometry and the temperature in the zones of plastic deformation around the shear plane and near to the tool-chip interface.

Oyane et al [76] have published data for the effect of temperature on the material flow stress at high strain rates and this is reproduced in Figure 17. With the strain-hardening index and with this information, it is possible to calculate the values of cutting force for a new tool using the above equation and those summarised in Figure 18, which illustrates the iterative procedure required using a flow chart. The appropriate additional equations are described in Appendix F which also contains a fuller description of the model.

The above model has been developed for the process of turning and in order to apply this to the milling process some minor changes in the notation are required, these being that t_1 must represent the feed per insert and w represent the depth of cut. As can be seen from Figure 11 the milling process removes material in an

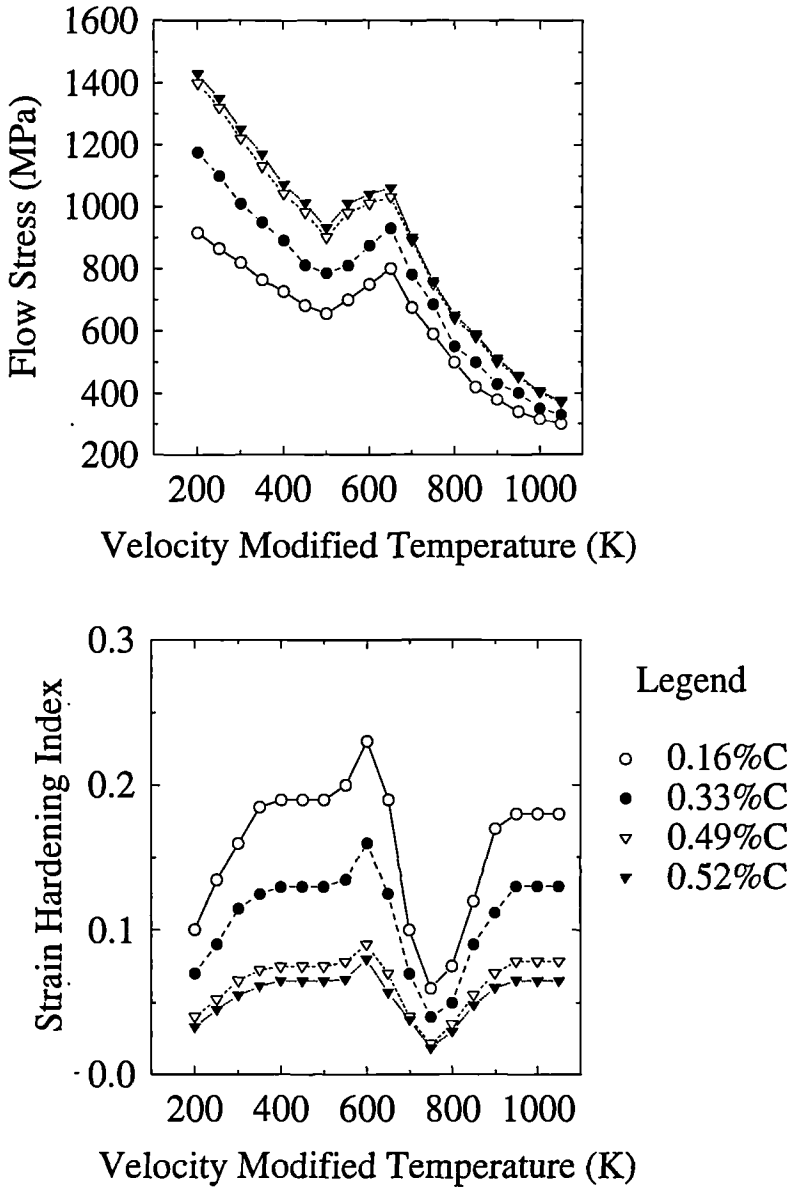

Figure 17: Variation of σ_1 and n with Temperature, after Oxley

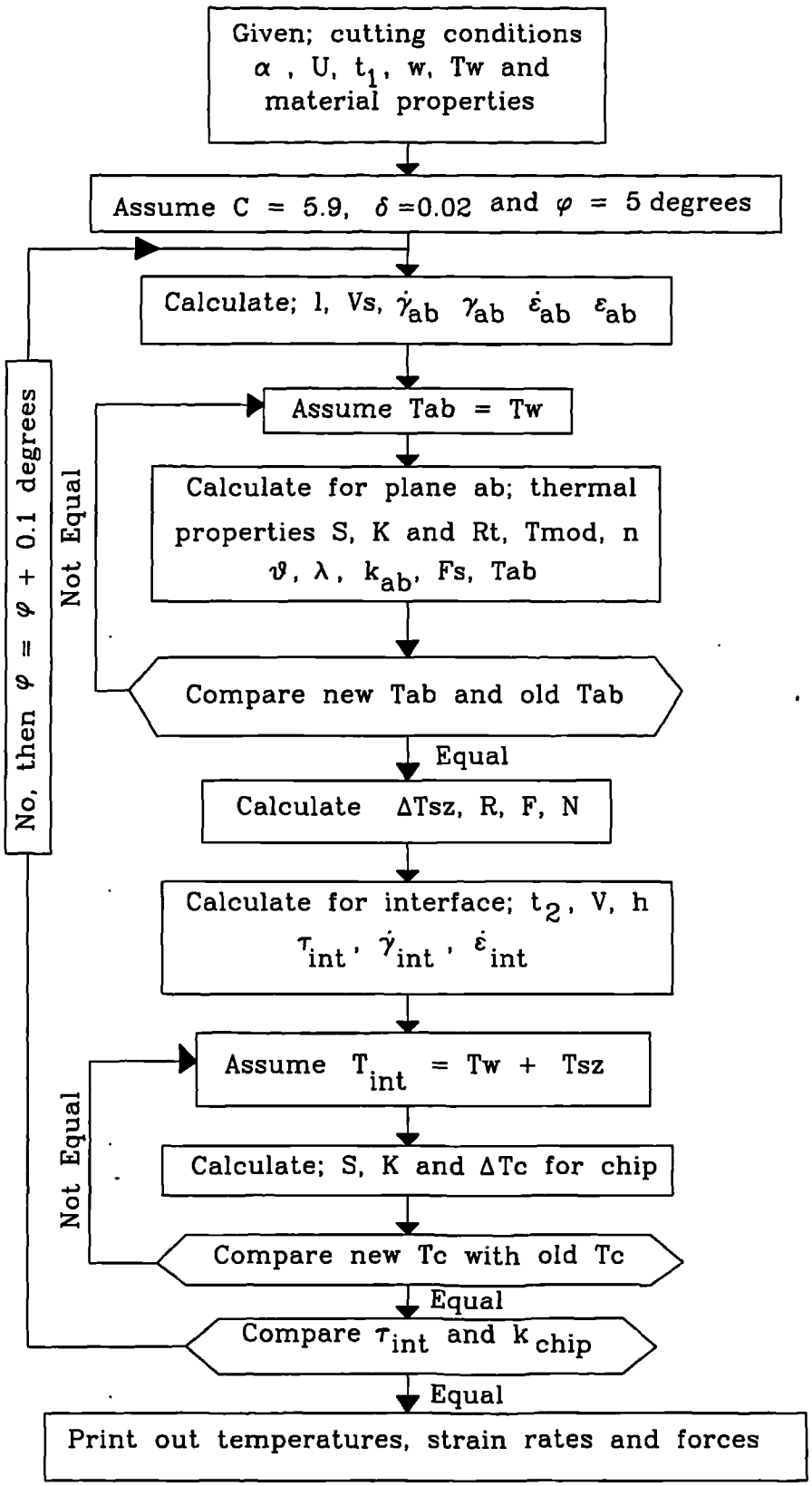

Figure 18: Model of Strain Rate after Oxley et al

arc, so the modified model only predicts the cutting parameters instaneously. In reality this does not matter too much if as in this work only relative magnitudes are required.

In applying the Oxley model to the milling process, and in particular to the materials and cutting conditions used in this work, two additional assumptions have been made.

(a) The material properties of En24 and En24T and En8 are the same. In particular the flow stress and strain hardening exponent, σ_1 and n, are assumed to vary with carbon content. The values for the appropriate carbon content have been extracted from the published work of Oxley et al [148] and are shown in Figure 17

(b) The specific geometry of the milling cutter used in this work approximates to semi-orthogonal milling, which is valid if the process is analysed on the plane defined by the cutting velocity and the chip velocity. This is a geometrical property of the tool that is independent of the angle of inclination of the tool. The effective rake angle can be calculated from the geometry and used in the machining model in place of the true rake angle.

These assumptions will affect the absolute values obtained for strain rate and other outputs of the model but the relative variation for changes in cutting conditions should be preserved as the variables in question are held constant in any one cutting test.

For comparison between tests on different materials it is necessary to examine the effect of the first assumption. The low temperature flow stress of En24T and En24 and En8 can be taken to be approximately 1000 N/mm^2, 800 N/mm^2 and 500 N/mm^2 respectively at low strain rates. No specific values could be found for strain hardening exponent even at low strain rates but Dieter [149] quotes values of 0.1 and 0.19 for a 0.6 %C steel which has been tempered respectively lightly and heavily. Such differences would be expected to disappear above about 650°C where any previous heat treatment would be removed by overtempering although the heating rate may raise this temperature somewhat. Tables 1 and 2 show the differences in chip temperature, strain rate, and cutting force when the material properties are changed in the following manner for rough face milling on En24T and En8 respectively. For the quenched and tempered En24 steel the flow stress will be approximately 20 % higher than for the annealed En24 (yield and UTS are that much higher) and the strain hardening index will be around 50 % of the annealed value. For the En8 material the flow stress will be approximately 50 % of the annealed En24, but the strain hardening index will be much higher, probably as much as 200 %. Since all of these materials have the same carbon content, the base values of En24 annealed were taken from Oxley in Figure 17.

As can be seen the only parameter to change significantly for the En24T is the total strain rate, with the other two parameters only varying by a small or negligible amount. Whereas for the En8 all values change substantially (Tables 1

	No Material Change	Material Change
Chip Temperature (C)	684	685
Total Strain Rate (s^{-1})	74250	138600
Cutting Force (N)	1437	1158

Table 1: Changes in Temperature, Strain Rate and Force when Material Properties are Taken into Consideration for En24T

	No Material Change	Material Change
Chip Temperature (C)	689	348
Total Strain Rate (s^{-1})	44500	79500
Cutting Force (N)	2400	500

Table 2: Changes in Temperature, Strain Rate and Force when Material Properties are Taken into Consideration for En8

and 2) of course these are the maximum expected changes since it is assumed that the room temperature differences are maintained. As noted before this error will not effect calculated values for any one material, but should be borne in mind when comparing for example strain rates during tests on the different materials.

As mentioned earlier, there are two main wear geometries which evolve on the insert; flank wear and crater wear. Sarwar and Thompson [21] suggest that, for the case of a blunt lathe tool, a 'dead metal area' appears in front of the cutting edge which partly fills in the region where the tool wears away. It would seem, therefore, that there is a mechanism for compensating for flank wear and that the main geometry changes during tool degradation which affect chip formation are associated with crater development rather than flank wear. Even if there is a change in chip flow caused by flank wear that is not compensated by a 'dead metal area' it is difficult to imagine how this would affect the chip formation characteristics.

However it is, relatively simple, to take crater wear into account in the above model as it constitutes a change in local rake angle. The effect can, in principle, be measured by profiling the crater and then changes in temperature, cutting force and the other metal removal parameters can be estimated using the model.

Table 3 lists some of the changes in calculated machining parameters as the local rake angle changes from -5° to 10°. It can be seen that, although the total strain rate (sum of interface and shear plane strain rates) decreases, the cutting force increases and the temperature increases both in the chip and at the tool-chip interface. In line with the drop in strain rate, the deformed chip thickness

	New	Worn
Rake Angle (rad)	-0.087	0.1671
Total Strain Rate (1/s)	92832	41384
Chip Temperature (C)	700	822
Cutting Force (N)	2058	2661
Interface Temperature (C)	2233	2387
Deformed Chip Thickness (mm)	0.815	1.34

Table 3: Changes in Metal Cutting Parameters for a Change in Local Rake Angle

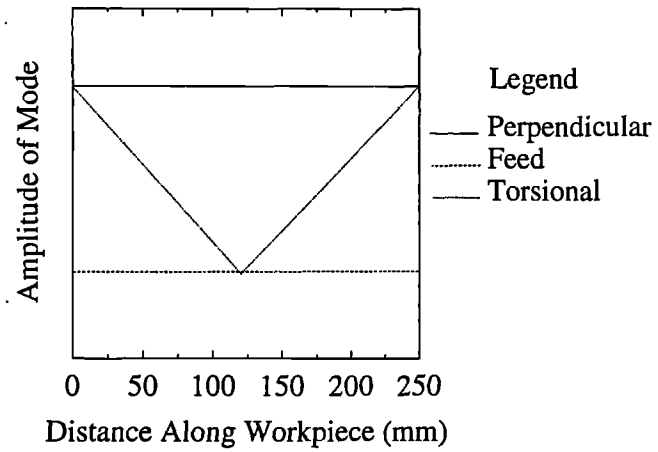

Figure 19: Variation in Mode Amplitude as the Tool Traverses the Workpiece

increases dramatically.

Any force measurement that is performed during metal cutting is made in the presence of large dynamic interaction between the workpiece and machine tool and this is particularly true of milling. A strain based force transducer will itself have dynamic properties and, as such, will affect the cutting process to some extent. Even if this were avoided by calibrating part of the machine tool for force measurements there would still be interaction between the headstock and the workpiece. The overall effect on force measurability will depend on the static and dynamic stiffnesses of the machine and transducer structures, and the frequencies of any resonances that occur. The transducer used in this work had three basic mode shapes; one feed, one transverse translational and one torsional mode and the relative dominance of these three basic mode shapes will change with cutter position in the workpiece. As the tool traverses the transducer, the excitation of different modes will occur in the manner shown in Figure 19, which illustrates schematically how mode amplitude might be expected to vary with distance along the workpiece. In the absence of coupling, the measured perpendicular and feed forces might be expected to remain constant throughout the cut.

Aside from the excitation caused by tooth impact, any non-uniform wear development on the tool, manifest as different wear land widths on the individual inserts, will generate a larger spread of frequencies thus exciting a greater number of resonances.

The balance of any force measurement will thus be made under the two competing phenomena of dynamic response and chip flow mechanics. It is quite probable that both will occur at the same time and it is obviously important to know which mechanism is the dominant one.

The effect of material will appear in the chip formation characteristics through the shear flow stress and strain hardening index and their variation with temperature. In addition, the material hardness and shear strength will affect the deflection of the force transducer which will, in effect, appear as a larger forcing function to the vibrational modes of the transducer. It would, therefore be expected that larger forces would be generated due both to increases in the force due to chip flow mechanics and also (artificially) due to larger levels of vibration.

The most obvious effect of insert breakage would be a reduction in cutting force at the instant of breakage. There would, of course, be a dynamic effect since the insert breakage will cause a recoil to be applied to the transducer. Similarly, there will be a reduced metal removal so that the force exerted by the following insert will increase. This latter effect may, indeed, be easier for the transducer to detect than the breakage event itself. Subsequent cutting force generated by the broken insert and the implications for the following one will depend upon the extent of edge damage vs feed per tooth and the detailed geometry of the damage.

3.4 Effect of Process on Acoustic Emission

There are three possible mechanical effects occurring during milling which might give rise to acoustic emission generation. These are the plastic deformation and fracture processes in the chip, the tribological effects at the tool wear sites (mostly flank and crater in this work) and the impacts as the insert hits the workpiece. In addition, there are secondary effects and noise due to components of the machine tool such as the spindle bearings and feed screw which might generate a background level of AE and a component related to cutting force.

It is widely argued that the AE generated during metal cutting is due to the dislocation motion in the material being machined and also to the fracture of hard inclusions in the deforming chip. The work of Gillis [63] and Rouby [81,82] points to the movement of dislocations as the probable generating mechanism for the AE signal. The precise mechanism is difficult to determine but, in the later work, Rouby expresses the view that the time of flight between obstacles is the important factor since there will be an impulsive displacement applied to the crystal lattice when a dislocation starts to move (or stops). This generation mechanism for the AE signal will be affected by several parameters in the

metal removal process. The strain rate and temperature will alter the number of dislocations and the mean distance that they can move. Higher strain rates will cause more dislocations to move, whereas higher temperatures will reduce the dislocation density through thermal recovery. In addition, the nature of the milling process is such that temperatures will be lower as the insert enters the workpiece, whereas the strain rate will be very large immediately. This would imply that the largest AE signal should occur as the insert enters the workpiece.

According to Oxley et al the shear strain rate in the shear zone can be expressed:

$$\dot{\gamma}_{AB} = \frac{CV_s}{l} \tag{15}$$

Where:

$\dot{\gamma}_{AB}$ is the strain rate on the shear plane

V_s is the shear velocity

l is the length of shear plane

and C is related to ϕ and θ by:

$$\tan\theta = 1 + 2(\frac{\pi}{4} - \phi) - Cn \tag{16}$$

Where n is the strain hardening index.

If the other cutting variables remain constant the shear strain rate is simply proportional to the shear plane angle. This means that as the rake angle changes, causing a reduction in the shear plane angle then the shear strain rate will also change. (This is a little simplistic as θ is dependent on geometry and temperature as well.)

For the tool-chip interface:

$$\dot{\gamma}_{int} = \frac{V}{\delta t_2} \tag{17}$$

Where:

$\dot{\gamma}_{int}$ is the tool-chip interface strain rate

V is the chip velocity

δ is the ratio of tool-chip interface plastic zone thickness to chip thickness

t_2 is the deformed chip thickness

As the shear plane angle and rake angle change with wear so V reduces and t_2 increases thus reducing the strain rate at the interface. In addition, there is a strong temperature dependence for all of these machining parameters.

The above changes in the strain rate and temperature would also be expected to cause changes in the power spectrum of the AE emitted from the cutting process. A reduction in strain rate and/or an increase in temperature will tend to increase the distance between dislocations and so it would be expected that a greater proportion of the AE signal will be concentrated at lower frequencies under such conditions. Thus, if cutting conditions, wear or material characteristics change so as to significantly affect the strain rate or temperature some changes in AE might be expected.

The most important effects of wear on the cutting mechanics have already been discussed briefly and it would appear that the formation of the crater is the most important from the point of view of chip formation. If this is the case, then it would be expected that wear will affect the strain component of the AE signal mainly through changes in the cutting geometry due to crater development. As the crater develops, it will affect the strain rate and temperature which will in turn increase the rate of crater development. The Oxley model allows an estimation of both of strain rate and temperature and Table 3 shows calculated values of strain rate and temperature as the local rake angle increases. Although the interface temperature calculation must be erroneous probably due to assumptions regarding thermal diffusivity it is probable that the temperature is well over 1000 °C. Both of these calculated parameters will affect the movement and number of dislocations which will affect the AE signal due to plastic deformation.

As discussed above the different steels used in this work will have different flow stress and strain hardening indices, especially at lower temperatures. The effect of this on strain rate and chip temperature has already been discussed and is summarised in Tables 1 and 2. The mean free path (for dislocation motion) will also be different for the steels used in this work since, besides dislocation density, it will also be dependent on the grain size and the size and distribution of carbides. The dominant effect on dislocation mean free path in the zones of high plastic deformation will probably be the dislocation density although this, itself, will be determined by the microstructural obstacle density. In the En8 material, the ferrite grain size was between 0.05 and 0.4 mm with a pearlite interlamellar spacing of about 0.25μm. A typical martensitic grain size will be around 1μm and the mean free distance between temper carbides will probably be somewhat less than this, reducing with the degree of temper. AE bursts associated with carbide fracture events might be expected to have an intensity related to carbide size (decreasing in order En8>En24>En24T) and be separated by a time associated with that for sufficient dislocations to cross the mean free

	Ferrite/Pearlite	Martensitic
Crossing Grain	4-32 kHz	1600 MHz
Between Carbides	6400 MHz	1600-32000 MHz

Table 4: Probable Frequencies Corresponding to One Dislocation Crossing a Microstructural Feature

distance to cause fracture of the particle. Dislocation velocities will vary with strain rate but are normally expected to saturate at the shear wave velocity (Dieter [149]) which, for steel, is about 3200 ms^{-1}. Table 4 shows frequencies corresponding to dislocation crossing of the principal microstructural features and it should be noted that the distribution of carbides in the ferrite/pearlite structure is heterogeneous whereas that in martensite is homogeneous.

The large frequency values corresponding to the motion of dislocations between obstacles demonstrates that the Rouby model of AE generation of the deceleration of dislocations at obstacles is a little simplistic. It is more likely that large numbers of dislocations building up at the carbide interfaces and causing internal fracture will generate significant events. Supposing the carbides to be of equal strength, the number of dislocations required will be approximately proportional to carbide cross-sectional area, A, which will decrease in the order indicated above. Dividing each of the frequencies in Table 4 by n.A (where n is the number of dislocations required to fracture a carbide of unit cross-sectional area) gives fracture frequencies which will be smaller than those indicated in Table 4 but with an order of increasing frequency En8>En24>En24T.

In order to understand what effect the wear process will have on the AE signal it is important to have an in-depth understanding of the cutting and wear processes. At the present time these phenomena are not completely understood but a considerable body of empirical and qualitative knowledge has built up over the last few decades on the wear mechanisms that are occurring on the tool. These can be classified as abrasion, adhesion, diffusion, attrition and fracture, the relative roles being determined mainly by the temperatures at the cutting tool-work interfaces.

The tool material used in this work was an un-coated tungsten carbide/titanium carbide/(tantalum, niobium) carbide mixture with a cobalt binder. The precise make-up is shown in Table 3.4. The concensus of current thinking on wear of such materials is that higher temperatures lead to diffusion becoming the dominant wear mechanism. With the migration of carbon from the WC and cobalt into the chip which weakens the tool structure and allows attrition of the other carbide particles. Trent [3] notes that, at high cutting speeds (such as those used in this work), the crater develops at a very rapid rate.

Type	Chemical Composition %				Grain	Strength	Hardness
	WC	TiC	(Ta,Nb)C	Co	Size μm	N/mm^2	HV
S25M	69.5	6.5	14.5	9.5	1-2	2000	1480

Table 5: Chemical and Mechanical Information for Carbide Inserts

Cook [4] has discussed the mechanisms of crater wear for this type of tool material and has found that the wear rate is quite strongly temperature dependent. This can be seen from Figure 20 reproduced from material published by Cook, who constructed an Arrhenius plot and showed that there was a sharp change in activation energy at around $730°C$ so that a fundamental change of mechanism might be expected here although the point is made that this may simply be a change in diffusion coefficient between the phases of iron. Cook notes that, when cutting with WC-TiC-TaC-Co tools, the crater wear particles have essentially the original carbide grain size of around 1 μm suggesting that they have not been abraded. He also notes that cobalt readily diffuses from the carbide tools and concludes that the wear rate is not limited by any mechanism involving cobalt. He believes that the wear mechanism is controlled by dissolution of the WC grains by the chip material, with the cobalt diffusing away at a greater rate from the interfacial layer. As the WC dissolves, the undissolved complex carbides stand proud and are mechanically removed from the weakened structure. He concludes that the rate of WC dissolution is probably controlled by diffusion out of the WC into the chip when temperatures are greater than about 730° C, i.e. above the iron-carbon eutectoid. Below the eutectoid, the rate of absorption is not as strongly thermally activated and wear is therefore likely to be mechanically dominated.

It would be expected that a similar wear mechanism will occur on the flank face as similar temperatures occur here with the same dependence of the wear rate on temperature occurring.

If significant AE were generated by the insert hitting the workpiece it would be expected that the largest level of AE would occur as the insert enters the workpiece with the AE signal decaying as the insert progresses through the workpiece. Figure 21 shows measured perpendicular force and the 0.5 ms rms AE as a four point tool rotates. It can be seen that the greatest level of AE occurs a short time period after the insert enters the workpiece but, for one insert engagement, there is little or no AE generated. This time delay is partly due to the rms processing unit, because the slew rate of the instrument is governed by the averaging time constant. If the generation of AE was simply related to insert engagement then the AE signal would be expected to be reflected in the force signal and would furthermore be expected to be sensitive to resonances. Neither of these effects have been observed and it can be concluded that the high level of AE generated as the tool enters the workpiece is a transient effect due to the fact that the chip

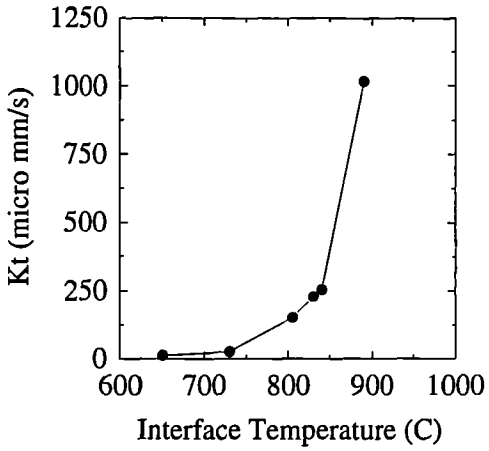

Figure 20: Crater Wear Rate vs Temperature for a WC-TiC-TaC-Co Tool, after Cook

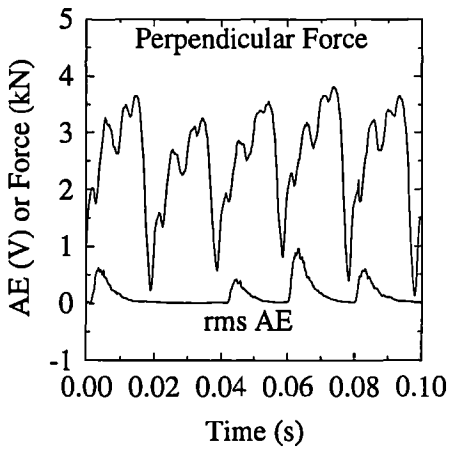

Figure 21: Perpendicular Force and rms AE as a Four Point Tool Rotates

and tool temperatures have not yet risen to the steady state level.

In summary, it is very difficult to imagine dissolution of carbon or cobalt from the tool into the workpiece as generating much AE, but it would be expected that the mechanical removal of carbides from the tool material might give rise to AE. The effect of chip deformation is likely to be rather complex with possible contributions from strainrate via dislocation movement but also via fracture of workpiece carbides. Both effects might be expected to show a frequency dependence and an intensity which depends primarily on strain rate, temperature and material type. Any effects of tool wear will, in fact, be secondary and would manifest itself through changes in strain rate or temperature. It seems unlikely that the impact of the tool on the workpiece is an important generator of AE during milling.

AE is potentially a very useful sensor for short-timescale event detection since it can be acquired with high temporal resolution and is, in principle, immune

from any resonance (electomagnetic or mechanical) which may be present. The effect of a tool breakage on the AE signal should appear above the general level of the cutting AE as it has been found that complete breakage of the insert or fracture of the insert generate large amounts of AE, Lan and Dornfeld [112]. The effect of incorrectly selected cutting conditions on the AE signal appears to be dependent on the strain rate, temperature and other factors such as changes in the way hard carbides are removed from the insert. As such it is expected that it would be possible to detect such an event but that the effect would vary with cutting conditions, amount of tool wear and other factors already identified. Hard patches in the workpiece, due perhaps to foreign objects, should be easier to detect as they will produce changes in the AE signal from a normal (for that material under those cutting conditions) level.

3.5 Artificial Intelligence

Two different AI methods have been used in this work, namely:

(a) Expert Systems

(b) Artificial Neural Networks

both have different capabilities and properties and their application to this work is outlined below.

3.5.1 Expert Systems

This work has used only a small part of the inference capabilities available in an Expert System simply to demonstrate the relative performance of such a system against a Artificial Neural Network. To be precise, linear regression lines were fitted to the sensorial data from a wear test for the spindle current, feed force, and acoustic emission sensors. These were then used to predict the wear level by combining the predicted wear value from all sensors, suitably weighted to give a greater precedence to the regressions with a higher correlation coefficient.

A wider set of data from this work was also input into a more general ES shell but that work will not be presented here. Even the limited ES simulation allows for combination of sensors to obtain one wear value but it does have limitations and uses very little of the Expert Systems capabilities. The real power of an ES lies in its inference capabilities when presented with empirical knowledge of a variety of different types and formats.

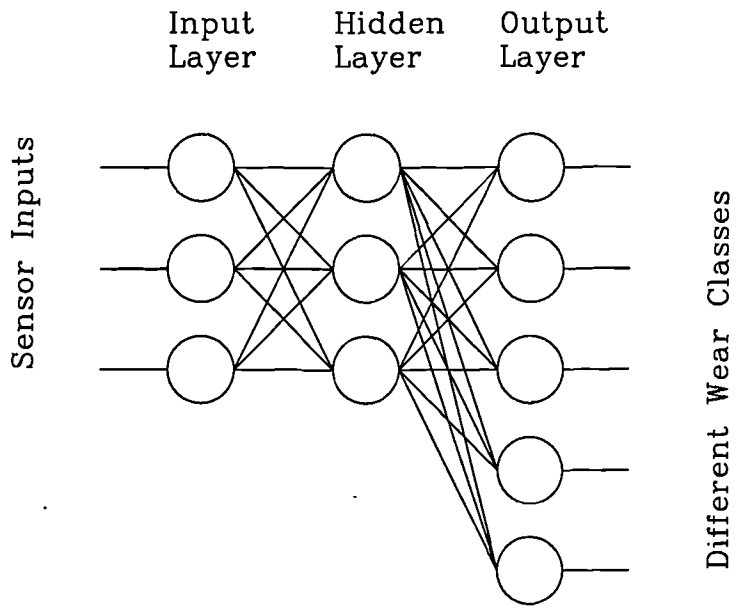

Figure 22: General Wear Detecting Artificial Neural Network

3.5.2 Artificial Neural Networks

The network used in this work is of the simple feed-forward type, trained by a backpropagation algorithm that ensures that all of the network is involved in storing the knowledge pertaining to the flank wear level. The wear levels can be quantified by creating a number of different classes which are represented by different output neurons as shown in Figure 22. The likelihood of breakage can be represented by one neuron in a separate network as shown in Figure 23. If a number of different breakage events can be identified, their likelihoods can be introduced by having an output neuron for each breakage event. The computer code for a general ANN is given in Appendix D.

The reason for this choice of network is relatively simple. The 'feed-forward' type of network has been shown to perform well in other situations and is relatively well developed. The training algorithm, 'back-propagation' has been developed for this type of network and has similarly been proven. For example, Rangwala and Dornfeld [5] successfully used a similar network to classify new and worn tools in turning operations.

The network functions by the combined effects of individual neurons which compute a weighted sum of their inputs to give an excitation (ϵ). This is then used in a 'sigmoid' function (the excitation function) of form:

$$f(\epsilon) = \frac{1}{1 + e^{-\epsilon}} \tag{18}$$

This type of function makes the neuron more 'decisive' as the state of the neuron

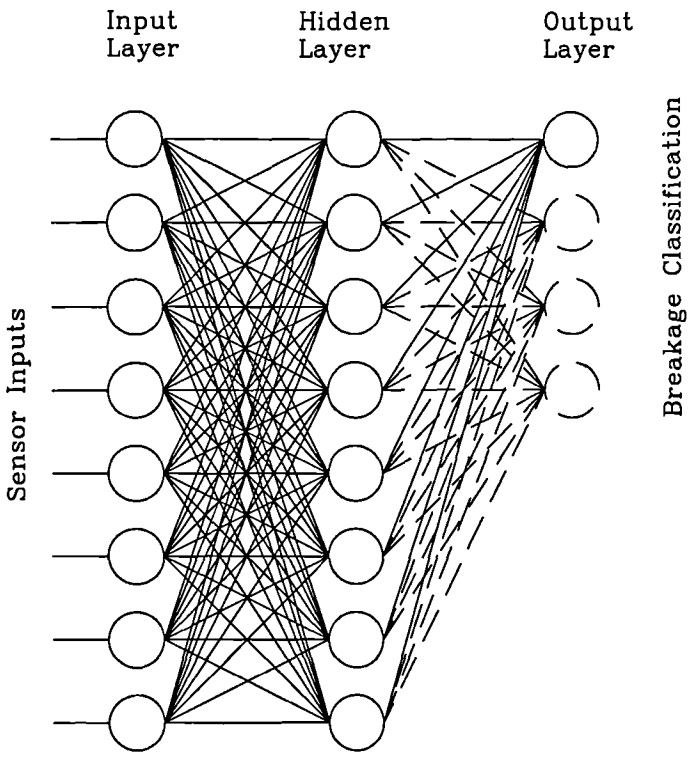

Figure 23: General Breakage Detecting Artificial Neural Network.

will switch from inactivity to activity very quickly around the central point of the function.

For each neuron the training rule is to:

(a) Present the network with the input. The neuron output is given by calculating:

$$o(i) = \Sigma w(j).i(j) \tag{19}$$

Where:

$o(i)$ is the output of the ith neuron

$w(j)$ is the weight of the jth input to the ith neuron

$i(j)$ is the input to the ith neuron on the jth input line

(b) For each neuron, compute the error given by:

$$\Delta(i) = [o(i) - do(i)].f'(\epsilon) \tag{20}$$

Where:

$\Delta(i)$ is the error of the ith neuron

$o(i)$ is the actual output of the ith neuron

$do(i)$ is the desired output of the ith neuron

$f'(\epsilon)$ is the derivative of the excitation function

(c) Adjust weight $w(i)$ by an amount given by $k.\Delta(i).i(j)$, where k is a constant that determines the rate of learning.

This training algorithm works for single layered networks but a bit more work is required for a multi-layer network as this method does not allow the hidden layers to be trained. If these layers are ignored in the training algorithm then they will not assist in the decision making process and are therefore redundant.

Hidden layers can be utilised by computing the error for each neuron in the output layer, $\Delta(i)$, and associating with each hidden unit in the layer below a proportion of the error of each output neuron to which it is connected. This proportion should obviously be the strength of the connection between the hidden neuron and the output neuron. This means that the hidden neuron's error will be a weighted sum of all the errors of all the output neurons to which it is connected, weighted again by the derivative of the excitation function. This approach is then propagated back through the network, a layer at a time, until the input layer is reached.

For wear estimation, an input can be used for each of the sensors and a number of different neurons can be used to represent different wear levels as seen in Figure 22. It is then possible to train the network to recognise progressive wear by the state of its inputs (the sensor outputs) from repeatedly presenting random selections from the sensors and telling the network the wear state to which each selection corresponds. If the training set is representive of, for example, a wear test, then the network can be presented with new data from a similar test and asked to make a prediction as to which wear state the data comes from. The output of each neuron will then be representative of the probability of the wear state being in that region. Obviously, the higher the probability the more certain the network is that the wear corresponds to this value. If the network cannot decide on the wear level then this will manifest itself as similar lower probabilities over several or all output neurons.

A rather different stategy can be adopted for breakage detection using the network scheme illustrated in Figure 23. If the inputs contain a value representative of each tooth pass and a series of consecutive tooth characteristics are input, then any abnormality in these characteristics which may be indicative of short-timescale events should be detectable as a disruption to the input pattern. Such a disruption could be characterised using a single output or the type of disruption could be identified by using a pattern of different ouputs.

Chapter 4

Experimental Apparatus and Procedure

This Chapter describes the apparatus and procedure used for the experiments that have been conducted as a part of this work. All the experiments were carried out using largely the same apparatus with a few modifications in each case and this is described in the first part of this Chapter. Next, the errors associated with each of the sensors are discussed and finally the experimental procedure is described in detail for each of the experiments; preliminary tests, systematic wear tests and other complementary tests.

Five sets of tests were carried out and these are summarised below:

(a) *Influence of Machine Stiffness on Sensorial Information*
An investigation, using a variable stiffness platform, of the effect of the machine stiffness on AE, workpiece vibration and cutting force, whilst machining on mild steel with a six point face milling cutter.

(b) *Influence of Insert Geometry on Sensorial Information*
An investigation of specific wear geometries and their effect on sensorial data. Artificial means were used to simulate progressive degradation including flank and crater wear and instantaneous degradation, particularly edge breakdown.

(c) *Progressive Degradation Studies*
An investigation of progressive wear using three tools, two face milling and one grooving, on three different steels.

(d) *Instantaneous Degradation*
An investigation of insert breakage under a variety of different circumstances, including a pre-cracked insert, hard patches in a workpiece, edge chipping, and operator/program error.

(e) *Influence of Cutting Conditions on Sensorial Information*
An investigation of the influence of cutting speed, feed rate and depth of

cut on AE, spindle current and cutting force whilst machining En24 with an eight point face milling cutter.

4.1 Apparatus

This section describes the apparatus used for all of the experiments highlighting, where necessary, any differences between tests.

4.1.1 Wadkin V5 Milling Machine

The Wadkin V5, three axis computer numerical control (CNC) milling machine formed the basis of all the experiments. The milling machine was instrumented with a set usually consisting of ten transducers and these were used to monitor the cutting operation throughout the preliminary tests, systematic wear experiments and other complementary tests. A photograph of this machine can be seen in Figure 24.

The machine has two tables, each of dimension 1150 mm x 600 mm, which can move horizontally and a spindle which is mounted on a headstock capable of being moved in the vertical direction.

The spindle is rotated by a d.c. motor with a maximum power rating of 18 kW, the power versus spindle speed curve for this motor being shown in Figure 25. It will be noticed that the actual power the motor is capable of delivering is dependent on the rotational speed of the spindle and that at a rotational speed of 900 RPM the power no longer increases with rotational speed.

4.1.2 Force Transducer

This sensor, a detailed description of which can be found in Appendix A, consisted of two rigid plates separated by four strain gauged pillars and was built specifically for this work. The sensing elements were so instrumented that the three mutually orthogonal cutting force components could be processed by the ancillary electronics (details also given in Appendix A).

During experimentation, the force transducer formed an artificial table for the machining operation raising the bed a total of 130 mm above the normal cutting level. A drawing of the force transducer can be seen in Figure 26.

Figure 24: Wadkin V5 Computer Numerical Control Milling Machine

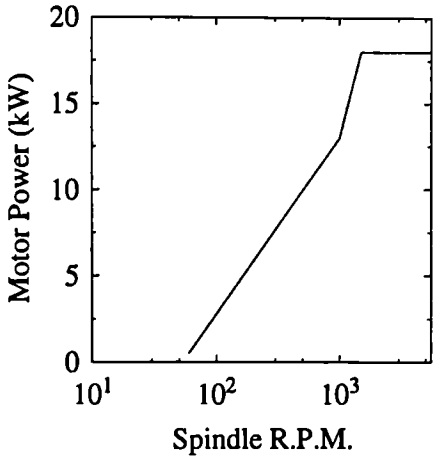

Figure 25: Wadkin V5 CNC Milling Machine Torque Curve

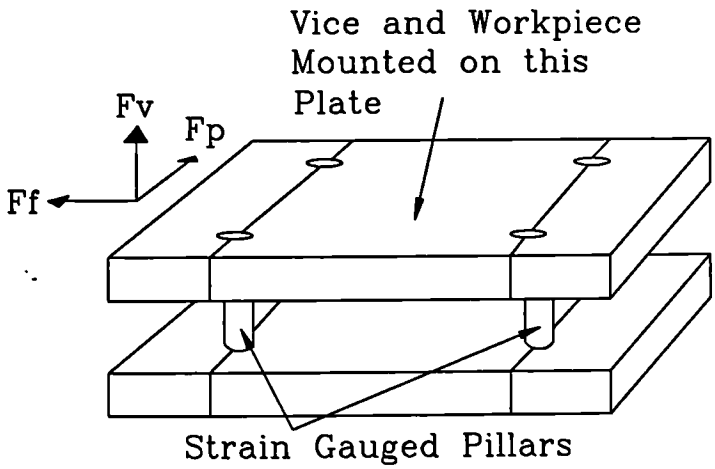

Figure 26: Drawing of Force Transducer

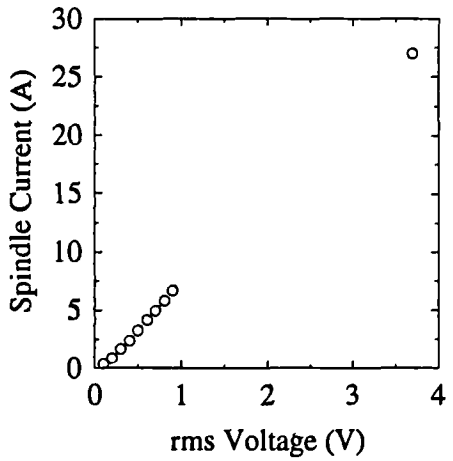

Figure 27: Calibration of the Spindle Current Meter

4.1.3 Spindle Current

The current sensing element provided in the machine consisted of an inductance coil on one armature of the three phase windings. The voltage detected by this sensor was measured by a digital rms volt meter (DVM), as installed on the machine. This meter, which was calibrated in amps, indicated the value of the current from the input voltage. For the purposes of this work, the voltage on which the DVM operated was isolated and then passed through a true rms converter and digitised using a computer based data acquisition system, details of which are described later in this section. Clearly, it is necessary to calibrate this rms voltage against actual spindle current and this was done by rotating the spindle off load and comparing the measured voltage with the current read from the machine meter.

Due to the difficulty in generating currents in the conductors supplying the motor that are of the order of that generated during cutting, it has only been possible to find a calibration constant for the very low end of the current range of the motor. It was also possible to make one calibration observation during cutting and it is clear from Figure 27 that this confirms the low current calibration curve.

4.1.4 Shaft Encoder

This sensor was constructed after the preliminary set of calibration experiments when it was found that it would be of considerable interest to monitor the cutting operations on a 'per insert' basis. This sensor made it possible to examine any variability in the sensorial data as different inserts performed the cutting operation and a detailed description can be found in Appendix B.

Briefly, the shaft encoder consisted of a reflective plate attached to the tool holder which was probed by a small fibre optic sensing element mounted on the headstock near to the rotating tool holder. Laser light was launched into one end of the

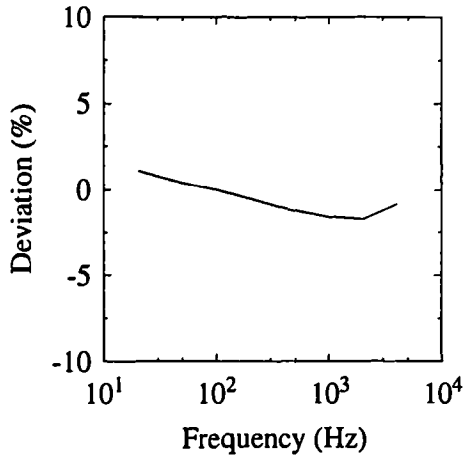

Figure 28: Calibration of Perpendicular Component Accelerometer

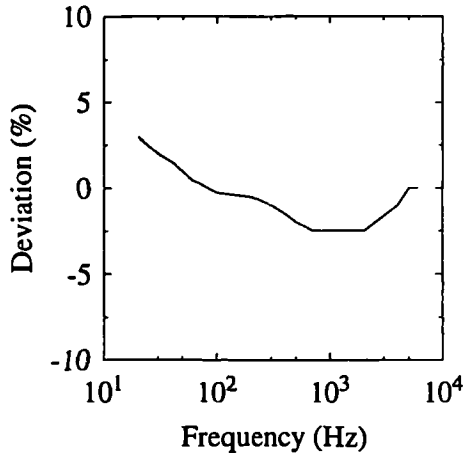

Figure 29: Calibration of Feed Component Accelerometer

fibre and the reflected beam was returned through the same fibre. On exit, the path was turned through ninety degrees using a beam splitter and converted into a voltage by a photodiode. Further detail is available in Appendix B.

4.1.5 Accelerometers

Endevco accelerometers were used to monitor the vibration of the top plate of the force transducer as an indication of the workpiece vibration. The calibration graphs for these two sensors can be seen in Figures 28 and 29. These curves were taken from the factory calibration and show deviation from a linear response over the frequency range of interest.

The charge amplifier used was manufactured by Birchal, and was the CA/04/FH model.

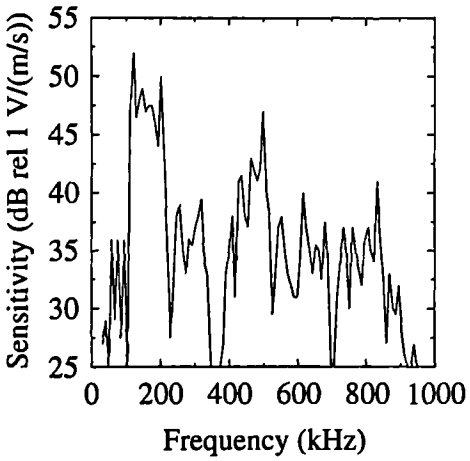

Figure 30: Calibration of the D9201A Acoustic Emission Sensor

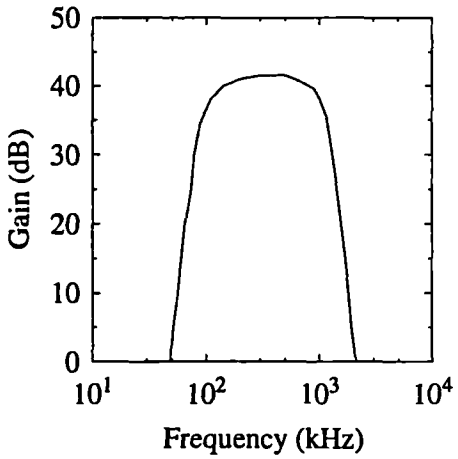

Figure 31: Calibration of the 1801 Acoustic Emission Amplifier and Bandpass Filter

4.1.6 Acoustic Emission

The AE sensor used throughout the experimentation was a Dunegan Endevco D9201A. This is a PZT based sensor with a relatively flat frequency response (for a commercial PZT sensor) and adequate sensitivity for the metal cutting operation. The calibration graph for this sensor can be seen in Figure 30.

The output of the sensor was amplified by 40 dB using an Endevco 1801 AE amplifier, fitted with a Butterworth bandpass filter. The frequency response of this amplifier and filter can be seen in Figure 31.

The output of the amplifier was recorded in two ways. The first of these was an analogue recording by a modified U-matic Video Cassette Recorder (VCR) a description of whose modifications can be seen in Appendix C. This provided a permanent record of 'raw AE' for future playback should it prove necessary to analyse the AE data with high temporal resolution.

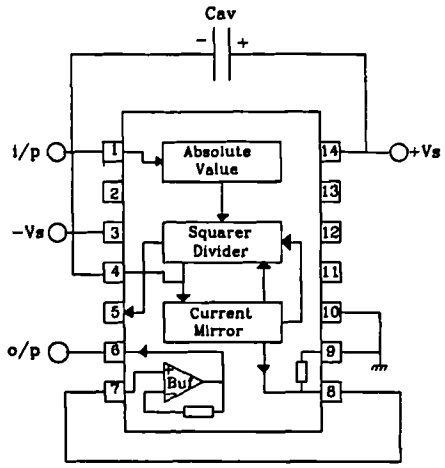

Figure 32: Manufacturer's Internal Layout of the rms Processing Chip

The second approach to AE recording was to process the analogue signal by an rms circuit, described in the following section with averaging constants of 0.5 ms and 250 ms. The 250 ms constant was chosen because the literature had shown a relationship between AE and tool wear using just such processing and the 0.5 ms averaging constant was chosen because it was felt that it would be of interest to examine the rms AE signal for variations, on a 'per insert' basis, with wear. (Although in the signal processing performed on the systematic wear test data the longer averaging time was simulated from the 0.5 ms averaging constant.)

4.1.7 RMS Processing

A unit was used that could process the rms of four channels simultaneously with a maximum bandwidth of 1 MHz. These channels were arranged so that one had an averaging constant of 0.5 ms, two had averaging constants of 250 ms and one had a time constant which could be varied between 2.5 μs and 250 ms. This allowed two channels of AE and one of spindle current to be processed leaving the fourth (variable time constant) as a spare. Figure 32 shows the manufacturer's layout of the internal workings of the hybrid chip and Figure 33 displays the circuit diagram of the four channel rms processing unit.

The hybrid chip chosen does have some limitations since only voltage levels greater than 1 V will have an rms calculation based on the full bandwidth of the circuit, (1 MHz). This is due to the automatic gain control of the system which increases the gain for small signal levels, typically less than 100 mV. In practice this was not found to be a problem as during metal cutting the signal usually only dropped below 100 mV in periods when there was no cutting being performed. This means that the circuit effectively only limits the bandwidth of the noise signal. The frequency response of the circuit is shown in Figure 34.

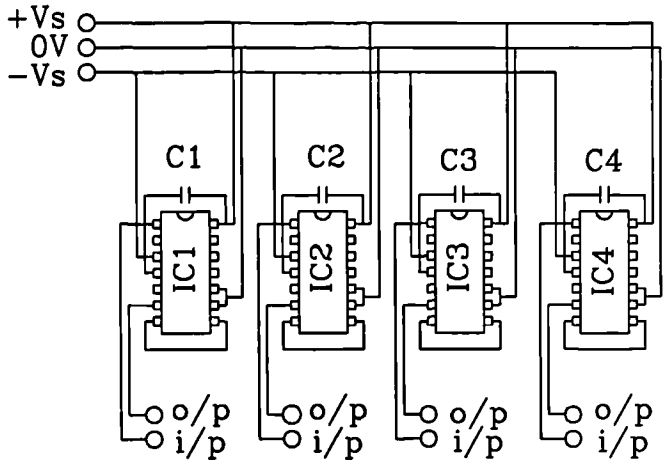

Figure 33: Circuit Diagram of the rms Processing Unit

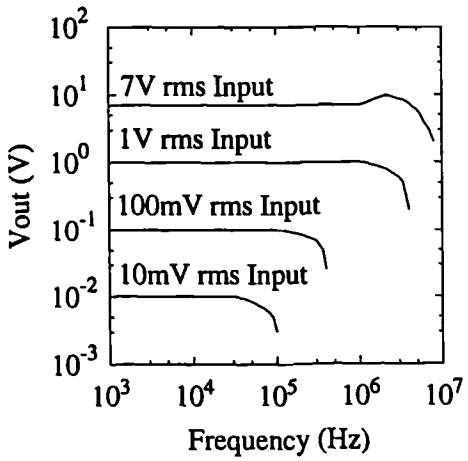

Figure 34: Frequency Response of the rms Processing Unit

Resolution	0.1 μm
Stylus	0.1 μm diameter diamond
Travel Length	12 mm

Table 6: Salient Features of Surface Finish Probe

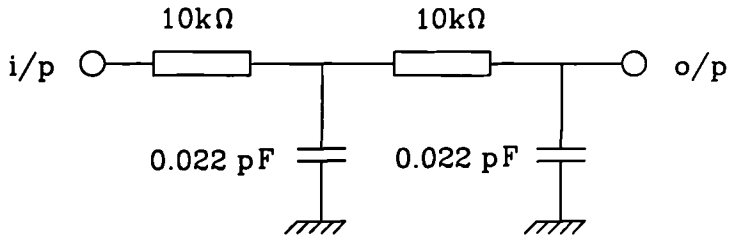

Figure 35: Circuit Diagram of the Anti-Aliasing Unit

4.1.8 Surface Finish Measurement

As it is normal, particularly in finishing operations, for the machinist to be more concerned with the surface finish than the tool wear level, surface finish was recorded by using a portable instrument that gave a direct reading of the R_a value. Table 6 shows the salient features of this instrument.

4.1.9 Anti-aliasing Filters

All channels of data were fed through a set of anti-aliasing filters, constructed from resistor-capacitor networks. A circuit diagram is shown in Figure 35 with the corresponding filter response characteristics being shown in Figures 36 and 37.

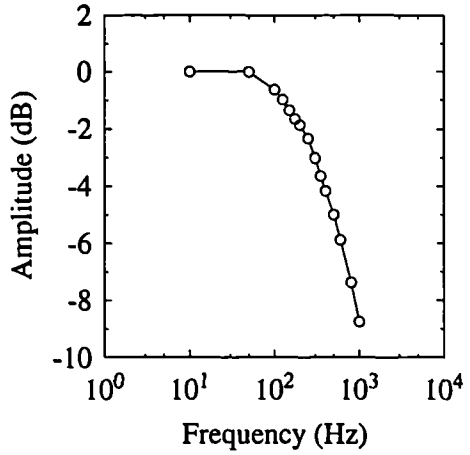

Figure 36: Frequency Response of the Anti-Aliasing Filter Unit

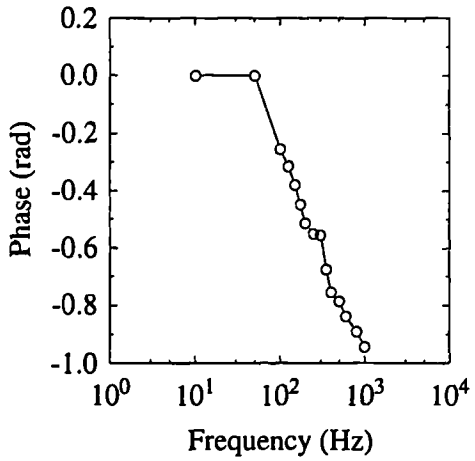

Figure 37: Phase Response of the Anti-Aliasing Filter Unit

4.1.10 Data Acquisition System

Experimental data was acquired by a wide range of different means of varying bandwidth and sophistication. These are described in turn below:

Tool Imaging System

During the systematic wear tests, it was necessary to measure the flank wear on each of the inserts in the tool holder. This was done off-process at intervals of approximately two minutes of cutting time.

Inserts were imaged using a charge coupled device (CCD) camera fitted with a standard lens which was mounted with a stand-off of 5 mm using an extension tube. This magnified the image by a factor of ten at the screen, and led to a practical resolution for measurement of flank wear of 0.01 mm.

Images of worn inserts were displayed on screen for in situ measurement as well as being recorded onto the U-matic VCR for later play-back. A diagram of the general set-up is shown in Figure 38.

Data Acquisition Boards for Digital Computers

Three different types of data acquisition board were used in this work. A brief description of each of these is listed below:

(a) *CompuScope 220*
The operating performance of this data acquisition board is shown in Table 7. This board was used for the digitisation of all full bandwidth AE signals and also in one of the calibration experiments which was conducted before the full experimental set-up was commissioned.

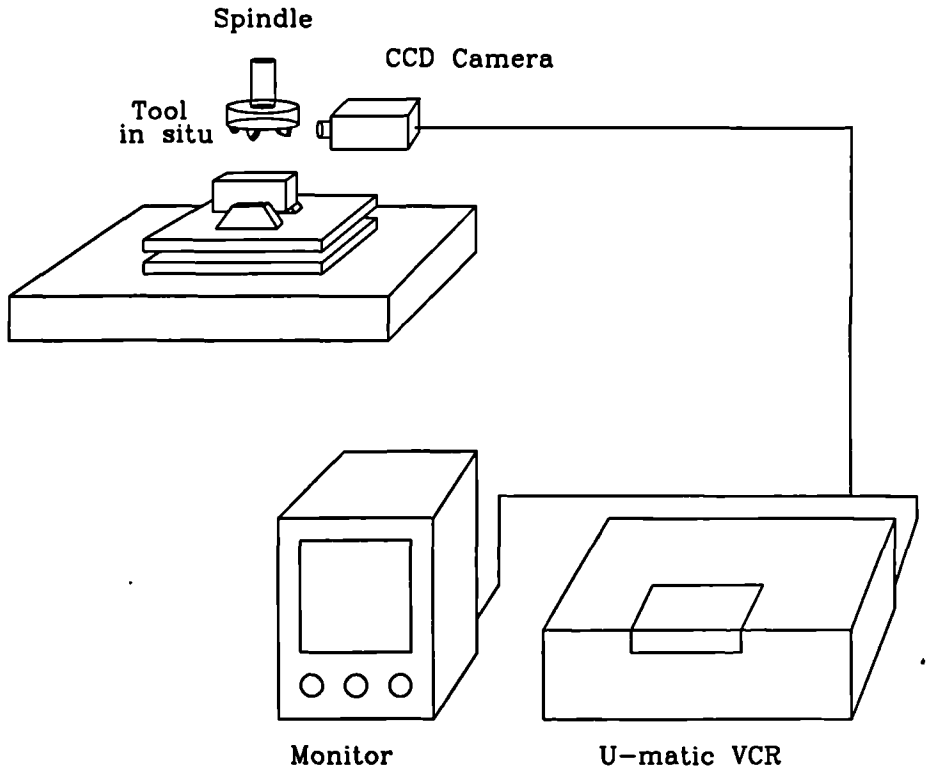

Figure 38: General Set-up of the CCD Camera Tool Imaging System

Maximum Sample Rate	40 MHz
Input Signals	± 10 V maximum
Number of Channels	2 Single Ended
Onboard Memory	256 kBytes

Table 7: Specification of the GAGE CompuScope 220

Maximum Sample Rate	100 kHz
Input Signals	± 10 V maximum
Number of Channels	16 S.E. or 8 D.E.
Onboard Memory	2 kBytes

Table 8: Specification of the AT-MIO-16L

The board operates by cyclically filling a 256 kByte on-board buffer on a continuous basis. When the board receives a trigger signal to capture data it stops this process and stores data in the manner requested by the user in an internal buffer. At this stage it is possible to download the buffer to hard storage in the personal computer in which the board is located. This takes around 15 s depending mainly on the time taken to give data buffers different file names for storage on the magnetic medium. The data is thus saved in a batch manner after the event has passed and the batch size is limited to 256 kBytes for both channels.

(b) *National Instruments AT-MIO-16L*
Table 8 shows the data pertaining to the operating performance of the National Instruments AT-MIO-16L board. For the systematic wear tests two such boards were used simultaneously at different sample rates of 1.4 kHz and 140 Hz. This allowed the signals of low bandwidth, such as spindle current and the 250 ms rms averaged AE signal to be acquired at a lower rate. Synchronisation was maintained by an inter-board bus that allowed one board to set the clock rate for the other. Typically, the 10 MHz clock on the card with the sample rate of 1.4 kHz was used to drive the clock for the other board. This then allowed the board operating at 140 Hz to count a set number of pulses (in this case ten) sent from the 1.4 kHz card before obtaining data.

The AT-MIO-16L board also fills its internal buffer in a cyclical manner but it is also possible for it to transfer the contents of these buffers continuously to the memory of the host personal computer (PC).

From the PC memory, it is possible to write the data directly to disk storage using a double buffering technique where, as one memory buffer is filled with data coming from the boards, the other buffer is being cleared and the data it contained is being written to hard disk storage. This obviously limits the data sampling rate over all channels to the bandwidth that it is possible to transmit through the disk controller and to the hard disk. In the current set-up it was found, through trial and error, that the maximum bandwidth that could be transmitted without error corresponded to 40 kHz and this was regarded as being adequate for the ten channels of data when anti-aliasing filters were used.

Maximum Sample Rate	235 kHz
Input Signals	± 10 V maximum
Number of Channels	16 S.E. or 8 D.E.
Onboard Processor	80C186 with 512 kBytes of memory
Digital Signal Processor	Motorola 560000 with 96 kBytes of memory

Table 9: Specification of the DAP 2400/6

(c) *DAP 2400/6 Data Acquisition and Signal Processing Board*
To be of commercial use, the overall monitoring system requires the capability to acquire data and to perform signal processing in order that other software can make on-line calculations of tool wear and make decisions.

In order to perform the data acquisition and signal processing in real time with the system using AT-MIO-16L boards, it would have been necessary to use several computers in a primitive parallel set-up, one to perform data acquisition, one to perform signal processing, another to perform the simulation of the neural network and perhaps another to run the expert system, depending upon the exact monitoring/control strategy. A more practical solution to this problem is to use a data acquisition board which has on-board processing capabilities. The DAP 2400/6 is such a board and its operating specification is shown in Table 9

The board acquires data in a similar manner to the AT-MIO-16L boards but communicates with the PC via a device driver. This device driver allows instructions pertaining to acquisition and signal processing to be downloaded prior to acquisition. Then, after acquisition and processing, the data is sent via a pipe to the device driver where it can be read by the PC. This allows the PC to interact with the user, run other processor intensive programs and save data whilst new data is being acquired and processed.

Personal Computer

The personal computer used during data acquisition and signal post processing was a 20 MHz 80386 DX AT compatible machine, fitted with a small computer systems interface (SCSI) disk controller, 240 MByte hard disk, 150 MByte tape streamer, 8 MByte of random access memory, VGA display device and 20 MHz 80387 numeric co-processor. The two AT-MIO-16L boards and the DAP 2400/6 board were fitted to this machine (at different times).

The CompuScope Board was fitted into a 12 MHz 80286 AT compatible machine, fitted with a 40 MByte hard disk and 640 Kbytes of memory and a 80287 numeric

Concentration %							
C	Si	Mn	P	S	Cr	Mo	Ni
0.50	0.26	0.69	0.02	0.03	0.02	0.01	0.01
Grain Size 0.05 to 0.4 mm diameter Hardness 170 HB							

Table 10: Metallurgical Analysis of the En8 Workpiece Material

Concentration %							
C	Si	Mn	P	S	Cr	Mo	Ni
0.41	0.20	0.52	0.01	0.04	1.08	0.25	1.37
Hardness 330 HB							

Table 11: Metallurgical Analysis of the En24T Workpiece Material

co-processor, although, in principle, it could equally have been fitted into the 80386 AT compatible machine.

4.1.11 Overall Data Handling and Measurement

A schematic of the entire sensor, amplifier, filter and acquisition system is shown in Figure 39. The accelerometers, the force transducer and the acoustic emission sensor were used in all experiments as were the rms processing unit, charge amplifiers, strain gauge amplifiers and AE amplifier. The anti-aliasing filters, spindle current sensor and shaft encoder were added for wear experiments on En24 and En24T.

4.1.12 Workpiece Materials Used

For the majority of experiments, two materials have been used as workpieces. These are both steels, En8 and En24, and were chosen to allow an investigation of the full range of machinable carbon-manganese and low alloy steel properties. The En24 was used in two different heat treatments; quenched and tempered, hereinafter referred to as En24T and fully softened by annealing. The En8 is not normally considered to be a heat treatable steel and was only investigated in the fully annealed condition. Table 10 shows a metallurgical analysis of the En8 material and the corresponding metallographic structure is shown in Figure 40. Tables 11 and 12 and Figures 41 and 42 display the corresponding information for the En24 and En24T workpiece materials.

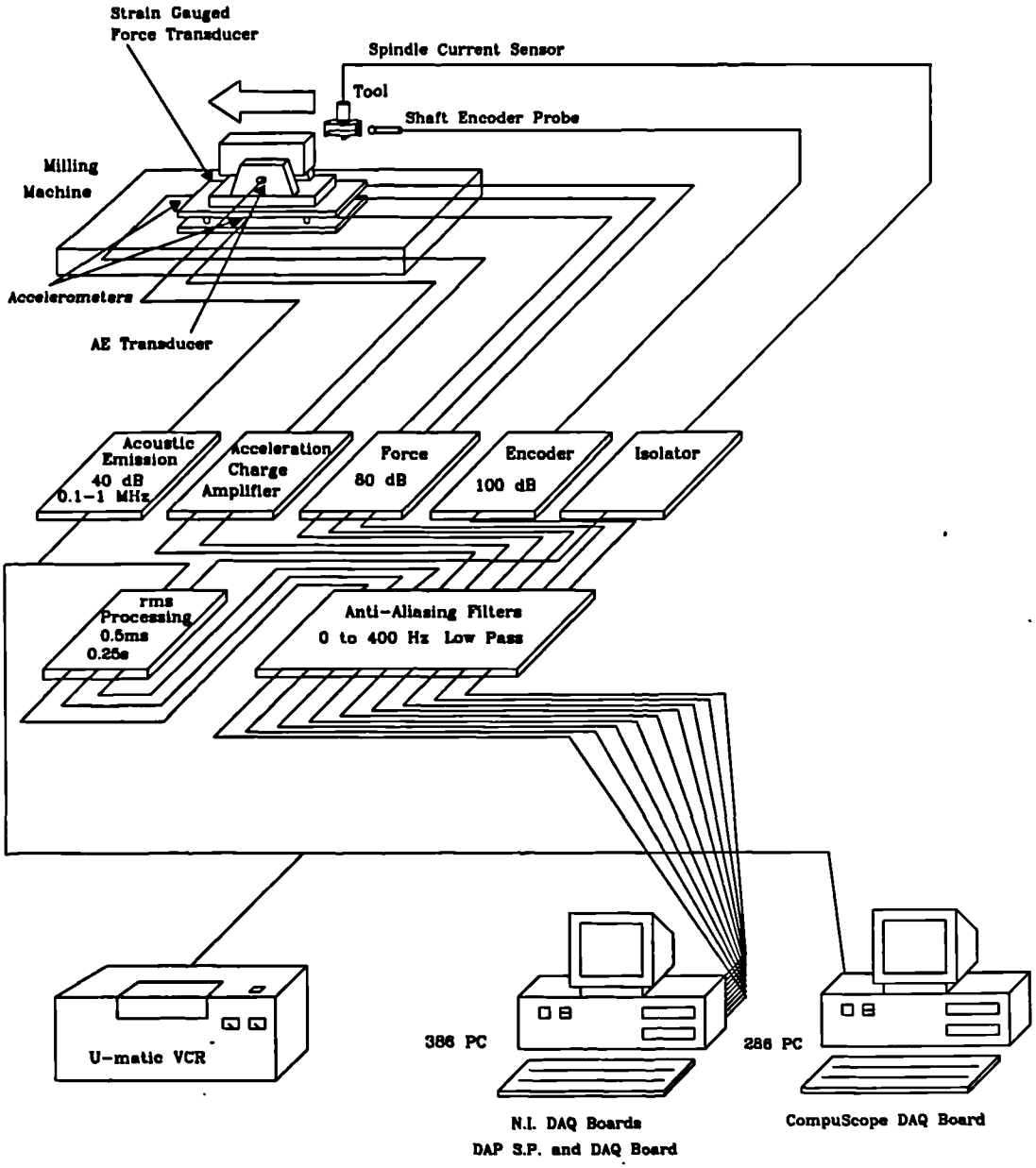

Figure 39: Entire Acquisition System and Sensors

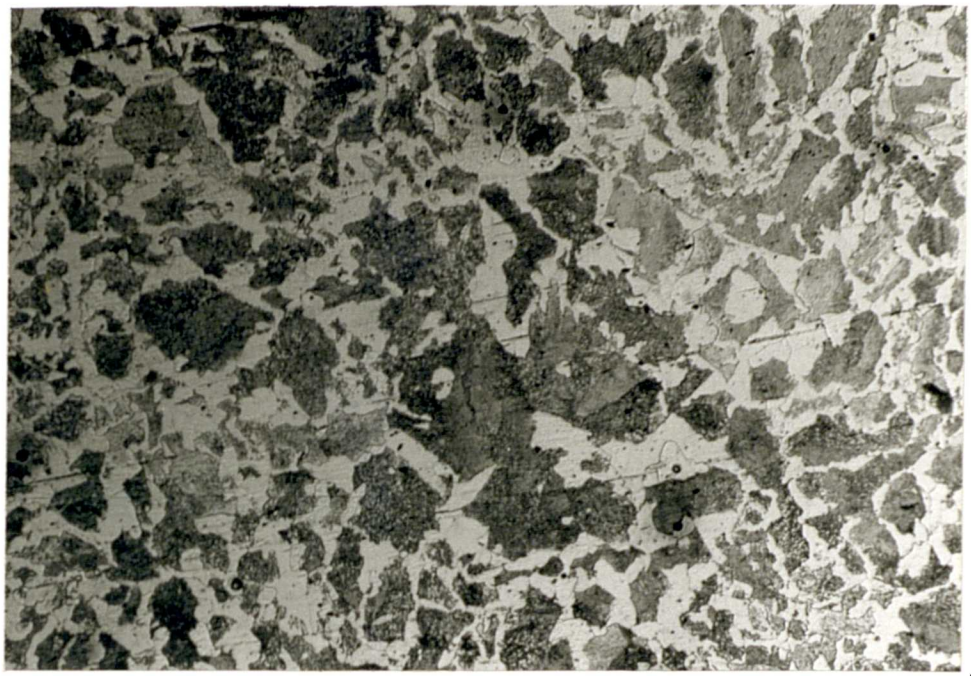

Figure 10: Metallographic Structure of the Annealed En8 Material (X100)

Concentration %							
C	Si	Mn	P	S	Cr	Mo	Ni
0.41	0.20	0.52	0.01	0.04	1.08	0.25	1.37
Hardness 230 HB							

Table 12: Metallurgical Analysis of the En24 Workpiece Material

Figure 41: Metallographic Structure in the Quenched and Tempered En24T Material (X400)

Figure 42: Metallographic Structure in the Annealed En24 Material (X400)

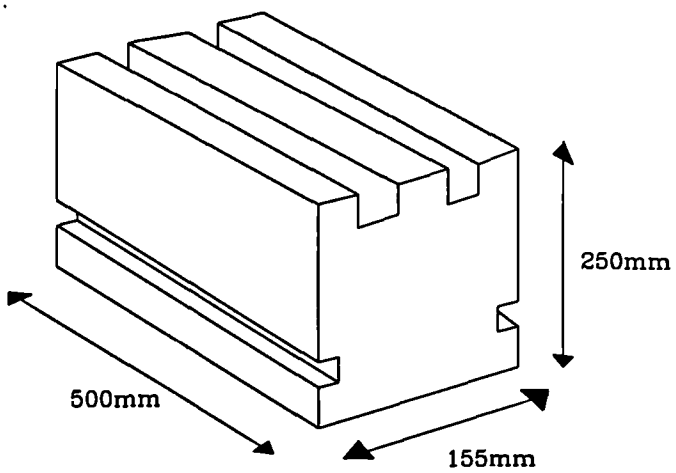

Figure 43: Sketch of the En8 Workpiece

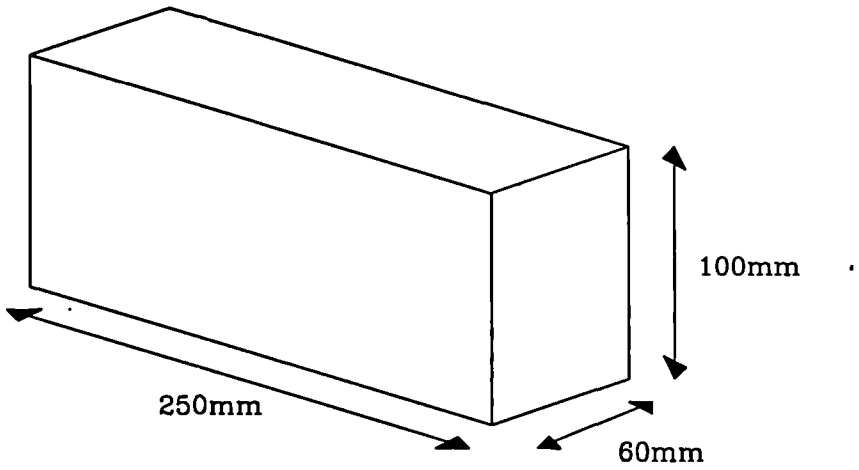

Figure 44: Sketch of the En24 Workpiece

Two sizes of workpiece were used. For the En8 material a large block measuring 500 mm by 150 mm by 200 mm was used. It was necessary to prepare the surface of the block for face milling by cutting grooves in the top of the block so that three 35 mm wide turrets were left. These were then machined away with the cutting conditions of interest. For the En24(T) material a standard block with dimensions of 250 mm by 60 mm by 100 mm was used for all the relevant cutting conditions and operations. It was not necessary to perform any preparation of this workpiece. Figures 43 and 44 show sketches of the two workpieces.

4.1.13 Cutting Tools

Three cutting tools were used. The first of these was an eight point face milling cutter, Table 13, which was used for rough and finish milling on En24 and En24T material. A two point grooving tool, Table 14, was used in the grooving tests, on the same materials. For rough face milling of the En8 material, a four point 50 mm diameter tool was used, Table 15.

Tool	SECO R220.74-0100-12
Diameter	100 mm
Number of Inserts	8 SNKN 1204EN
Cutting Rake	-5 degrees

Table 13: Geometry of the Eight Point Cutter

Tool	SECO R217.19-1612.4-06
Diameter	25 mm
Number of Inserts	2 CCMX 060304-79
Cutting Rake	-11° - -5°

Table 14: Geometry of the Two Point Cutter

Tool	SECO R220.13-0050-12
Diameter	50 mm
Number of Inserts	4 SEKN 1203AFN
Cutting Rake	12°

Table 15: Geometry of the Four Point Cutter

4.2 Accuracy of Measurements

Before presenting the results obtained from the experiments it is necessary to assess the accuracy of the various measurements made. This is done in the following sub-sections for each of the sensors in turn.

4.2.1 Force Transducer and Wadkin Milling Machine

The force transducer calibration graphs for static loading can be seen in Appendix A, Figures 336, 337 and 338 and it will be observed that these exhibit a linear variation with applied load.

In the case of metal cutting, however, the loading is dynamic and the dynamic response of the force transducer will affect the force value recorded. The first mode shape obtained by an eigenvalue analysis of the dynamic response of the force transducer is shown in Appendix A, Figures 329 to 333. This analysis was based on the assumption that the workpiece mass would be a maximum of 150 kg giving a first natural frequency of 237 Hz. This is appropriate for the experiments on En8 workpieces, at least at the start of the wear test and for every change of workpiece throughout the test. However, for the tests on En24 workpieces and the experiment to investigate the influence of machine/fixture stiffness, the mass placed on top of the force transducer was 12 kg with a vice, of mass 42.5 kg being used to attach it to the force transducer. The first natural frequency of this arrangement, which was 344 Hz, was measured by impulse techniques. As the workpiece is machined, its mass will change and so the natural frequency of the force transducer will change. If anything, this effect will reduce the contamination of the force signal by dynamic effects.

The frequencies of interest in the cutting process are of the order of 12 - 40 Hz and 50 - 100 Hz (the spindle and tooth passing frequencies, respectively) and so this resonance of the force transducer could affect the recorded force values. In fact, it was sometimes possible to observe the resonance in both the time domain and frequency domain of the force signal. The importance of this effect will depend on the exact cutting conditions selected as an integer sub-multiple of the natural frequency will cause excitation and larger feed rates will generate a larger forcing function.

In this work, no attempt was made to select cutting speeds which avoided these harmonics, as it was felt that it was of more importance to monitor realistic cutting conditions. The cutting force signals from any wear test therefore have a probability of some contamination from this source. The error introduced due to this effect was observed to be quite small ($< 5\%$ of the d.c. component of the force) for the wear tests conducted.

Besides this natural frequency effect, the feed force signal displayed some other interesting features. The peak d.c. value as measured by the force transducer

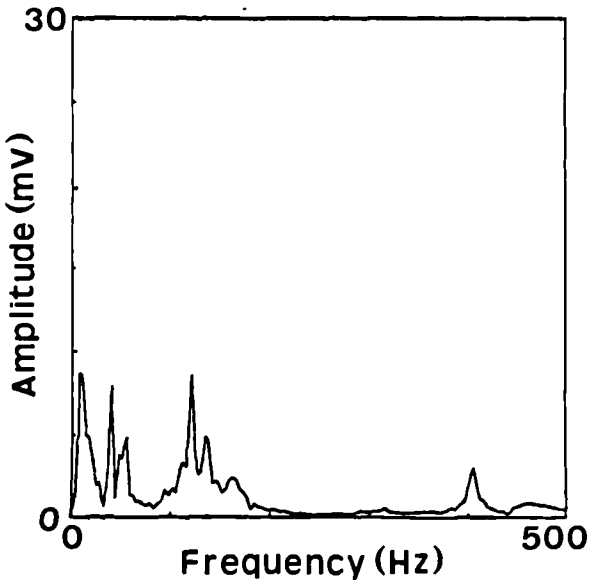

Figure 45: Direct Flexibility for the Perpendicular Direction

occurs at entry into the workpiece and, as the tool progresses, the d.c. component gradually reduces until the tool exits the workpiece. From the discussion in Chapter 3, it would appear that this is caused by mode coupling between the torsional and longitudinal modes of vibration and this results in an excursion of approximately 1 kN for a 250 mm cut across the workpiece. In order to minimise this effect, data was extracted from samples approximately in the region of the middle of the cut. However, there can still be a drop of around 0.5 kN and, for this component of the cutting force, this error can constitute quite a significant proportion of the d.c. signal, as much as 50 % for conditions where the force level is low, for example under finishing conditions.

Finally, the machine tool itself has a large number of natural frequencies, as it is a a rather complex structure. Figures 45, 46 and 47 show the power spectra for the three mutually perpendicular components of the direct flexibilities of the Wadkin machine tool. The pertinent information from these plots is summarised in Table 16. Not surprisingly, the machine is stiffer in the vertical direction, than in the feed or perpendicular directions. The important point to note is that these resonances lie in the same frequency range as the cutting frequencies and therefore there will be a very complex interaction between the cutting process and the machine tool. The force transducer is thus only one more part of the structure that will interact with the cutting process.

4.2.2 Acoustic Emission

The AE sensor used throughout the experiments was a contacting one and it was necessary to decide on a location for the sensor for each set of experiments. For the tests on En8 workpieces, it was mounted on the bottom plate of the force

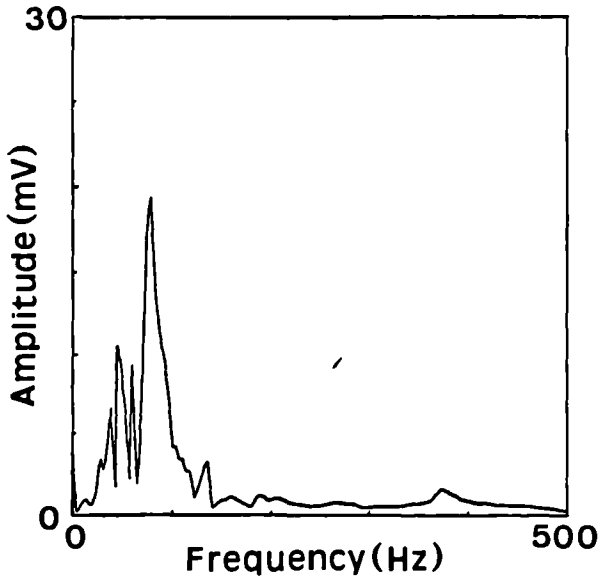

Figure 46: Direct Flexibility for the Feed Direction

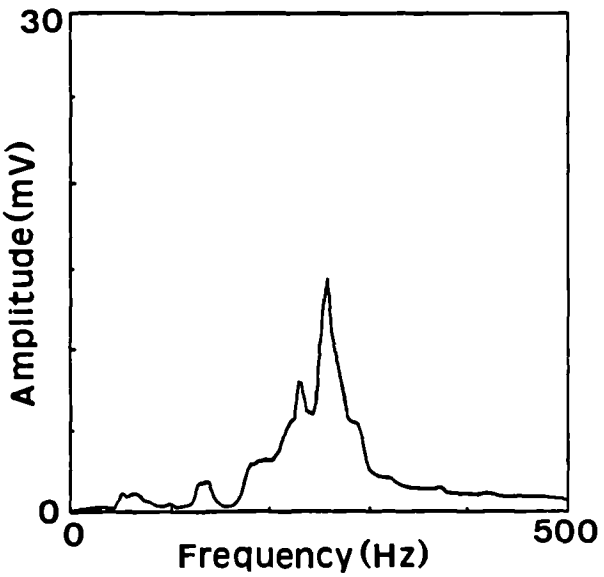

Figure 47: Direct Flexibility for the Vertical Direction

Direction	Flexibility ($\mu m N^{-1}$)	Frequency (Hz)
xz	$1.0x10^{-2}$	0
xz	$3.2x10^{-2}$	20
xz	$1.8x10^{-2}$	44
yz	$1.0x10^{-2}$	0
yz	$4.5x10^{-2}$	20
yz	$2.0x10^{-2}$	44
zz	$0.8x10^{-2}$	0
zz	$23.8x10^{-2}$	20
zz	$5.0x10^{-2}$	44

Table 16: Direct Flexibilities of Wadkin CNC Milling Machine

transducer and for the wear tests on En24 and En24T workpieces the sensor was mounted on the back of the vice. These two locations resulted in different propagation paths from the cutting source to the sensor and this in turn might be expected to affect the amplitude of AE and to a lesser extent, the frequency content of the signal. As tests were not conducted concurrently, it was necessary to decouple the sensor between tests, the exception to this being the series of wear tests on En24 and En24T workpieces, where the sensor remained coupled to the vice for all but one of the experiments. The effect of decoupling the sensor can be relatively small if the user is proficient and consistent in the application.

Another effect, which can be larger than decoupling, is that of variable clamping forces between the vice and workpiece. Figure 48 shows the effect of varying the clamping force between vice and workpiece on the amplitude of the 100 kHz peak of the power spectrum of the signal received by the AE sensor. This data was obtained by placing a pulser on the top of the workpiece, and then capturing signals for a range of torques applied to the vice with a torque wrench. Figure 49 shows the pulse that was sent to the pulser along with one of the resulting bursts of AE detected by the D9201A sensor.

As can be seen, the clamping effect is quite large for torques below 100 Nm. It was usual for a wear test to only consume one block of material, and so this effect could only influence the repeatability of the results obtained between tests and must be considered when using AE sensors in a workshop environment.

4.2.3 Acceleration of the Workpiece

The main source of error in the recorded acceleration signals was expected to be a result of the mounting location. The implications of mounting on the top plate of the force transducer have already been discussed.

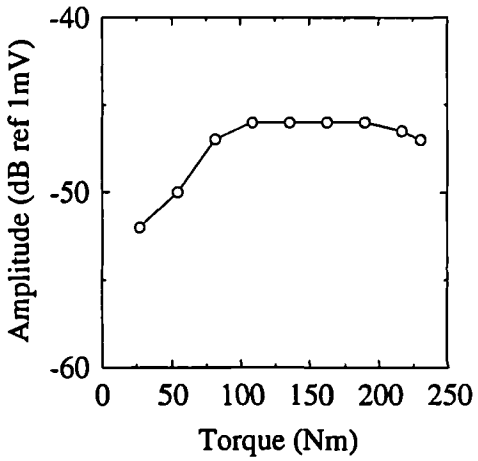

Figure 48: Variation in the 100 kHz peak, in the Power Spectrum of AE signals Acquired using Different Clamping Forces between the Vice and Workpiece

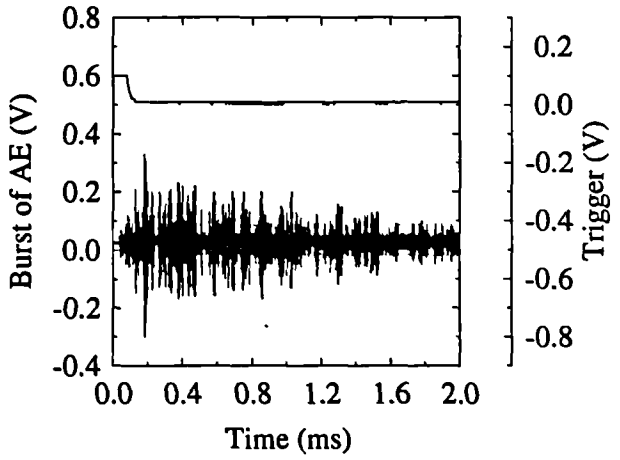

Figure 49: Pulse Applied to the Pulser and the Received AE Signal as Recorded by the D9201A AE Sensor.

4.2.4 Spindle Current

The measurement of spindle current is as accurate as the sensor used in the Wadkin machine. As it was not possible to acquire information from Wadkin on this matter the extent to which any noise or inaccuracies in the sensor would affect the recorded signal could not be assessed.

Other considerations as to how spindle current relates to power has already been covered in Chapter 3.

4.2.5 Wear Measurement

The method of wear measurement used in this work was not the most accurate that could have been used but was certainly one of the most convenient. As described earlier, the flank wear was measured by obtaining a magnified image of the wear land of each insert on a monitor and then a measurement of the wear land was made using a rule. Accuracy of measurement, at least in the initial stages of tool wear, was very good with a resolution of around 0.01 mm. As wear progressed, however, the profile became non-uniform and a certain amount of subjectivity resulted, corresponding to an error of approximately 0.05 mm. Error bars shown later on the wear evolutions correspond to the range of flank wear measured on the two, four or eight inserts and this value is in general larger than the estimated error in measurement.

4.2.6 Surface Finish Measurement

The accuracy of surface finish measurement, as quantified by the R_a value, was determined by the accuracy of the sensing instrument. This instrument was capable of making measurements with a resolution of 0.01 μm over the tracking length of the sensing element which, for this small probe, was only 12 mm. In order to obtain a measure of the variability in surface finish of the cut surface, six measurements were made; three along the length of the workpiece and three across the width. In each case, these tracks were located around the centre of the opposite dimension. Again, the variability between measurements generally exceeded the measurement error.

4.2.7 Variability of the Workpiece Material

The workpieces used for the wear tests were quite large, close to the limiting ruling section for heat treatment, and it might therefore be expected that some variability in hardness would be found through the cross-section of the block. In addition, some variability between workpieces might be expected if they had been heat treated individually.

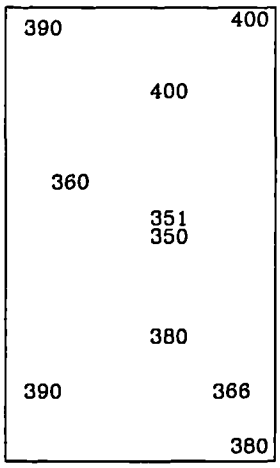

Figure 50: Variation in Hardness for the En24T Material

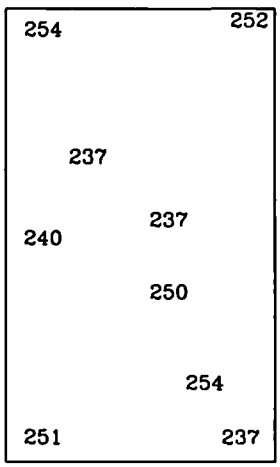

Figure 51: Variation in Hardness for the En24 Material

In fact, the variation in hardness through the depth of all the workpieces was found to be very small. Figures 50, 51 and 52 show this variation for the En24T, En24 and En8 materials, respectively.

4.2.8 Expression of Errors in Presentation of Results

The following convention for expressing measurement variability, has been used in Chapter 5 to maximise the clarity of presentation. Variability of each sensor in a cut is generally expressed by the spread of data points. During the systematic wear tests, two tests were carried out and these are represented by hollow and filled circles. Variability in VB_B over the tool is shown as an error bar. However, because of the closeness of the data points for some of the wear tests, error bars have only been introduced for one set of data points in order to improve the clarity of presentation.

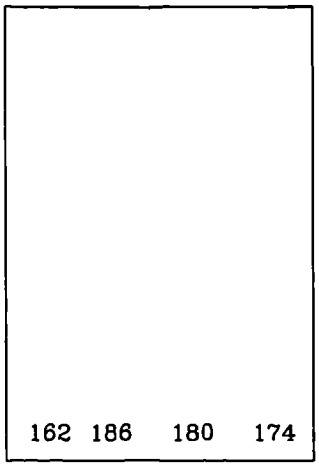

Figure 52: Variation in Hardness for the En8 Material

4.3 Experiment to Investigate the Direct Flexibilities of the Machine Tool

This short experiment was conducted to investigate the direct flexibilities of the machine tool, as it was felt that these values could have an effect on the tool life, and so would be of interest in the development of a monitoring system which is to be applicable to a variety of machines, each with its own dynamic properties.

The experiment consisted of placing accelerometers on the machine table and head stock. Then, by clamping a 'shaker' on to the table and by using a pseudo-white noise source to excite it, the flexibility of each of the three mutually orthogonal components was calculated for the spindle.

Figure 53 shows the experimental set-up, and accelerometer locations used during this experiment. The accelerometers were those described in Section 4.1.5.

4.4 Investigation of the Influence of Machine/-Fixture Stiffness on AE and Workpiece Vibration Generated during Face Milling on Bright Mild Steel.

Many workers [78,123] have suggested the use of AE as a measurand for use in condition monitoring of the machining process, proposing a variety of different signal processing schemes. As described in Chapter 2, Dornfeld [73,94] and Blum [105], for example, have made extensive use of AE for condition monitoring in turning and milling operations. However, there is little published data to support the claim that AE is unaffected by the low frequency, high amplitude machine vibrations which affect other measurands such as force.

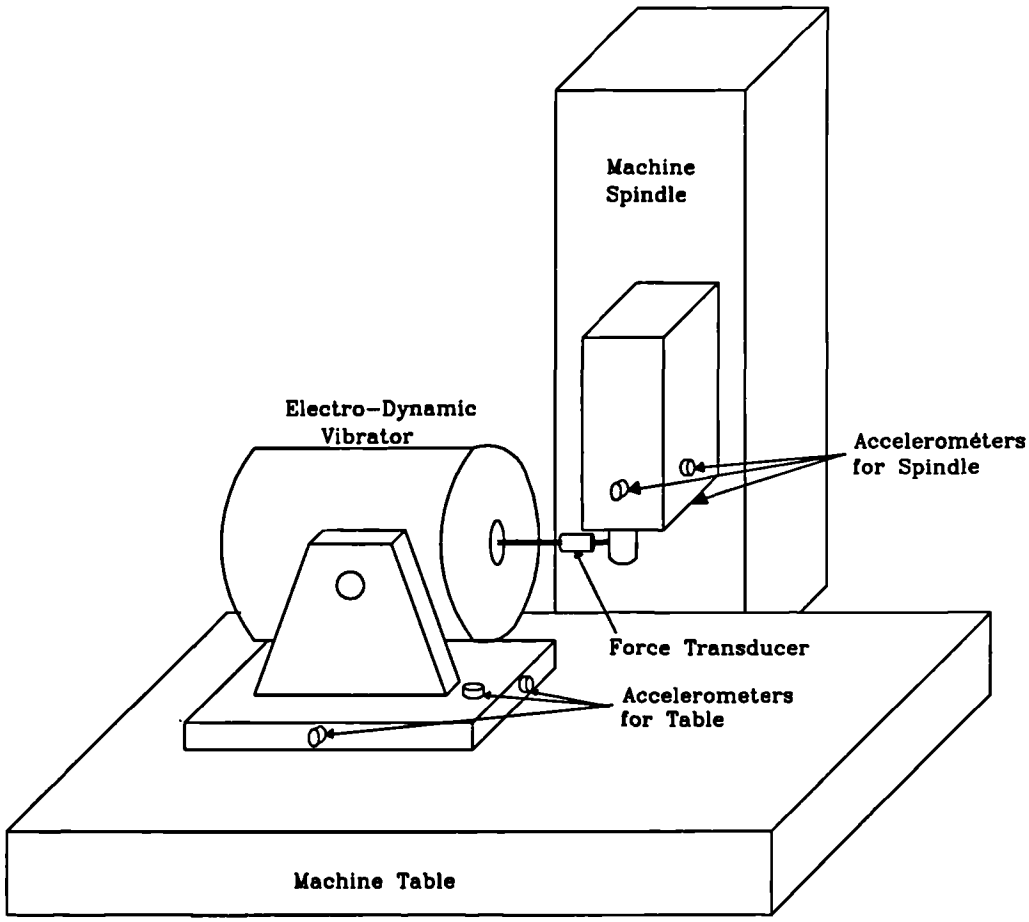

Figure 53: Set-up of Experiment to Perform a Flexibility Analysis of the Wadkin CNC

Diameter	Stiffness	Relative Stiffness	Natural Frequency
20mm	150 $kNmm^{-1}$	1.0	344Hz
30mm	763 $kNmm^{-1}$	5.1	440Hz
40mm	2412 $kNmm^{-1}$	16.1	460Hz

Table 17: Theoretical Stiffness of Slender Pillar Sets for Influence of Stiffness Experiments

It is reasonable to suppose that the machine/fixture stiffness will have an effect on the sensorial information that is recorded if the frequency response of the sensor is in the same range as the machine frequency response. However, if the frequency response of the sensor is an order of magnitude higher than the machine characteristics then it can be expected that the sensor will be unaffected by those machine characteristics.

In order to address this effect it was decided to investigate the influence of machine/fixture stiffness on the AE and workpiece acceleration by varying the static stiffness of the workpiece fixture. Since the overall stiffness in the cutting process is determined by the machine tool/workpiece/fixture combination. Varying of one of these components is not quite the same as varying the machine tool itself but is more realisable and controlled and should give an indication of the likely effect machine stiffness will have on sensorial information.

4.4.1 Experimental Apparatus

The variation in effective machine stiffness was achieved by mounting the vice and workpiece on a stiff platform supported above the existing milling machine table by four 'slender' pillars which could be changed to vary the diameter (Figure 26). This platform is essentially the same as the force transducer but without the strain gauges and with a variable pillar diameter.

Three sets of pillars were used, giving the overall theoretical stiffnesses shown in Table 17, calculated by assuming a maximum deflection based on a beam built in at one end with the other end free to move parallel to the fixed end. The natural frequencies shown in Table 17 were measured using impulse techniques with a calibrated hammer. These frequencies and stiffnesses can be compared with the milling machine static stiffness, governed mainly by the headstock, of around 100 $kNmm^{-1}$ with natural frequencies of 20 Hz and 48 Hz.

AE was measured with the Dunegan D9201A broadband piezoelectric transducer described earlier and this was coupled directly to the workpiece. The AE signal was amplified with the combined AE amplifier and filter. This signal was then processed by a true rms converter to yield the rms AE signal over a time period

Tool	6 Point, 100mm Diameter Sandvik T-Max
Workpiece	50mm x 50mm x 210mm, Bright Mild Steel
Depth of Cut	2.5mm
Cutting Velocity	295 m/min
Feed Rate	0.07 mm/insert

Table 18: Cutting Conditions for the Influence of Stiffness Experiments

of 5.5 ms. The analogue signal was then digitised with the CompuScope board in the 80286 PC with a sample rate of 5 kHz, allowing approximately a 150 mm section of the workpiece traverse to be recorded, and this was arranged to be around the centre of the workpiece.

Workpiece vibration was measured by positioning an accelerometer in the feed direction on the top plate of the stiff platform and this signal was analysed in real time with a spectrum analyser. The overall experimental set-up is shown in Figure 54.

4.4.2 Experimental Procedure

The experiment consisted of machining a block of general purpose mild steel (dimensions of 250 mm x 50 mm x 50 mm) held in a vice attached to the top plate of the platform described above. A single traverse of the workpiece was then made with a six point face milling cutter using the cutting conditions in Table 18 for each of three sets of pillars.

4.4.3 Signal Processing

Signal processing consisted of using the spectrum analyser to estimate the power spectrum of the workpiece acceleration. Whilst for the AE signal the power spectrum was estimated off-line, as was the amplitude distribution.

4.5 Influence of Insert Geometry on Sensorial Information

The aim of this experiment was to assess the influence that different wear geometries had upon the sensors used in the systematic wear experiments as there was some evidence from the literature that, for example, crater wear affects the AE signal through lowering of the strain rate. It might also be expected that insert

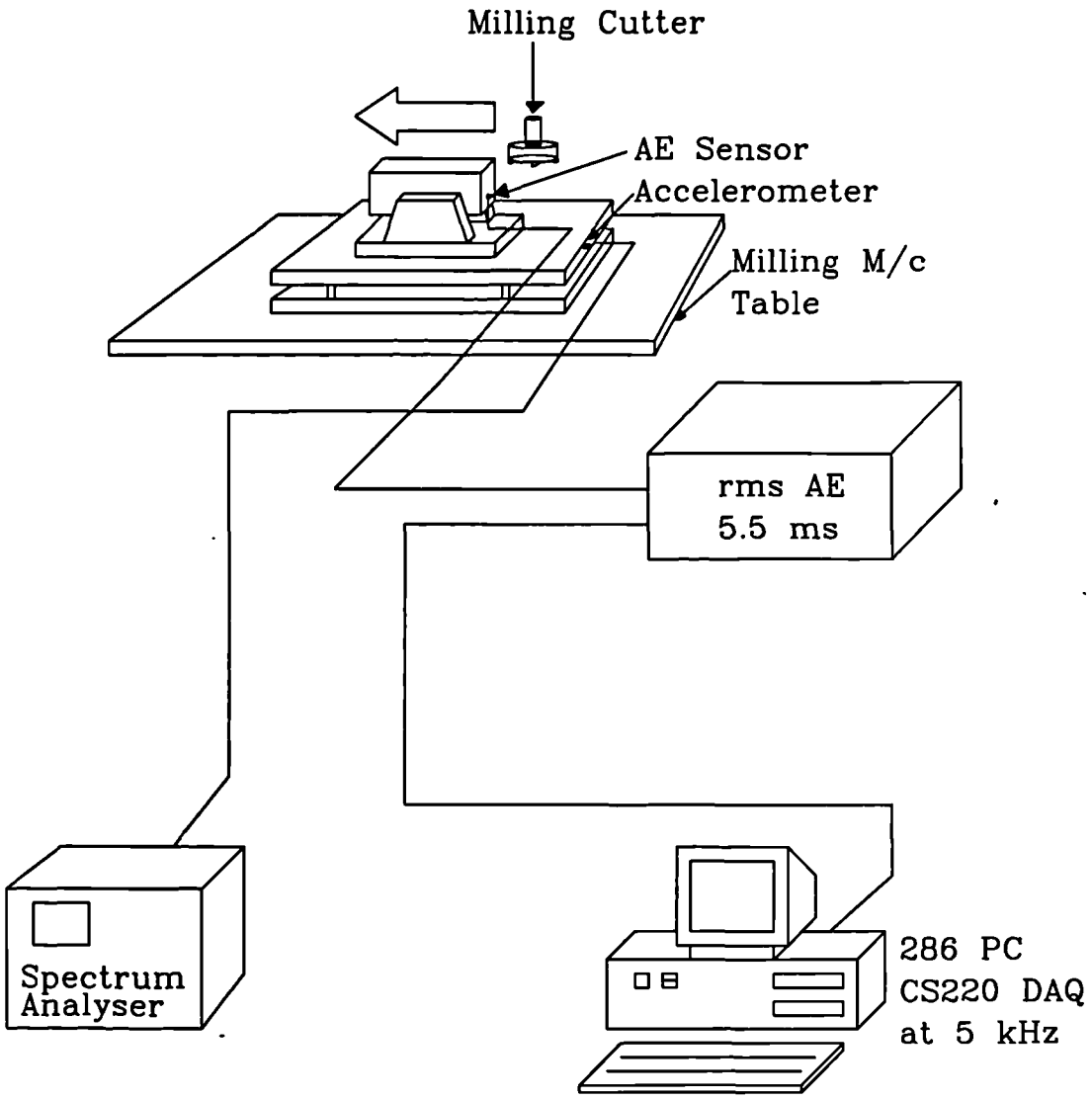

Figure 54: Experimental Set-Up for Influence of Stiffness Experiment

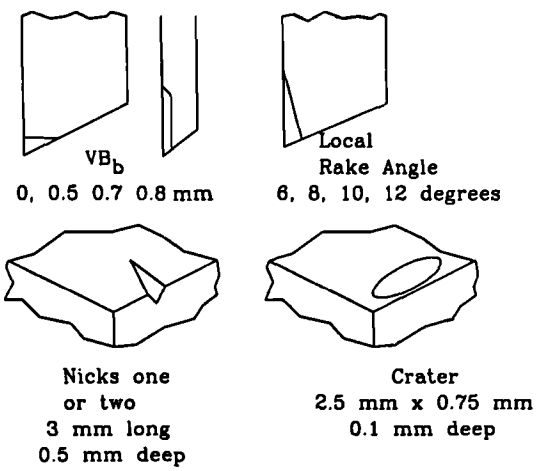

Figure 55: Drawing of the Different Geometries Investigated in the Influence of Geometry Experiments

set-up and cutting geometry may have an influence on other sensors such as the cutting force and workpiece vibration.

4.5.1 Experimental Apparatus

Apparatus consisted of the three axis mechanical force transducer, with the two horizontal components of workpiece acceleration and the AE processed with the rms unit at 0.5 ms. Data was stored on the 386 PC after being digitised with the National Instruments AT-MIO-16-L data acquisition boards.

4.5.2 Experimental Procedure

The experiment consisted of acquiring data corresponding to the three components of cutting force, two components of acceleration and AE by using the ground inserts shown in Figure 55. These consisted of four new inserts that had been precision ground to include the following geometries; differing local rake angle, major flank wear simulations, a crater, and simulations of edge breakdown.

During the experiment all four slots in the tool holder were used, three of the slots containing new 'control' inserts and the fourth containing the insert with the ground geometry. Three 'bedding in' cuts were performed followed by three cuts when data was acquired. The cutting conditions used for these tests are shown in Table 23.

Sensor	Signal Processing
Cutting Force	Mean + Standard Deviation
0.5 ms rms Acoustic Emission	Mean + Standard Deviation
Feed Acceleration	Standard Deviation

Table 19: Signal Processing for the Influence of Geometry Experiment

4.5.3 Signal Processing

Analysis of the data consisted of calculating the parameters shown in Table 19. The analysis was conducted on all the data from a tool rotation, not simply the results corresponding to the insert with the specific geometry as it was not possible to decide which of the features in the time evolution corresponded to the insert with the artificial geometry.

4.6 Long Timescale Event Detection using Spindle Current, Cutting Force, Workpiece Vibration and Acoustic Emission during Face and Groove Milling Operations.

This set of experiments was carried out in order to provide a database on which to demonstrate the relative merits of an expert system and neural network for long-timescale event detection.

The work presented here examines the wear evolution during several cutting operations on three different conditions of two steels, En8 and En24, treated to give hardnesses of 180 HB, 220 HB and 330 HB. A range of sensors were employed to monitor the cutting operations, these being detailed in Table 20, with most tests being conducted twice to assess repeatability. Each test consisted of wearing out all of the inserts of the tool of interest under a set of normal production cutting conditions for each tool.

4.6.1 Experimental Apparatus

Figure 39 is a block diagram of the experimental set-up for the various tests, the differences between tests on En24(T) and En8 materials as explained in Section 4.1.10.

For the En24 material, nine sensors were used and these are shown in Table 20. The surface finish was logged manually. During a typical wear test, data was

Workpiece Acceleration, the 3 Orthogonal Components
Cutting Force, the 3 Orthogonal Components
rms AE, averaging constant, 0.5 ms and 0.25 s
AE recorded on analogue format tape, bandwidth 1 MHz
Spindle Current
Fibre Optic Shaft Encoder

Table 20: Sensors Employed in Systematic Wear Tests

	Roughing	Finishing	Grooving
Cutting Speed (m/min)	150	200	100
Feed Rate (mm/insert)	0.15	0.1	0.15
Depth of Cut (mm)	2.5	0.5	2.5

Table 21: Cutting Conditions for the Tests using En24T as a Workpiece

collected on every third cut (a cut being one pass along the top of the workpiece with the tool and cutting conditions of interest), with data for the entire cut being recorded at that time. The size of the test blocks allowed for almost a complete wear test to be conducted on one block for each of the cutting conditions selected, the exception being the test on En8 where approximately three and a half blocks were used. This resulted in a variable amount of data per wear test but, typically, each test resulted in 20 Mbytes of digital data and one hour of analogue recording.

4.6.2 Experimental Procedure

The cutting conditions used in the different experiments are summarised in Table 21 for rough and finish face milling and for groove milling of the En24T material. Similarly, Table 22 displays the data pertaining to systematic wear tests carried out on En24 in the fully annealed condition.

	Roughing	Finishing	Grooving
Cutting Speed (m/min)	250	300	170
Feed Rate (mm/insert)	0.2	0.1	0.1
Depth of Cut (mm)	2.5	0.5	2.5

Table 22: Cutting Conditions for the Tests using En24 as a Workpiece

	Roughing
Cutting Speed (m/min)	125
Feed Rate (mm/insert)	0.2
Depth of Cut (mm)	2.5

Table 23: Cutting Conditions for Wear Test using En8 as a Workpiece

Only one systematic wear test was conducted on En8 (in the fully annealed condition) and the data relating to the rough machining of this material is displayed in Table 23

A typical wear test consisted of taking a tool with new inserts and, under the appropriate cutting conditions for the tool and material, performing enough cuts to wear out the inserts. A worn-out tool was considered to be one with a mean VB_B value of 0.7 mm. Periodically throughout the life of the tool, typically at every third cut, data from the sensors employed was acquired using the data acquisition boards and PC. After this, images of the wearing inserts were obtained by using the CCD camera and recording the images onto the U-matic video cassette recorder, as described previously. Finally, a measure of the surface quality was made with the portable R_a meter. This procedure allowed data pertaining to the different sensors and R_a values to be correlated with wear, without generating excessive amounts of data.

4.6.3 Signal Processing

For the examination of the evolution of sensor output with wear, five segments of data corresponding to around 40 revolutions of the tool were recovered from magnetic storage and analysed. Each segment was processed to produce five data points for each cut analysed. Each point corresponds to between 20 mm and 40 mm of tool travel along the workpiece and was taken from an area in the middle of the cut. The process is illustrated schematically in Figure 56.

The general form of the time series collected from each of the sensors employed is displayed in Figures 57 to 61. Each (approximately 40 revolution) segment was analysed by calculating the parameters shown in Table 24.

4.7 Short Timescale Event Experiments

This series of experiments was conducted, sometimes fortuitously, in order to assess the affect that short-timescale degradation has on the sensor output. After analysis, this would allow a recommendation as to the most appropriate sensor

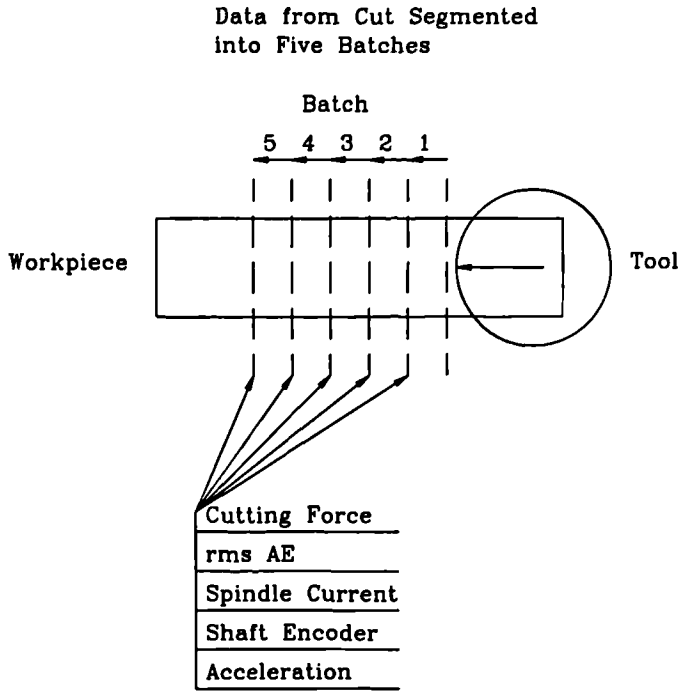

Figure 56: Sample Point and Data Analysis of the Systematic Wear Tests

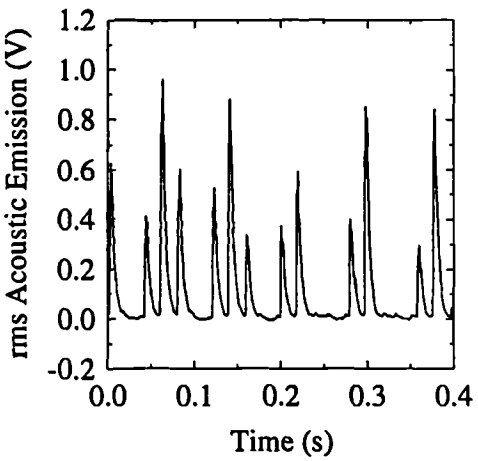

Figure 57: Typical Time Series of the rms AE at 0.5 ms

Sensor	Signal Processing
Spindle Current	Mean
Cutting Force	Mean + Standard Deviation
0.5 ms rms AE	Mean + Standard Deviation
Workpiece Acceleration	Standard Deviation

Table 24: Signal Processing Applied during Systematic Wear Tests

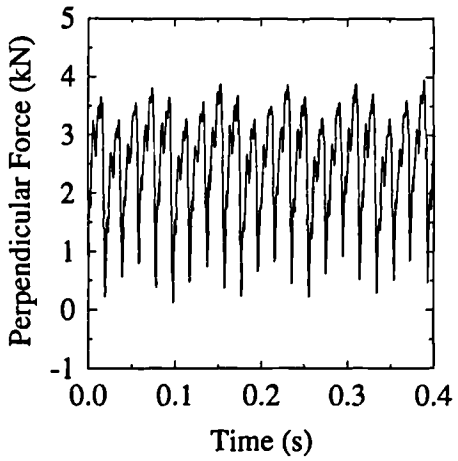

Figure 58: Typical Time Series of the Perpendicular Force

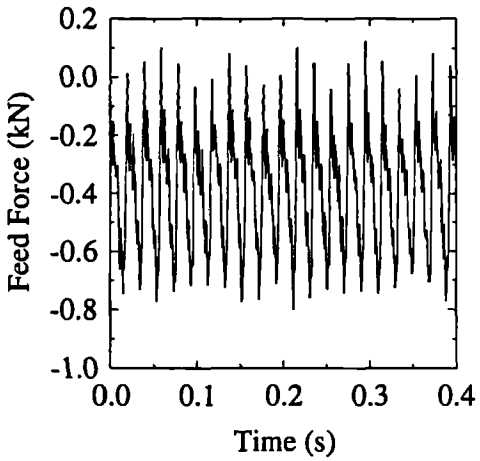

Figure 59: Typical Time Series of the Feed Force

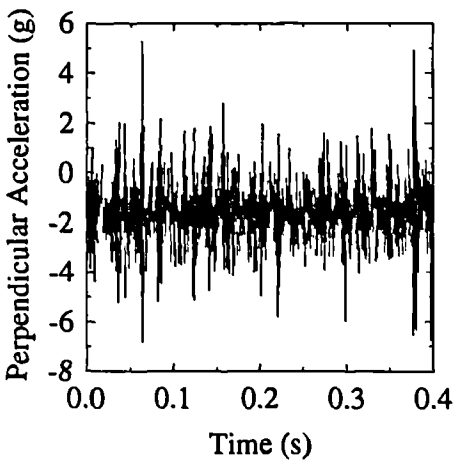

Figure 60: Typical Time Series of the Perpendicular Acceleration

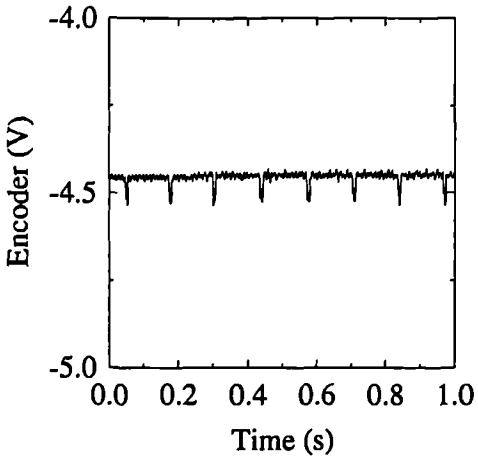

Figure 61: Typical Time Series of the Optical Shaft Encoder

to use for recognition of such events.

4.7.1 Experimental Apparatus

In general the apparatus used consisted of the same set-up as that used for systematic wear tests. Therefore cutting force, vibration, AE and spindle current were sensors that were used for some or all of the experiments. Again Figure 39 provides a schematic of the set-up.

4.7.2 Experimental Procedure

The work presented under this heading arises from a variety of experiments and events. Some are sub-sets of the systematic wear tests described in the previous section, and others were short individual experiments that investigate, for example, the effect of localised hard patches on sensorial information. One was the result of an operator error which caused the machine spindle to jam, breaking an insert. These experiments are described in the following sub-sections.

Traverse Through a Weld Bead and Heat Affected Zone.

This experiment consisted of running the milling cutter along the workpiece and through a weld bead and its heat affected zone under rough face machining conditions. The weld bead had been deposited by first grinding out part of the workpiece to a depth of 5 mm and a cross-section of 35 mm by 30 mm and then laying in weld material until the ground portion was filled. This was then ground flush with the original workpiece. The workpiece material was En8 and the four point 50 mm diameter tool was used with the cutting conditions shown in Table 23. Figure 62 shows a section through the weld bead and Figure 63 shows

Cutting Velocity	150 m/min
Depth of Cut	5 mm
Feed Rate	0.15 mm/insert

Table 25: Accidental Cutting Conditions used to Stall Spindle and Break an Insert

the variation in hardness in the direction of the tool traverse.

Pre-Cracked Insert and its Resulting Breakage

This experiment was conducted by using insert that had been accidentaly cracked in place of an insert in good condition. The cutting tool was brought into contact with the En8 workpiece under roughing conditions (Table 23) and the breakage of the insert followed within a few revolutions of the tool. The extent of the crack after failure is shown in Figure 64 although the initial pre-crack size is not known.

Insert Failure and Machine Stall under Inappropriate Cutting Conditions

In an experiment under roughing conditions on En24T material, the depth of cut was accidentally set at 5 mm instead of 2.5 mm, as shown in Table 25. This doubling of the depth of cut resulted in the breakage of one of the inserts, shown in Figure 65, rapidly followed by the stalling of the spindle.

Edge Chipping Whilst Conducting a Roughing Wear Test

This result forms a small part of a systematic wear test on En8 steel with a four point face milling tool when edge chipping of one of the inserts occurred towards the end of the wear test at a mean flank wear of 0.5mm. Table 23 gives cutting conditions applicable to this event and Figure 66 shows the extent of material loss on the insert.

4.7.3 Signal Processing

Signal processing to detect the above events has been kept to a minimum and, in most cases, only the time series have been used. The reason for this is that, with a minimal set of signal processing, any detection system will have the best

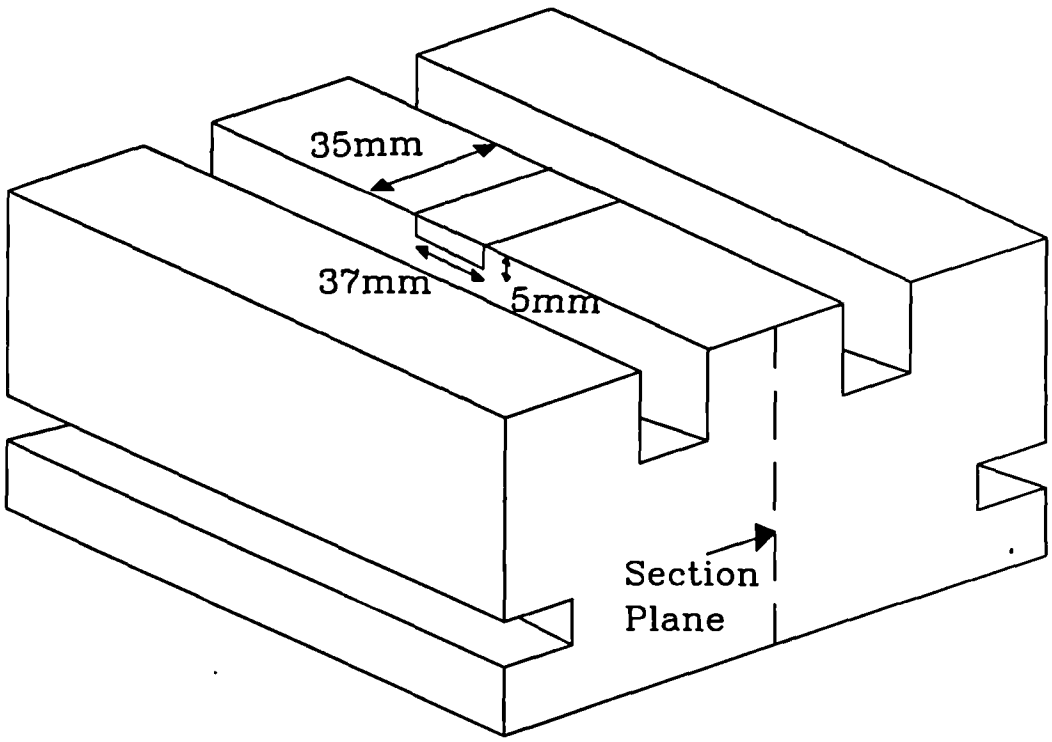

Weld Bead in Workpiece

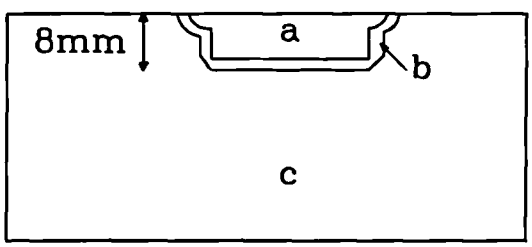

Hardness	
a	160 HB
b	350 HB
c	160 HB

Section through Weld Bead

Figure 62: Weld Bead Location and Section

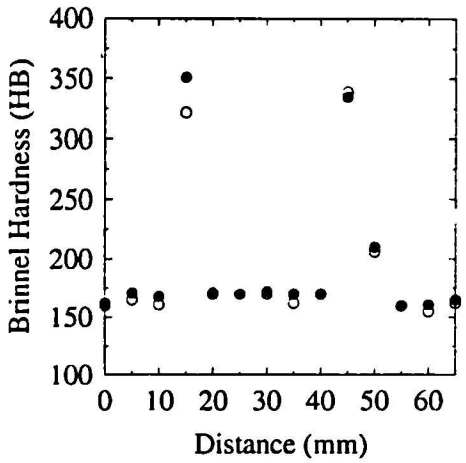

Figure 63: Weld Bead Hardness Profile in the Feed Direction

Figure 64: Extent of Failure of Pre-Cracked Insert (X4)

Figure 65: Extent of Failure of Insert During Abnormal Cutting Conditions (X4)

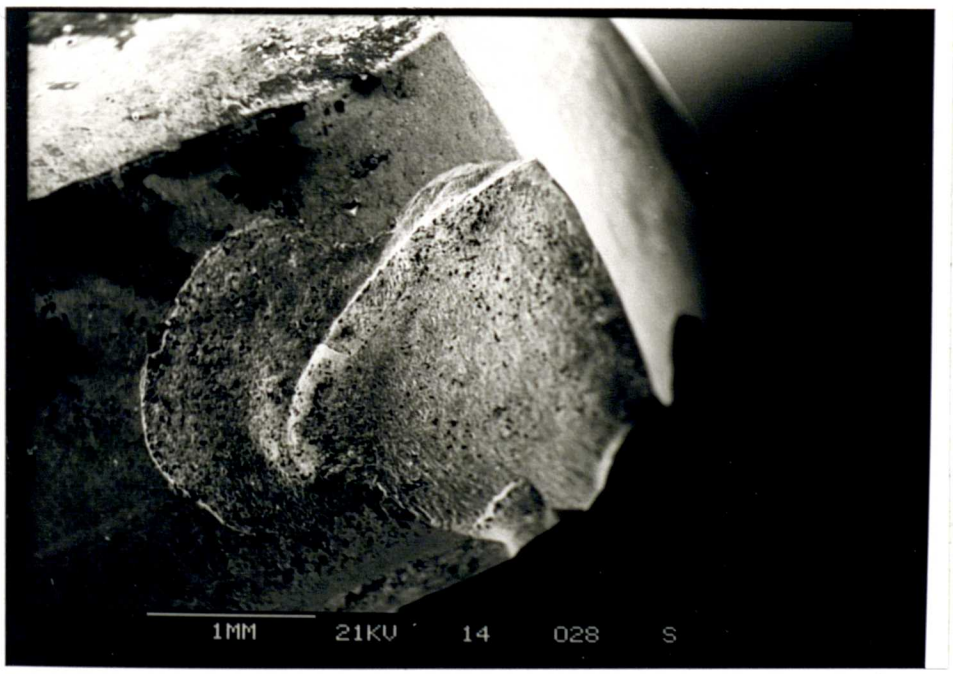

Figure 66: Extent of Edge Chip

chance of real-time processing the data encoded in the sensorial information, thus allowing prompt action.

4.8 Influence of Cutting Conditions on Sensorial Information

This series of experiments was designed to assess the influence that cutting conditions have upon the outputs of the sensors employed in the systematic wear tests. As a by-product of the experiments it has been possible to assess the effect of tool wear on the sensorial information at a variety of cutting conditions.

4.8.1 Experimental Apparatus

Throughout the five sets of random walks data was collected from four sensors, these being the feed and perpendicular components of the cutting force, rms AE at 0.5 ms, AE at the full bandwidth of the sensor, and the spindle current. Figure 67 shows the experimental set-up. Data was captured onto two PC-based data acquisition cards, one low sample speed board and the other the CompuScope board, Table 7.

4.8.2 Experimental Procedure

One cutting tool and one material were selected for this study, these being the 8 point SECO cutter and annealed En24 material (Tables 12 and 13 respectively). The maximum range of cutting speeds and feed rates recommended in the machining literature [29] were used to generate a set of twenty cutting conditions at varying depths of cut. Table 26 shows the range of cutting conditions considered. In order to proceed, the selected cutting conditions were randomised and a total of five sets of randomly chosen conditions (random walk) were carried out. There was a weighting introduced into the experiment towards the central point of the cutting condition space such that there were five cuts carried out at this point and only one at the others.

Obviously, the tool wore as the process of performing twenty random cuts proceeded and the amount of flank wear that occurred during each random walk is shown in Table 28. The wear rate was such that it was possible to allocate each random walk to a distinct wear class; new (VB_B = 0.0 mm to 0.2 mm), partly used (VB_B = 0.2 to 0.3), used (VB_B = 0.3 to 0.4), worn (VB_B = 0.4 to 0.5) and worn out (VB_B = 0.5 to 0.6).

Data was acquired from a region approximately in the middle of the cut synchronised by a position indicator on the CNC. Twelve blocks of 256 points were

Number	Cutting Speed m/min	Feed Rate mm/insert	Depth of Cut mm
1	125	0.16	0.5
2	255	0.16	0.5
3	125	0.34	0.5
4	255	0.16	0.5
5	125	0.16	1.7
6	255	0.16	1.7
7	125	0.34	1.7
8	255	0.34	1.7
9	80	0.25	1.1
10	300	0.25	1.1
11	190	0.1	1.1
12	190	0.4	1.1
13	190	0.25	0.1
14	190	0.25	2.1
15	190	0.25	1.1
16	190	0.25	1.1
17	190	0.25	1.1
18	190	0.25	1.1
19	190	0.25	1.1
20	190	0.25	1.1

Table 26: Cutting Conditions for Random Walk Through Cutting Condition Space

	Random Selection of Cutting Conditions
1	6 3 20 10 4 19 12 14 15 5 18 7 8 17 11 1 16 13 9 2
2	8 12 13 18 7 4 1 6 10 11 17 20 9 14 3 19 15 5 2 16
3	4 16 3 17 1 8 14 11 13 6 20 10 2 19 9 15 12 18 7 5
4	17 20 16 14 4 9 1 3 10 2 19 11 12 18 8 7 5 6 13 15
5	13 8 5 1 4 17 20 12 10 6 16 14 19 11 3 15 9 7 2 18

Table 27: Order of Random Walks

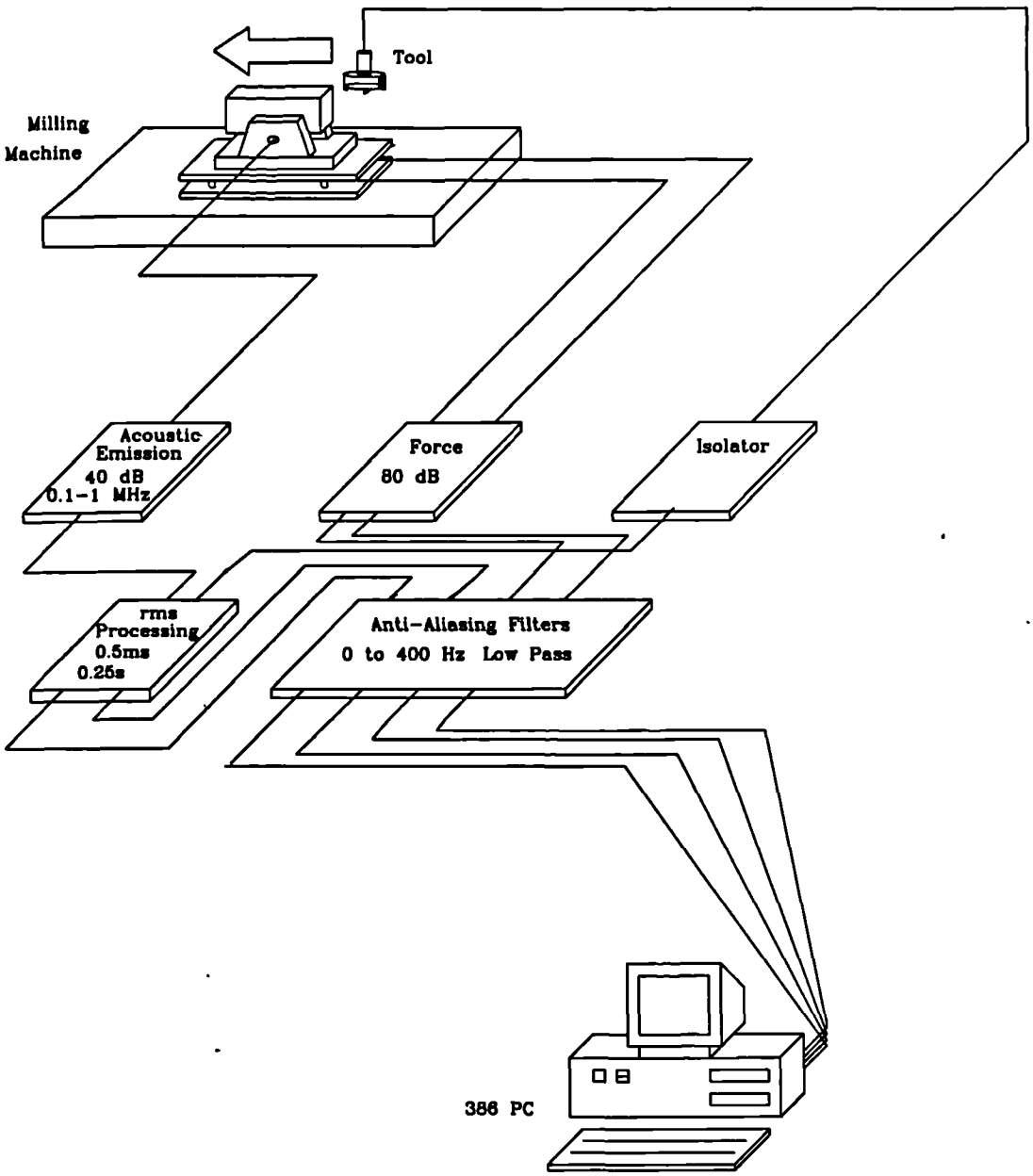

Figure 67: Experimental Set-up for Random Walk Experiments

Amount of Tool Wear per Random Walk	
Random Walk One	0.0 to 0.2
Random Walk Two	0.2 to 0.3
Random Walk Three	0.3 to 0.4
Random Walk Four	0.4 to 0.5
Random Walk Five	0.5 to 0.6

Table 28: Amount of Tool Wear per Random Walk

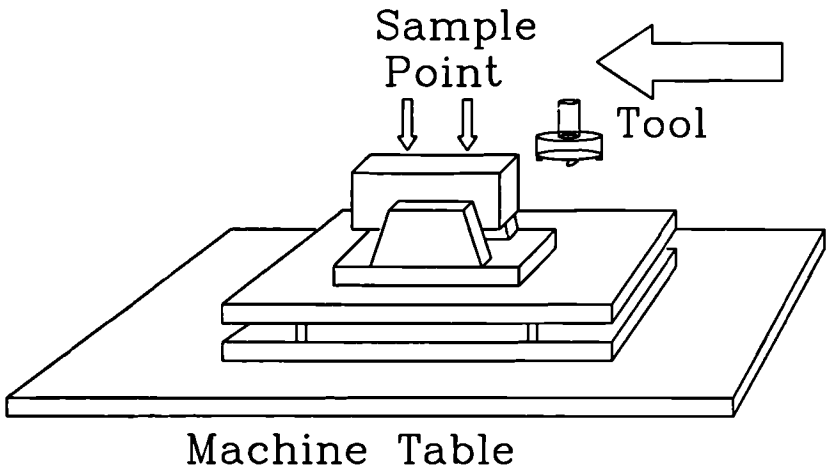

Figure 68: Sample Point in Relation to Workpiece for Random Walk and Accelerated Wear Tests

acquired at the rate of 1.6 kHz per channel from each cut in each of the 20 cutting conditions for the five wear classes and on the CompuScope board one sample of AE was recorded from an approximate position in the middle of each cut. Each set of 12 by 256 data points corresponded to a cutting length of between 24 mm and 111 mm, depending on the feed rate selected. Figure 68 shows the approximate position of the area of data sampling in relation to the workpiece.

4.8.3 Signal Processing

Once the low bandwidth data had been acquired the processing described in Table 29 was performed on it. For the high bandwidth AE data the power spectrum was estimated using the Fast Fourier Transform, with the mean frequency calculation and a band analysis being performed and plotted against the cutting conditions.

Cutting Force	Mean + Standard Deviation
Spindle Current	Mean
rms AE at 0.5 ms	Mean + Standard Deviation
Raw AE	Mean of Fifty Power Spectrum Estimations using FFT

Table 29: Signal Processing Performed on Data Acquired during Random Walks

Cutting Speed	190 m/min
Feed Rate	0.25 mm/insert
Depth of Cut	1.1 mm

Table 30: Cutting Conditions for Accelerated Wear Test Data Acquisition

4.8.4 Verification of the Wear Test obtained at the Central Point

This test was performed in order to verify the reproducibility of the random walk experiments described above but itself provided additional data. The verification was carried out at the central point in cutting condition space for the random walk experiments.

Experimental Apparatus, Procedure and Signal Processing

As for the random walk experiments, the eight point tool was used on the En24 material with a single set of cutting conditions as shown in Table 30.

As it had been found that the tool wear rate was very low at these cutting conditions, the harder En24T material and a set of separate cutting conditions (Table 31) was used to provide accelerated wear between data acquisition cuts.

The experiment was conducted by first performing a bedding in cut on the En24 with a new set of inserts. Then two data acquisition cuts were performed with the

Cutting Speed	300 m/min
Feed Rate	0.1 mm/insert
Depth of Cut	1.1 mm

Table 31: Cutting Conditions for Accelerated Wear

Mean VB_B = 0.00 mm
Mean VB_B = 0.19 mm
Mean VB_B = 0.40 mm
Mean VB_B = 0.55 mm
Mean VB_B = 0.70 mm

Table 32: Wear Levels for Which Data was Acquired

cutting conditions shown in Table 30. The workpiece material was then changed to En24T and the wear-inducing cutting conditions were selected. A varying number of cuts were performed, no fewer than three and no more than six, in order to increase the wear on the tool to one of the levels in Table 32. These levels were selected to roughly coincide with the wear classes defined in the random walk experiments. When the tool reached the new wear level the workpiece material and cutting conditions were returned to those shown in Table 30 and then a bedding-in cut was again performed, followed by two data acquisition cuts.

Data acquisition and signal processing were identical to that carried out in the random walk experiments.

4.9 Summary of Experimental Work

The experiments that have been conducted and the data that has been acquired are summarised below:

(a) *Stiffness Tests*
Face milling on mild steel using a 6 point tool whilst monitoring AE and vibration.

(b) *Geometry Tests*
Face milling on En8 using a 4 point tool whilst monitoring force, AE and vibration.

(c) *Wear Tests*
Face and groove milling on En8, En24 and En24T using 2, 4 and 8 point pools whilst monitoring using force, AE, vibration, surface finish and spindle current.

(d) *Breakage Tests*
Face milling on En8 and En24T using 4 and 8 point tools whilst monitoring using force, AE, vibration and spindle current.

(e) *Cutting Conditions*
Face milling on En24 using a 8 point tool whilst monitoring force, AE, spindle current and surface finish.

Chapter 5

Experimental Results

This Chapter describes the results obtained during the series of experiments conducted on the En8 and En24 workpiece materials. Analysis and discussion of these results is deferred to the next Chapter. The experiments performed and the objectives are listed again below in the order in which they are presented:

(a) *Influence of Machine Stiffness on Sensorial Information*
An investigation, using a variable stiffness platform, of the effect of the machine stiffness on AE, workpiece vibration and cutting force, whilst machining on mild steel with a six point face milling cutter.

(b) *Influence of Insert Geometry on Sensorial Information*
An investigation of specific wear geometries and their effect on sensorial data. Artificial means were used to simulate progressive degradation including flank and crater wear and instantaneous degradation, particularly edge breakdown.

(c) *Progressive Degradation Studies*
An investigation of progressive wear using three tools, two face milling and one grooving, on three different steels.

(d) *Instantaneous Degradation*
An investigation of insert breakage under a variety of different circumstances, including a pre-cracked insert, hard patches in a workpiece, edge chipping, and operator/program error.

(e) *Influence of Cutting Conditions on Sensorial Information*
An investigation of the influence of cutting speed, feed rate and depth of cut on AE, spindle current and cutting force whilst machining En24 with an eight point face milling cutter.

5.1 Influence of Machine/Fixture Stiffness on AE and Workpiece Vibration.

The first machining experiment conducted was one to determine the effect of the machine/fixture stiffness on the Acoustic Emission signal. As it is to be expected that the cutting force, vibration and spindle current readings will be machine specific, it was hoped that the AE signal would remain independent of the particular machine that was performing the cutting.

5.1.1 Results Obtained from Monitoring the Acceleration of the Workpiece

Figures 69, 70 and 71 show the spectra of acceleration in the feed direction for rough face milling. These were obtained using a spectrum analyser to calculate thirty two consecutive averages of five hundred and twelve points from the output of the accelerometer. As can be seen, the first peak in the power spectra corresponds to the tooth passing frequency. The peaks at higher frequencies are harmonics of this fundamental cutting frequency, and it can be seen that these are larger in amplitude when one of these harmonics lies close to the natural frequency of the platform. This being 344 Hz for the 20 mm pillars, 380 Hz for the 30 mm pillars and 420 Hz for the 40 mm pillars. A comparison of amplitudes at these frequencies shows that there is a general drop in amplitude as the pillar diameter increases, the larger difference being between the 20 mm and 30 mm pillar sets.

5.1.2 Results from Monitoring the rms AE

Amplitude Distribution of the rms AE

Table 33 shows the variation in the amplitude distribution parameters of the rms AE signal for pillar diameters of 20 mm, 30 mm and 40 mm. The values were obtained from the AE signal by first using the true rms processor with an averaging time of 5.5 ms and then performing an amplitude distribution analysis of the resulting rms time series. Figures 72 to 74 show the resulting distributions and it can be seen that there is no obvious systematic difference between them.

Frequency Analysis

The estimates of the power spectra, obtained from the Fast Fourier Transform (FFT) of the rms AE signal, can be seen in Figures 75 to 77 for each of the pillar diameters. The amplitude scale is in decibels referenced to 1 mV and it can be

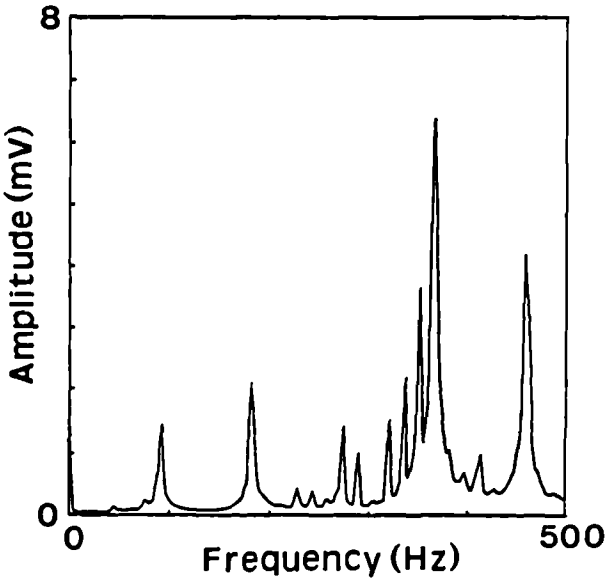

Figure 69: Power Spectrum of the Acceleration for 20mm Pillars

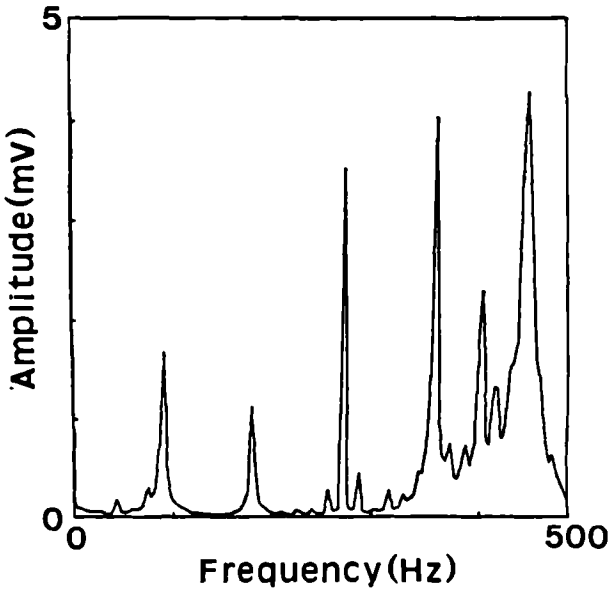

Figure 70: Power Spectrum of the Acceleration for 30mm Pillars

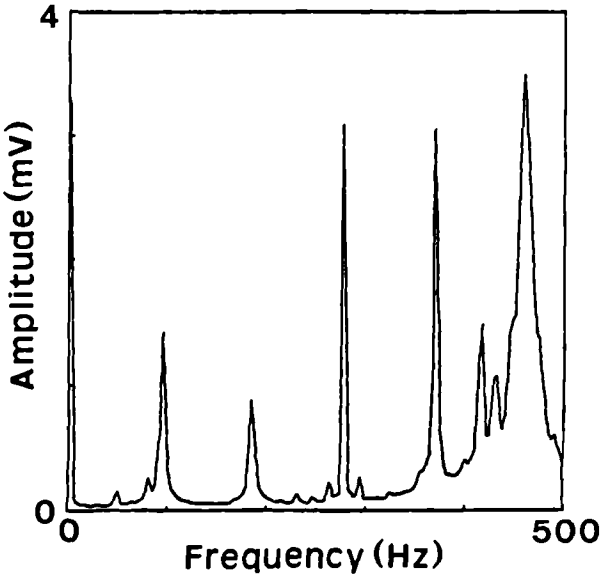

Figure 71: Power Spectrum of the Acceleration for 40mm Pillars

Pillar Diameter	Mean	Standard Deviation	Skew	Kurtosis
20mm	1.7	0.4	0.08	2.7
30mm	1.6	0.4	0.6	3.7
40mm	1.7	0.4	0.4	3.1

Table 33: Amplitude Distribution Parameters

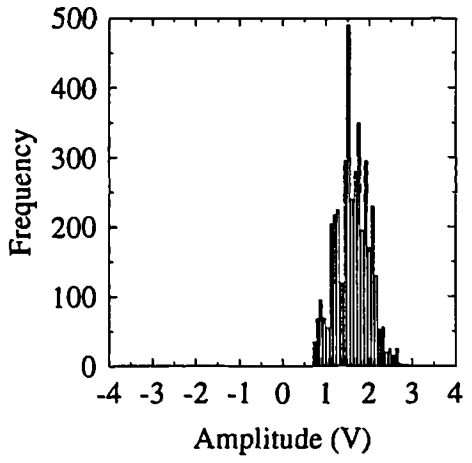

Figure 72: Amplitude Distribution of the rms AE for Cutting on the 20 mm Pillars

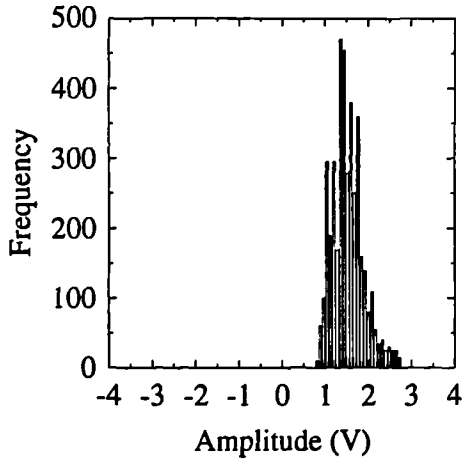

Figure 73: Amplitude Distribution of the rms AE for Cutting on the 30 mm Pillars

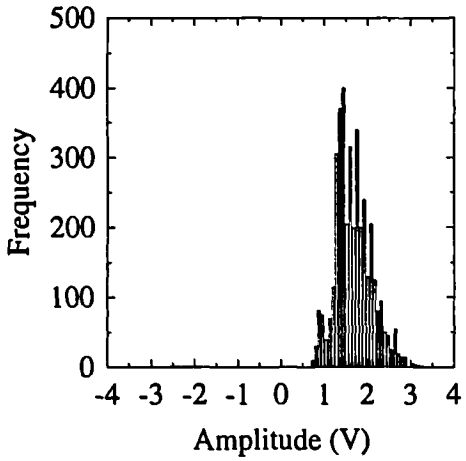

Figure 74: Amplitude Distribution of the rms AE for Cutting on the 40 mm Pillars

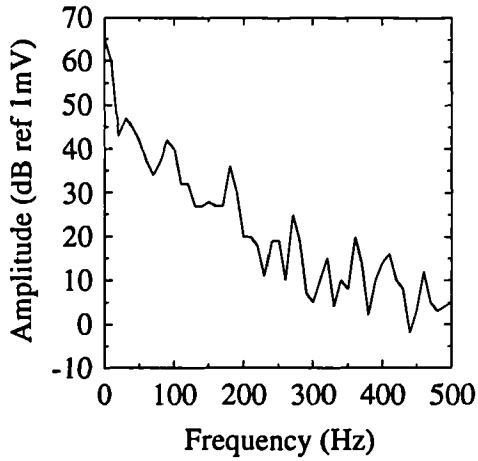

Figure 75: Power Spectrum of the rms AE Signal for Cutting on the 20mm Pillars

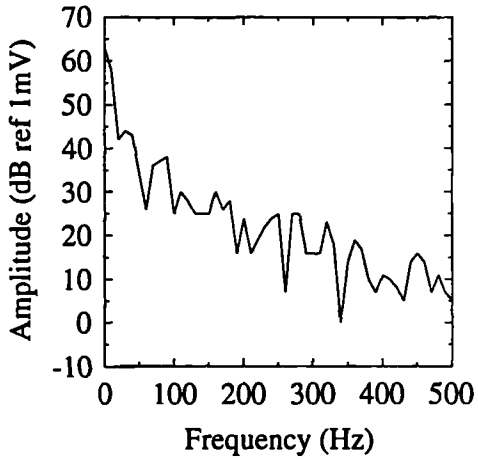

Figure 76: Power Spectrum of the rms AE Signal for Cutting on the 30mm Pillars

seen that there is no amplification of the rms AE signal in the region at which amplification was found in the corresponding acceleration spectra.

5.2 Results from Investigating the Influence Artificial Inserts have on Sensorial Information

As has already been described, four inserts were precision ground to include such geometries as different local rake angles, major flank wear, craters and simulations of edge breakdown. This was an attempt to isolate the various effects such wear geometries have on sensorial information, as it is normal for some or all of these profiles to evolve together when a tool wears. In order to analyse the effects of the artificial geometries, one insert was placed in the tool holder with three control

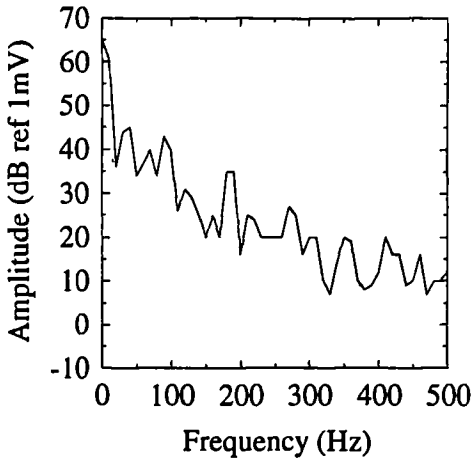

Figure 77: Power Spectrum of the rms AE Signal for Cutting on the 40mm Pillars

inserts which had neither simulated nor natural wear. Three cuts were then performed to 'bed' the geometry in before three cuts were performed to acquire data. The results from each of the different types of artificial wear geometry are presented below.

5.2.1 Simulation of Major Flank Wear

Figures 78 to 81 show the results obtained from an analysis (across all inserts in the tool holder) of the data obtained whilst machining with one insert having simulated flank wear.

Figure 78 shows that there is a general tendency for the perpendicular component of the cutting force to decrease with increasing flank wear although the point corresponding to zero flank wear is anomalously low. The feed component of force, shown in Figure 79 displays a much more linear trend with tool wear and tends to increase with simulated wear.

The plot of the 0.5 ms rms AE, shown in Figure 80 reflects that shown by the perpendicular cutting force. However, the variations between data points at the same wear level are as large as the variations across the flank wear range.

The perpendicular component of workpiece acceleration, does not exhibit any noticeable variation with artificial tool wear. This can be seen in Figure 81, where the data values for this sensor lie on an almost horizontal line with a high degree of scatter.

5.2.2 Artificial Craters and Cutting Edge Degradation

Figures 82, 84, 86 and 88 show the results from the perpendicular and feed components of cutting force, 0.5 ms rms AE and the perpendicular acceleration

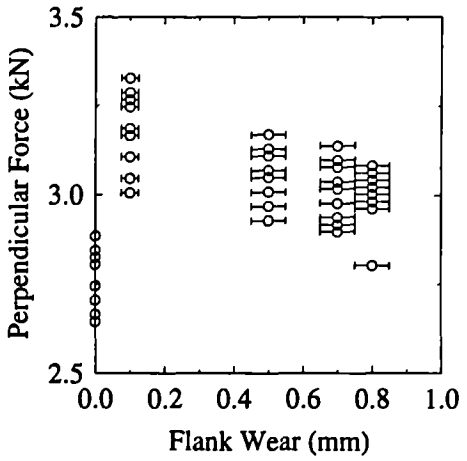

Figure 78: Changes in Perpendicular Cutting Force for Simulated Flank Wear in one Insert

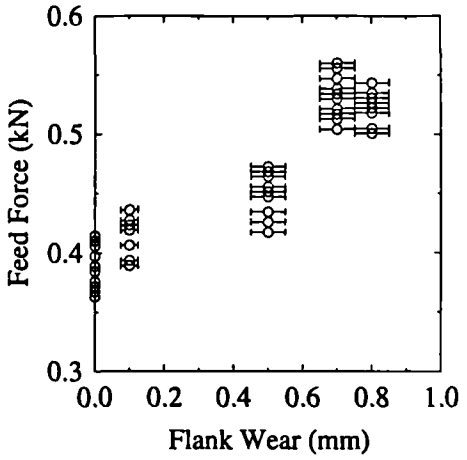

Figure 79: Changes in Feed Cutting Force for Simulated Flank Wear in one Insert

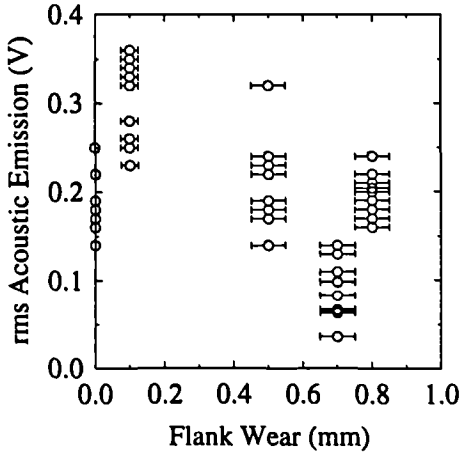

Figure 80: Changes in 0.5 ms rms AE for Simulated Flank Wear in one Insert

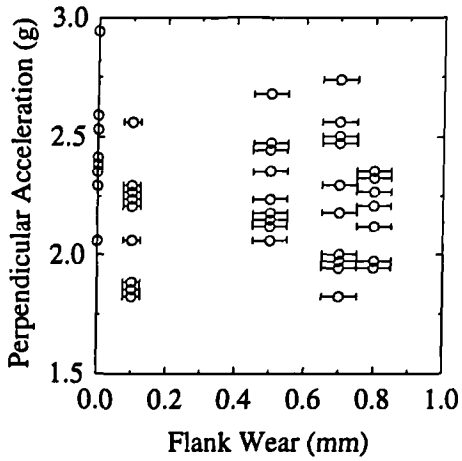

Figure 81: Changes in Perpendicular Acceleration for Simulated Flank Wear in one Insert

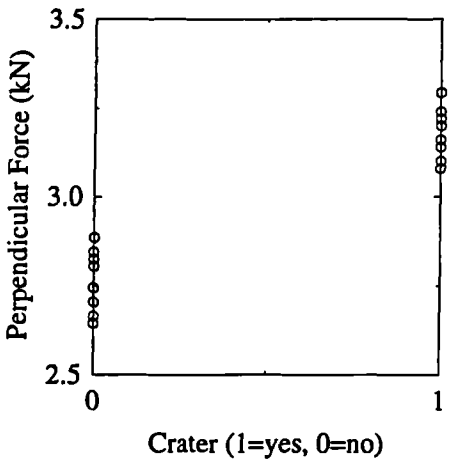

Figure 82: Changes in Perpendicular Cutting Force for an Artificial Crater in one Insert

respectively for crater wear and Figures 83, 85, 87 and 89 display results from the same sensors for the simulation of cutting edge breakdown with nicks on the rake face.

Results for these two different geometries will be presented together, as they both have the effect of disrupting the flow of chips over the rake face, and so some similarities might be expected between the results obtained.

The perpendicular force exhibits a similar variation for the two types of rake face geometry. For the case of one nick, or a crater, on the rake face, the level of the force increases from the level measured with control inserts. When an extra nick is added, no further increase is observed.

For the feed force any variation is within the spread of data from one cut. In general, it appears that these geometries cause a reduction in the feed force

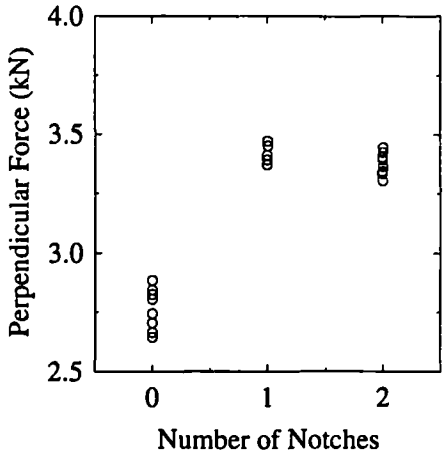

Figure 83: Changes in Perpendicular Force for a Simulated Edge Breakdown in one Insert

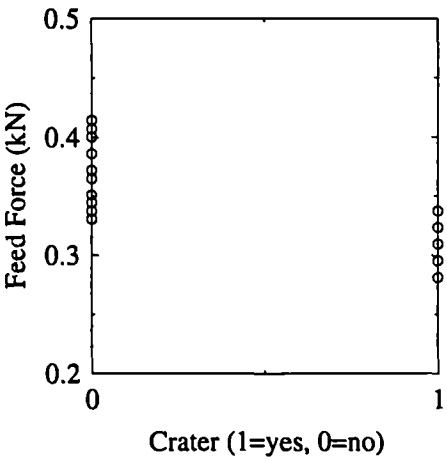

Figure 84: Changes in Feed Force for an Artificial Crater in one Insert

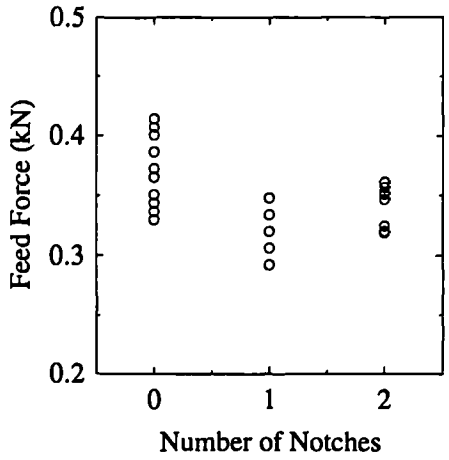

Figure 85: Changes in Feed Force for a Simulated Edge Breakdown in one Insert

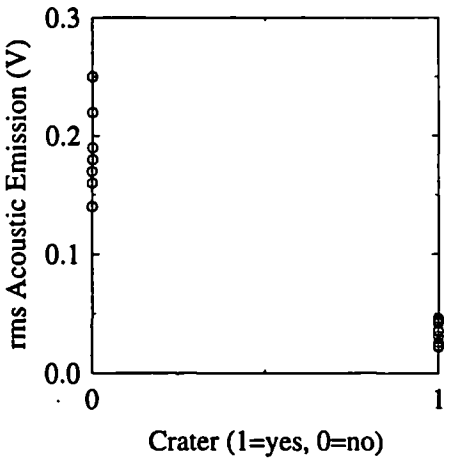

Figure 86: Changes in 0.5 ms rms AE for an Artificial Crater in one Insert

required for cutting. For the case of nicks on the rake face the effect on the level of the feed force again does not appear to depend greatly upon whether one or two nicks are present on the rake face.

The variation in the rms AE is perhaps the most consistent and, for both geometries, there is a marked reduction in the AE signal giving a rms value which is similar for all these types of geometry on the rake face.

The perpendicular acceleration is also quite a repeatable parameter to measure for the geometries tested. There appears to be a monotonic reduction in the acceleration with increasing numbers of nicks on the rake face and, for the artificial crater, there is a small but repeatable reduction of the vibration level.

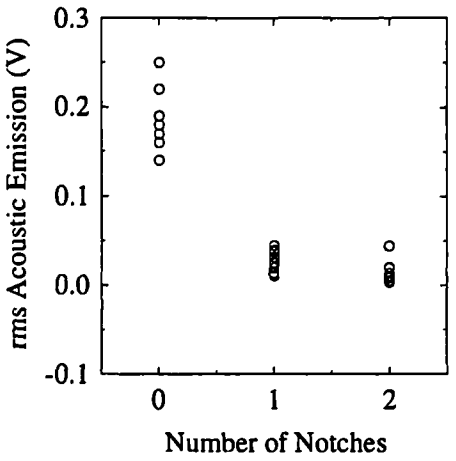

Figure 87: Changes in 0.5 ms rms AE for a Simulated Edge Breakdown in one Insert

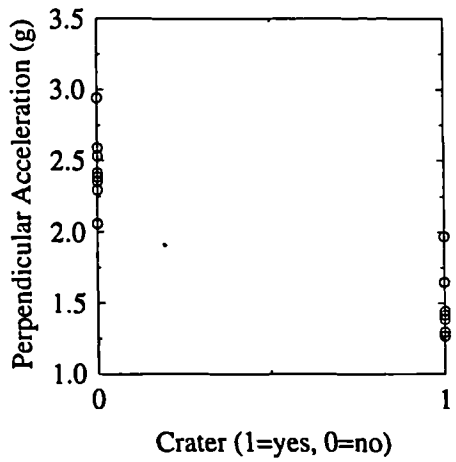

Figure 88: Changes in Perpendicular Acceleration for an Artificial Crater in one Insert

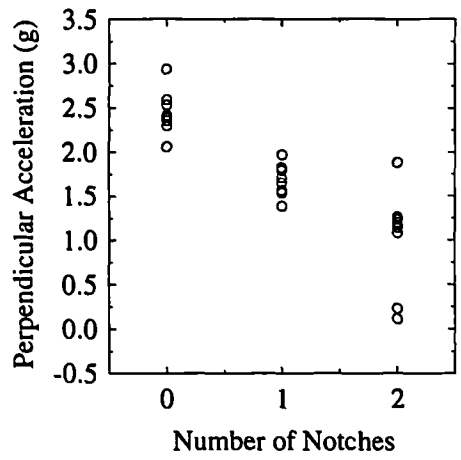

Figure 89: Changes in Perpendicular Acceleration for a Simulated Edge Breakdown in one Insert

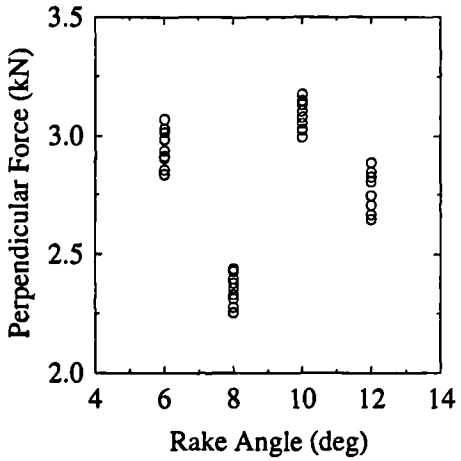

Figure 90: Changes in Perpendicular Cutting Force for Changes in Local Rake Angle

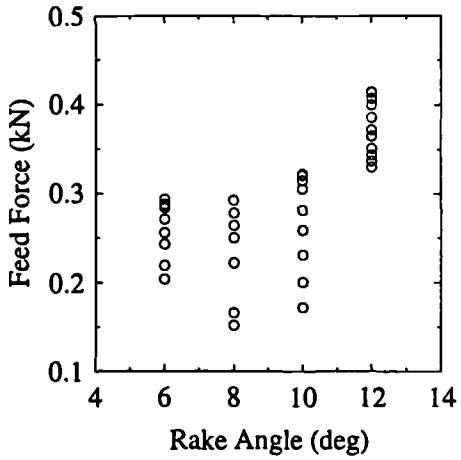

Figure 91: Changes in Feed Cutting Force for Changes in Local Rake Angle

5.2.3 Changes in the Local Rake Angle

Figures 90 to 93 display results from the perpendicular and feed components of cutting force, the 0.5 ms rms AE and the perpendicular acceleration respectively for changes in the local rake angle of one of the inserts.

Although there are some variations in sensor output for changes in local rake angle, it would appear that none shows a consistent trend with the possible exception of feed force.

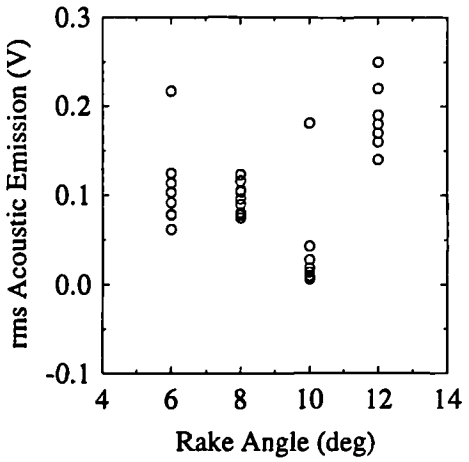

Figure 92: Changes in rms AE for Changes in Local Rake Angle

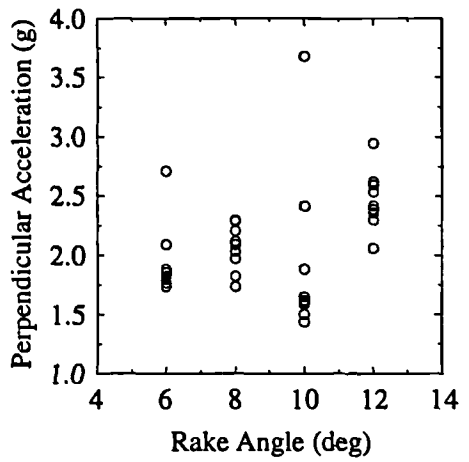

Figure 93: Changes in Perpendicular Acceleration for Changes in Local Rake Angle

Material	Cutting Operation
En8	Roughing
En24T	Roughing, Finishing and Grooving
En24	Roughing, Finishing and Grooving

Table 34: Summary of Wear Experiments Conducted

5.3 Results from Systematic Wear Tests on En8 and En24 Workpiece Materials

As mentioned earlier, results from systematic wear tests have been obtained on two different materials under a variety of cutting operations and conditions. Table 34 summarises these experiments and the results will be presented below in the order in which they appear in this Table.

5.3.1 Results for Machining En8 in the Fully Annealed Condition

The first test conducted was a face milling test on En8 material using roughing conditions.

Face Milling using Roughing Conditions

Figure 94 shows the wear evolution of the tool with time and it can be seen that, at the start of tool life, the wear rate is relatively high, levelling off in the middle, and increasing again towards the end of the tool life. The wear rate for the test on En8 is very different from that on En24(T), with a tool life of 350 minutes as opposed to around 30 minutes. It should also be noted that rather a long time was spent with VB_B between 0.4 and 0.6 mm and the following data should be interpreted in that light.

Figure 95 shows the variation in the perpendicular cutting force with mean flank wear. This component of the cutting force exhibits a general increase with increasing tool wear. The variation in the feed component of cutting force is rather less consistent with some very large scatter and even negative values at larger VB_B levels (Figure 96).

Figure 97 displays the variation of the perpendicular component of acceleration. It can be seen that this component shows a similar trend to the perpendicular force.

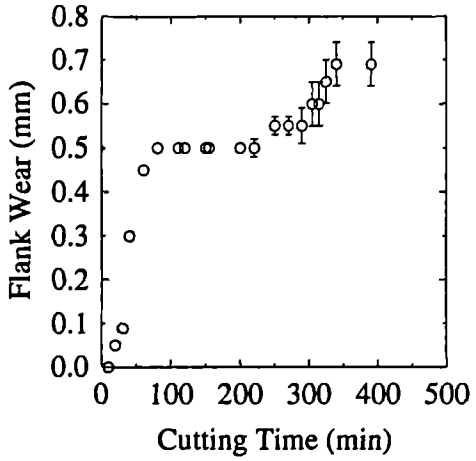

Figure 94: Flank Wear vs Cutting Time for Face Milling under Roughing Conditions of En8 Material

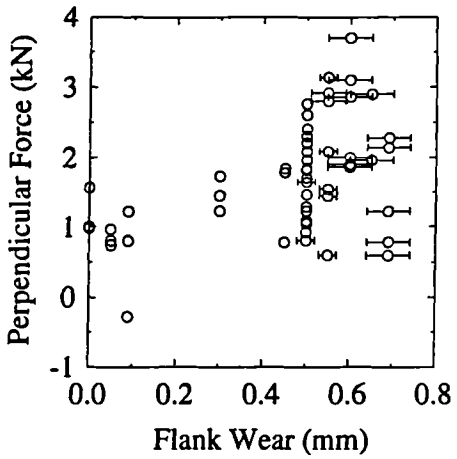

Figure 95: Perpendicular Force vs Flank Wear for Face Milling on the En8 Material under Roughing Conditions

For the remaining sensors, It can be seen that the rms AE exhibits a general trend to increase with tool wear (Figure 98) and the surface finish (R_a) tends to decrease with wear initially and then begins to increase at an approximate VB_B level of 0.5 mm, although there is variability in both VB_B and R_a (Figure 99). This behaviour is also exhibited in later experiments.

For later consideration, the chip temperature was estimated by temper colour and Figure 100 shows that the temperature increases consistently with tool wear.

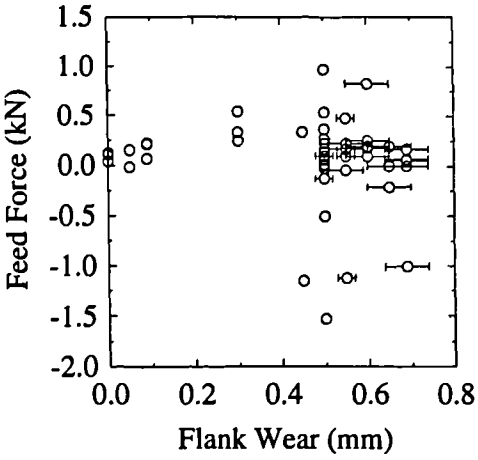

Figure 96: Feed Force vs Flank Wear for Face Milling on the En8 Material under Roughing Conditions

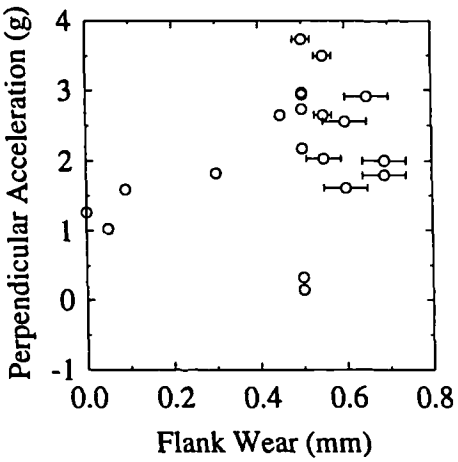

Figure 97: Perpendicular Acceleration vs Flank Wear for Face Milling on the En8 Material under Roughing Conditions

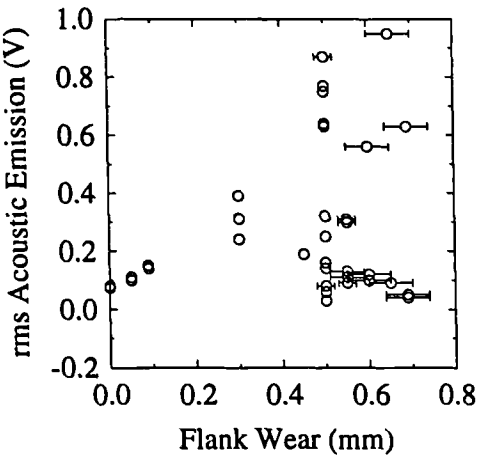

Figure 98: Variation in the rms AE vs Flank Wear for Face Milling on the En8 Material under Roughing Conditions

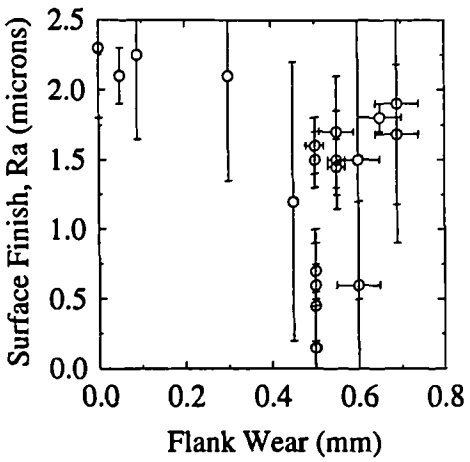

Figure 99: Surface Finish, R_a vs Flank Wear for Face Milling on the En8 Material under Roughing Conditions

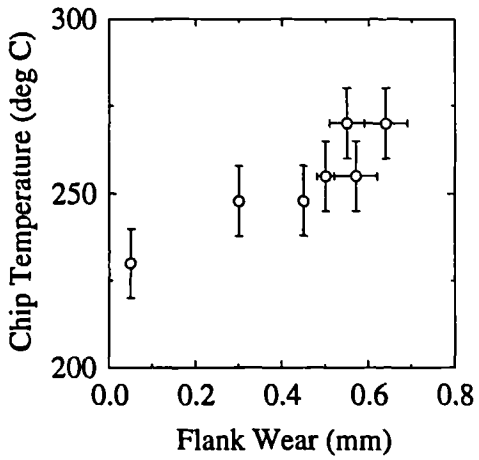

Figure 100: Chip Temperature vs Flank Wear for Face Milling on the En8 Material under Roughing Conditions

5.3.2 Results for Machining En24 in the Quenched and Tempered Condition

As mentioned earlier, the following tests on En24 material were each repeated under nominally identical conditions and the two sets of results are illustrated as solid and open circular points in the following Figures.

Face Milling using Roughing Conditions whilst Machining En24T

It can be seen from Figure 101 that the wear evolution is a broad linear one with only minor differences between the two tests, one exhibiting a generally higher wear rate and a slightly different evolution.

As seen from Figure 102, spindle current shows an almost linear evolution with flank wear. The perpendicular component of the cutting force, in Figure 103, follows a quite unexpected trend with wear. Starting with a new tool, the force exhibits a slight decrease as wear increases to around 0.4 mm. Then there is a significant jump from around 6 kN to just under 8 kN, after which this force component continues to decrease up to the end of the tool life. This behaviour is seen very clearly in one of the tests (solid points) but less so in the other (open points). The feed component of the cutting force, presented in Figure 104, exhibits a linear trend with flank wear and, although the slope of this evolution is similar for both tests, the intercepts are significantly different. The perpendicular acceleration generally decreases as tool wear increases (Figure 105), but again the two sets of data are quite different especially at the start of the wear tests. The discontinuities observed in the perpendicular force do not seem to be exhibited in the corresponding perpendicular acceleration.

Figure 106 shows the variation in the rms AE with tool wear and, despite some scatter, it will be noticed that the rms AE signal generally decreases with increasing tool wear with a very large drop in amplitude for the last few cuts of the test. For this test the cumulative rms AE shows a sigmoid-shaped variation with tool wear, as seen in Figure 107. Figures 106 and 107 only show one data set due to an error during data collection. Apart from one point, the mean AE frequency shown in Figure 108 lies around 100 kHz and does not appear to vary with wear but there is a small degree of scatter, around 50 kHz wide. Some interesting points arise from a band analysis of the AE, shown in Figure 109. There is a distinct rise in the energy in the 100 - 200 kHz band at a flank wear level of 0.25 to 0.3 mm and the next two frequency bands, 200 - 300 kHz and 300 - 400 kHz, either show no obvious increase in energy or the energy in the band drops slightly with wear.

Figure 110 shows the variation in the R_a value. From this plot it can be seen that the surface finish remains broadly constant with tool wear, although it might be noticed that there is a slight dip in the value of R_a at a value of around a mean flank wear value of 0.3 mm. Mean values are reasonably repeatable between the

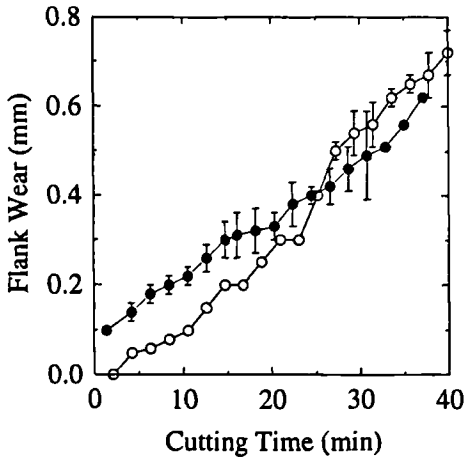

Figure 101: Flank Wear vs Cutting Time for Rough Machining of the En24T Material

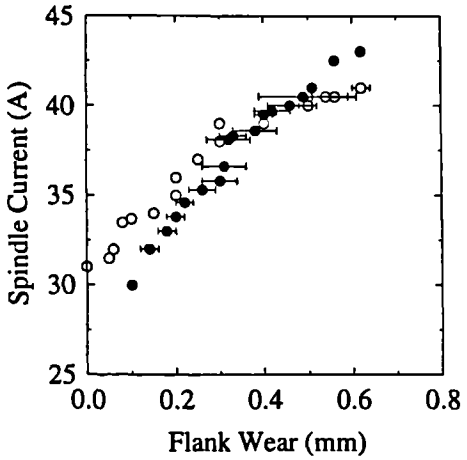

Figure 102: Spindle Current vs Flank Wear for Rough Machining of the En24T Material

two tests, although the test with solid points does not exhibit the same evolution with wear and the error bar is large for both tests.

Face Milling using Finishing Conditions Whilst Machining En24T

For wear tests on En24T using finish face milling, flank wear was very rapid so that for one of the wear tests (open points in Figure 111), only five data points were acquired through the life of the tool. The wear rate in this particular test was more rapid than the repeat test and was also not as linear as the repeat. The variation in spindle current (Figure 112) with flank wear for the two tests follows the wear evolutions with time in a very repeatable manner with two different gradients of spindle current with tool wear for the two nominally identical tests. The perpendicular component of cutting force (Figure 113) exhibits a linear

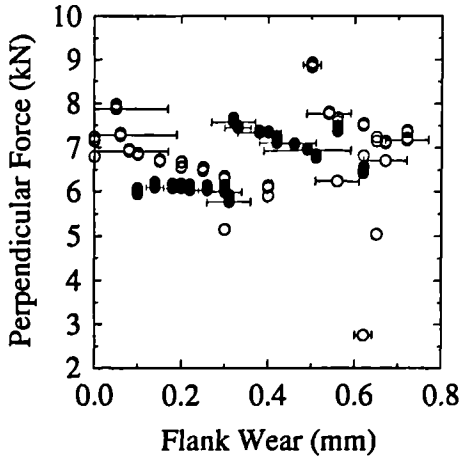

Figure 103: Perpendicular Force vs Flank Wear for Rough Machining of the En24T Material

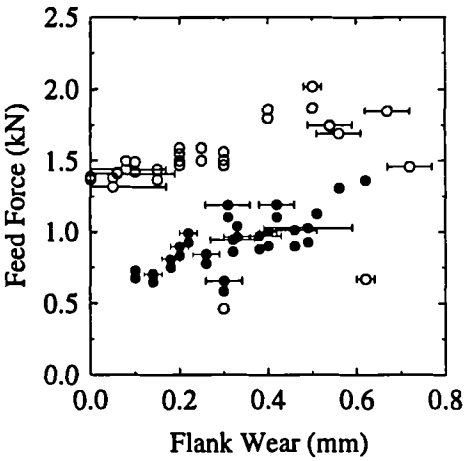

Figure 104: Feed Force vs Flank Wear for Rough Machining of the En24T Material

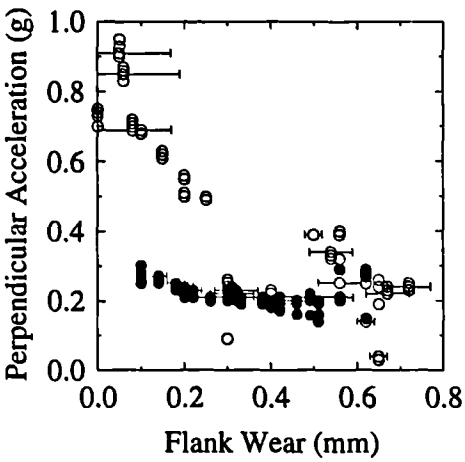

Figure 105: Perpendicular Acceleration vs Flank Wear for Rough Machining of the En24T Material

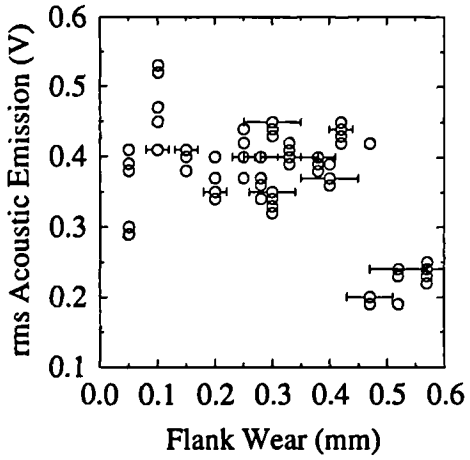

Figure 106: rms AE vs Flank Wear for Rough Machining of En24T

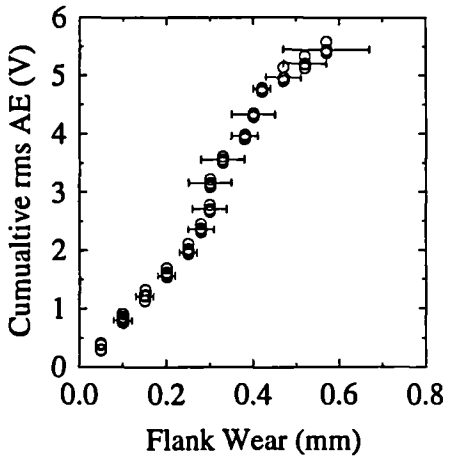

Figure 107: Cumulative rms AE vs Flank Wear for Rough Machining of the En24T Material

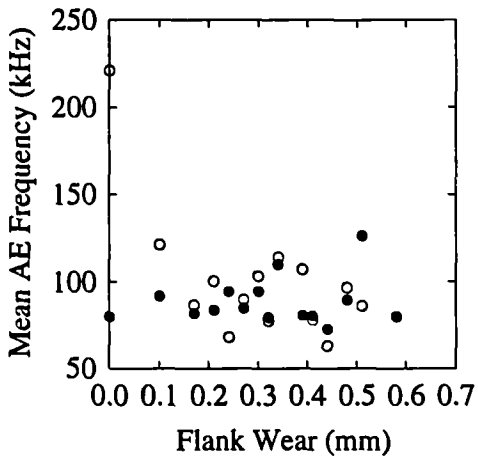

Figure 108: Mean AE Frequency vs Flank Wear for Rough Machining of the En24T Material

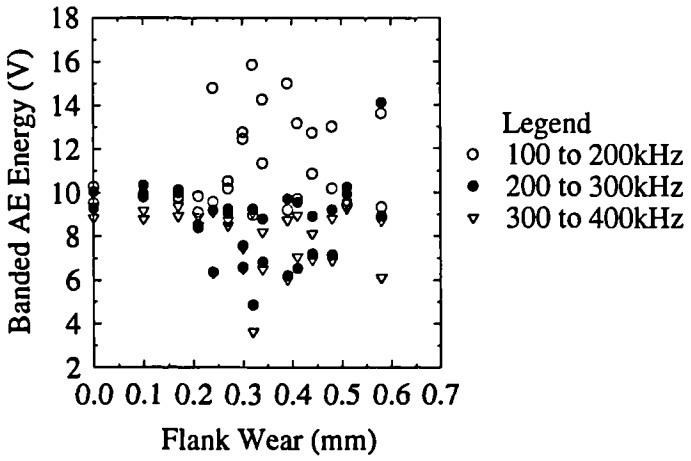

Figure 109: Banded AE Energy vs Flank Wear for Rough Machining of the En24T Material

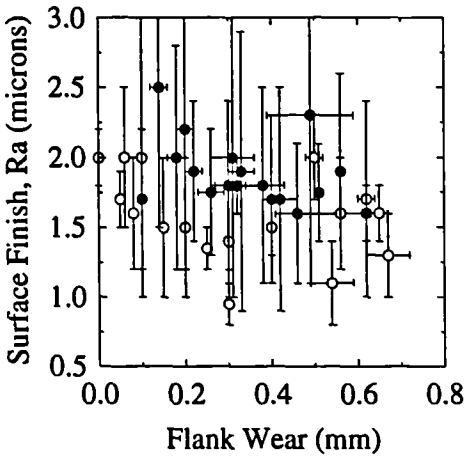

Figure 110: Surface Finish (R_a) vs Flank Wear for Rough Machining of the En24T Material

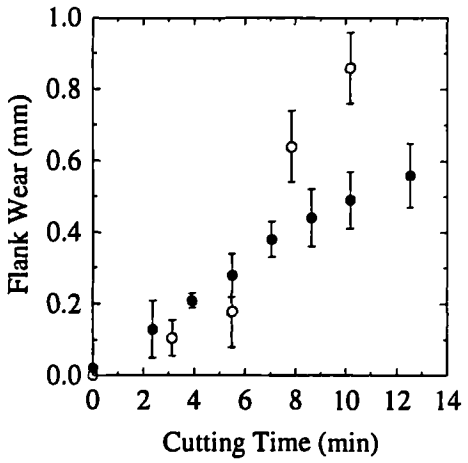

Figure 111: Flank Wear vs Cutting Time for Finish Machining of the En24T Material

and repeatable decrease with increasing tool wear although the feed component (Figure 114) seems to indicate some anomalous effect during the first test (open points) where the evolution is less linear and exhibits a wider variation than the repeat. It is also evident in both tests that the feed force displays a greater scatter at the end of cutter life than at the beginning. The data on perpendicular acceleration, Figure 115, shows a wide scatter both with and between cuts.

Acoustic emission is perhaps the most repeatable of the sensors in this experiment and is shown in Figure 116. For this set of conditions, the rms AE shows a general increase with flank wear and, of course, the cumulative rms AE also rises monotonically with tool wear, as shown in Figure 117. Figure 118 shows a plot of mean AE frequency against flank wear and it appears that there is a slight tendency for the mean AE frequency to decrease with flank wear but the data are generally a little too sparse to draw firm conclusions. In Figure 119, it can be seen that the energy in the 100 - 200 kHz band increases quite dramatically at around 0.3 mm of flank wear whereas there appears to be a slight tendency for the energy in the next two bands to drop with increasing wear. Surface finish for these tests exhibits a tendency for the minimum value for R_a to occur at around 0.3 to 0.4 mm of flank wear (Figure 120). The repeatability between tests is good, but, as usual, there is quite a large variation in the R_a values measured from any one cut.

Groove Milling using Roughing Conditions whilst Machining En24T

Grooving on En24T workpieces has been one of the most repeatable of all wear tests, with very little difference between the two experiments in the manner in which flank wear evolved with time spent cutting, Figure 121. Both evolutions are almost linear with time, although there is a small drop in the wear rate at a point approximately half way through the life of the tool. Spindle current variations with flank wear (Figure 122) reflect this linear, repeatable trend with

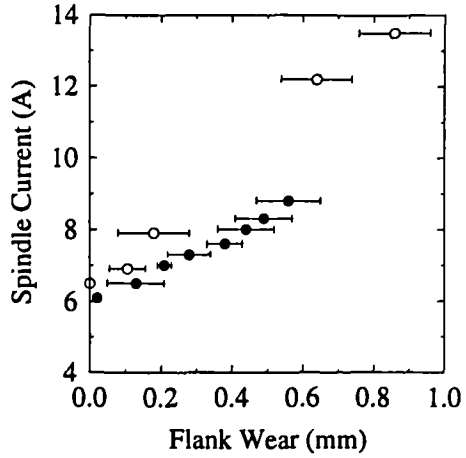

Figure 112: Spindle Current vs Flank Wear for Finish Machining of the En24T Material

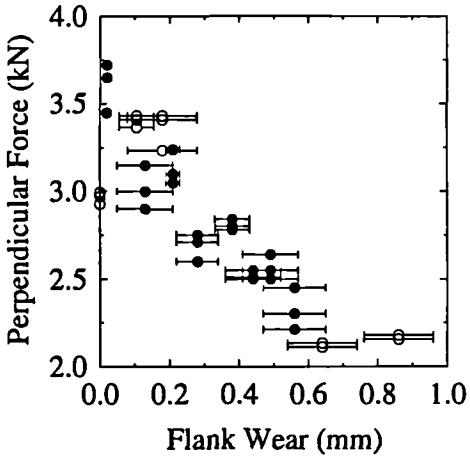

Figure 113: Perpendicular Force vs Flank Wear for Finish Machining of the En24T Material

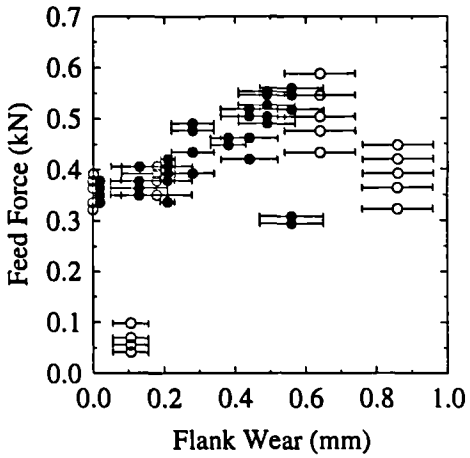

Figure 114: Feed Force vs Flank Wear for Finish Machining of the En24T Material

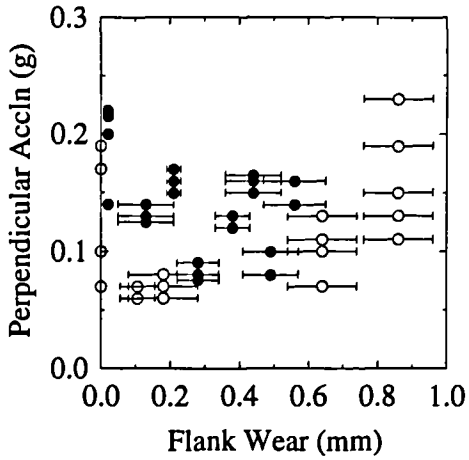

Figure 115: Perpendicular Acceleration vs Flank Wear for Finish Machining of the En24T Material

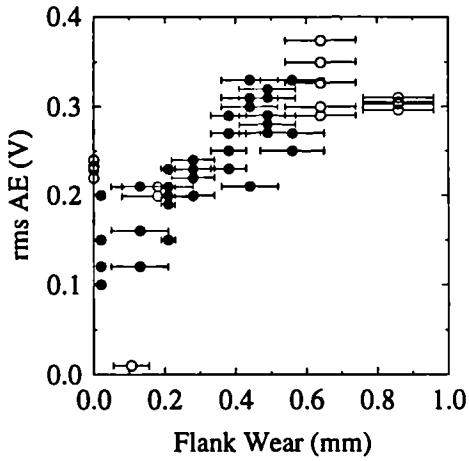

Figure 116: rms AE vs Flank Wear for Finish Machining of En24T

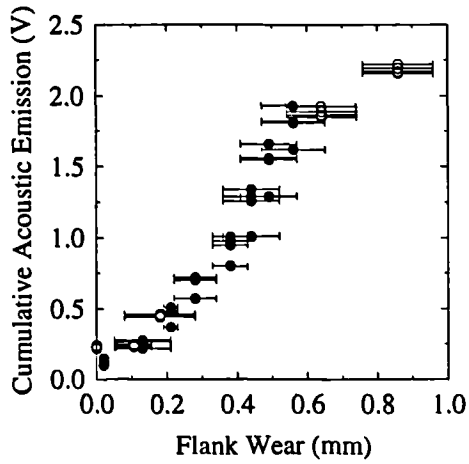

Figure 117: Cumulative rms AE vs Flank Wear for Finish Machining of the En24T Material

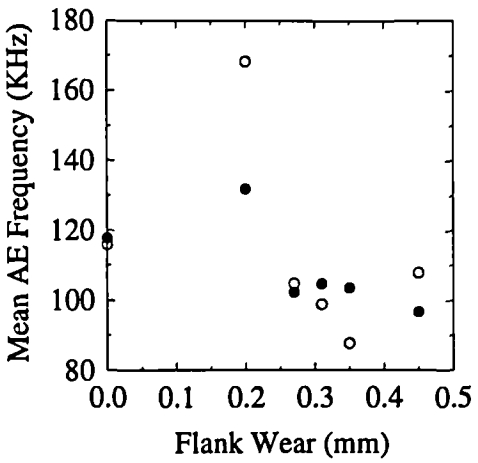

Figure 118: Mean AE Frequency vs Flank Wear for Finish Machining of the En24T Material

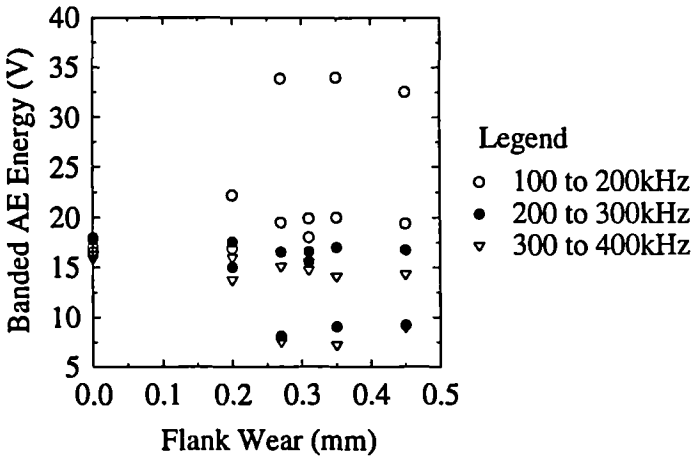

Figure 119: Banded AE Energy vs Flank Wear for Finish Machining of the En24T Material

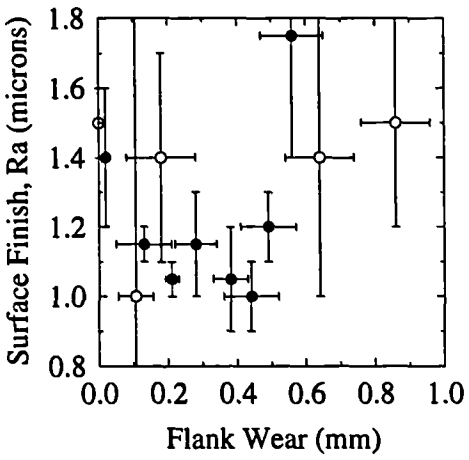

Figure 120: Surface Finish (R_a) vs Flank Wear for Finish Machining of the En24T Material

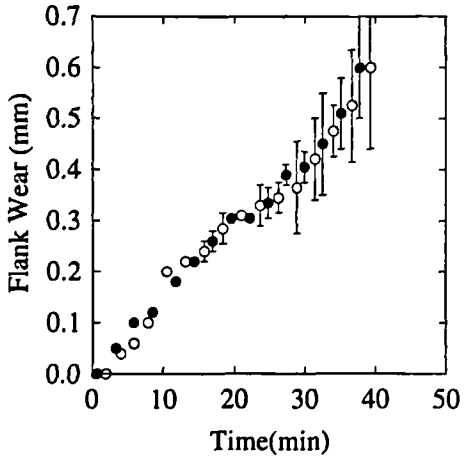

Figure 121: Flank Wear vs Cutting Time for Groove Machining of the En24T Material

one anomalous point (P1 in Figure 122). This demonstrates the sensitivity of this transducer to cutting conditions, as this data record was obtained when the feed rate was accidentally set at 65 % of the programmed value. The perpendicular force exhibits a similar trend to the spindle current, in that it generally increases with flank wear (Figure 123) although the scatter of results is much larger than for spindle current and there is an abnormally high value at VB_B=0 mm for one of the tests. The feed component of the cutting force (Figure 124) also increases monotonically with flank wear but does not display the sensitivity to the change in cutting conditions seen in the spindle current sensor. Figure 125 shows the evolution of the standard deviation of the perpendicular acceleration with wear and it can be seen that there is a very repeatable increase in this parameter with tool wear, although there are some points that lie higher than the general data set.

The rms AE signal, in Figure 126, is again fairly repeatable between tests and very repeatable during cuts but, under this set of conditions, the AE does not exhibit any clear trends to increase or decrease with flank wear although the values for a new tool appear to be lower than the general data set. The plots of cumulative rms AE shown in Figure 127 are broadly the same for both tests, with only a small difference occurring due to the slightly lower amplitudes for the second test. Figure 128 shows the variation in the mean AE frequency with wear. It appears that there is quite a large scatter in the mean values or, perhaps more importantly, that there are two values around which the mean value resides, 100 kHz or 130 kHz. In this particular test there does not appear to be any variation in the mean frequency with increasing wear. From the band analysis (Figure 129) it can be seen that there is a strong reduction in the energy in the 300 - 400 kHz band with tool wear. For the 100 to 200 kHz band there appears to be a small increase in energy with wear, whereas for the 200 to 300 kHz band there is no noticeable change with wear.

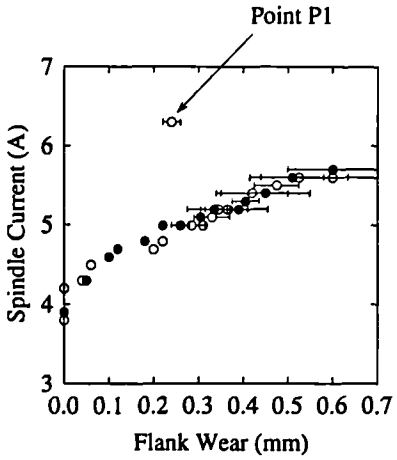

Figure 122: Spindle Current vs Flank Wear for Groove Machining of the En24T Material

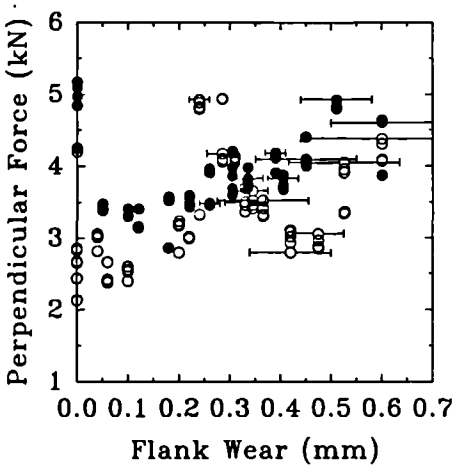

Figure 123: Perpendicular Force vs Flank Wear for Groove Machining of the En24T Material

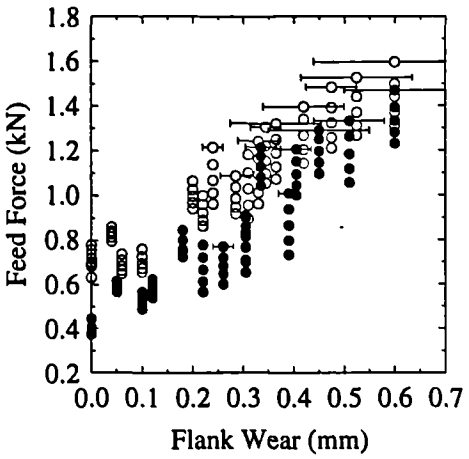

Figure 124: Feed Force vs Flank Wear

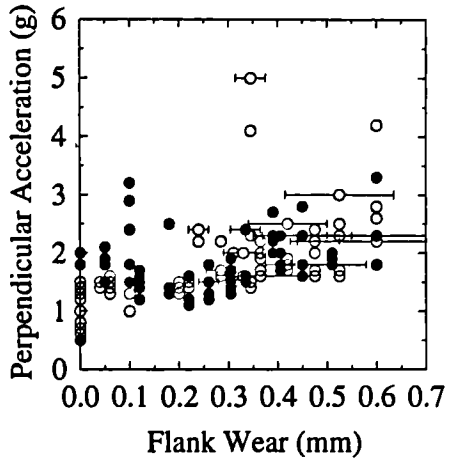

Figure 125: Perpendicular Acceleration vs Flank Wear for Groove Machining of the En24T Material

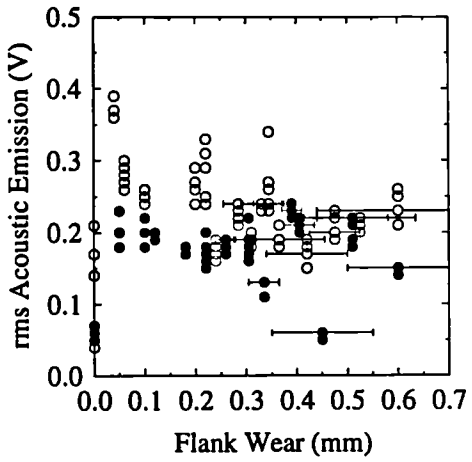

Figure 126: rms AE vs Flank Wear for Groove Machining of En24T

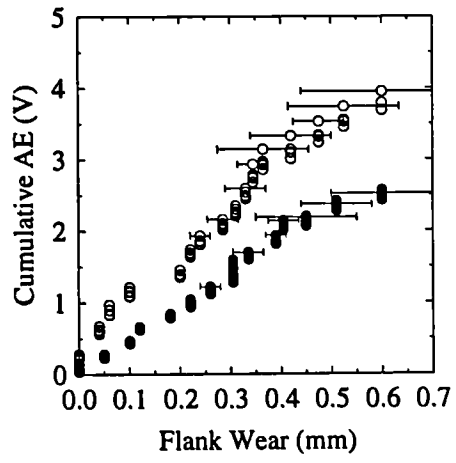

Figure 127: Cumulative rms AE vs Flank Wear for Groove Machining of the En24T Material

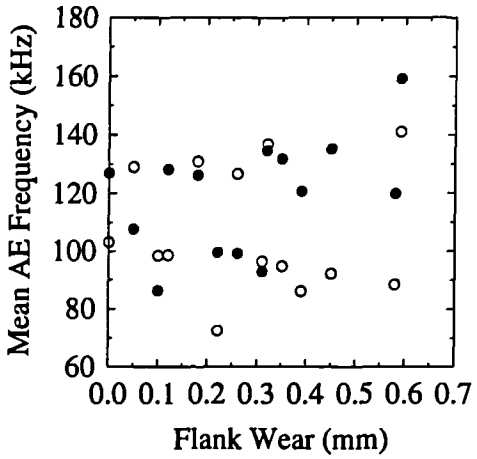

Figure 128: Mean AE Frequency vs Flank Wear for Groove Machining of the En24T Material

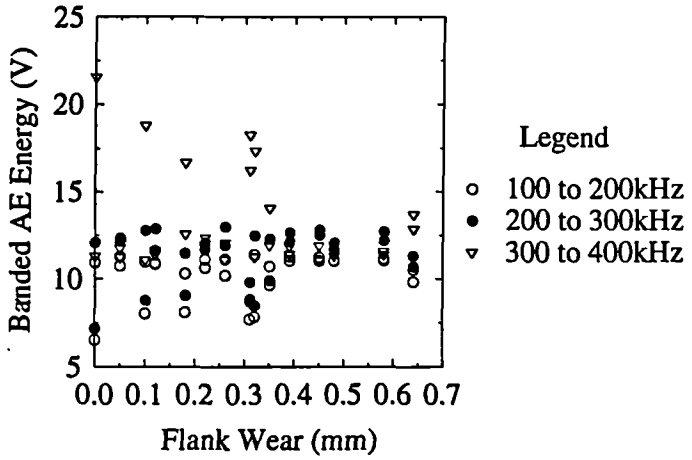

Figure 129: Banded AE Energy vs Flank Wear for Groove Machining of the En24T Material

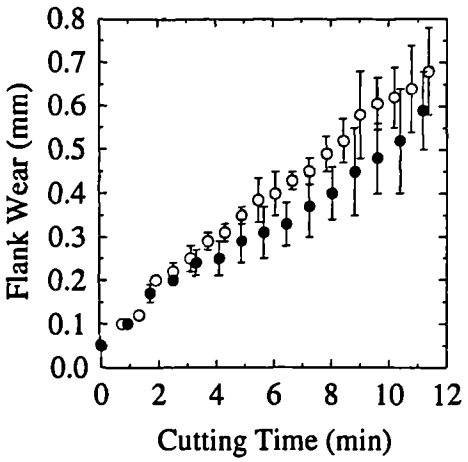

Figure 130: Flank Wear vs Cutting Time for Rough Machining of the En24 Material

5.3.3 Results for Machining En24 in the Fully Annealed Condition

Face Milling using Roughing Conditions whilst Machining En24

Increases in flank wear with cutting time (Figure 130) for this particular set of conditions are very repeatable and linear with time and this is reflected by the spindle current, Figure 131. The perpendicular component of the cutting force, shown in Figure 132, exhibits quite a consistent increase for one set although there is some scatter in the data values for the first test. The feed force (Figure 133) is quite repeatable between tests but the variation during a cut can be quite marked, (as much as 1 kN). The perpendicular acceleration (Figure 134), does not appear to vary much with tool wear and the rms AE (Figure 135) shows a tendency to increase but with some scatter. The cumulative rms AE shows a repeatable evolution with tool wear, as can be seen from Figure 136. There is a slight divergence of the two plots but this only occurs towards the end of the wear tests. Surface finish variations with tool wear are similar to those observed in other wear tests, Figure 137.

Face Milling of En24 using Finishing Conditions

Finishing conditions for this workpiece material produced a very repeatable set of wear evolutions with time (Figure 138) again with spindle current variations (Figure 139) which directly correspond with the variation in flank wear with time. The perpendicular component of cutting force (Figure 140) generally increases with increasing tool wear but the trends are not repeatable with around 1.5 kN separating the starting values of force between the two tests. Neither the feed force variation (Figure 141) nor the perpendicular acceleration (Figure 142) are

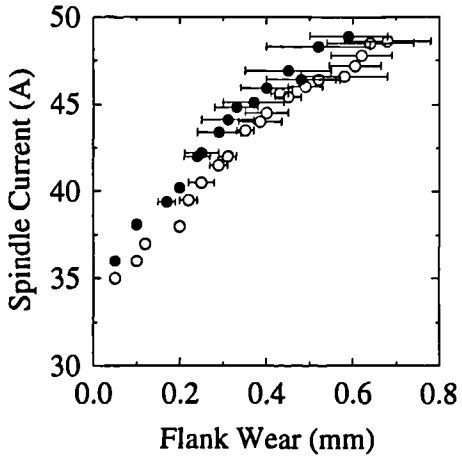

Figure 131: Spindle Current vs Flank Wear for Rough Machining of the En24 Material

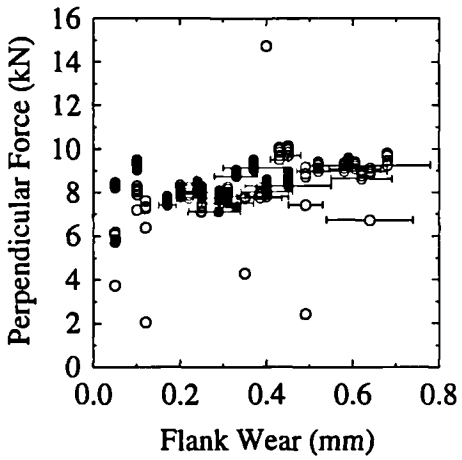

Figure 132: Perpendicular Force vs Flank Wear for Rough Machining of the En24 Material

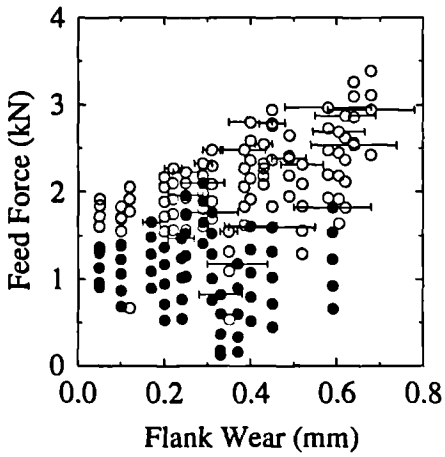

Figure 133: Feed Force vs Flank Wear for Rough Machining of En24

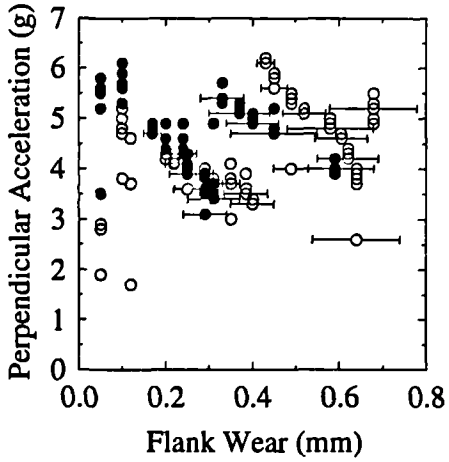

Figure 134: Perpendicular Acceleration vs Flank Wear for Rough Machining of the En24 Material

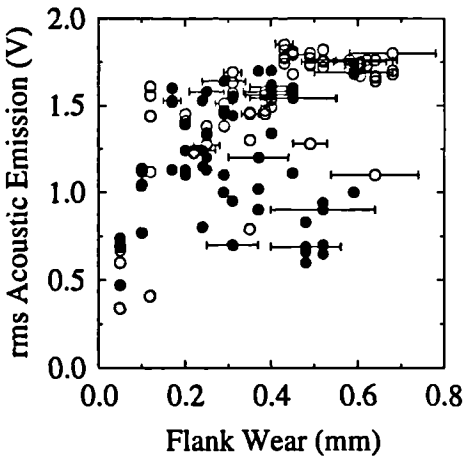

Figure 135: rms AE vs Flank Wear for the Rough Machining of En24 Material

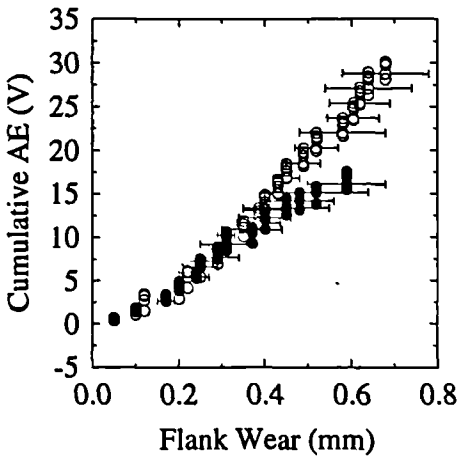

Figure 136: Cumulative rms AE vs Flank Wear for the Rough Machining of En24 Material

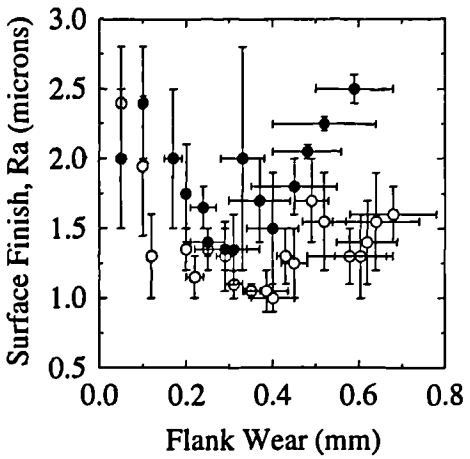

Figure 137: Surface Finish, R_a, vs Flank Wear for the Rough Machining of the En24 Material

as linear or repeatable as that of the spindle current but both could still be used as tool wear monitors even though the level of confidence would not be high.

The rms AE signal variation with tool wear (Figure 143) varies in a similar manner between tests but the level of the signal was markedly different. It should however, be noted that there was a change of workpiece between these two tests. The plot of cumulative rms AE can be seen in Figure 144 and there is a considerable difference between the two evolutions resulting from these different levels. In Figure 145, a plot of the mean AE frequency with increasing tool wear can be seen. Apart from the disparate values for a new tool, the mean frequency does not vary with tool wear to any noticeable degree. For this wear test there is no discernable change in the relative energy bands in AE with tool wear up to a flank wear value of 0.5 mm (Figure 146) where energies diverge, the 100 to 200 kHz value becoming the highest. From Figure 147 it is just possible to discern that for medium values of flank wear R_a values tend to be smaller than either for new or worn tools.

Groove Milling of En24 using Roughing Conditions

Flank wear varied fairly linearly with cutting time in this test (Figure 148), although it is not possible to assess the repeatability of this result. Again, spindle current (Figure 149) reflected the behaviour of flank wear. The perpendicular component of the cutting force also exhibits quite a linear trend with tool wear, as shown in Figure 150, but again the data tend to spread towards the end of the test. The feed force variation in any one cut can be quite large the spread again being largest towards the end of the cut, Figure 151. The perpendicular component of workpiece acceleration generally exhibits an increase with increasing tool wear. although again there is quite a large spread of data points commencing at around 0.6 mm of flank wear (Figure 152).

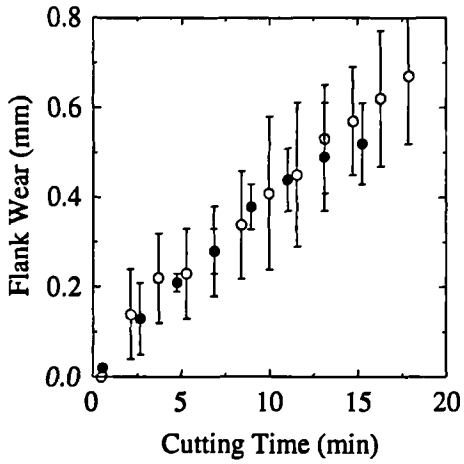

Figure 138: Flank Wear vs Cutting Time for the Finish Machining of the En24 Material

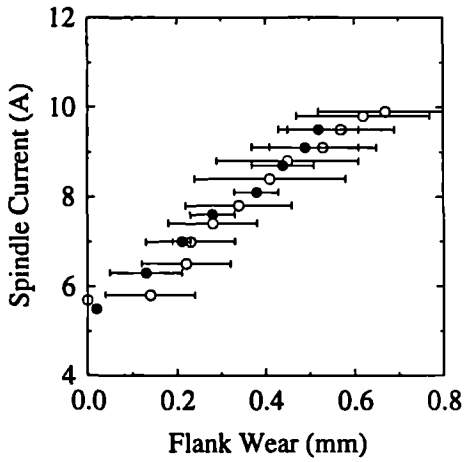

Figure 139: Spindle Current vs Flank Wear for the Finish Machining of the En24 Material

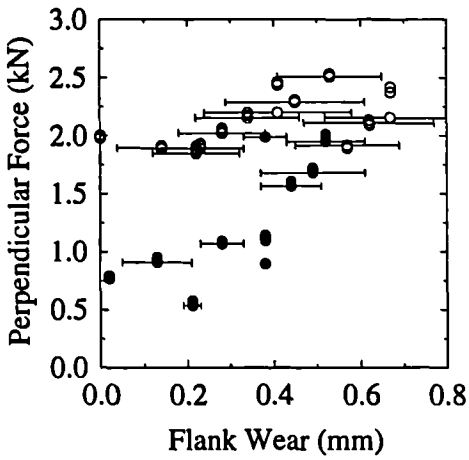

Figure 140: Perpendicular Force vs Flank Wear for the Finish Machining of the En24 Material

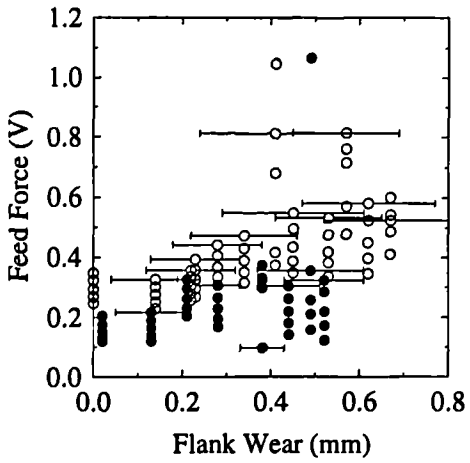

Figure 141: Feed Force vs Flank Wear for the Finish Machining of the En24 Material

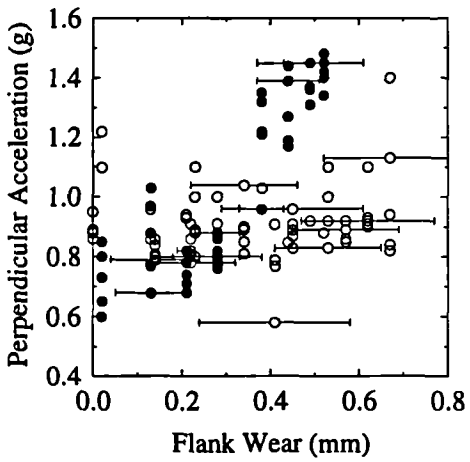

Figure 142: Perpendicular Acceleration vs Flank Wear for the Finish Machining of the En24 Material

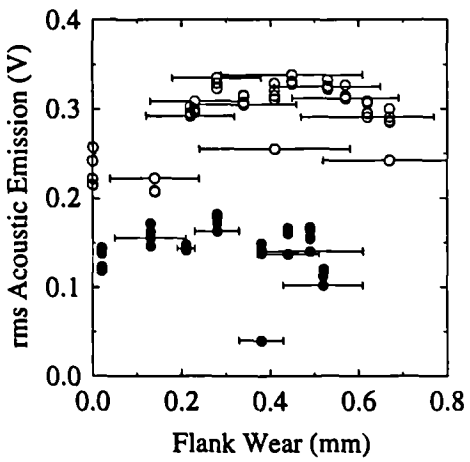

Figure 143: rms AE vs Flank Wear for the Finish Machining of En24

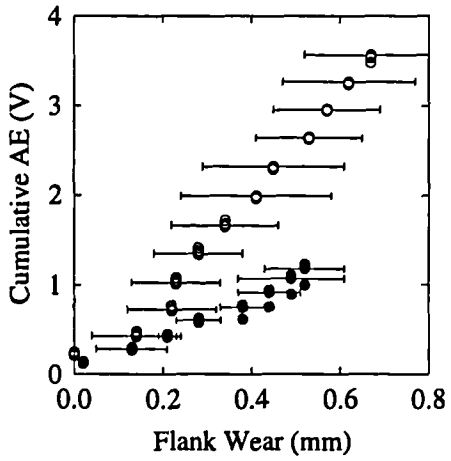

Figure 144: Cumulative rms AE vs Flank Wear for the Finish Machining of the En24 Material

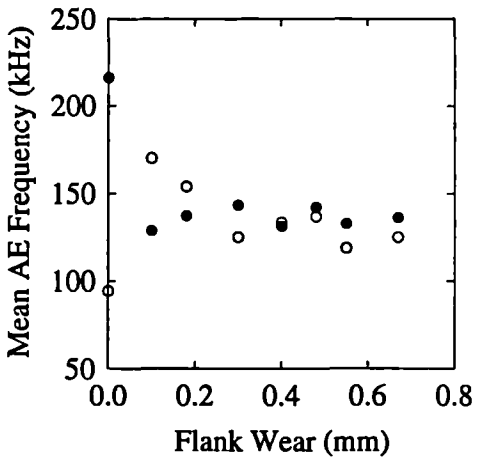

Figure 145: Mean AE Frequency vs Flank Wear for the Finish Machining of the En24 Material

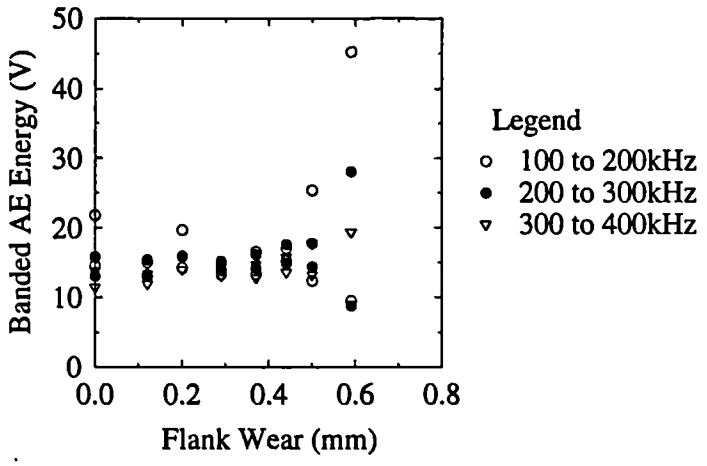

Figure 146: Banded AE Energy vs Flank Wear for the Finish Machining of the En24 Material

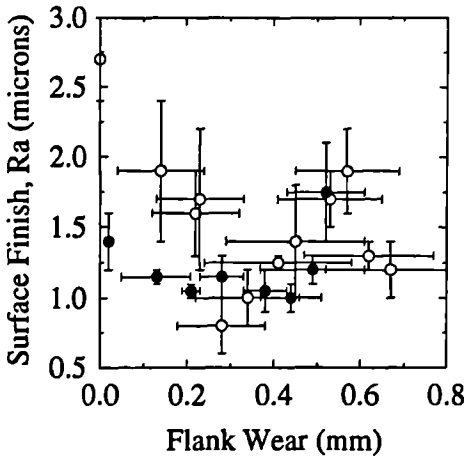

Figure 147: Surface Finish, R_a, vs Flank Wear for the Finish Machining of the En24 Material

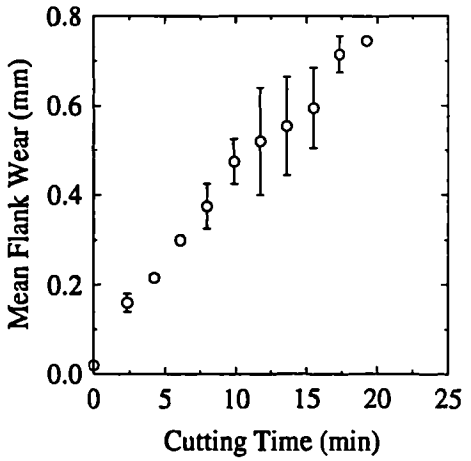

Figure 148: Flank Wear vs Cutting Time for the Groove Machining of the En24 Material

As with some of the other tests, the rms AE values (Figure 153) are quite consistent during a cut but the variation with flank wear is non-monotonic. The cumulative rms AE is almost linear with wear, (Figure 154). For this wear test the mean AE frequency is scattered around the range of 80 to 150 kHz (Figure 155) although there does appear to be a slight general trend for the mean frequency to reduce with increasing tool wear. The banded AE energy with flank wear (Figure 156) shows a similar trend to other tests, in that the energy contained in the 100 to 200 kHz frequency range increases slightly after a value of flank wear of 0.3 mm, whereas the energy contained in the other bands, either remains the same or reduces slightly.

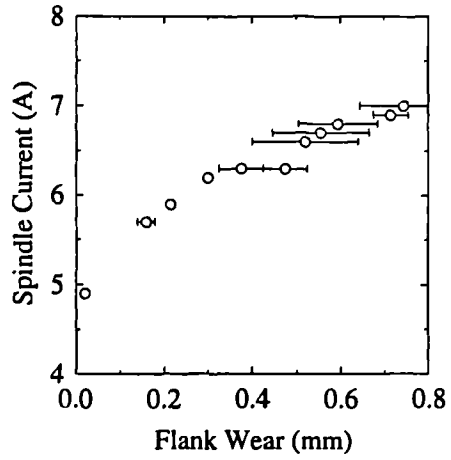

Figure 149: Spindle Current vs Flank Wear for the Groove Machining of the En24 Material

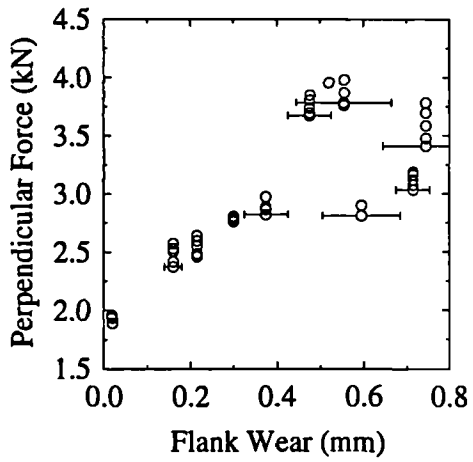

Figure 150: Perpendicular Force vs Flank Wear for the Groove Machining of the En24 Material

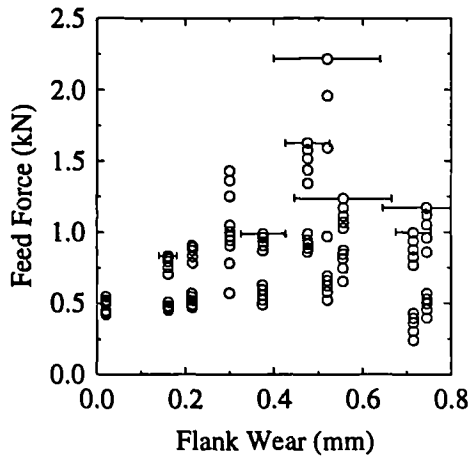

Figure 151: Feed Force vs Flank Wear for the Groove Machining of the En24 Material

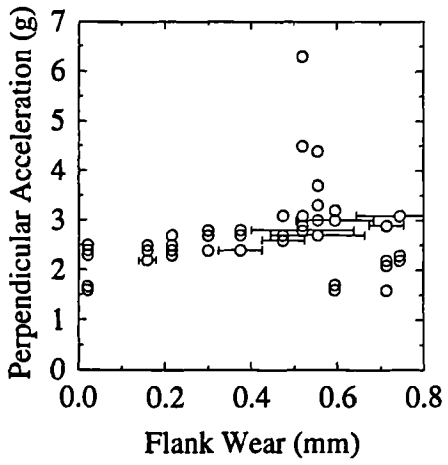

Figure 152: Perpendicular Acceleration vs Flank Wear for the Groove Machining of the En24 Material

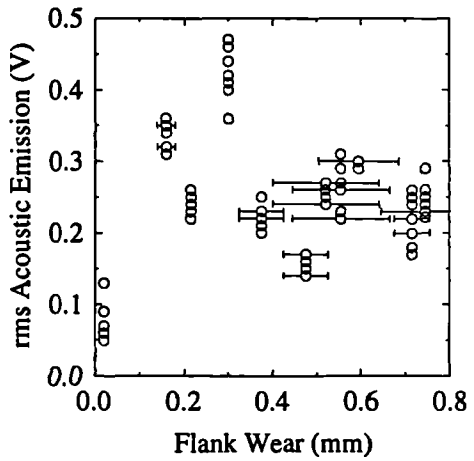

Figure 153: rms Acoustic Emission vs Flank Wear for the Groove Machining of the En24 Material

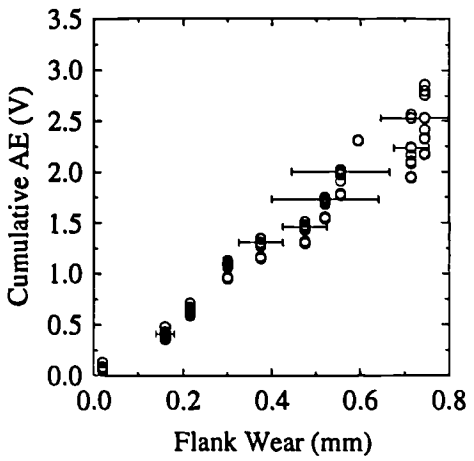

Figure 154: Cumulative rms Acoustic Emission vs Flank Wear for the Groove Machining of the En24 Material

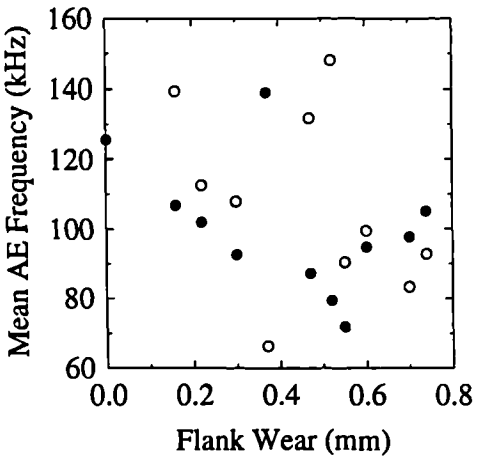

Figure 155: Mean AE Frequency vs Flank Wear for the Groove Machining of the En24 Material

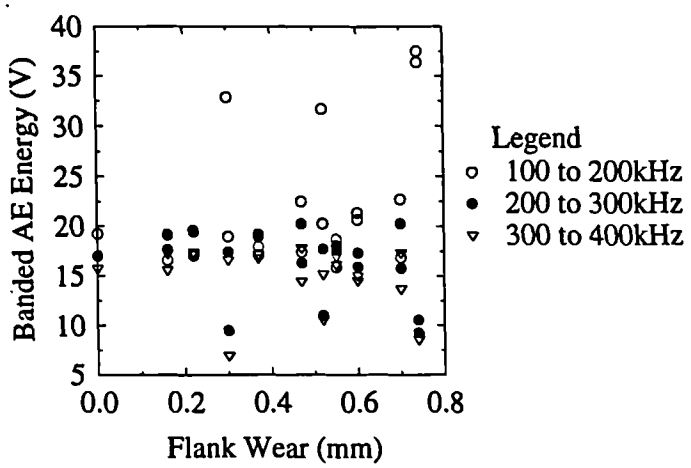

Figure 156: Banded AE Energy vs Flank Wear for the Groove Machining of the En24 Material

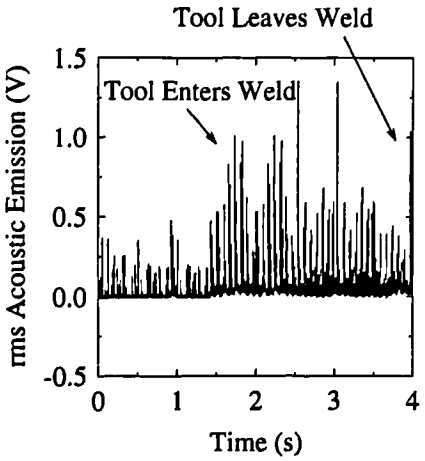

Figure 157: rms AE from a Traverse Through a Weld Bead

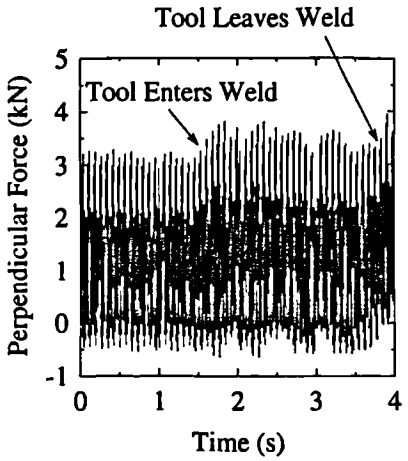

Figure 158: Cutting Force from a Traverse Through a Weld Bead

5.4 Short Timescale Event Results for Cutting Force and Acoustic Emission during Face Milling Operations.

5.4.1 Weld Traverse

Figures 157 and 158 show the traverse of the tool through the weld and its heat affected zone recorded by the force transducer and AE sensor. It can be seen that the AE signal increases by around 200 % average, whereas the cutting force increases by around 20 % on entry into the heat-affected zone.

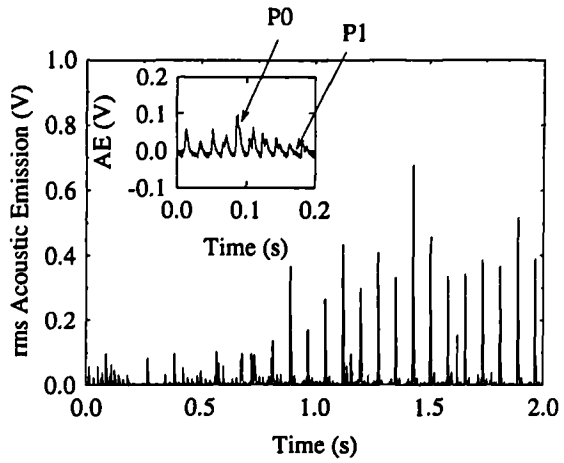

Figure 159: rms AE Record of the Entry of a Tool with a Pre-Cracked Insert

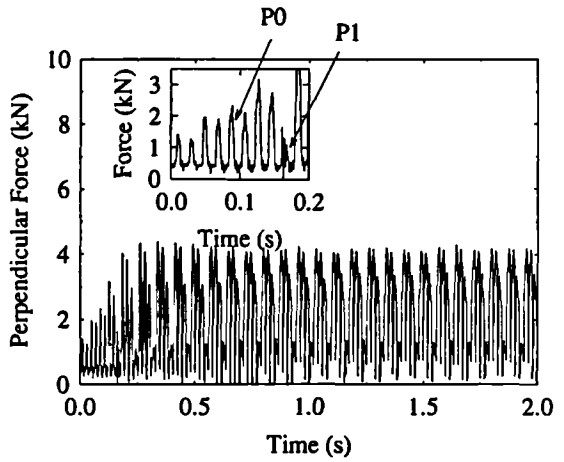

Figure 160: Cutting Force Record of the Entry of a Tool with a Pre-Cracked Insert

5.4.2 Pre-Cracked Insert

Figures 159 and 160 show the rms AE at 0.5 ms and perpendicular cutting force as a sample of the information displayed by all sensors as the pre-cracked insert failed. The tool entry into the workpiece can be observed in both Figures as an increasing mean peak height. The fracture of the insert manifests itself as a low cutting force at point P1. At this point the insert is not cutting and so it is likely to have fractured one rotation prior to this. If this point, P0, is examined the rms AE can be seen to be considerably larger than the surrounding peaks. In contrast the cutting force exhibits no particular features which might suggest failure was taking place. Further into the cut it is possible to see the increased strain that is being imposed, on the insert following the broken one, by a large peak of AE and an increased cutting force (although the latter effect is less pronounced).

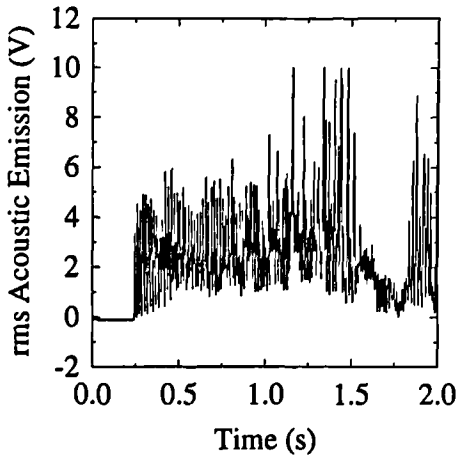

Figure 161: AE during Abnormal Cutting and Spindle Stall

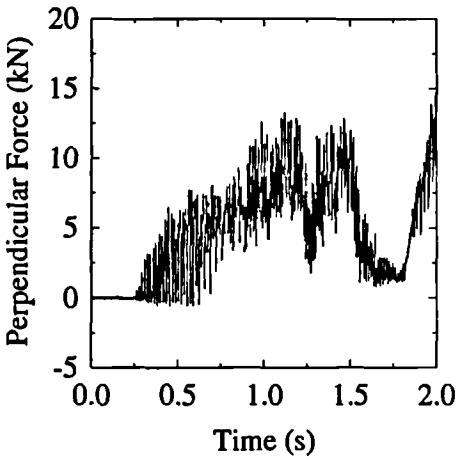

Figure 162: Perpendicular Force during Abnormal Cutting and Spindle Stall

5.4.3 Insert failure and machine stall under inappropriate cutting conditions

Figures 161 to 164 show the sensorial information from the rms AE, cutting force, shaft encoder and spindle current from the roughing cut on En24T under abnormal cutting conditions. As soon as the tool enters the workpiece it can be seen that the rms AE signal is very large compared to that obtained from a normal cut. The cutting force also shows the tool entering the workpiece and, as the tool progresses, the force level rises steadily, until the load becomes too great for the spindle to rotate and a stall occurs followed by some slippage as the drive is still being applied to the spindle. The shaft encoder shows this slippage by an increased duration between pulses and also signals the complete stop of the spindle as would be expected. The spindle current displays similar information to the cutting force, in that the spindle current steadily rises as the tool progresses and, as the spindle stops rotating, the current value levels off at around 60 A.

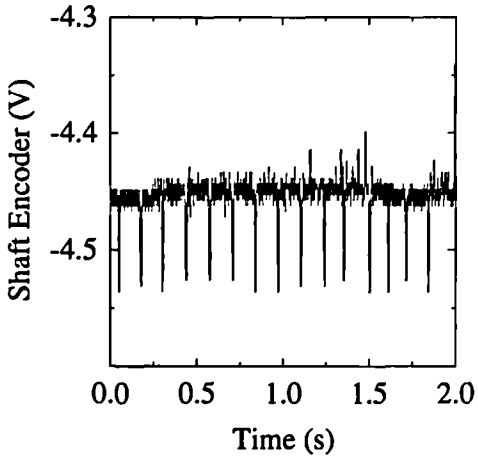

Figure 163: Shaft Encoder Output for the Abnormal Cutting and Spindle Stall

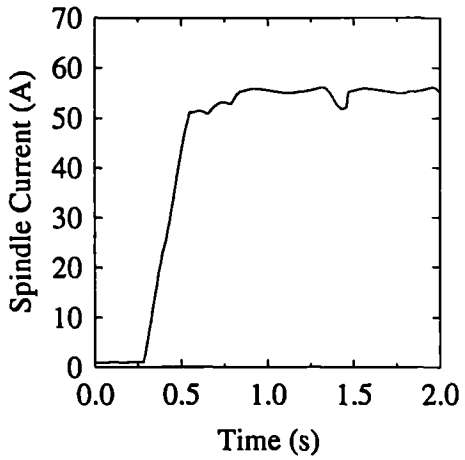

Figure 164: Spindle Current during Abnormal Cutting and Spindle Stall

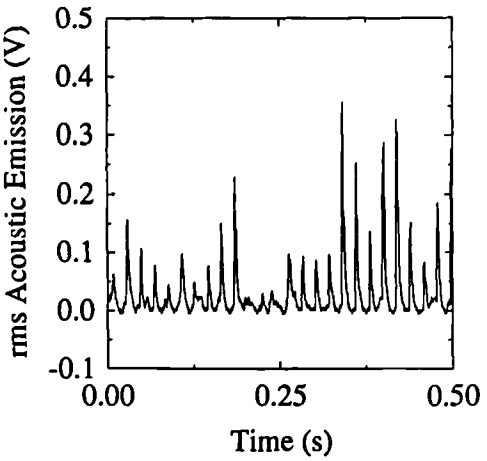

Figure 165: Time Evolution of rms AE Before Edge Chipping

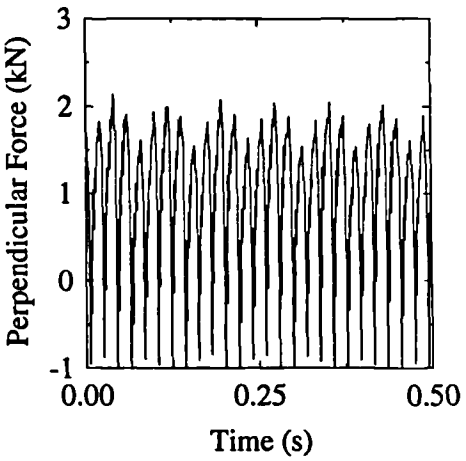

Figure 166: Time Evolution of the Cutting Force Before Edge Chipping

5.4.4 Insert Edge Breakdown

Figures 165 and 166 show the rms AE and the tangential cutting force recorded before the edge chipping event described earlier and Figures 167 and 168 show the same information after this event.

It can be seen that there is a significant change in the amplitude and form of the AE signal before and after edge chipping. Before, the AE is periodic with clear tooth passing information being observable and after it becomes more random in appearance, and it is very difficult to observe the passing of inserts over the workpiece. The cutting force, on the other hand, does not lose the tooth passing information from its time evolution, rather it is enhanced after the edge chipping event, with the standard deviation of the signal increasing and the envelope of the tooth passing peaks changing from a sinusoid before the event to a saw tooth shape after the event.

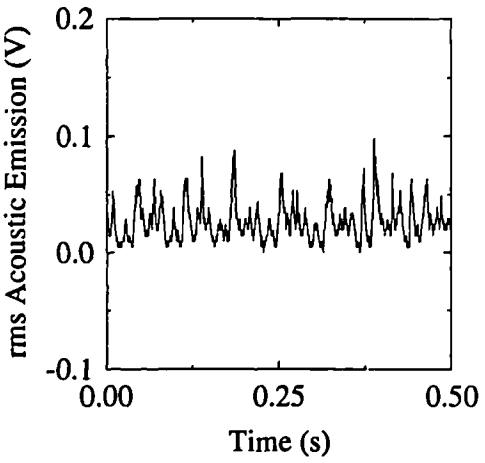

Figure 167: Time Evolution of rms AE After Edge Chipping

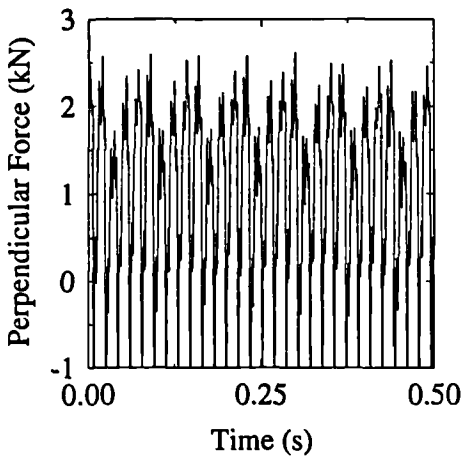

Figure 168: Time Evolution of the Cutting Force After Edge Chipping

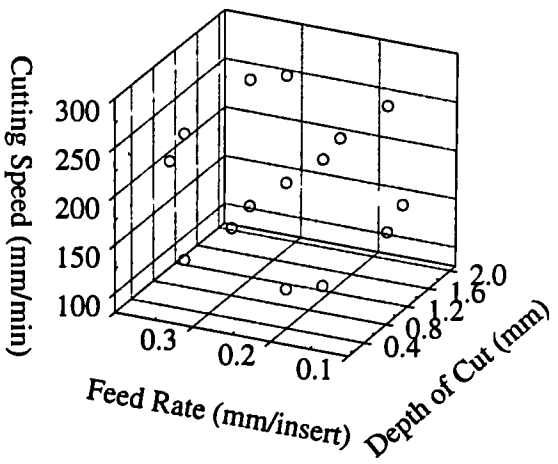

Figure 169: Cutting Conditions used to Assess their Influence on AE, Force and Current

5.5 Influence of Cutting Conditions on AE, Cutting Force and Spindle Current

As described in Chapter 4, an experiment was conducted to assess the influence that cutting conditions have on the spindle current, the cutting force, the acoustic emission and the surface finish. Each sensor will be discussed in turn for the first random walk described in Chapter 4 and illustrated in Figure 169. This test was conducted with a nominally new tool ($VB_B < 0.2$ mm) and the effect of wear on some of the points in cutting condition space is examined in the next Section.

Only one random walk of the cutting condition space is presented here, as similar trends for sensor variation with cutting conditions could be observed at other flank wear levels. As before, the mean of the spindle current, the mean plus one standard deviation of the two horizontal components of cutting force, and the mean plus one standard deviation of the 0.5 ms rms AE are used as sensor features. For later discussion the strain rate and metal removal rate have been calculated for each of the cutting conditions.

To give a picture of the effect of wear on sensorial information as a function of the cutting condition space identified in Figure 169 seven points in this space have been selected consisting of the extreme locations of depth of cut, feed and speed and the central point. Also, the accelerated wear test results will be discussed.

5.5.1 Influence of Cutting Conditions on Sensorial Output

Figures 170, 171 and 172 show the effect of depth of cut, feed and speed on spindle current. As can be seen, an increase in either of the first two of these parameters

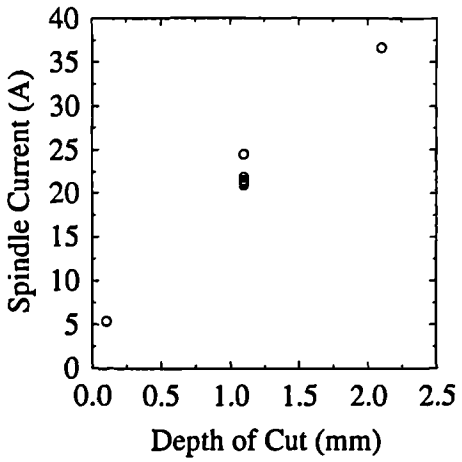

Figure 170: Variation in Spindle Current with Increasing Depth of Cut

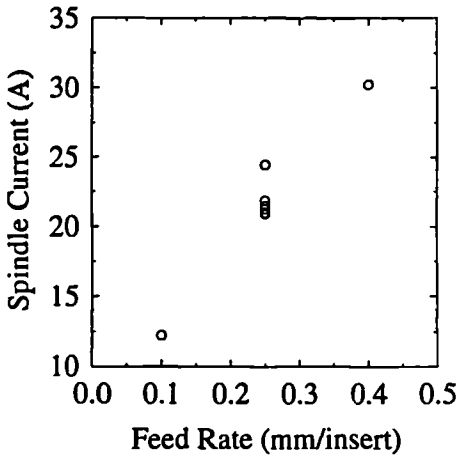

Figure 171: Variation in Spindle Current with Increasing Feed Rate

leads to an increase in spindle current with the sensorial output not varying much with speed.

Similarly, perpendicular force increases with depth of cut and feed rate, and varies very little with speed (Figures 173, 174 and 175). Similar evolutions for feed force can be observed, although the scatter of data points is larger (Figures 176, 177 and 178).

From Figures 179, 180 and 181 it can be seen that the rms AE appears to increase with depth of cut, and not to vary outside of the scatter of data points for feed and speed.

For the mean AE frequency, there is little evidence for variations with any of the conditions (Figures 182 to 184).

For the banded AE energy (Figures 185, 186 and 187) there does not appear to be any consistent variation in energy with depth of cut for any of the frequency bands, although the last point for each of the bands all lie around the same value.

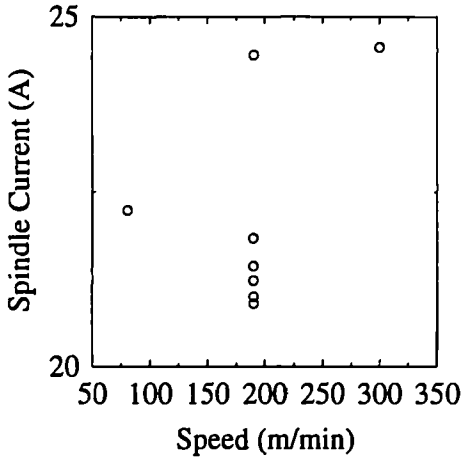

Figure 172: Variation in Spindle Current with Increasing Cutting Speed

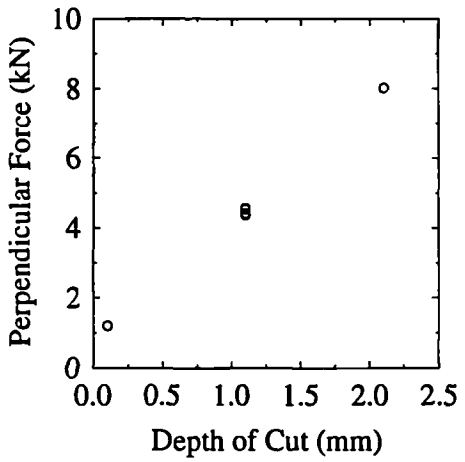

Figure 173: Variation in Perpendicular Force with Increasing Depth of Cut

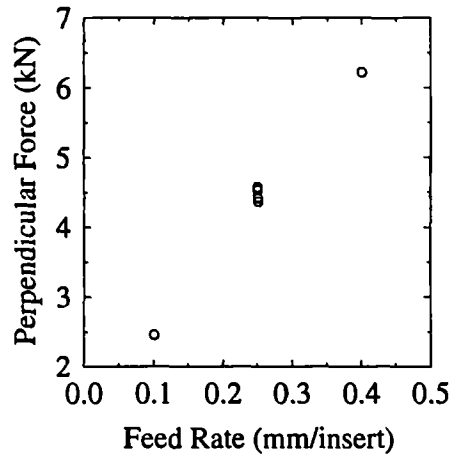

Figure 174: Variation in Perpendicular Force with Increasing Feed Rate

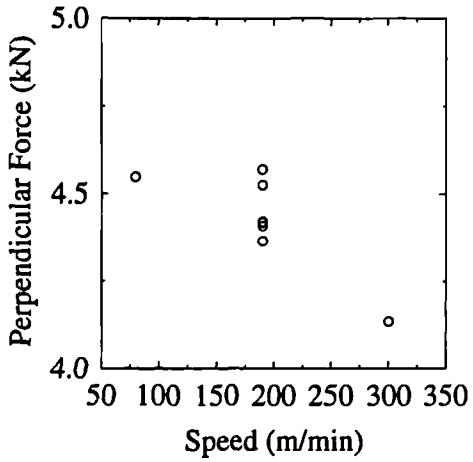

Figure 175: Variation in Perpendicular Force with Increasing Cutting Speed

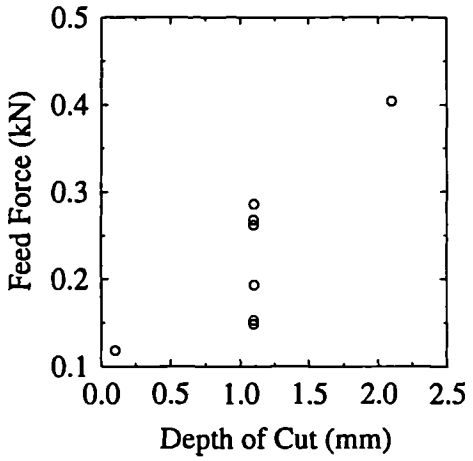

Figure 176: Variation in Feed Force with Increasing Depth of Cut

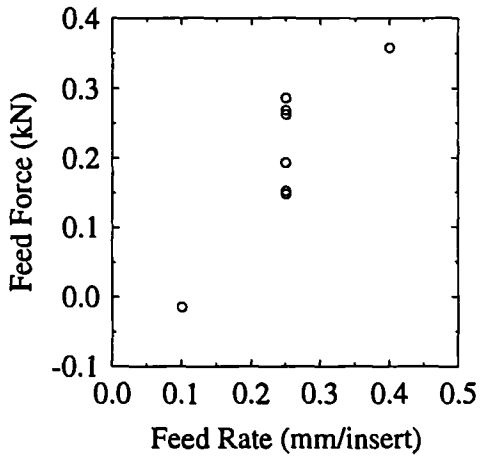

Figure 177: Variation in Feed Force with Increasing Feed Rate

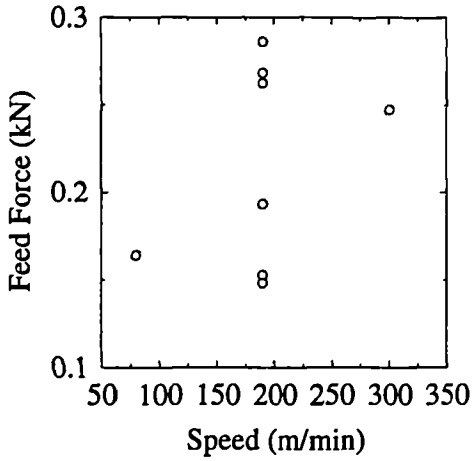

Figure 178: Variation in Feed Force with Increasing Cutting Speed

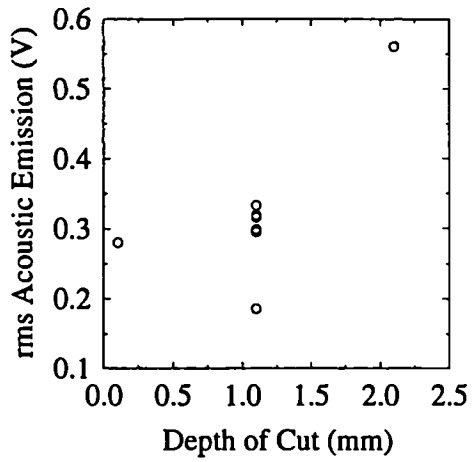

Figure 179: Variation in rms AE with Increasing Depth of Cut

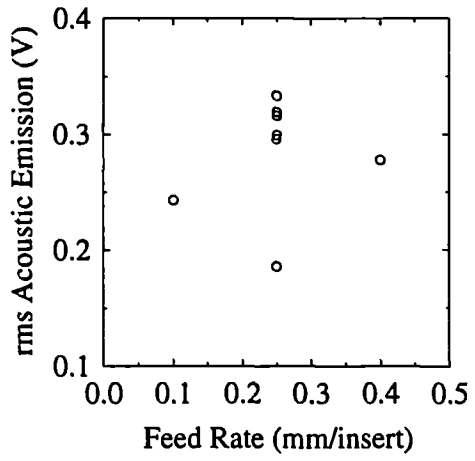

Figure 180: Variation in rms AE with Increasing Feed Rate

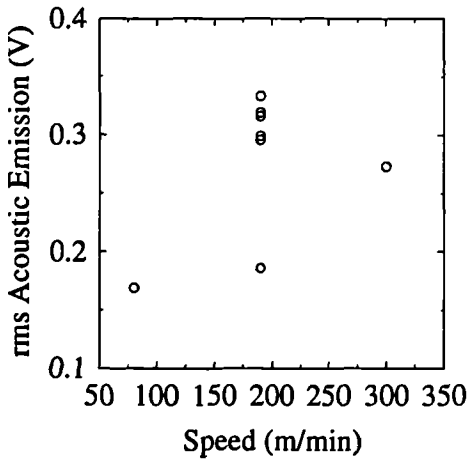

Figure 181: Variation in rms AE with Increasing Cutting Speed

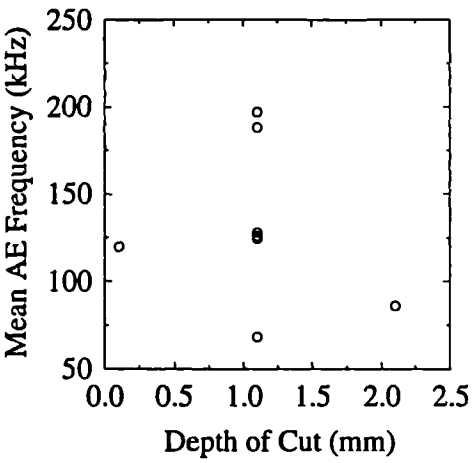

Figure 182: Variation in Mean AE Frequency with increasing Depth of Cut

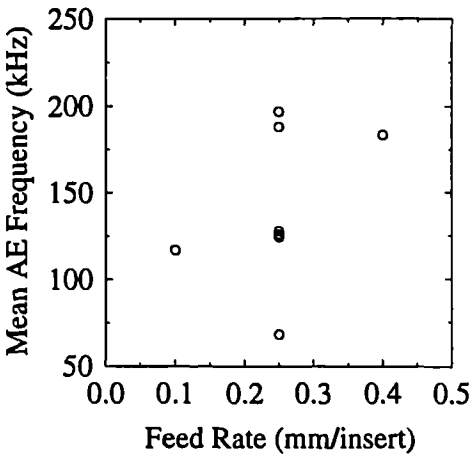

Figure 183: Variation in Mean AE Frequency with Increasing Feed Rate

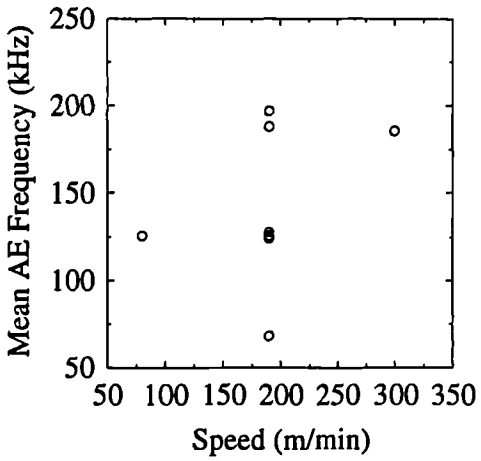

Figure 184: Variation in Mean AE Frequency with Increasing Cutting Speed

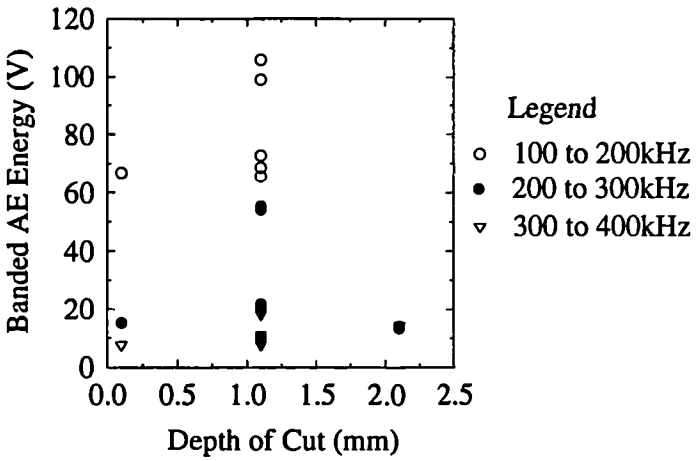

Figure 185: Variation in Banded AE Energy with Increasing Depth of Cut

There appears to be an increase in both the 100 to 200 kHz and 200 to 300 kHz bands with both feed and speed, and no variation for the 300 to 400 kHz band.

Somewhat surprisingly, no systematic variation of R_a was found with any of the cutting conditions. However, the relatively small number of points and the variability of R_a measurements may have probably obscured any trends (Figures 188 to 190).

5.5.2 Variations in Sensorial Information with Wear

Central Point of Cutting Condition Space

In common with other wear tests, the spindle current (Figure 191) increases with wear in a quite linear manner for the central point in cutting condition space. Both the feed and perpendicular forces decrease with wear but with a sharp increase in both cases at the highest value of VB_B (Figure 192 and 193).

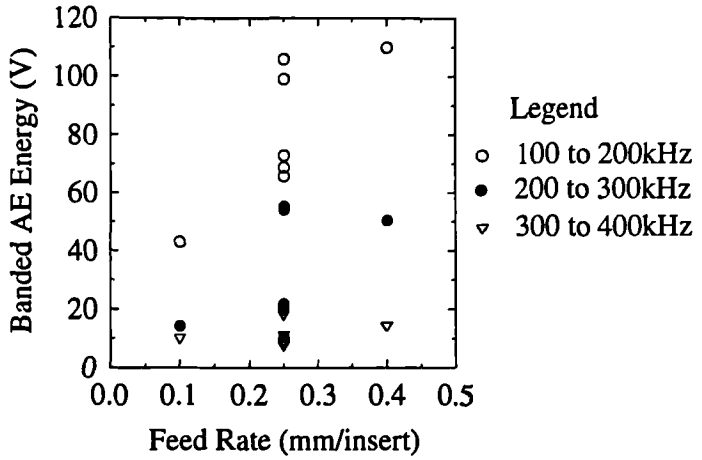

Figure 186: Variation in Banded AE Energy with Increasing Feed Rate

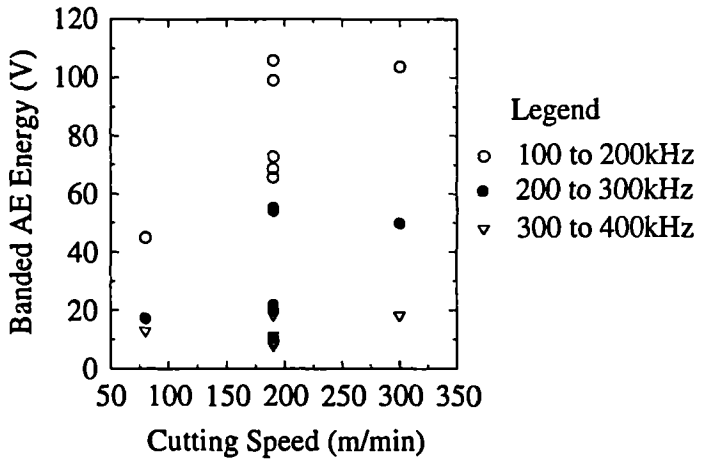

Figure 187: Variation in Banded AE Energy with Increasing Cutting Speed

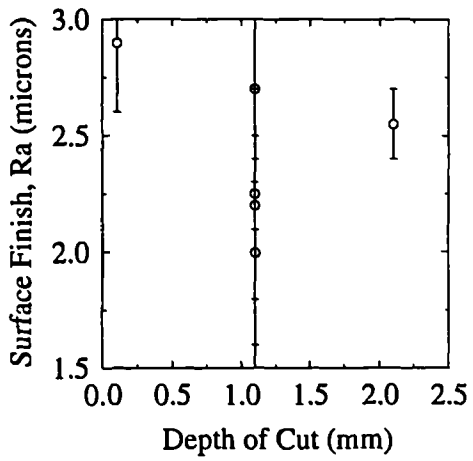

Figure 188: Variation in Surface Finish with Increasing Depth of Cut

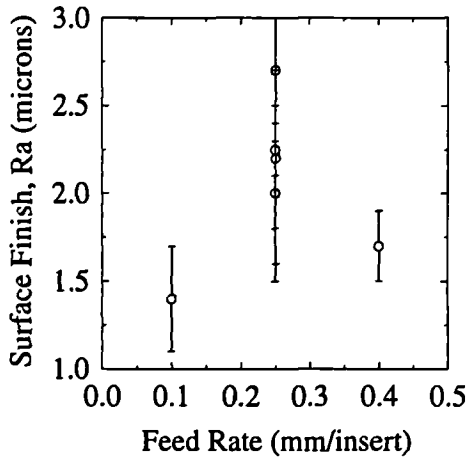

Figure 189: Variation in Surface Finish with Increasing Feed Rate

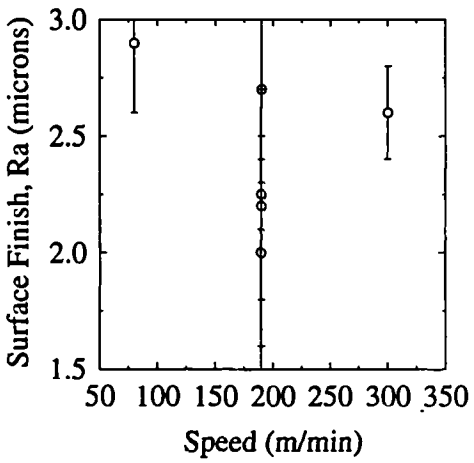

Figure 190: Variation in Surface Finish with Increasing Cutting Speed

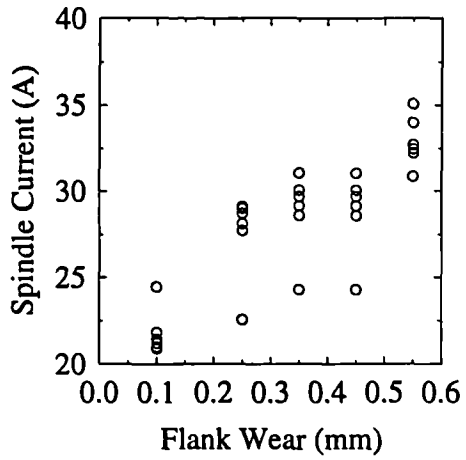

Figure 191: Variation in the Spindle Current with Wear for the Central Point of the Space

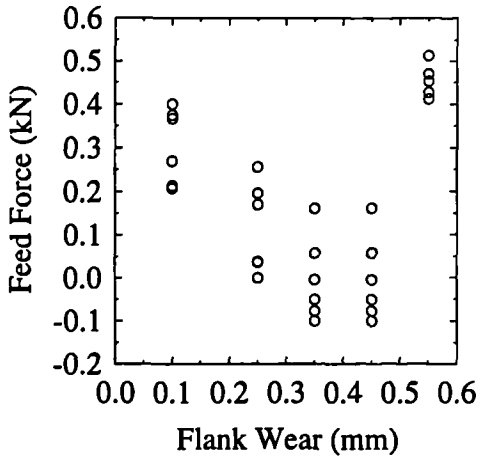

Figure 192: Variation in the Feed Force with Wear for the Central Point of the Space

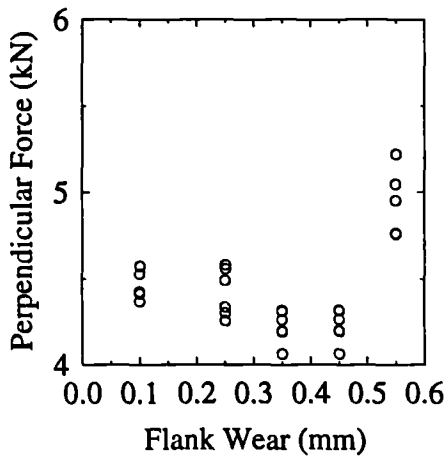

Figure 193: Variation in the Perpendicular Force with Wear for the Central Point

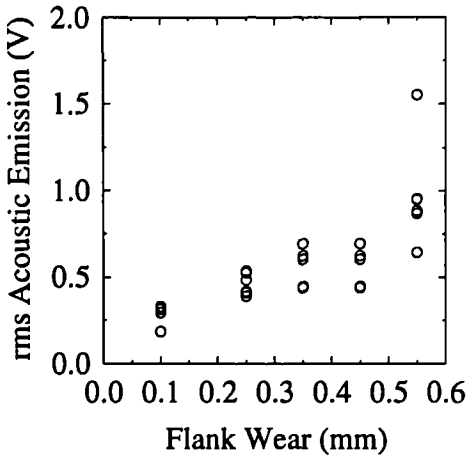

Figure 194: Variation in the rms AE with Wear for the Central Point of the Condition Space

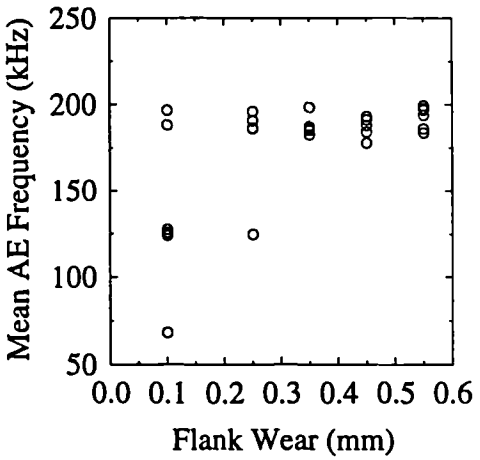

Figure 195: Variation in the Mean AE Frequency with Wear for the Central Point of the Condition Space

The rms AE increases in a linear fashion with flank wear (Figure 194) and, in commmon with other wear tests, the mean AE frequency does not vary with tool wear (Figure 195). From Figure 196 it can be seen that there is a small increase in the 100 to 200 kHz AE band with wear but that this nearly all takes place over the the wear step of 0.1 to 0.25 mm. There is a similar step for the 200 to 300 kHz band and no increase for the last band.

Figure 197 shows a similar variation to other wear tests for R_a with flank wear.

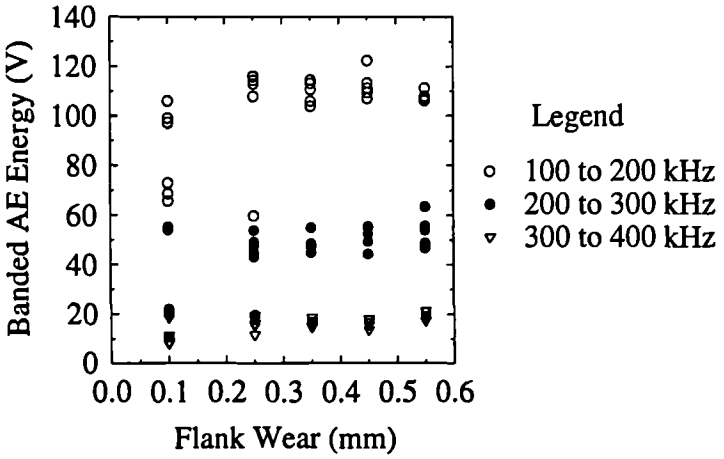

Figure 196: Variation in the Banded AE Energy with Wear for the Central Point of the Condition Space

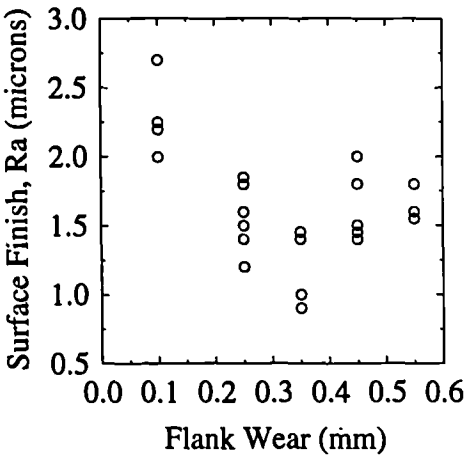

Figure 197: Variation in the Surface Finish with Wear for the Central Point of the Condition Space

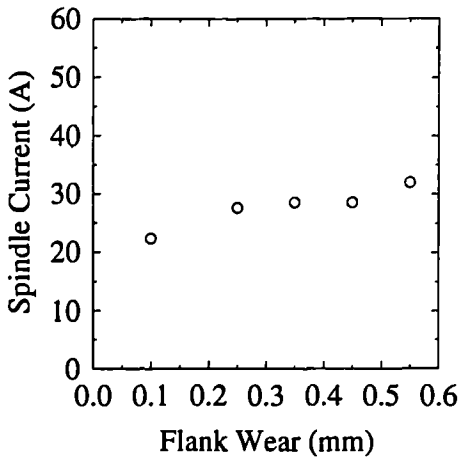

Figure 198: Variation in the Spindle Current with Wear for a Cutting Speed 80 m/min

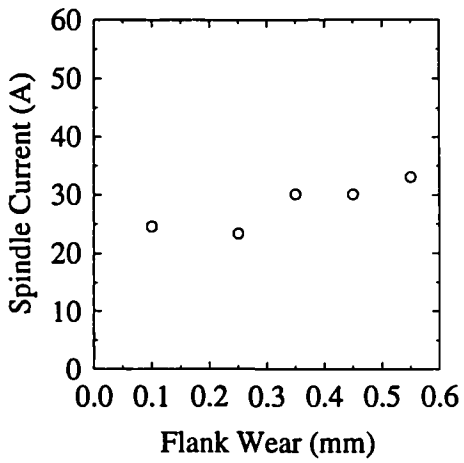

Figure 199: Variation in the Spindle Current with Wear for a Cutting Speed of 300 m/min

5.5.3 Variations in Sensorial Information for the Extreme Values of the Condition Space with Flank Wear

The Extremes of Cutting Speed

For both 80 m/min (Figure 198) and 300 m/min (Figure 199), the spindle current exhibits a modest linear increase with tool wear.

Both the feed and perpendicular forces decrease with wear at a cutting speed of 80 m/min (Figure 200 and 201) with an increase in both cases for the highest value of VB_B. For a cutting speed of 300 m/min, the feed force (Figure 202) and perpendicular force (Figure 203) show almost exactly the same variation as they did at 80 m/min.

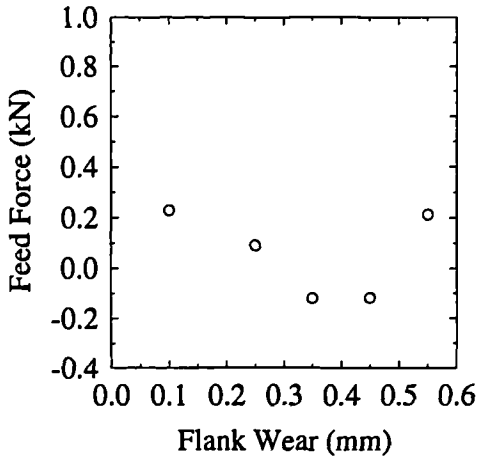

Figure 200: Variation in the Feed Force with Wear for a Cutting Speed of 80 m/min

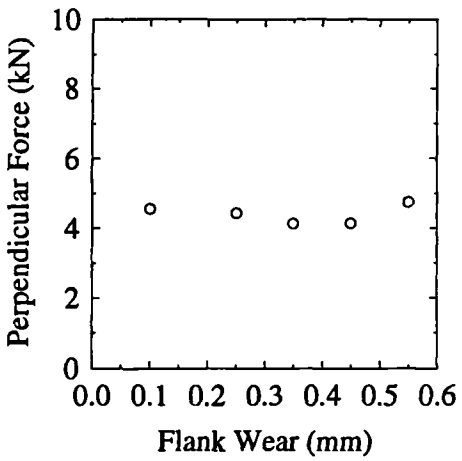

Figure 201: Variation in the Perpendicular Force with Wear for a Cutting Speed of 80 m/min

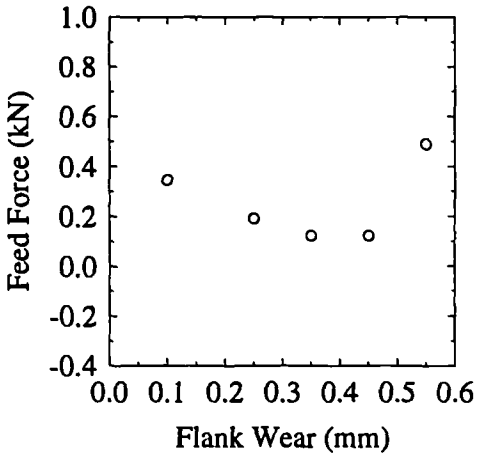

Figure 202: Variation in the Feed Force with Wear for a Cutting Speed of 300 m/min

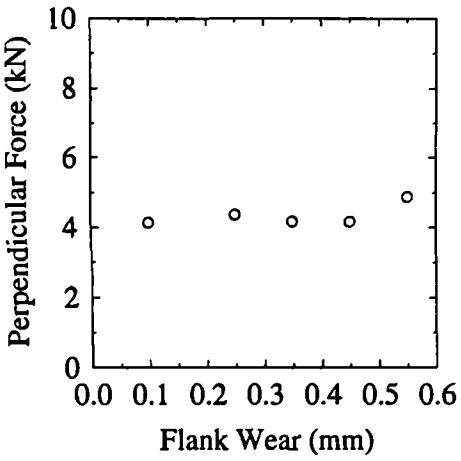

Figure 203: Variation in the Perpendicular Force with Wear for a Cutting Speed of 300 m/min

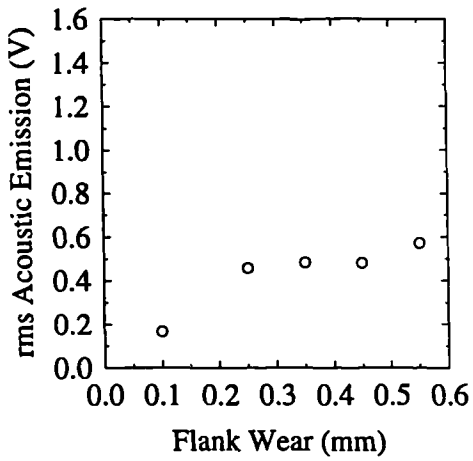

Figure 204: Variation in the rms AE with Wear for a Cutting Speed of 80 m/min

The rms AE for a speed of 80 m/min (Figure 204) shows a modest increase with wear and this is repeated for a speed of 300 m/min (Figure 205). The mean AE frequency for both a cutting speed of 300 m/min, Figure 207, displays no significant variation with tool wear and if the first point is disregarded the same can be said for a cutting speed of 80 m/min Figure 206.

For a cutting speed of 80 m/min there is no change in the AE energy level for any of the frequency bands (Figure 208), whereas for a speed of 300 m/min there is a large increase for the first wear increment and then little change with wear for both the 100 to 200 kHz and 200 to 300 kHz bands. The 300 to 400 kHz band does not vary with wear.

Surface finish variations with tool wear for a speed of 80 m/min (Figure 210) exhibits no particular trends with wear increases, whereas for a speed of 300 m/min (Figure 211) the 'U' shaped trend observed in other wear tests can be seen.

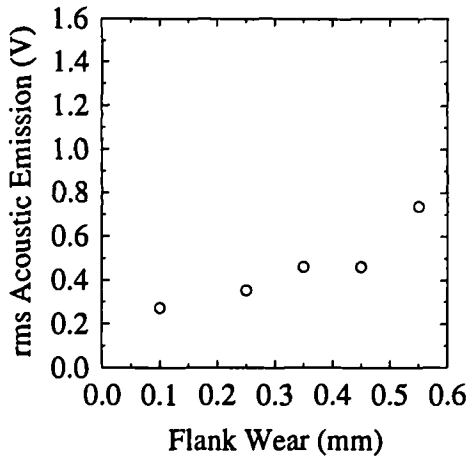

Figure 205: Variation in the rms AE with Wear for a Cutting Speed of 300 m/min

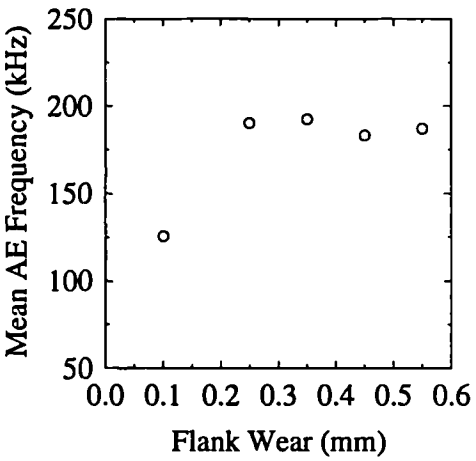

Figure 206: Variation in the Mean AE Frequency with Wear for a Cutting Speed of 80 m/min

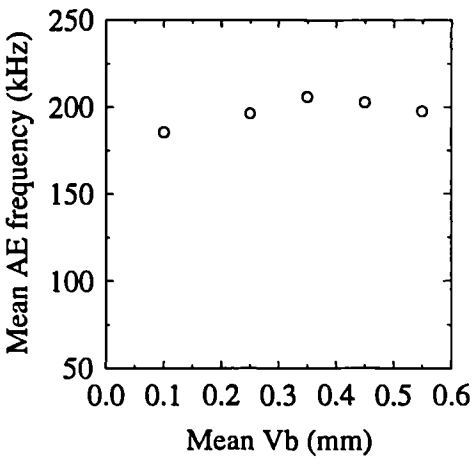

Figure 207: Variation in the Mean AE Frequency with Wear for a Cutting Speed of 300 m/min

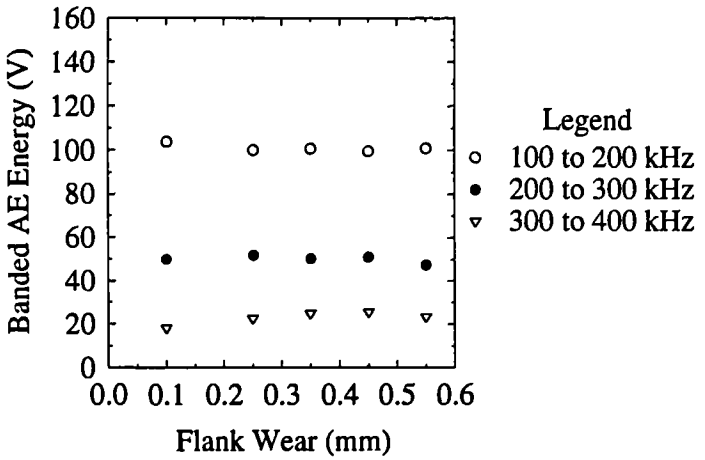

Figure 208: Variation in the Banded AE Energy with Wear for a Cutting Speed of 80 m/min

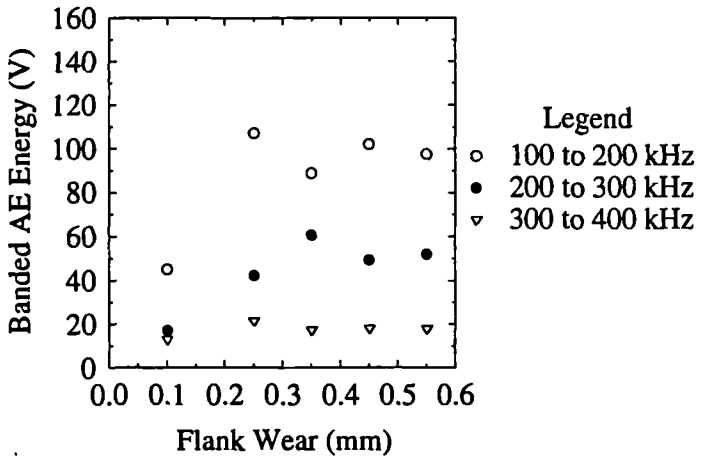

Figure 209: Variation in the Banded AE Energy with Wear for a Cutting Speed of 300 m/min

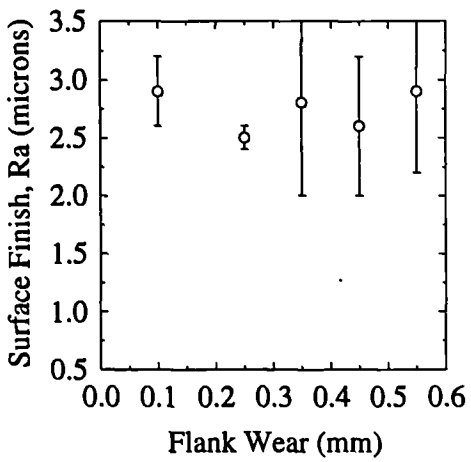

Figure 210: Variation in the Surface Finish with Wear for a Cutting Speed of 80 m/min

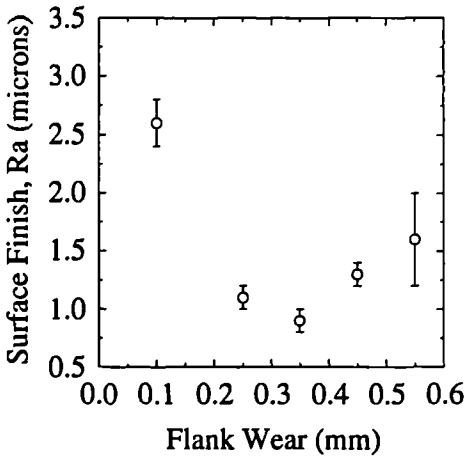

Figure 211: Variation in the Surface Finish with Wear for a Cutting Speed of 300 m/min

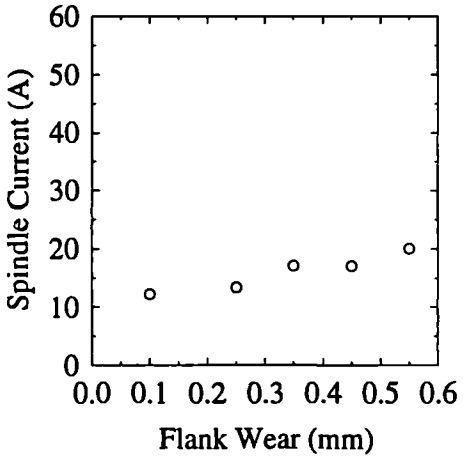

Figure 212: Variation in the Spindle Current with Wear for a Feed Rate of 0.1 mm/insert

The Extremes of Feed Rate

For a feed rate of 0.1 mm/insert (Figure 212) spindle current exhibits a small but linear increase with wear. For a feed rate of 0.4 mm/insert (Figure 213) a similar linear trend is exhibited although the level of current is much higher.

Feed force variations with wear for a feed rate of 0.1 mm/insert (Figure 214), are small in line with the spindle current, however, a drop for medium wear values is again observed. The perpendicular component of cutting force (Figure 215) exhibits no observable changes with tool wear. It is noticeable that the actual values are much lower than for other tests. For a feed rate of 0.4 mm/insert the feed force (Figure 216) hardly varies at all with wear except for the last increment when it again increases. The perpendicular force (Figure 217) displays a similar variation.

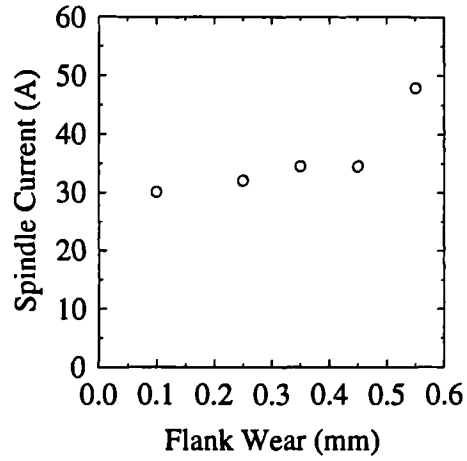

Figure 213: Variation in the Spindle Current with Wear for a Feed Rate of 0.4 mm/insert

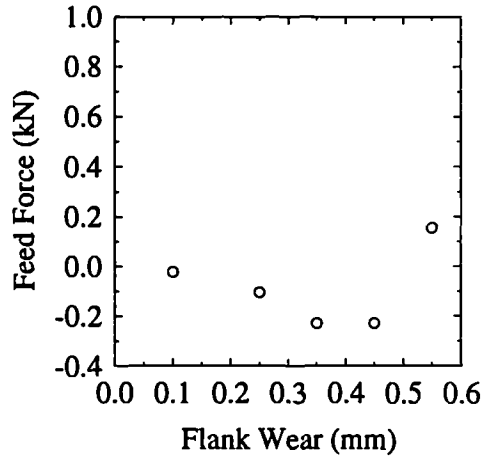

Figure 214: Variation of Feed Force with Wear for a Feed Rate of 0.1 mm/insert

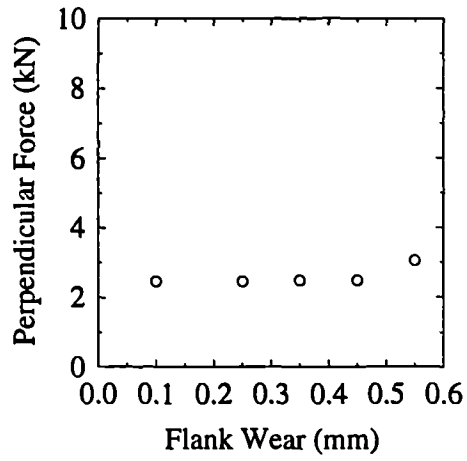

Figure 215: Variation of Perpendicular Force with Wear for a Feed Rate of 0.1 mm/insert

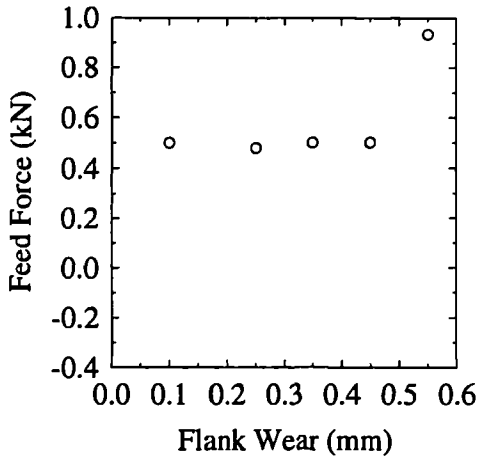

Figure 216: Variation of Feed Force with Wear for a Feed Rate of 0.4 mm/insert

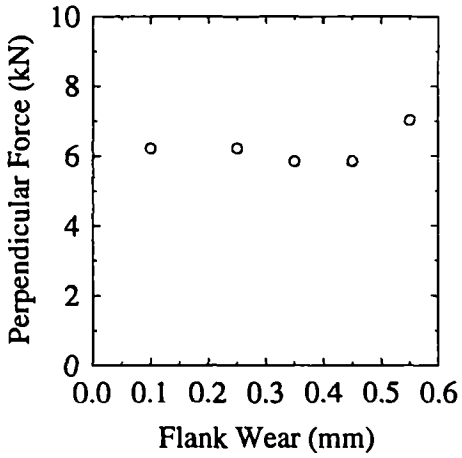

Figure 217: Variation of Perpendicular Force with Wear for a Feed Rate of 0.4 mm/insert

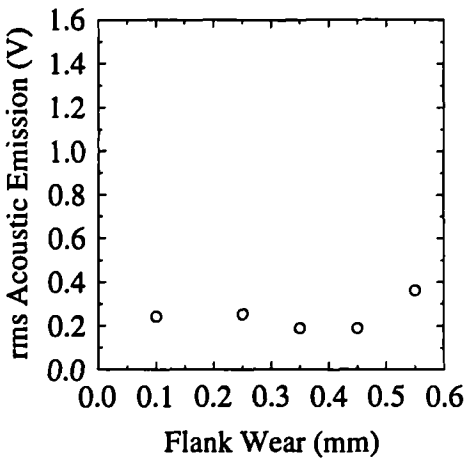

Figure 218: Variation in the rms AE with Wear for a Feed Rate of 0.1 mm/insert

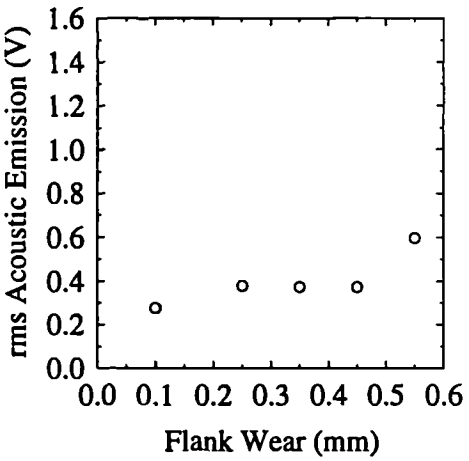

Figure 219: Variation in the rms AE with Wear for a Feed Rate of 0.4 mm/insert

The rms AE for a feed rate of 0.1 mm/insert (Figure 218) shows a small increase with wear and a similar, although slightly more pronounced pattern can be seen for a feed rate of 0.4 mm/insert (Figure 219).

With one exception in both Figures 220 and 221) for a feed rate of 0.1 mm/insert and 0.4 mm/insert there is no variation with wear. It is probable that both points are anomalous.

In a similar manner to the mean frequency variation, the energy changes with wear show no change with wear (Figures 222 and 223) except for these same points, adding weight to the hypothesis that these points are incorrect.

The surface finish for a feed rate of 0.1 mm/insert (Figure 224) displays a slight tendency to increase with tool wear, this variation is very small, and is within the error bars. For a feed rate of 0.4 mm/insert there is no systematic variation with tool wear, Figure 225.

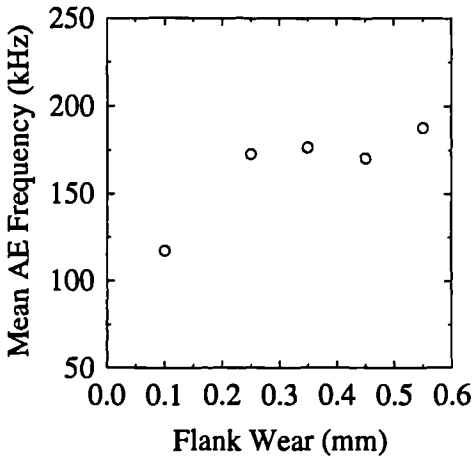

Figure 220: Variation in the Mean AE Frequency with Wear for a Feed Rate of 0.1 mm/insert

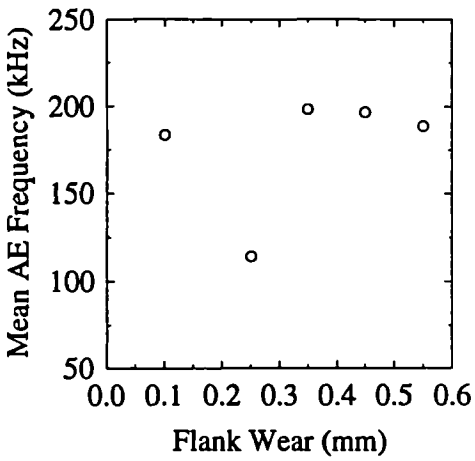

Figure 221: Variation in the Mean AE Frequency with wear for a Feed Rate of 0.4 mm/insert .

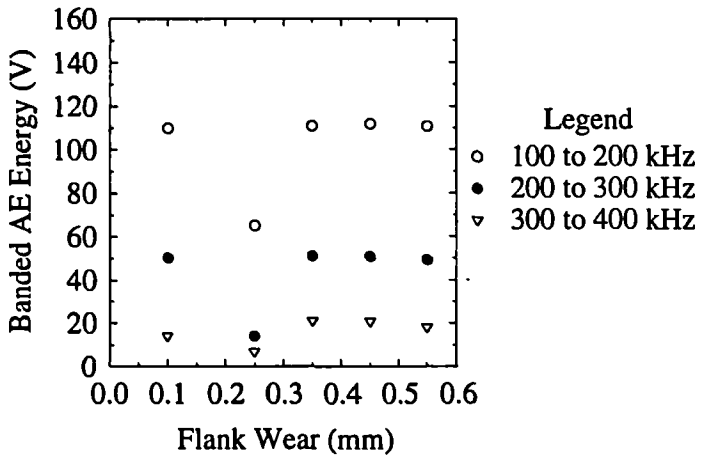

Figure 222: Variation in the Banded AE Energy with Wear for a Feed Rate of 0.1 mm/insert

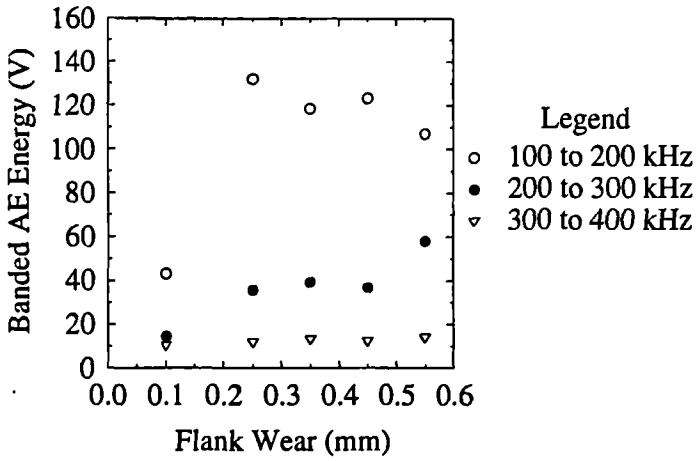

Figure 223: Variation in the Banded AE Energy with Wear for a Feed Rate of 0.4 mm/insert

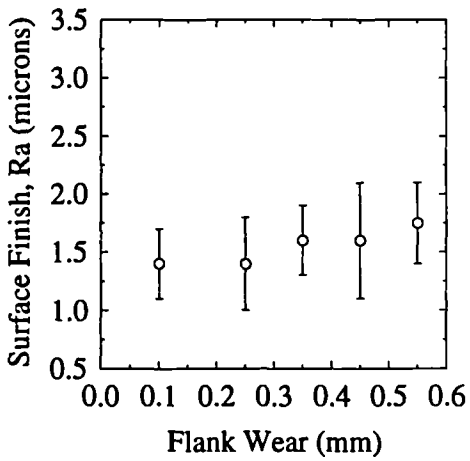

Figure 224: Variation in the Surface Finish with Wear for a Feed Rate of 0.1 mm/insert

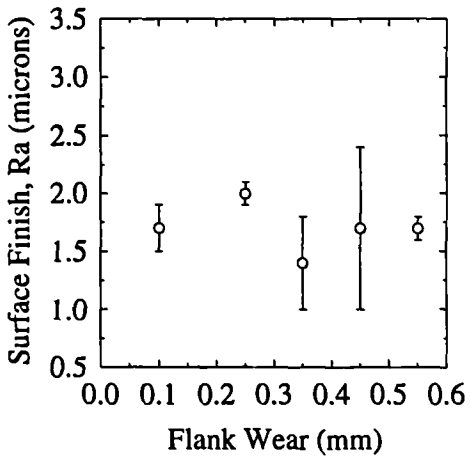

Figure 225: Variation in the Surface Finish with Wear for a Feed Rate of 0.4 mm/insert

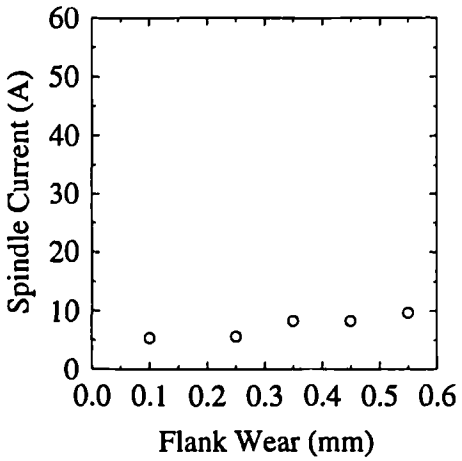

Figure 226: Variation in the Spindle Current for a Depth of Cut of 0.1 mm

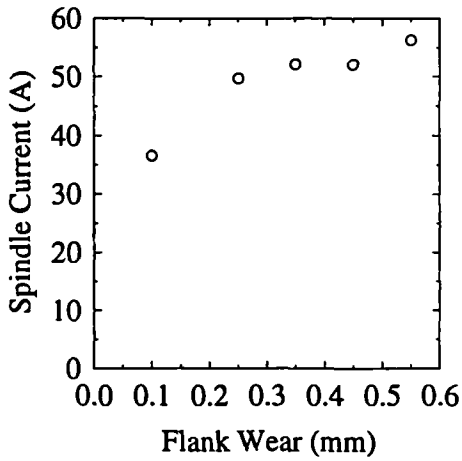

Figure 227: Variation in the Spindle Current with Wear for a Depth of Cut of 2.1 mm

The Extremes of Depth of Cut

Even for the 0.1 mm depth of cut there is still a small rise in spindle current with wear (Figure 226). For the 2.1 mm depth of cut (Figure 227) the gradient is, of course, much greater.

The feed and perpendicular forces show no variation with wear for a 0.1 mm depth of cut (Figures 228 and 229), although the feed force again exhibits lower values for medium values of flank wear. For a 2.1 mm depth of cut the feed force (Figure 230) displays a similar trend with wear to a low depth of cut, except the variation is larger. Perpendicular force (Figure 231), shows virtually no variation with wear. The values are very large at around 8 kN.

The rms AE signal for a 0.1 mm depth of cut (Figure 232), shows almost no change with wear whereas for a 2.1 mm depth of cut (Figure 233) the rms AE signal exhibits a large and quite linear increase with flank wear, although the last

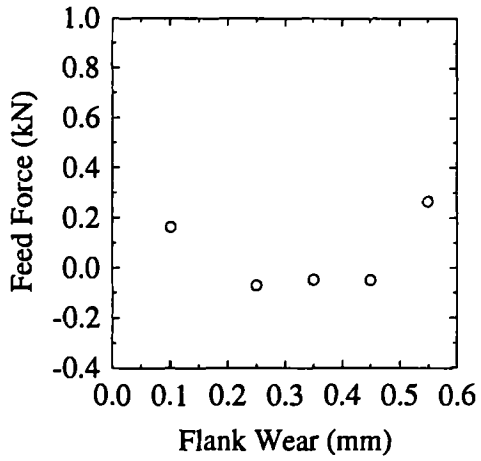

Figure 228: Variation in the Feed Force with Wear for a Depth of Cut of 0.1 mm

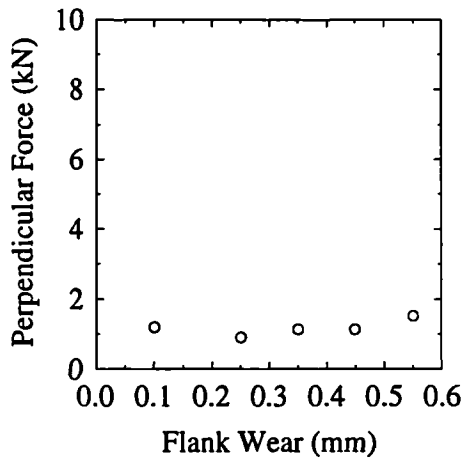

Figure 229: Variation in the Perpendicular Force with Wear for a Depth of Cut of 0.1 mm

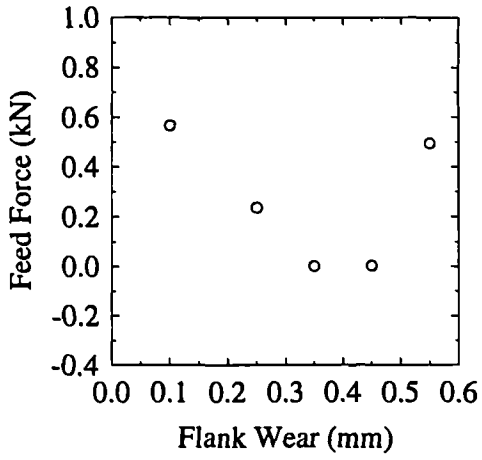

Figure 230: Variation in the Feed Force with Wear for a Depth of Cut of 2.1 mm

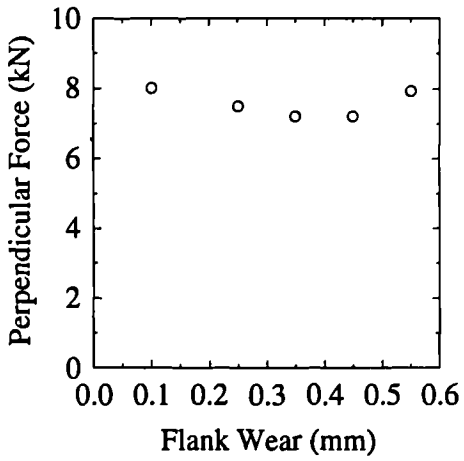

Figure 231: Variation in the Perpendicular Force for a Depth of Cut of 2.1 mm

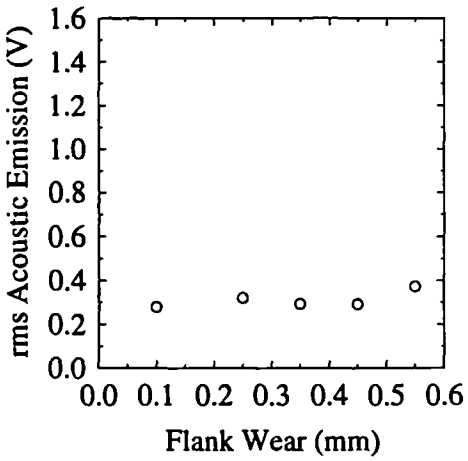

Figure 232: Variation in the rms AE with Wear for a Depth of Cut of 0.1 mm

point deviates from this trend by a small amount.

The mean AE frequency appears to increase with wear for both extremes of depth of cut (Figures 234 and 235). Although there appears to be little change in any of the AE energy bands with wear in either case (Figure 236 and 237).

The surface finish for both depth of cuts (Figure 238 and 239) displays a tendency towards lower values for medium values of flank wear.

5.5.4 Variations in Sensorial Information for an Accelerated Wear Test

As was mentioned in Chapter 4, this test was performed in order to verify whether the data collected from the central point was consistent when another tool was used.

Spindle current and both components of forces can be seen to increase with tool

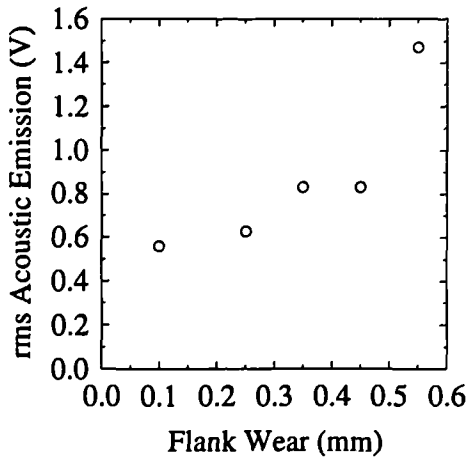

Figure 233: Variation in the rms AE with Wear for a Depth of Cut of 2.1 mm

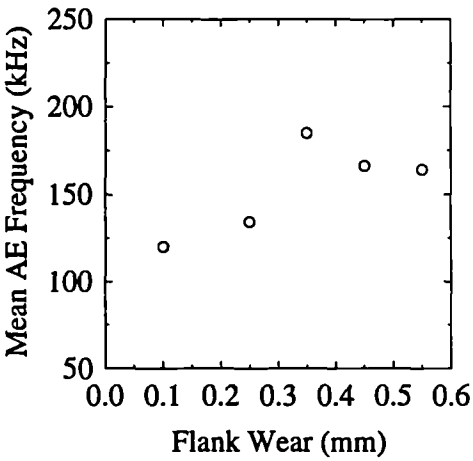

Figure 234: Variation in the Mean AE Frequency with Wear for a Depth of Cut of 0.1 mm

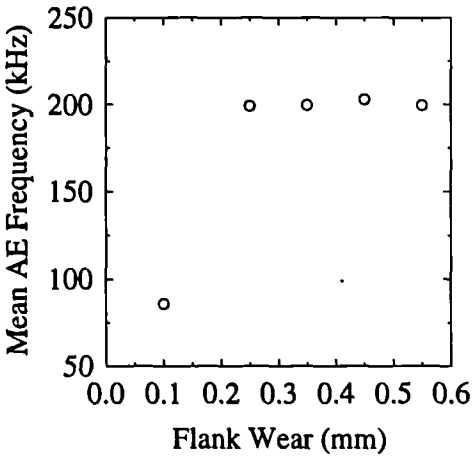

Figure 235: Variation in the Mean AE Frequency with Wear for a Depth of Cut of 2.1 mm

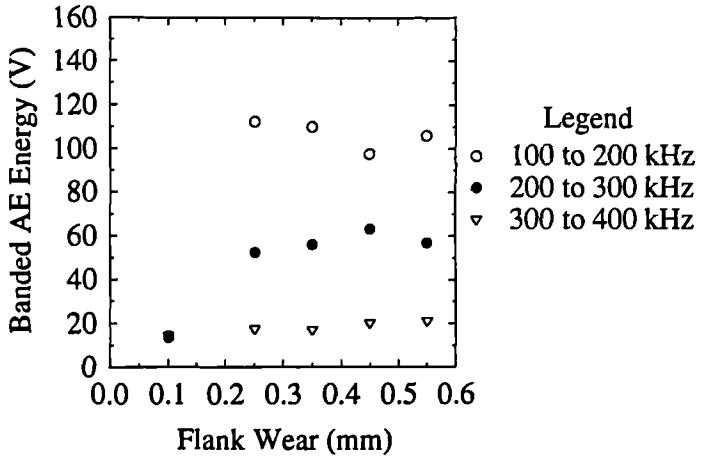

Figure 236: Variation in the Banded AE Energy with Wear for a Depth of Cut of 0.1 mm

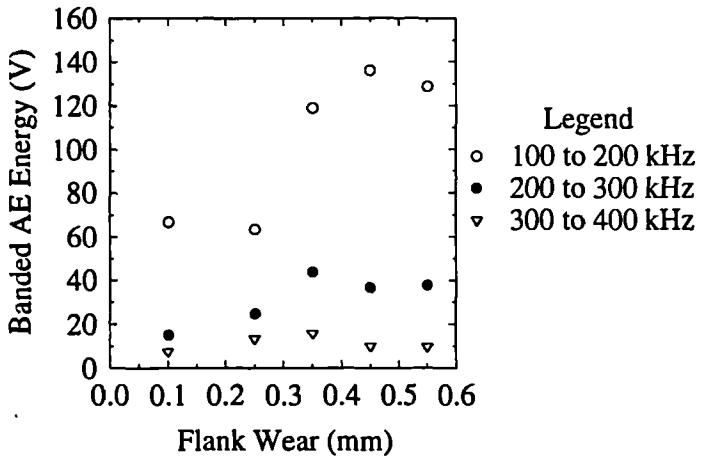

Figure 237: Variation in the Banded AE Energy with Wear for a Depth of Cut of 2.1 mm

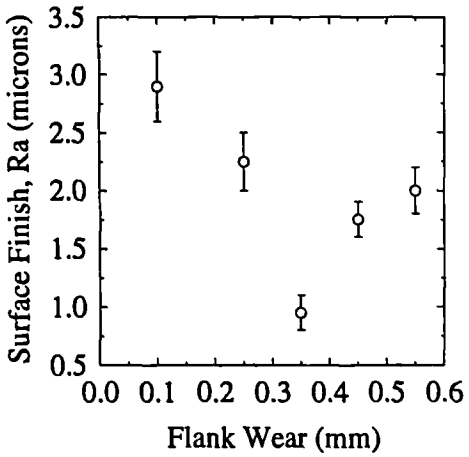

Figure 238: Variation in the Surface Finish with Wear for a Depth of Cut of 0.1 mm

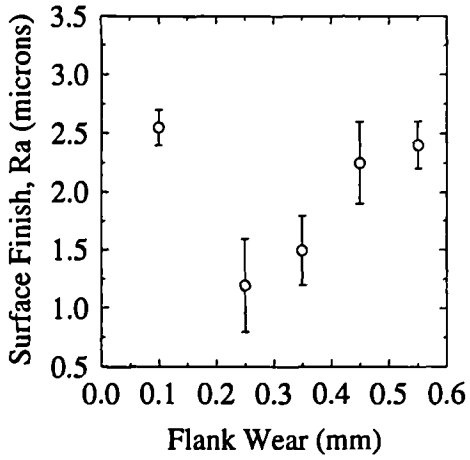

Figure 239: Variation in the Surface Finish with Wear for a Depth of Cut of 2.1 mm

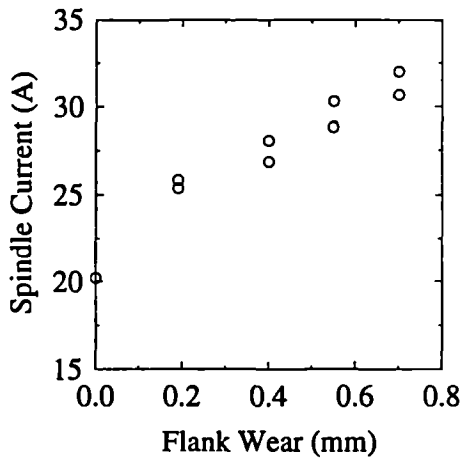

Figure 240: Variation in the Spindle Current with Wear for the Accelerated Wear Test

wear, Figures 240, 241 and 242. In contrast to the behaviour at the central point the rms AE appears to decrease with wear as can be seen in Figure 243 and apart from one point there are only small variations in the mean AE frequency with wear (Figure 244).

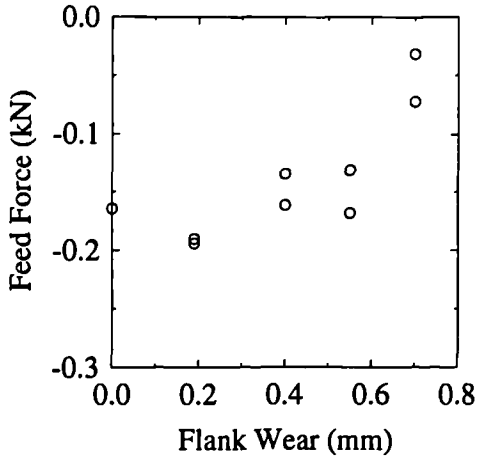

Figure 241: Variation in the Feed Force with Wear for the Accelerated Wear Test

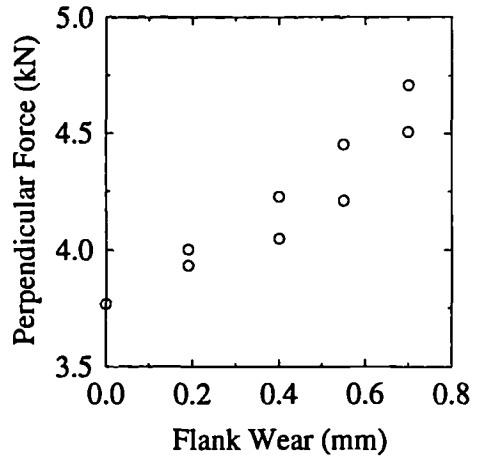

Figure 242: Variation in the Perpendicular Force with Wear for the Accelerated Wear Test

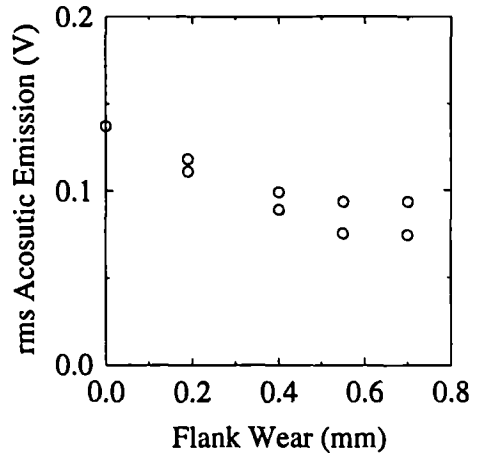

Figure 243: Variation in the rms AE with Wear for the Accelerated Wear Test

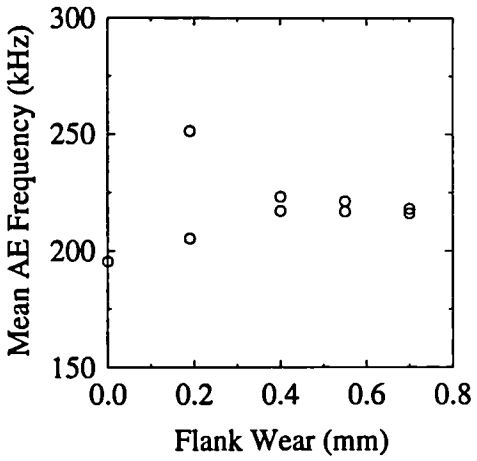

Figure 244: Variation in the Mean AE Frequency with Wear for the Accelerated Wear Test

Chapter 6

Discussion (of Results)

In this Chapter the results presented in Chapter 5 will be discussed in the light of observations made in Chapter 3. The discussion is organised into sections, each of which covers one set of the experiments that have been conducted to form this work. These sections are then sub-divided to cover each of the sensors used in that set of experiments, so that it is possible to assess the suitability of a given sensor, or set of sensors, to provide optimum cover for the monitoring task.

6.1 Preliminary Experiments

This section covers experiments which can be regarded as being of a calibratory or preliminary nature and, in particular, addresses the stiffness and insert geometry experiments discussed in Chapter 5.

6.1.1 Influence of Machine/Fixture Stiffness

From the experiments on machine/fixture stiffness (Section 5.1), it was seen that the general level of acceleration increases with the reduction in the effective machine stiffness (Figures 69, 70 and 71), as might have been expected and, to amplify this, Table 35 shows the variation in maximum acceleration variation with pillar diameter. It is important to note that the accelerations at the tooth passing frequency hardly change at all with pillar diameter, whereas those near to the natural frequency of the platform change dramatically.

For tool wear monitoring, the implication is that the cutting force and the workpiece vibration are likely to show behaviour which is heavily influenced by resonances. There will inevitably be cutting conditions which coincide with resonances of the force transducer and, even if a force transducer such as the one used in this work were not employed, there would be machine resonances that have a similar effect on the workpiece vibration. For this reason, any signal processing

Pillar Diameter	Maximum Acceleration
20 cm	7.1 mV
30 cm	4.7 mV
40 cm	3.8 mV

Table 35: Variation in Maximum Acceleration with Pillar Diameter

Pillar Diameter	Maximum Amplitude	Mean	Standard Deviation
20 cm	65 dB	1.7 V	0.4 V
30 cm	63 dB	1.6 V	0.4 V
40 cm	65 dB	1.7 V	0.4 V

Table 36: Variation in AE with Pillar Diameter

for force and/or acceleration would need to be filtered. This would be a complex operation as most headstocks display resonances in the same range of frequencies as that of spindle rotation and tooth passing, with the resonances of the vice usually occurring in a much higher region.

As was seen in Section 5.1 (Figures 72, 73, 74 and Figures 75, 76, 77) neither the amplitude distribution nor the power spectrum of the rms AE appear to be affected by the fixture vibration. The pertinent information from these Figures is shown in Table 36 for each of the pillar sets. This has two implications for monitoring, the first being that the AE signal should be independent of type of machine or fixture. Secondly, the clear tooth passing and rotational frequencies visible in the spectra indicate that a frequency analysis of the rms AE could, in principle, give information on the cutting process and the state of the inserts. This suggests possibilities for long-and short-timescale degradation monitoring and is independent of any effects seen in the power spectrum of the 'raw' AE.

This result adds weight to the suggestion made in Chapter 3 that the AE is not principally generated by the impact of inserts on the workpiece.

6.1.2 Influence of Insert Geometry on Sensorial Data

This set of tests will be discussed in the same order that the results were presented in Chapter 5 but first some general points will be made concerning all the experiments. As there was only one insert with the ground geometry in a tool holder with three other new inserts acting as 'controls', it can be expected that there would be quite a large dilution of the effect of the 'geometry insert' in the time-averaged sensorial information. Also, the fact that the inserts were

	Gradient (kN/mm)	Intercept (kN)
Feed Force	0.18	0.38
Perpendicular Force	0.63	2.75
Acceleration	0.0	2.25
rms AE	-0.04	0.22

Table 37: Summary of Results from a Simulation of Flank Wear

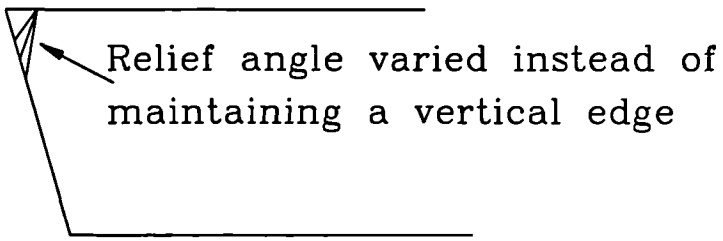

Figure 245: Specification of the Artificial Flank Wear

constantly removed and reset into the tool holder will increase the variability of the data.

Artificial Flank Wear Effect on Sensors

As was seen in Section 5.2 (Figures 78 to 80) a general trend for the sensorial data to increase with wear can be observed. These results are summarised in Table 37 by linear regression coefficients.

For the cutting force, a positive gradient is what would be expected by reference to the literature as it is generally accepted that the force requirement will increase as tool wear increases although, as discussed in Chapter 3, such observations may be due to crater wear which naturally accompanies flank wear. If this is so, the effect of an artificial crater should be larger than that of artificial flank wear. From the respective figures it seems that the two components of force exhibit opposite variations between the two artificial geometries and so the result is inconclusive.

The scatter in the results can probably be explained by the nature of the artificial geometry. In order to produce the artificial wear land, the insert was precision ground. This necessitated specifying the dimensions to be machined from the insert and, in so doing, it was found that the geometry was not identical to that occurring naturally. Figure 245 shows the specification of the artificial flank wear. The nature of this specification resulted in a variable relief angle with artificial VB_B and this could have introduced a retrograde variability in sensor output.

The perpendicular acceleration, Table 37, exhibits no variation with artificial wear. This is different from the majority of results obtained during systematic

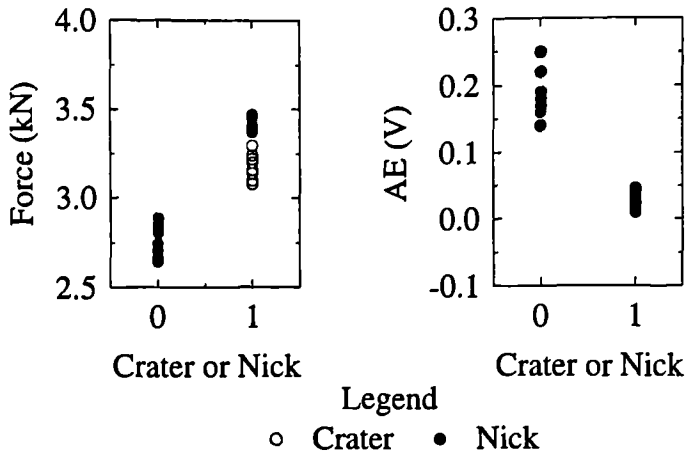

Figure 246: Summary of Sensor Ouput Changes with a Crater and Nicks on the Rake Face

wear tests, and so this would suggest that the variation in this experiment is too small for this sensor to detect or that the vibrations resulting from the inbalance introduced by the single modified insert are dominating the response. It is, however, interesting to note the difference between the perpendicular force and perpendicular acceleration. In principle, the two evolutions should be related to each other but, as was seen in Section 5.2, force increases and acceleration shows no variation.

For AE measurements there is no consistent trend with artificial flank wear. Also, there is a much larger spread of values in any one cut than for any of the other sensors, something that has been observed throughout the complete range of experiments conducted. The latter effect is probably inevitable in AE monitoring but the lack of any variation with flank wear is not surprising in the light of observations made in Chapter 3.

Crater and Edge Breakdown effect on Sensors

As seen in Section 5.2. and summarised in Figure 246, both components of the cutting force and workpiece acceleration are sensitive to the presence of a crater or nicks on the rake face although this is marginal for the feed component of force and perpendicular component of acceleration.

The above variations are almost certainly due to changes in the way in which the force transducer responds to the dynamic force regime. Since the insert geometry results in a different forcing function, and since there is an 'out of balance' in the insert set-up, the force level appears to rise as the vibration increases.

Again as seen in Section 5.2. (Figures 87 and 86) and summarised in Figure 246, the AE shows good sensitivity to both geometries and it appears that any disruption on the rake face, be it a crater or nicks, causes a reduction in the rms

Figure 247: Photograph of a Cutting Produced by the Insert with two Rake Face Nicks

AE of a roughly constant magnitude. A real edge breakdown event has been recorded during the systematic wear tests and forms part of the presentation of short-timescale events. The correlation between the simulated and real events is very encouraging. This suggests that at least part of the AE comes from chip flow mechanics over the rake face.

Table 38 shows the calculated change in chip temperature, force and total strain rate when a crater is introduced. It can be seen that there is a substantial change in all of these parameters that, as outlined in Chapter 3, will alter the motion of dislocations in the chip which will reduce the AE signal and increase the force both of which are in accord with the observations. It should be noted that such calculations can, at best, be seen as comparative and that any predicted effects will be diluted by the control inserts.

For the presence of nicks on the rake face it was not possible to accurately estimate the change in local rake angle, but from an observation of the chips produced by these inserts it is possible to observe the effect of that the geometry has as one or two ridges appear on the back of the chip in direct correspondence with the geometry. This can be seen in Figure 247 where a photograph of the cutting from an insert with two nicks is shown.

	Normal	Crater	Local Rake
Rake Change (degrees)	0	27	-6
Chip Temperature (C)	349	433	354
Strain Rate (s^{-1})	79500	53800	82600
Cutting Force (N)	500	1257	484

Table 38: Changes in Force, Strain Rate and Temperature with the Presence of a Crater and Small Change in Local Rake Angle

Local Rake Angle effect on Sensors

As was seen in Chapter 5, neither components of the cutting force nor the workpiece acceleration (Figures 90 to 93) show any clear trend with changes in local rake angle. Since it was found in the previous section that force and acceleration are sensitive to a crater or rake face nicks, it must be concluded that the artificial change in rake angle is not large enough to produce measurable changes in the force or acceleration. In this experiment the maximum change in local rake was -6° whereas, for the crater in the previous section, the change was of the order of 15°. The calculated values in Table 38 suggest that for the maximum local rake angle variation there is little change in temperature, force, or strain rate. This is stark contrast to the effect of the artificial crater and this is again consistent with the observations.

6.1.3 Summary Considerations from Preliminary Experiments for Long and Short-Timescale Tool Degradation

From the foregoing discussion of the preliminary experiments, the following considerations can be carried forward into the discussion of the major series of experiments, namely those for short and long-timescale degradation.

(a) *Force and Acceleration*
Both these sensors are subject to contamination from resonance of the force transducer which can lead to a greater sensitivity but is unreliable due to the fact that the dynamic properties of the machine and fixture will change with cutter position. Force is generally a better sensor to use than acceleration as it contains a d.c. component.

(b) *Acoustic Emission*
High variability within a cut generally masks any geometrical effect, except for disruptions in the rake face where a definite reduction in AE can be

observed. The insensitivity of the AE to vibration allows the sensor to be used as a monitor in a variety of dynamic situations and its high temporal resolution allows frequency analysis within a tooth pass.

Therefore, it would be expected that AE would be a suitable sensor for short-timescale degradation and possibly for wear (as rake face discontinuities appear). An rms analysis of the AE signal is therefore worthwhile, but other processing schemes might reveal further sensitivity.

It would be expected that force might be useful for wear monitoring, although possible variable contamination of the signal due to resonance effects has to be considered.

Spindle current was not monitored during these preliminary experiments as it was felt that enough was known about this sensor to allow it to be carried directly to the short and long-timescale experiments.

6.2 Discussion of Results obtained from Systematic Wear Tests on En8 and En24 Workpiece Materials

The results for wear tests will be discussed here on a sensor by sensor basis in order to bring out commonality in the results and to highlight any inconsistencies or repeatability problems that the sensor has suffered. Spindle current has been introduced into the analysis almost as a control sensor as its evolution with wear is quite well known and it will provide a benchmark against which to evaluate the other sensors. Force has been carried forward as has the perpendicular component of acceleration (which appeared to be the most sensitive component) along with the AE, which has been analysed in several different ways. The results from the preliminary experiments will be used to compare/contrast with the results obtained in these systematic wear tests.

6.2.1 Flank Wear Evolutions

As was seen in Section 5.3. the evolution of flank wear for machining of En8 follows a trend not exhibited during any of the other tests (Figure 94). This is almost certainly due to the combined factors of the relatively low cutting speed of 125 $m.min^{-1}$ and the large grain size of the material after it had been annealed. Figure 248 shows all wear evolutions from systematic wear tests, and clearly the wear rate during the En8 roughing test is very different from the remainder. The En24 wear evolutions are also plotted separately in Figure 249 to highlight the differences between them, not discernable from Figure 94.

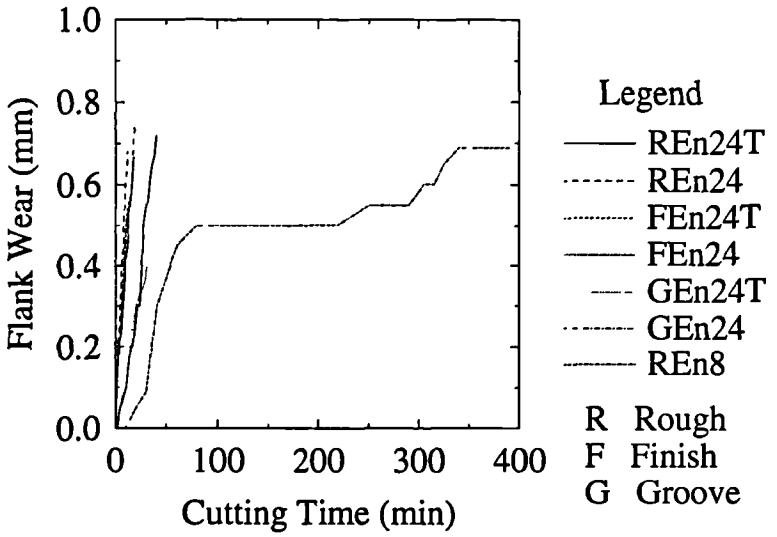

Figure 248: Evolution of Flank Wear for all Systematic Wear Tests

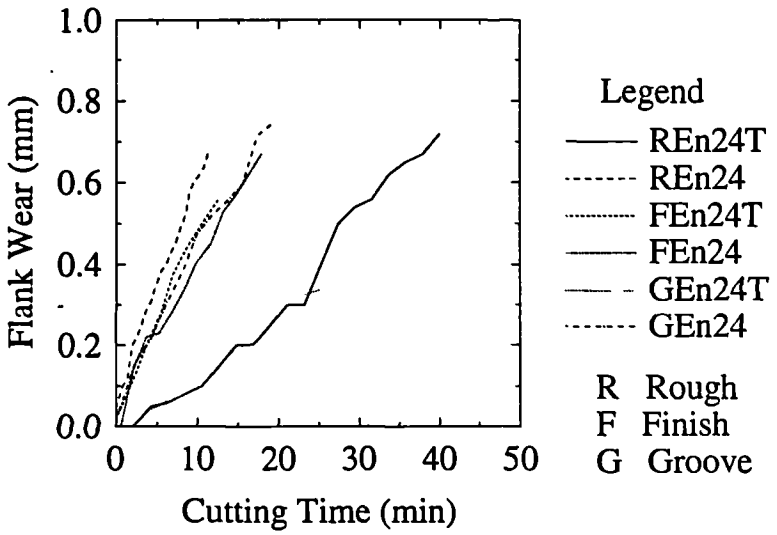

Figure 249: Evolution of Flank Wear for Systematic Wear Tests on En24

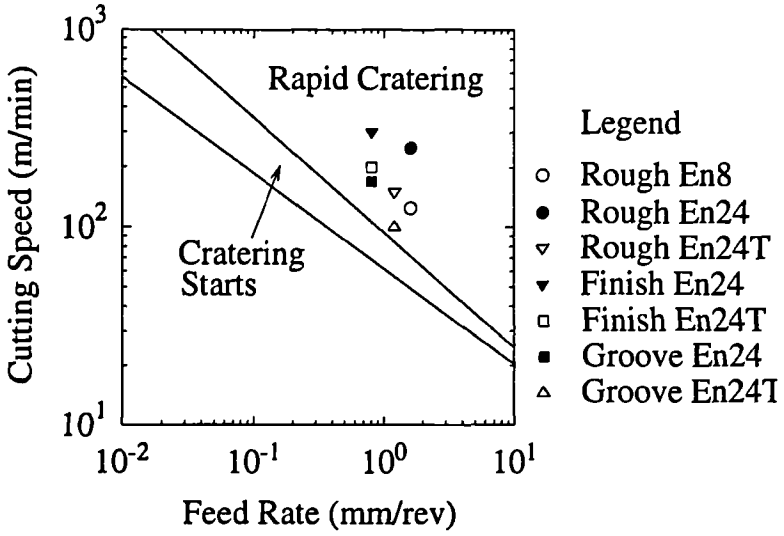

Figure 250: Severity of the Systematic Wear Tests

To assess the severity of these wear tests a machining diagram from Trent [3] has been reproduced (Figure 250) and the test conditions used here are marked on. From this, it can be seen that all tests are severe with the majority of tests on En24 being the most severe.

The repeatability of flank wear trends, shown in Figures 248 and 249, demonstrates the level of accuracy required from any monitoring system that is going to use sensors to measure tool wear rather than simply measuring the time the tool has been cutting, although, as discussed in Chapter 2, this latter method does have some logistical problems.

6.2.2 Spindle Current

It is clear from Figure 251 that the spindle current is generally well correlated with wear. As pointed out previously, no spindle current measurements are available for the En8 material.

As discussed in Chapter 3, it would be expected that the power required to perform the cutting operation will rise by approximately 30 to 40 % between a new and old tool and this is certainly confirmed by the observations.

6.2.3 Cutting Force and Workpiece Acceleration

From the results obtained in the 'Influence of Geometry' experiment it would be expected that both components of force would increase with both crater and flank wear.

In fact, seven out of the eight wear tests showed a reasonably linear increase with

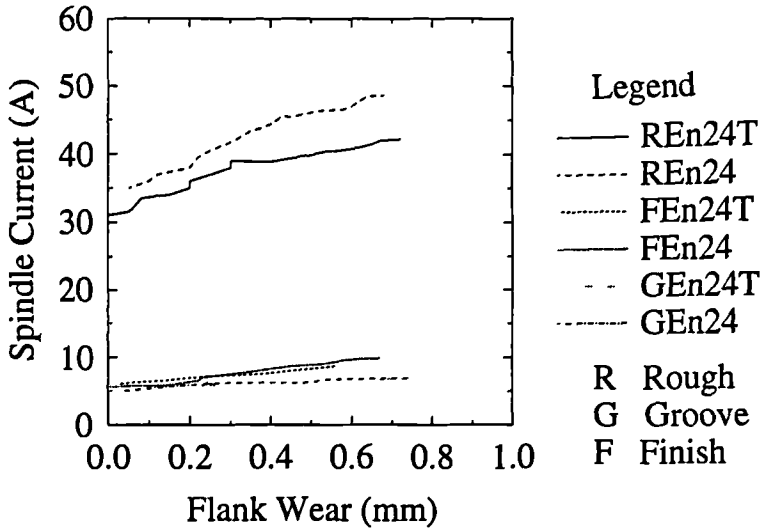

Figure 251: Spindle Current Variations for Wear Tests on En24(T)

	En24			En24T			En8
	R	F	G	R	F	G	R
Perp. Force (kN)	5.0	2.14	2.14	2.5	-2.1	3.75	2.85
Feed Force (kN)	0.5	0.53	0.61	1.1	0.42	2.5	-0.7
Wear Rate (mm/min)	0.04	0.04	0.04	0.02	0.05	0.02	0.002

Table 39: Gradient of Force Variation with Wear for Systematic Wear Tests

flank wear for both components of the cutting force as shown by the gradients of the evolutions summarised in Table 39. Table 40 shows a summary of the intercepts of the force and it can be seen that severe cutting conditions correspond to a large intercept (both roughing conditions show a very large intercept) but that the differences between materials are quite small. In general there is no correlation between intercept and wear rate as can be seen by considering the variations for tests on annealed En24. Similar observations can be made about the effect of wear rate on the gradient of the force variation with wear.

One point that is common to all plots of force is that values taken from one cut tend to spread out as the tool wears. This is almost certainly due to a dynamic interaction between the tool and force transducer, with the increasing load required to cut the workpiece acting as a larger forcing function and so amplifying the resonance of the sensor. One other effect that may play a part, as in the 'geometry' tests, is that inserts may perform different amounts of cutting due, for example, to variable wear, so generating periodic variations in force as the tool rotates. This effect would generate a broader range of frequencies and so would be expected to stimulate more resonances. Finally, the cutter position in relation to the strain gauged pillars will determine which of the perpendicular, feed or rotational mode shapes will be dominant, as was shown in Chapter 3.

	En24			En24T			En8
	R	F	G	R	F	G	R
Perp. Force (kN)	5.8	1.0	2.0	5.5	3.5	2.8	0.4
Feed Force (kN)	1.0	0.2	0.5	0.75	0.27	0.5	0.0
Wear Rate (mm/min)	0.04	0.04	0.04	0.02	0.05	0.02	0.002

Table 40: Intercept of Force Variation with Wear for Systematic Wear Tests

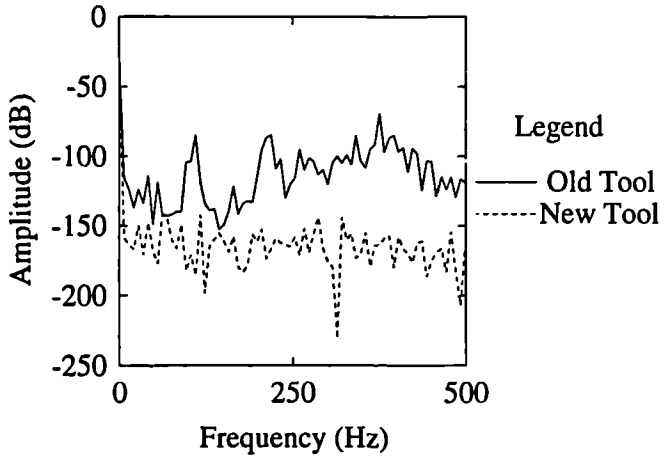

Figure 252: Power Spectra of the Feed Force for a New and Worn Tool, whilst Rough Machining on En24

In order to assess the affect of a possible resonance a power spectrum calculation has been conducted on what appeared to be the worst case of resonance contamination. The result is shown in Figure 252 where it is clear that there is indeed contamination of the signal due to resonance effects.

The workpiece acceleration is closely related to the cutting force and generally follows a similar trend with tool wear. In a similar manner to the force there is a spread of values as the tool wears. This again will be due to resonance effects although no frequency analysis has been undertaken.

6.2.4 Acoustic Emission

The rms AE signal is capable of providing a prediction of tool wear, for some of the wear tests conducted. However, the sensor is not very repeatable and can produce a non-monotonic variation with wear.

A reduction in the rms AE signal with wear can be explained by changes in the chip flow over the rake face due to the appearance of crater wear (Figure 253 shows the profile of a crater from one insert from a roughing test on the En24

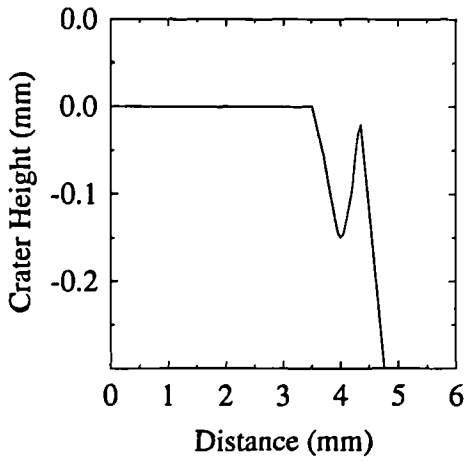

Figure 253: Profile of a Crater for one of the Inserts, from one Wear Test

Crater	Strain Rate	Chip Temperature
New(No)	92832	700 C
Old(Yes)	41384	822 C

Table 41: Changes in Strain Rate, based on Oxley model, for rough machining on the En24 Material

material and Table 41 displays the calculated changes in strain rate). However, there is little evidence of a systematic reduction of the AE signal in this manner occurring during the systematic wear tests which would make this feature useful for wear prediction. Furthermore, the sensorial output can increase or decrease with wear, as the gradients of the rms AE and cumulated rms AE in Table 42 shows.

If the rms AE were only dependent on the strain rate and temperature then it would be expected that the AE would change in the manner suggested above. Since this is not the case there must be more phenomena on which the AE signal is dependent. Amongst these might be competing geometrical effects which a simple crater analysis does not take into account.

Some authors [26,27] have presented data that suggest that the cumulative rms AE signal is related to the wear. If the cumulation is related to the wear, then it would be expected that the general level of AE would be related to the wear rate, and to assess, this both have been gathered in Table 42. As can be seen low wear rates can correspond to low AE signals but that this result is not consistent. This may simply mean that there is not a large enough variation in wear rate to detect any effect above those due to metal removal rate, strain rate and temperature.

The low repeatability of the AE sensor can also be a problem, as was shown in Section 5.3.2. The worst case of lack of repeatability between two nominally

	En24			En24T			En8
	R	F	G	R	F	G	R
Wear Rate (mm/min)	0.04	0.04	0.04	0.02	0.05	0.02	0.002
Metal Removal (mm^3/s)	3449	414	1414	1550	276	1252	1066
AE level (V)	1.4	0.25	0.22	0.4	0.2	0.22	0.4
Cum. AE (V/mm)	29.5	3.3	3.3	7.9	2.8	5.8	5.0
Strain Rate (s^{-1})	90000	88000		138000	210000		80400
Chip Temp. (C)	700	700		685	730		348

Table 42: Wear Rates and Other Parameters for Wear Tests Conducted on En24 and En8

identical tests is shown in Figure 143. It is possible that this problem can be explained by coupling variations between the vice and workpiece. As was shown in Section 4.1. (Figure 48) the AE signal drops when the clamping force between the vice and workpiece reduced to the extent that it is possible to produce variations of a few dB by varying the torque in the region of 80 to 100 Nm. Although the clamping torque was not calibrated it is probable that the clamping force varied between tests and this torque level is in the region that would be applied by a vice handle.

The other question over repeatability arises from variable coupling of the AE sensor to the vice but, during this set of tests, the sensor remained coupled for all but the test on En8 and one roughing test on En24. Therefore, this cannot be used to explain problems arising from repeat wear tests.

In view of the limited capabilities of time-domain AE processing to detect wear, it was decided to analyse the AE signal over its complete bandwidth for a limited data set. This, however, brings the analysis much closer to the shortcomings of the sensor, i.e. crystal resonances. The simplest types of processing that minimise the effect of resonance are to calculate the mean frequency and to perform an analysis of the energy contained within specific frequency bands.

For the plots of mean frequency with wear, presented in Section 5.3, there is little evidence to suggest that there is any shift with wear. Most of the plots exhibit no change with wear with the mean frequency lying within the first resonance of the sensor (not surprisingly).

From the band analysis of the AE signal it has been found that there are small

Test	Wear Condition	Mean shear plane separation
En24T Roughing	New	550μm
En24T Roughing	Old	600μm
En24 Roughing	New	500μm
En24 Roughing	Old	550μm
En24T Finishing	New	900μm
En24T Finishing	Old	850μm
En24 Finishing	New	700μm
En24 Finishing	Old	800μm
En24T Grooving	New	600μm
En24T Grooving	Old	700μm
En24 Grooving	New	500μm
En24 Grooving	Old	350μm

Table 43: Variation in Shear Plane Separation, New to Old Tools, for the Tests on En24 and En24T Workpiece Materials

but consistent shifts in energy with wear. Most of this shift is towards lower frequency, i.e. the 100 to 200 kHz energy band tends to increase with wear, while other bands show no change or reduce slightly with wear.

This change in the energy contained in the different frequency bands appears to tie in with proposals made in Chapter 3, where a lowering of the strain rate and increase in the temperature will cause more AE power to be concentrated in the lower frequency bands. An investigation of micrographs of new and worn chips is inconclusive in showing any variation in the shear plane separation (Table 43) between a new and worn out insert for the wear tests on En24. This analysis is rather coarse as it does not take into account changes in the temperature at the tool-chip interface as the tool wears, as was shown in Figure 100. This effect would allow for a greater mean free path which would cater for the increase in energy in the lower frequency band as the dislocations travel further, generating lower frequencies.

6.2.5 Surface Finish

The surface quality, as measured by the R_a value, and shown in Section 5.3., shows rather a wide variation in any one cut. There is a general trend for the R_a values produced by tools with medium values of flank wear to exhibit lower values than that produced by either a new or worn tool. It is worth noting that the actual surface quality is observably different between a new and worn tool. To the eye the surface produced by a new tool appears to have been cut more 'cleanly' than that produced by an old tool. The surface produced by an old tool

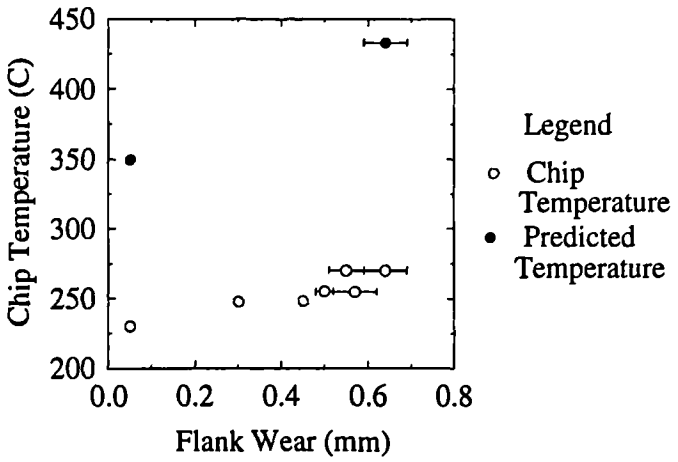

Figure 254: Observed Variation in Chip Temperature and Calculated Chip Temperature

appears to the eye to be 'smeared', rather than cut and clearly this variation is not picked up by the parameter R_a.

6.2.6 Chip Temperature

Figure 254 shows the assessed and predicted temperatures for rough milling on En8. The calculation was made based on expected rake angle variations due to the development of a crater and, although the absolute values are high, the variation with wear is roughly the same as that estimated from chip temper colour.

6.2.7 Summary of the Systematic Wear Tests

For the range of materials tested and the particular tools used it has been seen that the best sensors to use in a tool wear monitoring system would be spindle current, feed force, and acoustic emission although the latter two are less reliable for reasons outlined in the text.

The form of signal processing of the spindle current and force sensors is very simple and could easily be implemented. For the acoustic emission sensor, however, a more complicated range of analysis may be required. It is a simple matter to rms the output of the AE sensor and arrange for the result to be cumulated but, in order to use the band analysis of the full bandwidth AE signal, it is necessary to use acquisition equipment which also possesses a large bandwidth. Further, in order to gain confidence in the data points, a large frequency analysis would be required. This would result in a large amount of data being collected every cut, and some sophisticated data handling routines would have to be implemented in the analysis software in order to cope with this.

It might be thought that the best component of the cutting force to implement would be the perpendicular component as, for some of the tests, its output is better correlated with tool wear than the feed component. It is, however, more difficult to implement a perpendicular force sensor into a commercial machine than it would be to implement a feed force sensor.

6.3 Discussion of Short Timescale Event Results using Cutting Force and Acoustic Emission during Face Milling Operations.

The results for short-timescale degradation will be discussed for each particular experiment in turn. In general only force and AE are discussed as it was found that these two sensors provided the best sensitivity to the events.

6.3.1 Weld Traverse

Figure 255 shows the evolution of the time series of sensor outputs (the full plots were presented in Section 5.5.) from the AE and force sensors respectively along with the variation in hardness across the weld bead. As the tool traverses the weld bead it can be seen that both AE and force increase but that the AE increase is greater.

Within the weld metal itself, the AE peak height is generally higher than in the parent material but also shows a wide variation, such as one might expect when traversing a region of variable hardness such as that caused by the overlap of weld beads. It would be expected from the change in structure of the base to weld material that dislocations would have a shorter time of flight between obstacles (smaller grain size and more inclusions in the weld material) which according to current thinking on the generation mechanisms of AE would result in a larger signal.

6.3.2 Pre-Cracked Insert

As was seen in Section 5.4 the AE signal responds to the insert breakage with a large peak as the insert breaks whereas the force responds to the event one rotation later. The argument made in Section 5.5 is summarised in Figure 256.

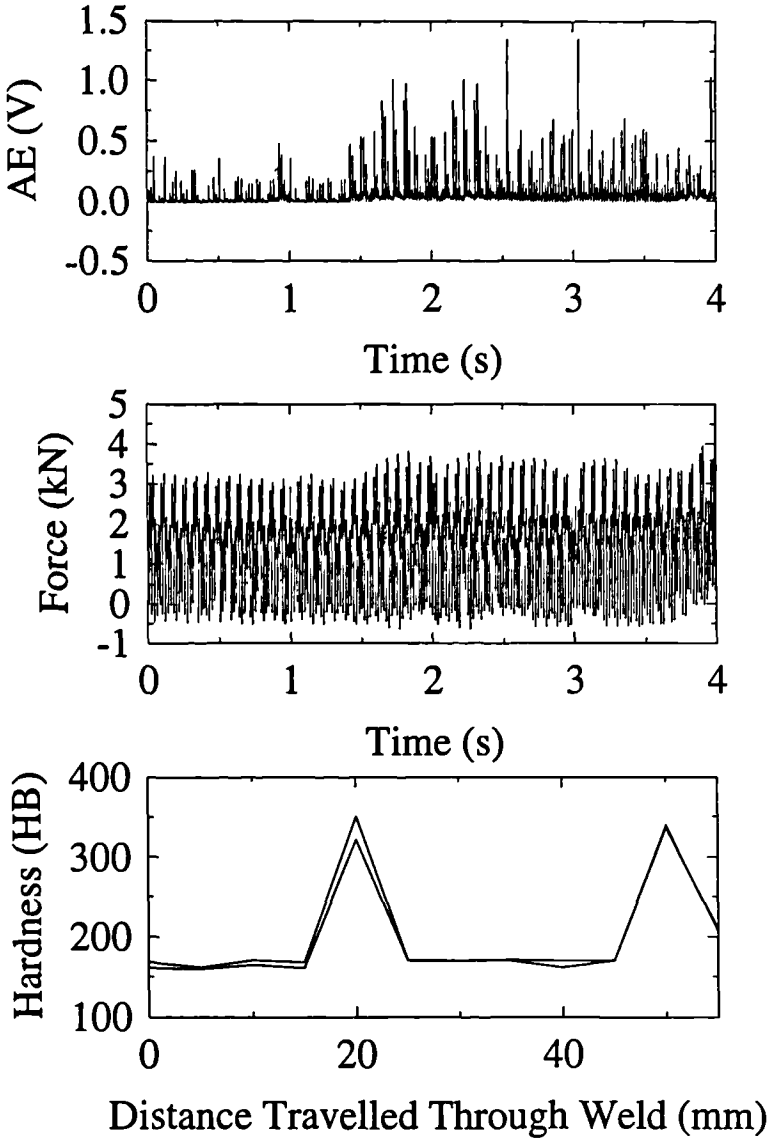

Figure 255: Schematic of the Variation in Sensor Output with Weld Hardness

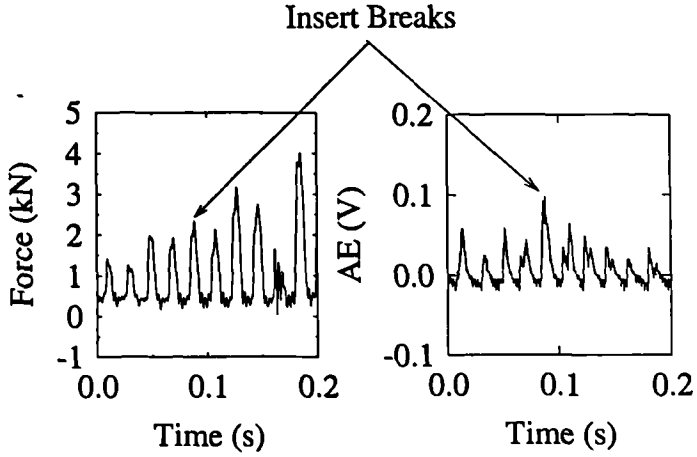

Figure 256: Summary of Pre-Cracked Insert Event

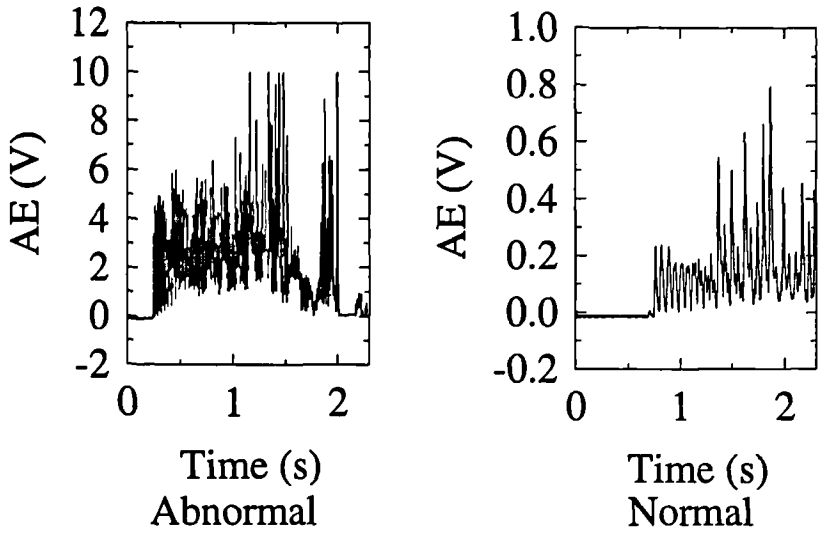

Figure 257: Normal and Abnormal rms AE

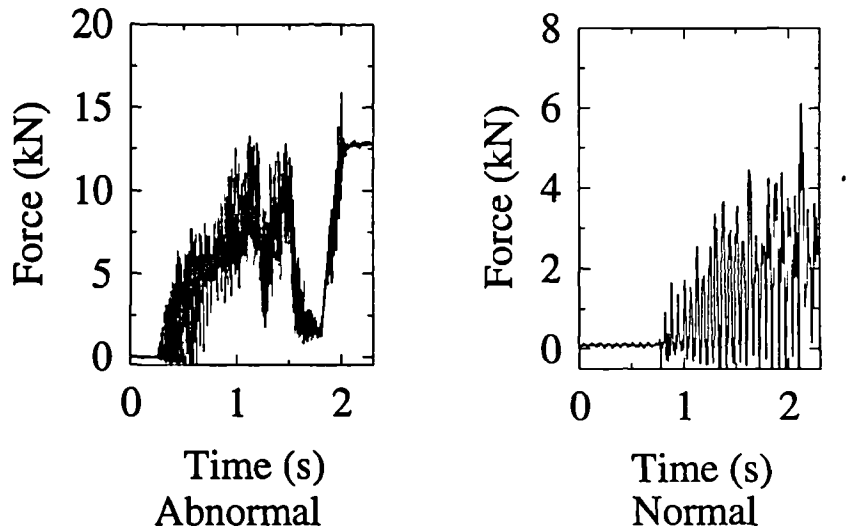

Figure 258: Normal and Abnormal Perpendicular Force

6.3.3 Insert Failure and Machine Stall under Inappropriate Cutting Conditions

Figures 257 and 258 show plots of normal and abnormal AE and force as the cutting tool enters the workpiece.

It is important in this instance to note that the rms AE, in Figure 257, for an abnormal cut is much higher than that for a normal cut. Whereas Figure 258 shows that the cutting force does not show any unusual levels until the tool has performed considerably more cutting than that necessary for the AE to detect the event.

It can be seen that the force (and other sensorial information) first exhibit features that would suggest that something is amiss with the cutting conditions some ten

rotations of the tool after the rms AE.

6.3.4 Insert Edge Breakdown

As was suggested in Section 6.2 the edge chipping event is very similar to that obtained with the artificially generated edge breakdown in the 'geometry' tests.

It was seen in Section 5.4 that the tooth passing information in the rms AE signal is severely reduced after the edge chipping event, whereas a slight increase can be observed in the perpendicular cutting force. This result is exactly what would be expected from the simulation of an edge break down that was discussed in Section 6.2, and was predicted in Chapter 3 when large changes in strain rate and temperature were observed for changes in local rake angle produced by a crater.

Although the edge chip is not like a crater, it does produce a change in the rake angle of the cutting insert and the explanation carried forward from Chapter 3 is that the secondary deformation zone on the chipped insert is much larger (the Oxley model does predict a much thicker chip for local rake angle increases), thus generating a higher temperature and a lower strain rate in the chip and surrounding area of the workpiece. In Chapter 3 it was seen that AE activity will decrease as temperature increases and also the stress-strain characteristic will be altered perhaps altering the length of time a chip is in contact with an insert. Certainly the chip form was observed to change when one of the inserts became damaged, changing from a three dimensional helix to a two dimensional spiral and, although this would only be expected to affect the one insert, it is clear from the AE signal that the signatures from all inserts have been disrupted.

There are subtle changes in the perpendicular force from before and after edge chipping but the effect is not as dramatic as that of the rms AE. There is a modest increase in the standard deviation of the signal and there are changes in the form of the force peaks for each tool rotation, which might be explained by the change in tool geometry exciting a resonance of the mechanical force transducer. This increase in force was also predicted in Chapter 3.

The corresponding plots for the feed component of cutting force show no significant change from before and after edge chipping.

6.4 Discussion of the Influence of Cutting Conditions on Sensorial Information

Again, the experiments on influence of cutting conditions will be discussed sensor by sensor in order to facilitate the isolation of effects due to cutting conditions from those due to wear.

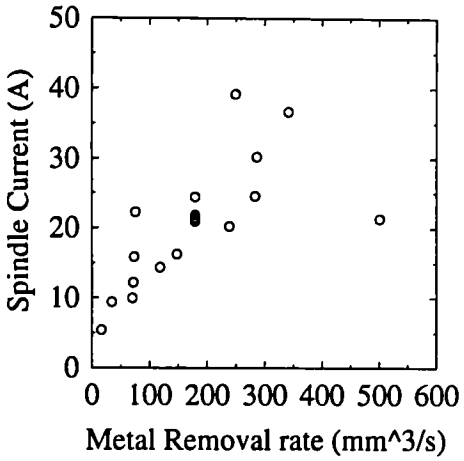

Figure 259: Variation in the Spindle Current with the Metal Removal Rate

6.4.1 Spindle Current

From Section 5.5. the spindle current was seen to vary in a linear manner for variations with depth of cut and feed rate with little variation with cutting speed (Figures 170 to 172). This result is well known and could have been recovered from most machining handbooks.

If the spindle current is plotted against the metal removal rate, as in Figure 259, it can be seen that there is a general linear relationship between the two parameters if the current value for 500 mm^3/s is disregarded. As was mentioned in Chapter 3 the current is only directly related to power for constant rotational speeds, as the rotational speed determines the voltage applied to the motor. This explains why the evolution of current with metal removal rate is not as linear as might be expected from Equation 7.

6.4.2 Cutting Force

In common with the spindle current, both components of the force required to remove material from the workpiece are linearly related to the depth of cut and feed rate, and not influenced by the cutting speed in any systematic manner, as was seen in Seciton 5.5. (Figures 173 to 178).

Both components of the cuttinng force show similar trends with the metal removal rate (Figures 260 and 261) with the feed component exhibiting a greater scatter, a result that would be expected from the systematic wear rates. Since cutting power is generally considered to be proportional to metal removal rate, this relationship is not at all unexpected and the scatter is again explainable in terms of transducer resonances.

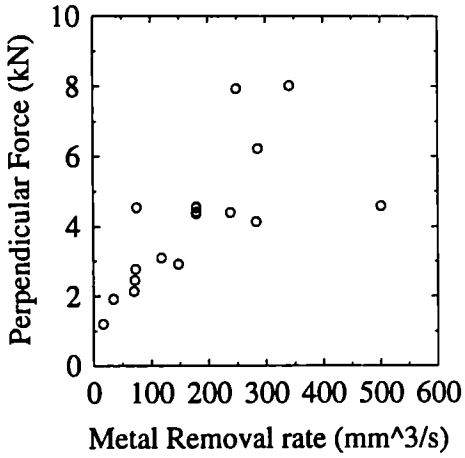

Figure 260: Perpendicular Force Variation with the Metal Removal Rate

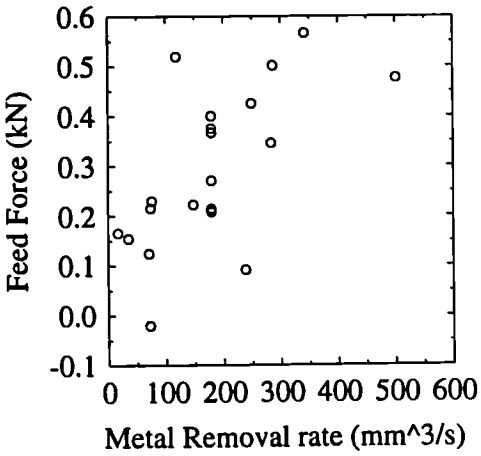

Figure 261: Variation in the Feed Force with the Metal Removal Rate

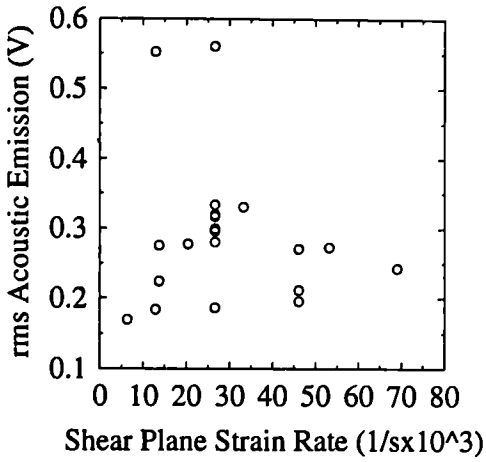

Figure 262: Variation in the rms AE with the Shear Plane Strain Rate

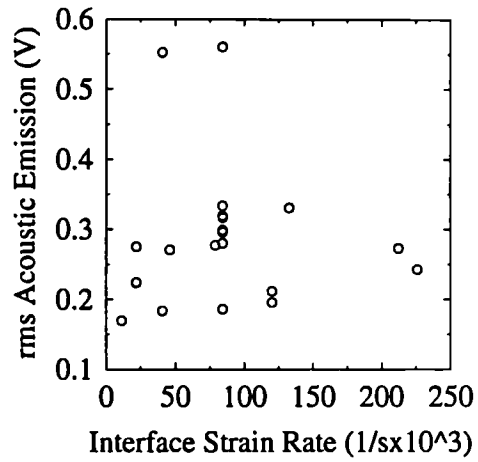

Figure 263: Variation in the rms AE with the Interface Strain Rate

6.4.3 Acoustic Emission

From Chapter 5 (Figures 179, 180 and 181) it appears that the rms AE increases as the depth of cut increases, and this is a result that would be expected from the short-timescale experiments although there are only a few points that can be plotted. Again, as was seen in Chapter 5, there are no systematic variations of the AE with the other cutting parameters.

Figures 262 and 263 show the rms AE signal plotted against the shear plane strain rate and interface strain rate from the model of Oxley as outlined in Chapter 3. Firstly, it can be seen that both plots follow very similar trends and, with the exception of two points, the rms AE values remain almost constant, showing very little tendency to increase or decrease with strain rate.

The rms AE signal shows a similar correlation with the metal removal rate, with the same two exceptional points giving the impression that the AE increases (Figure 264).

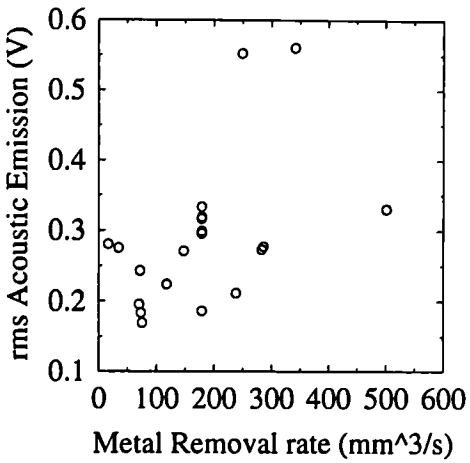

Figure 264: Variation in the rms AE with the Metal Removal Rate

As discussed in Chapter 5, the mean frequency (as was seen in Figures 182 to 182), shows little tendency to vary with the cutting parameters and the band analysis of the AE signal exhibits an inconclusive variation with the cutting parameters.

6.4.4 Surface Finish, R_a

It is generally accepted that high cutting speeds and low feed rates when combined, lead to a better surface finish. However, as discussed in Chapter 5 there has been very little observable variation in R_a values over the range of conditions investigated.

6.5 Discussion of the Variations of Sensorial Output for Different Cutting Conditions with Wear

Since the object of the cutting conditions experiment was to allow an extension of the systematic wear data to other cutting conditions it was necessary also to carry out a limited investigation of the effect of wear over the range of cutting conditions and this is discussed in the next section.

The results from the various sensors used during the random walks, will be discussed sensor by sensor as the tool wears.

6.5.1 Spindle Current

It is stated that the cutting power [29], although providing a good correlation with wear for large values of the cutting parameters, does not perform well for

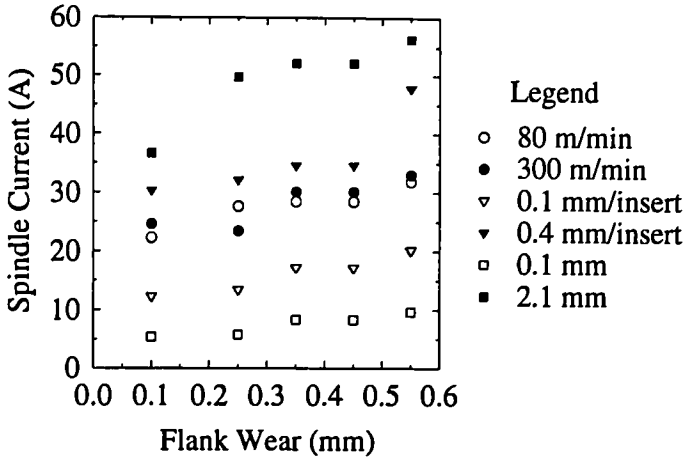

Figure 265: Variation in Spindle Current with Wear for the Extremes of Conditions

small values due to a disadvantageous signal-to-noise ratio.

In this work, this has not been found to be the case as can be seen in Figure 265 where there is a systematic increase in the sensorial output with wear for all conditions.

The accelerated wear test which was conducted to verify the central point of the condition space also exhibits a very linear variation with tool wear.

6.5.2 Cutting Force

The general linear increase with wear for the different conditions observed during the systematic wear tests does not appear to occur in this experiment. It might have been expected that there would be little variation with wear for small depths of cut or low feed rates, but even the high feed rate and high depth of cut tests do not exhibit the expected variation with wear. The sensitivities of the cutting forces to cutting conditions are quite good, however, so from that point of view the sensor should perform better than it appears to do in this test.

6.5.3 Acoustic Emission

At the start of this work, the aim was to use a variety of sensors, in a tool wear monitoring role, so that a greater number of cutting conditions, and materials could be monitored. The AE sensor was looked upon to provide a reliable wear monitor for the areas where the more traditional sensors do not perform so well, something that for spindle current at least does not appear to be necessary.

It is possible to observe very good correlations of AE with increasing tool wear, for the central point of the condition space. Figure 266 shows a summary of all

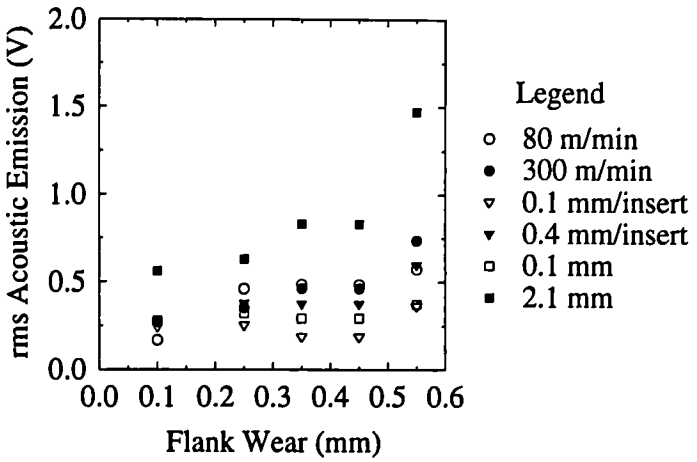

Figure 266: Variation in rms AE for the Extremes of Cutting Conditions

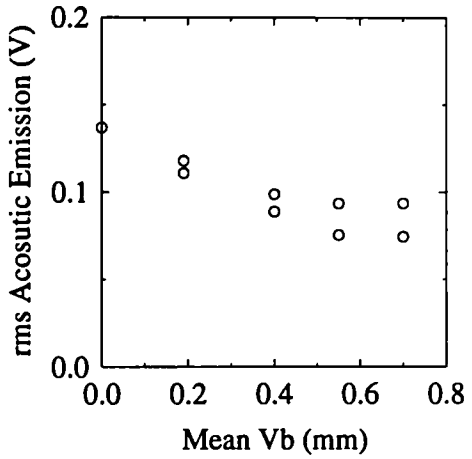

Figure 267: Variation in rms AE for the Accelerated Wear Test

the conditions and it can be seen that there is generally a linear increase with wear. In the corresponding plot for the accelerated wear test (Figure 267) the rms AE reduces in amplitude. This may be due to differences in the wear profile which are generated with the rapid wearing of the tool on the hard material. It would be expected that rapid wearing would cause high temperatures, leading to rapid cratering, whereas for the random walk tests the mean cutting speed was much lower, leading to a lower rate of crater development. This, as was discussed in Chapter 3, would lead to a lowering in the AE for the development of craters. This observation reinforces a very important point concerning the use of the AE sensor as a tool wear monitor in that it is perhaps too sensitive to the cutting geometry to be used reliably in a progressive wear monitoring role.

The other point to be made is that the AE sensor does not appear to perform as well as the spindle current sensor for the lower end of the cutting condition space. As can be seen in Figure 266 the AE signal does not vary very much with wear for the case of a small depth of cut.

As was seen from the plots of mean AE frequency and energy with increasing

tool wear (Section 5.5), it is difficult to see any evidence for systematic variations with tool wear. For many of the plots the number of points is too small to make considered judgements. When these results are taken together with the systematic wear tests it seems that there is little, if any, shift in the mean AE frequency with tool wear but that there is probably a change in the energy contained in the different frequency bands as a tool wears.

6.5.4 Surface Finish, R_a

The variation of surface finish, as measured by R_a, follows a very familiar pattern for the majority of plots. The general 'U' shaped variation with wear is repeated again pointing to the desirability of having a different parameter to describe surface finish.

6.6 Tool Condition Monitoring

From a broad consideration of the foregoing discussion it would appear that the best sensors to monitor tool wear are spindle current, the feed component of cutting force and the AE in decreasing order of reliability [29,45,73,94,104]. For breakage detection the same three sensors would be useful but in the opposite order of reliability [112,39,40].

Apart from its sensitivity the other constraint on using any sensor in a tool condition monitoring role is the one of how to implement it on a production machine. This is easily answered for the spindle current sensor, but for the others it is more difficult. It is possible to implement a feed force transducer by calibrating the feed motor but it would be very difficult to implement a perpendicular component force sensor in the same way. The AE sensor could not be placed on the vice or table as these are changed quite regularly in a machine shop [114]. A non-contacting AE probe would solve this problem [84], as it would then be possible to measure the AE signal on the rotating tool holder. A number of means might even be conceived to carry out surface measurement in-process.

It seems, then, that it is possible to implement the majority of sensors into the machine tool but the cost would, of course, have to be balanced against the benefit. Annual tooling costs in a normal machine shop would probably be around 5 % of the cost of the machine tool. If the tool wear monitoring system can gain an (optimistic) extra 10 % [111] in tool life then the cost of the system, based on a typical computer hardware pay back period of one year, should not be higher than 0.5 % of the cost of the machine. These are stringent constraints to meet, and the cost of a system to monitor tool wear would have to be spread over several machines in a normal workshop. The ability to cope with different materials, tools and machines, and all their different effects on tool wear is therefore very important.

The type of wear monitor to be implemented could in fact be tailored to the type of machine shop in question. If the machine shop produces high added value components then it should be possible to implement several sensors, maybe even optical fibre based AE sensors (McBride et al [84]) and then monitor tool wear and breakage based on the full set of sensors, as used in this work. If, however, the machine shop is producing large numbers of low added value components, then it would probably only be possible to use one sensor, and this would have to be the spindle current. Most modern machines have this sensor fitted, so it would be relatively easy to retrofit the wear monitoring system to a large number of establishments. However, this would afford only modest predictive capabilities for breakage detection in any but the most severe of circumstances. If this was a necessary requirement, then the next best sensor to incorporate in this role would be a PZT AE sensor, fixed permanently to a part of the machine that is not moving.

If the primary concern is surface quality and not wear the surface finish could be monitored using, for example, novel fibre based techniques so that in-process surface quality could be monitored, Hand et al [150].

In summary, it appears that the type of monitoring system to be used depends on the primary function of the machine shop in which the system is to be installed, and a variety of different solutions could be envisaged.

The next Chapter describes two approaches to the use of the sensorial data to build a tool wear monitoring system using spindle current, feed force and AE, and one for a tool breakage system, using only AE.

Chapter 7

Application of Artificial Intelligence

In the foregoing it has been seen that, although some sensors are more suitable for wear detection than others, it would be benificial to combine the information from several sensors to give a more reliable and verifiable indication of wear state. Further, special techniques will be necessary for detection and action in the event of short-timescale degradation.

This Chapter therefore presents the application of some AI techniques to some of the data which has been acquired, taking into account the foregoing analysis of sensor suitability.

As a direct comparison between the approach of an Expert System and a Neural Network, both have been applied to the same set of data in an attempt to bring out the relative advantages and disadvantages in a progressive tool wear monitoring role.

It has been observed that the short-timescale events that occurred during this work (Section 5.4) cause complex changes to sensorial information. It would therefore be very difficult to define rules for an Expert System to use this information to detect tool breakage and so only a neural network has been applied to the tool breakage data.

For long-timescale monitoring, data from one wear test has been selected, the central point of the random walk experiments described in Section 5.6.2. This set of data was used because the tool life had already been divided into five separate wear classes (necessary if the data is going to be used in an ANN) but, in principle, it would have been possible to use any of the wear test data.

For the Expert System simulation, a correlation line was calculated for five of the six data points with the remaining point from each of the sensors being used by the Expert System to estimate the flank wear of the tool. For the Neural Network, the same data as was used to calculate the correlation lines for the Expert System

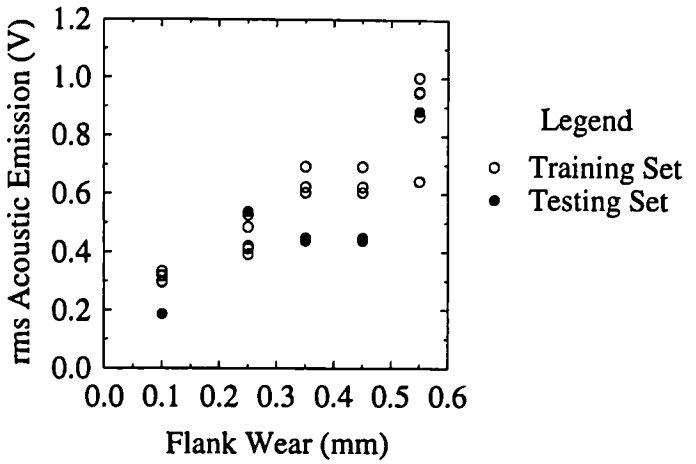

Figure 268: Training and Test Data from the Acoustic Emission Sensor

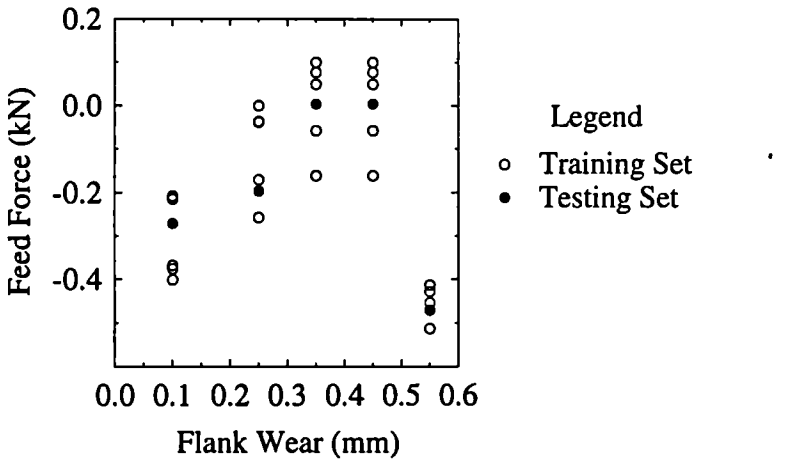

Figure 269: Training and Test Data from the Feed Force Sensor

was used to train the network. Following this, the data not shown to the network during training was used to ascertain the accuracy of the tool wear prediction.

As discussed in Chapter 6 the best three sensors to employ in a tool wear monitoring system are probably spindle current, feed force and acoustic emission. It would be possible also to include for example feed acceleration but the present analysis has been kept to three sensors in order to reduce the complexity of the system and also because it is felt that these sensors are the most practicable to employ in a commercial system.

The data from the acoustic emission, feed force and spindle current sensors, used to train the network and form the correlation line for the expert system are shown in Figures 268 to 270 along with the data used to test both systems.

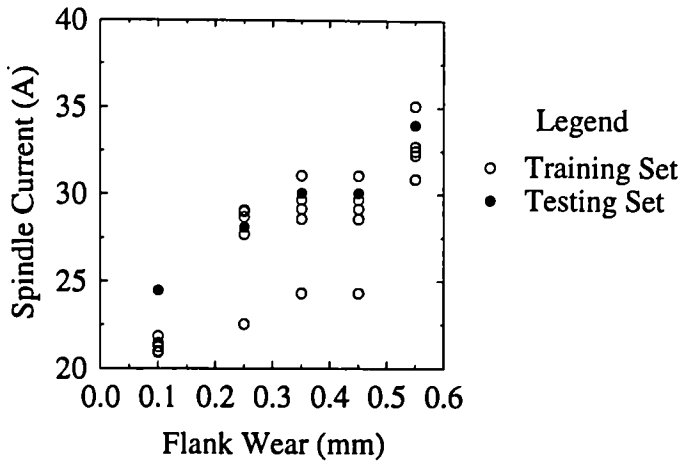

Figure 270: Training and Test Data from the Spindle Current Sensor

7.1 Application of Neural Network Techniques to Long-Timescale Progressive Tool Wear Detection

A feed-forward neural network simulation using a back-propagation training algorithm was used (Aleksander [151]) of topology shown in Figure 271 and described in Chapter 3.

Training of the network consisted of randomly presenting the network with data from the training set from Figures 268, 269 and 270. Between 1000 and 9000 iterations were used (an iteration being a randomly selected presentation of one of the training points appropriately labelled), as previous experience had shown that the optimum training time normally occurred between these two values.

7.1.1 Results from Network for all Three Inputs

The results from presenting the data to the network with five outputs are shown in Figures 272 to 276. For the neurons which go high at VB_B=0.15 mm and $VB_B \geq$0.6 mm corresponding to a new and worn out tool respectively it can be seen that the outputs are near to optimum with excellent classification of the new and worn tools. The other three neurons progressively representing greater levels of tool wear do not perform nearly as well. In fact, if a plot of the output of all the neurons is examined, Figure 277, it can be seen that the network is very confused as to what the tool wear level is for the central three values of flank wear. The network is, in fact, almost correct in its prediction of the tool wear for these central points, but the level of confidence is very small and could not really be used in a condition monitoring system. An important point to note is that the network is sure the data is not from a new or worn tool.

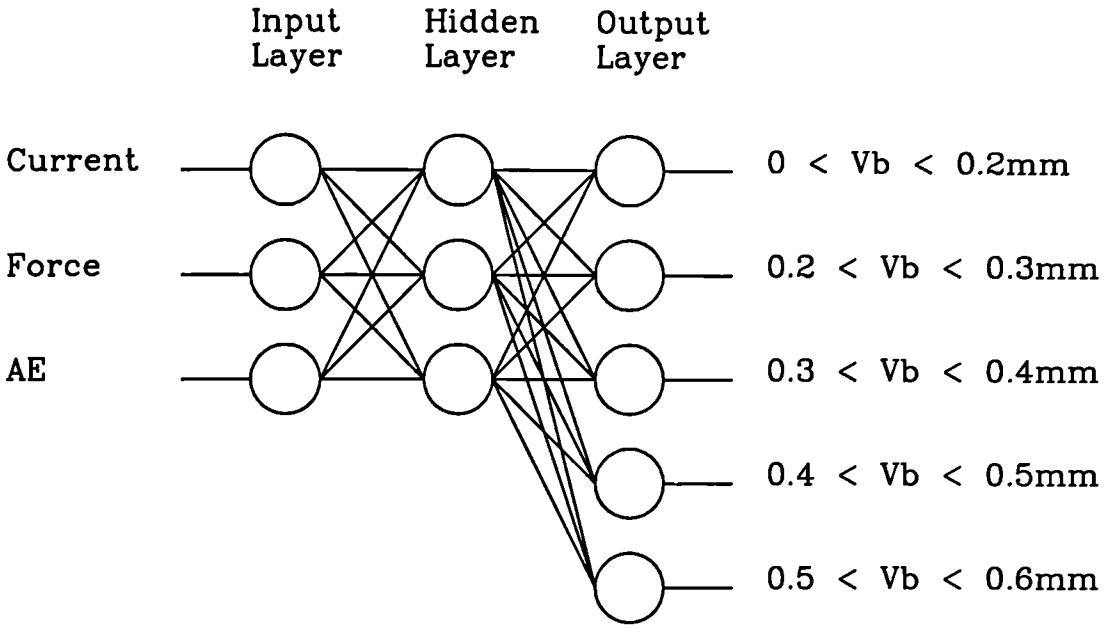

Figure 271: Neural Network Topologies for the Prediction of Progressive Tool Wear

It was not found to be of any benefit to increase the number of hidden layers in the network from one to two, even though the training time increased quite dramatically.

7.1.2 Neural Network performance when Two out of the Three Sensors are used in the Training Process

In order to assess the role played by each individual sensor in the global prediction of tool wear, it was decided to train the same network with the three possible combinations of two inputs selected from the spindle current, feed force and AE sensors.

Results from using Spindle Current and Feed Force

When the outputs of the individual 'wear level' neurons are observed, Figures 278 to 282, it can be seen that the network is not making a very good prediction of any wear state other than a worn out and nearly worn out tool. This can be seen as low levels of neural activity from output neurons one, two and four. This observation is amplified by a plot of all neurons vs wear (Figure 283) for six thousand iterations.

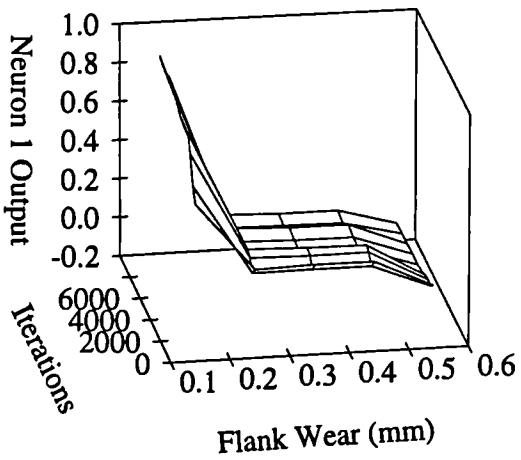

Figure 272: Prediction of a New Tool by Neuron 1

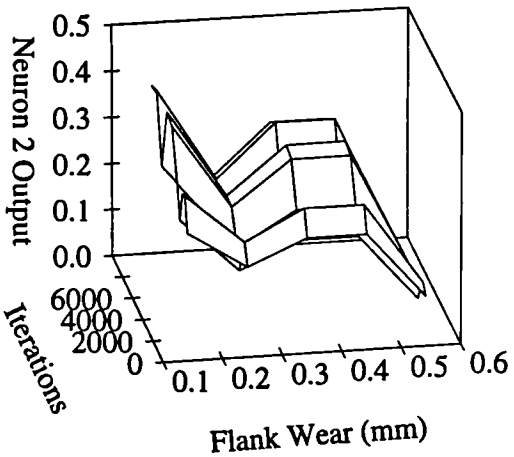

Figure 273: Prediction of 0.25 mm of Flank Wear by Neuron 2

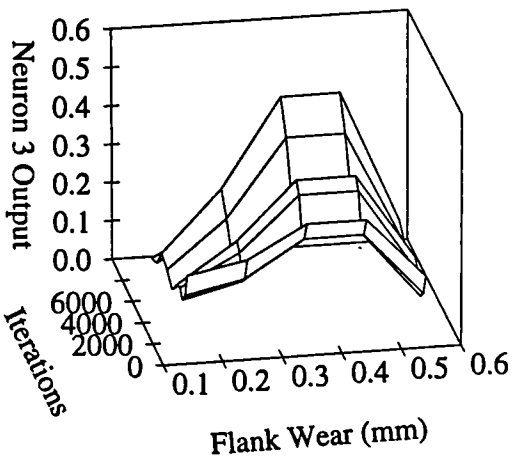

Figure 274: Prediction of 0.35 mm of Flank Wear by Neuron 3

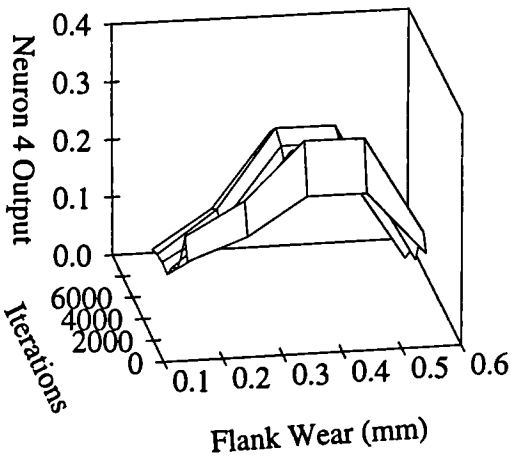

Figure 275: Prediction of 0.45 mm of Flank Wear by Neuron 4

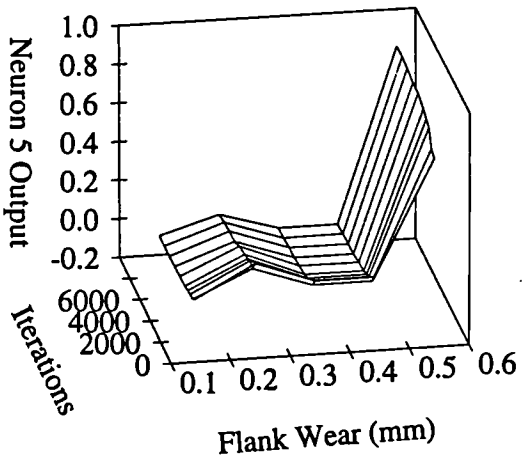

Figure 276: Prediction of a Worn Tool by Neuron 5

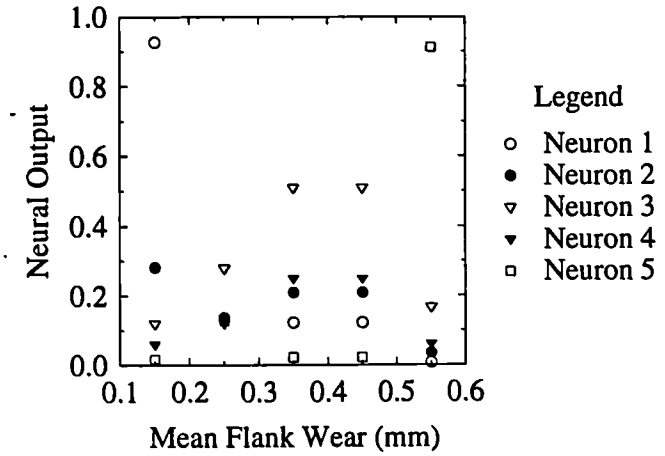

Figure 277: Prediction of Wear by all Neurons for 6000 Iterations

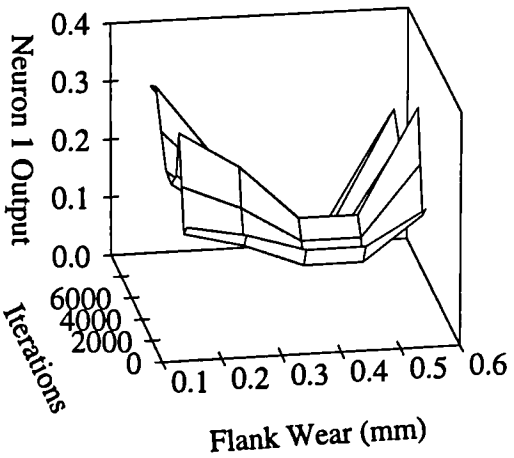

Figure 278: Prediction of a New Tool by Neuron 1, using Spindle Current and Feed Force

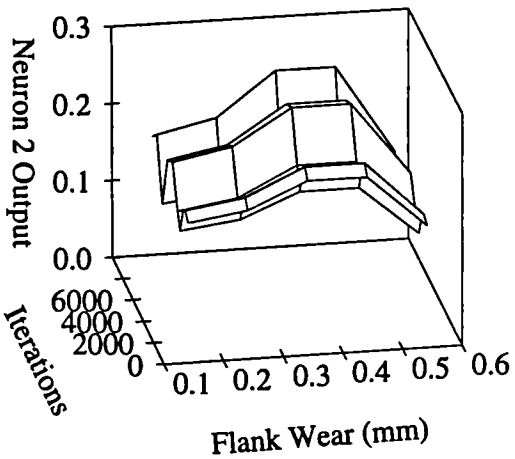

Figure 279: Prediction of 0.25 mm of Flank Wear by Neuron 2, using Spindle Current and Feed Force

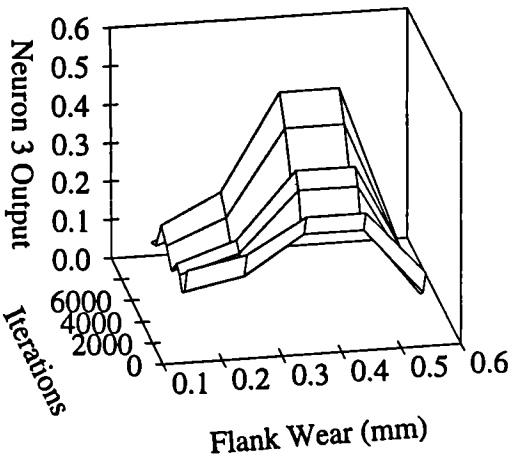

Figure 280: Prediction of 0.35 mm of Flank Wear by Neuron 3, using Spindle Current and Feed Force

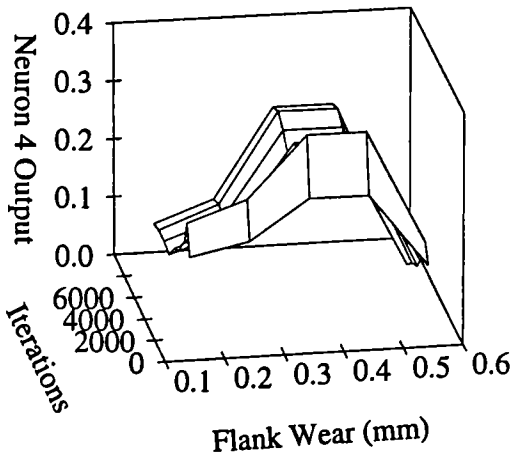

Figure 281: Prediction of 0.45 mm of Flank Wear by Neuron 4, using Spindle Current and Feed Force

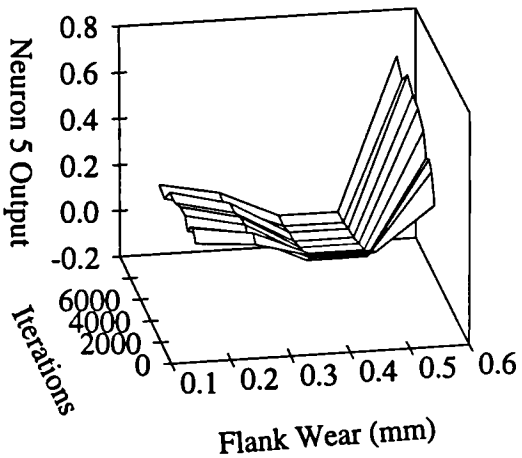

Figure 282: Prediction of a Worn Tool by Neuron 5, using Spindle Current and Feed Force

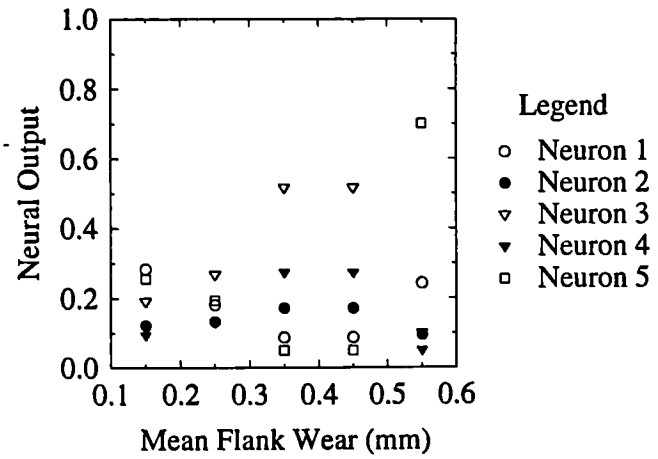

Figure 283: Prediction of Wear by all Neurons for 6000 Iterations, using Spindle Current and Feed Force

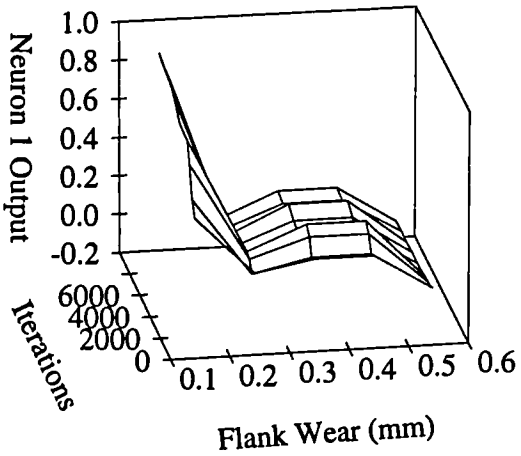

Figure 284: Prediction of a New Tool by Neuron 1, using Spindle Current and rms AE

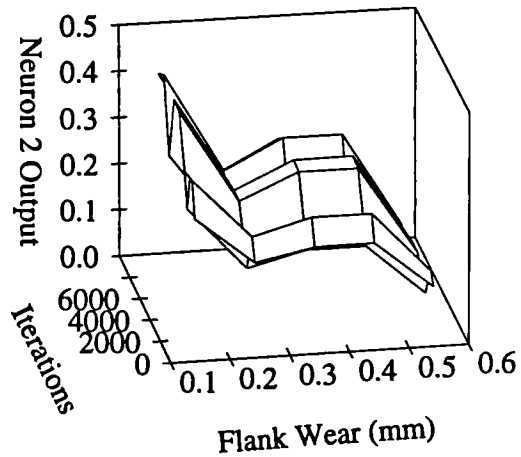

Figure 285: Prediction of 0.25 mm of Flank Wear by Neuron 2, using Spindle Current and rms AE

Results based on Spindle Current and AE

In contrast to using spindle current and feed force, the spindle current and rms AE combination is not noticeably worse than using all three sensors, as can be seen from Figures 284 to 288. Again the distinction between a new tool and a worn tool is excellent, whereas recognition of a partly worn tool, although correct for the middle wear value, is not of a high enough significance to allow reliable prediction. This result is evident in Figure 289, a plot of the output of all 'output neurons' vs flank wear using six thousand training iterations. In this Figure it is possible to classify a new tool with a Vb value of 0.1 mm at nearly 100 % confidence, with a similar success rate occurring with a tool with 0.55 mm of flank wear. It is again true to say that the network does not 'think' that the data from the middle wear values corresponds to a new or worn tool, at least for VB_B=0.35 and 0.45 mm.

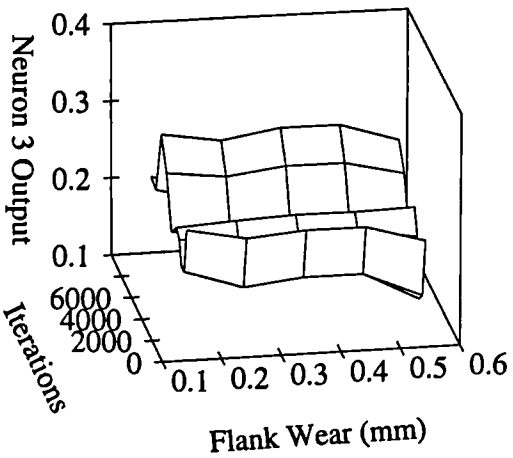

Figure 286: Prediction of 0.35 mm of Flank Wear by Neuron 3, using Spindle Current and rms AE

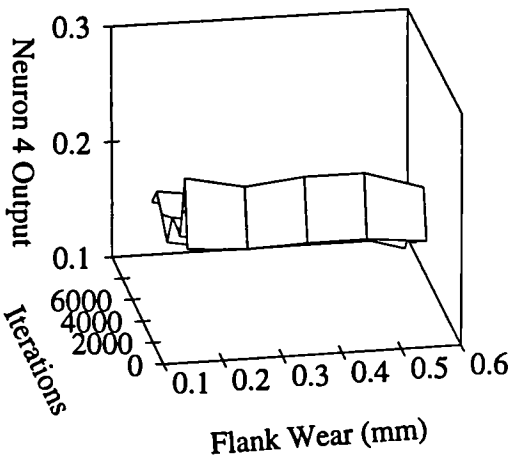

Figure 287: Prediction of 0.45 mm of Flank Wear by Neuron 4, using Spindle Current and rms AE

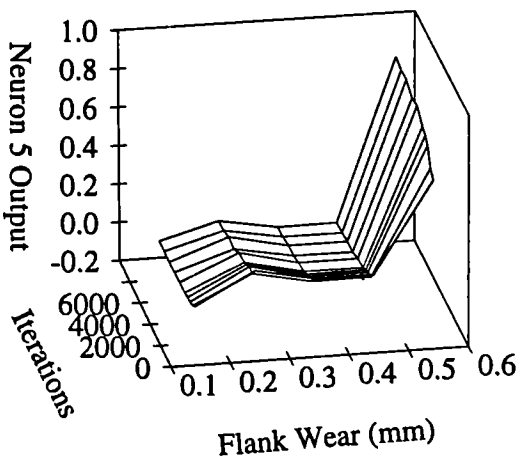

Figure 288: Prediction of a Worn Tool by Neuron 5, using Spindle Current and rms AE

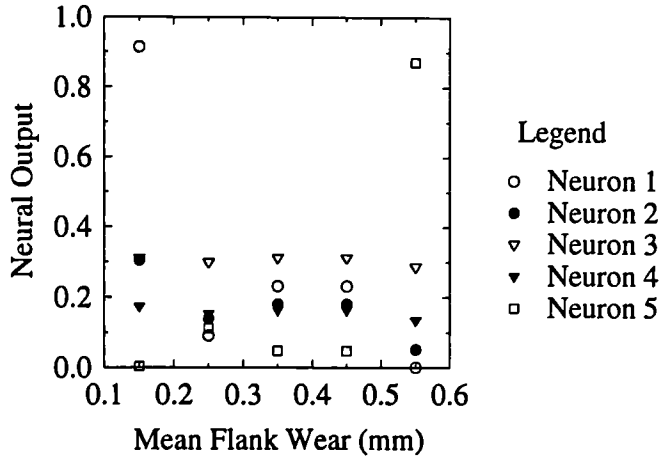

Figure 289: Prediction of Wear by all Neurons for 6000 Iterations, using Spindle Current and rms AE

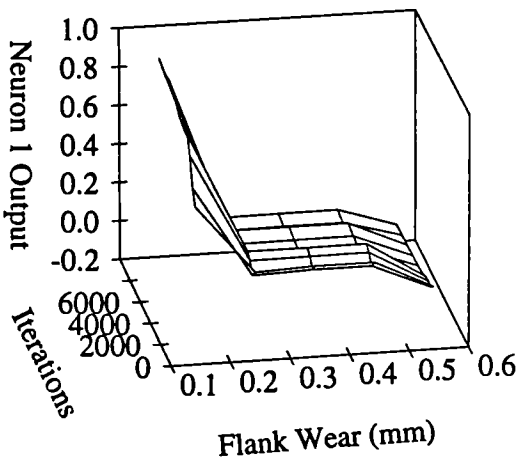

Figure 290: Prediction of a New Tool by Neuron 1, using rms AE and Force

Results based on Feed Force and AE

The rms AE and Feed Force combination is probably the best one tried, as can be seen from Figures 290 to 294. However, as with the network using all sensors, the classification of a partly worn tool is not really acceptable, except that the network does not think the data is from a new tool. Again, the distinction between a new tool and a worn tool is excellent and this level of significance is probably high enough to allow reliable detection of these wear states. This result is seen clearly in Figure 295, a plot of the output of all 'output neurons' vs flank wear again for six thousand training iterations. In this Figure it is possible to observe similar levels of distinction to using all three sensors and to using rms AE and spindle current.

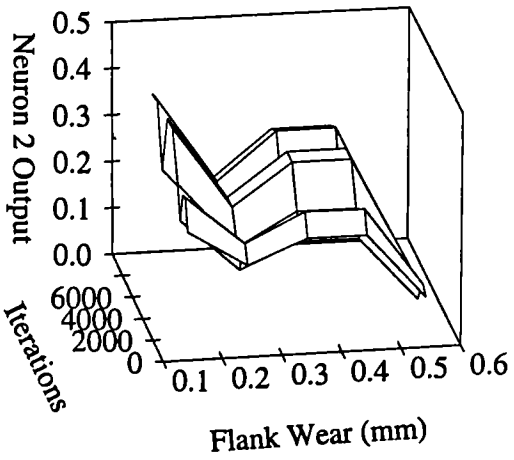

Figure 291: Prediction of 0.25 mm of Flank Wear by Neuron 2, using rms AE and Force

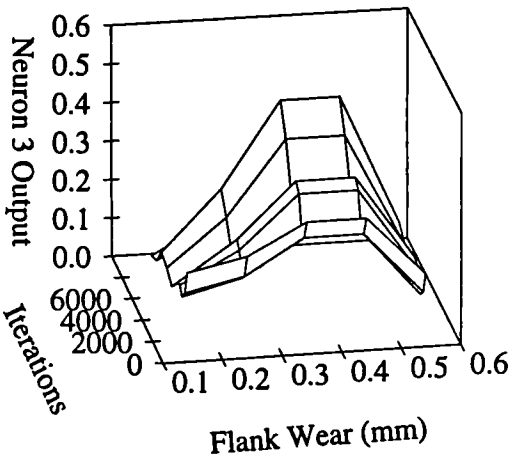

Figure 292: Prediction of 0.35 mm of Flank Wear by Neuron 3, using rms AE and Force

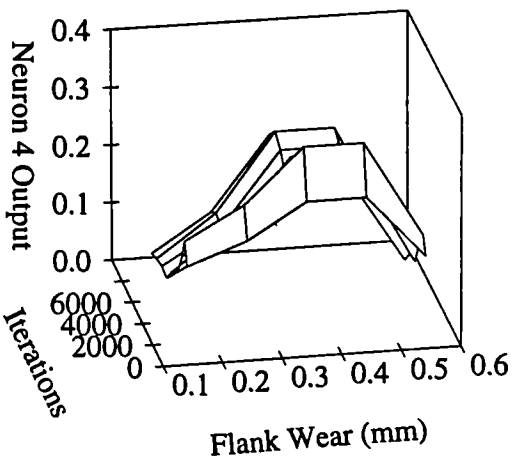

Figure 293: Prediction of 0.45 mm of Flank Wear by Neuron 4, using rms AE and Force

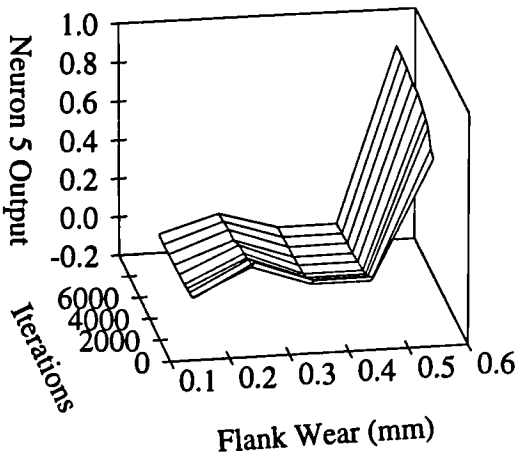

Figure 294: Prediction of a Worn Tool by Neuron 5, using rms AE and Force

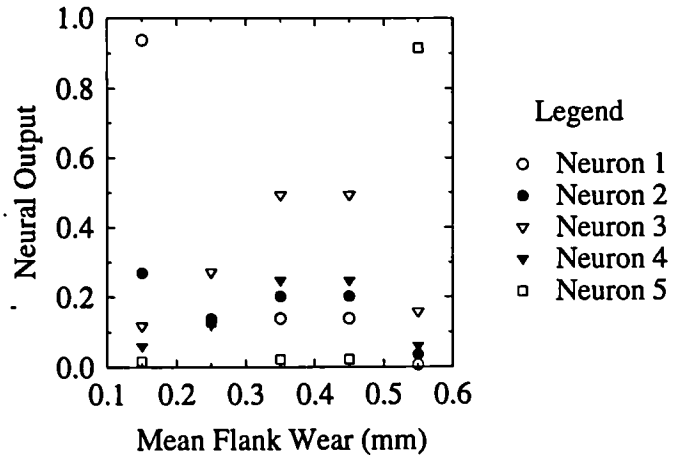

Figure 295: Prediction of Wear by all Neurons for 6000 Iterations, using rms AE and Force

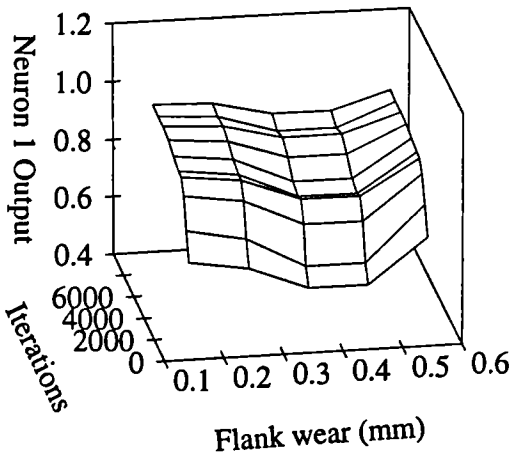

Figure 296: Prediction of a New Tool by Neuron 1 with no AE

7.1.3 Robustness of the Neural Network

In order to simulate the effect of a malfunctioning sensor, the output of one of the sensors, in this case the AE sensor, was modified to have either zero or random values, in the test data. The first of these situations simulates a sensor that has detached itself from its mounting position or has suffered a broken cable, a passive malfunction, and the second represents a sensor that has suffered some internal damage, such as a PZT crystal that has become detached from its base in an AE sensor, an active malfunction. The training of the network remained the same as described in Section 7.1.

A Network that is Presented with no AE but with normal Feed Force and Spindle Current values.

The results obtained by presenting a zero value of AE for a range of iterations for each of the output neurons are shown in Figures 296 to 300. It is obvious that the network is performing very poorly, and it is clear from the general performance (Figure 301) that, because the AE values are consistently low, the network is induced into a diagnosis that the tool is new at all values of actual VB_B.

A Network that is Presented with random values of AE but with normal Feed Force and Spindle Current Values.

The random values of AE that were presented to the network during testing are shown in Figure 302 along with the training data as used before.

From Figures 303 to 307 it is clear that, again, the network is not capable of making a decision based on the input of correct force and current readings when the AE sensor is giving conflicting information to the network. From Figure 308 it can be seen that the network only gets the classification of a new tool and a

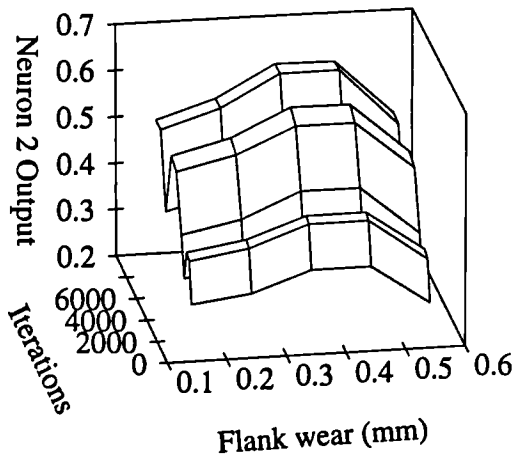

Figure 297: Prediction of 0.25 mm of Flank Wear by Neuron 2 with no AE

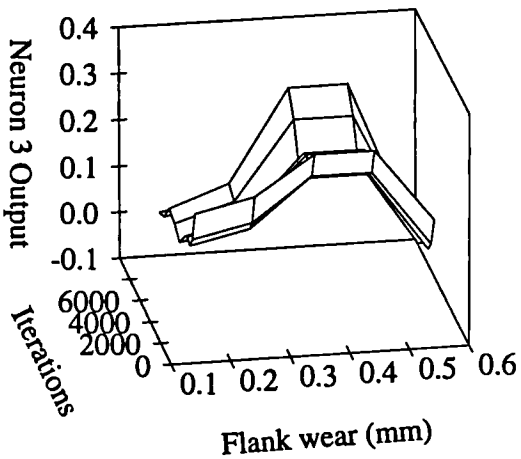

Figure 298: Prediction of 0.35 mm of Flank Wear by Neuron 3 with no AE

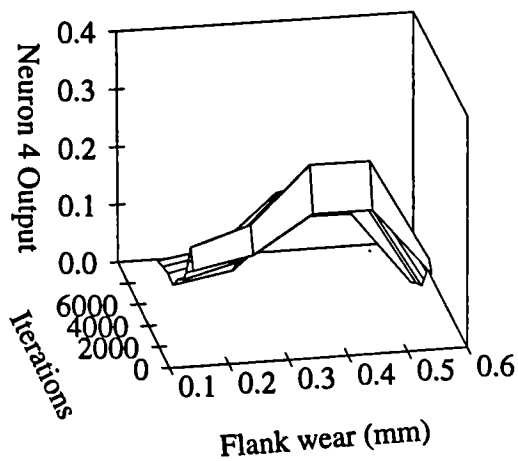

Figure 299: Prediction of 0.45 mm of Flank Wear by Neuron 4 with no AE

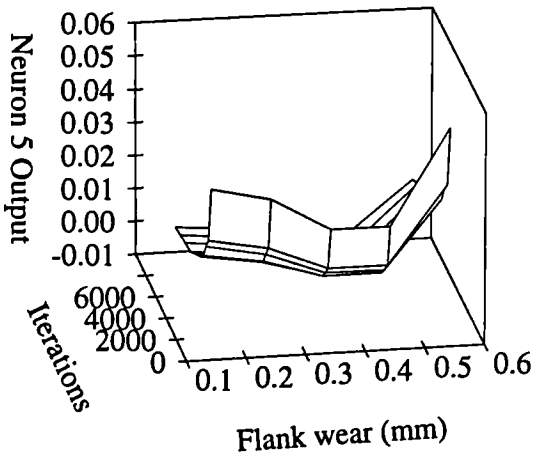

Figure 300: Prediction of a Worn Tool by Neuron 5 with no AE

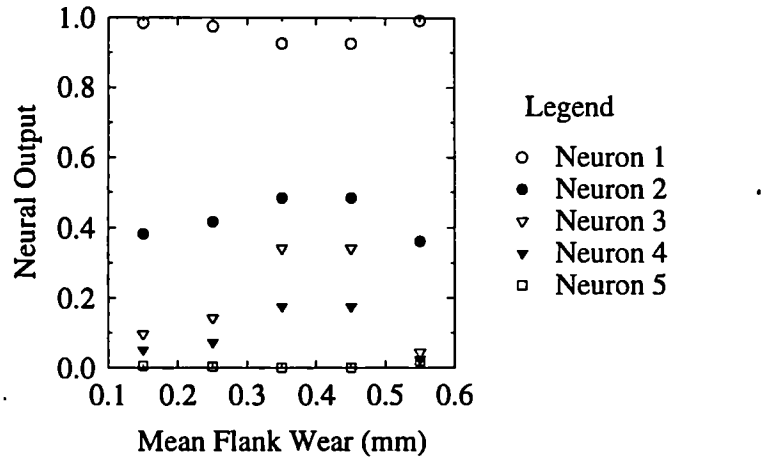

Figure 301: Prediction of Wear by all Neurons for 6000 Iterations, when no AE is Presented

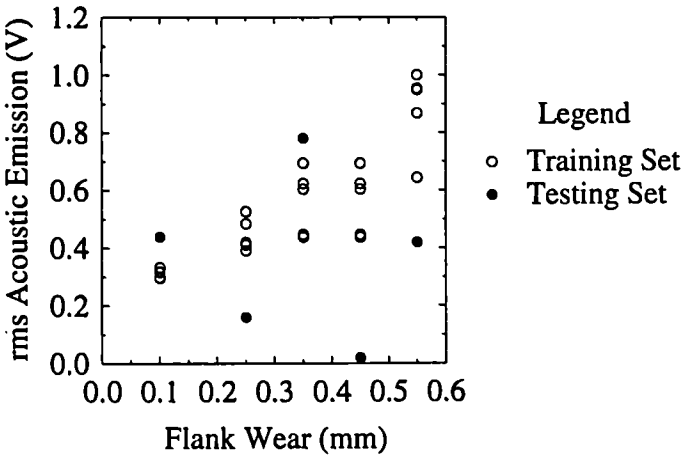

Figure 302: Training and Random Test Data for the AE Sensor

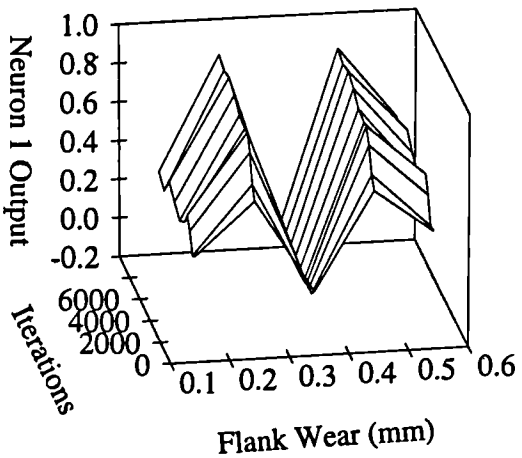

Figure 303: Prediction of a New Tool by Neuron 1 with random AE values

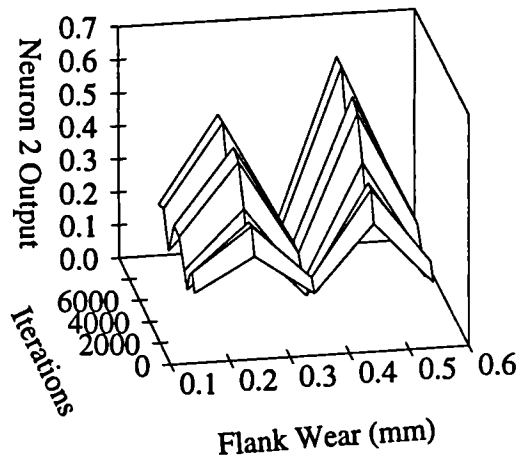

Figure 304: Prediction of 0.25 mm of Flank Wear by Neuron 2 with random AE values

medium worn tool correct and this is probably only due to the fortuitous values of the random data at these points (Figure 302). As when the AE is low the network predicts a new tool is cutting and vice versa.

7.2 Simulation of an Expert System to Long-Timescale Progressive Tool Wear Detection

In this very simple simulation a prediction based on the output of all the sensors was made by first fitting linear regression lines for each sensor vs VB_B and then combining the predictions from each sensor to give a single value weighted according to correlation coefficients obtained from the linear regression.

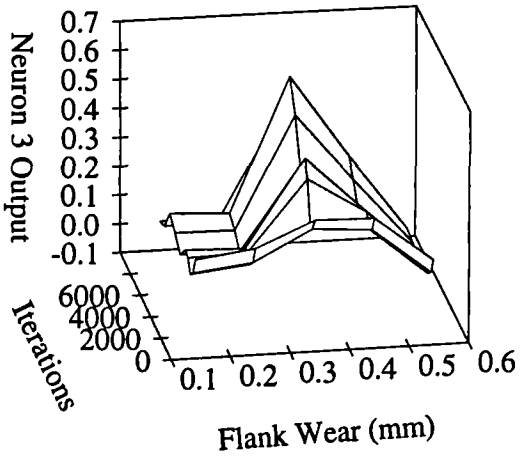

Figure 305: Prediction of 0.35 mm of Flank Wear by Neuron 3 with random AE values

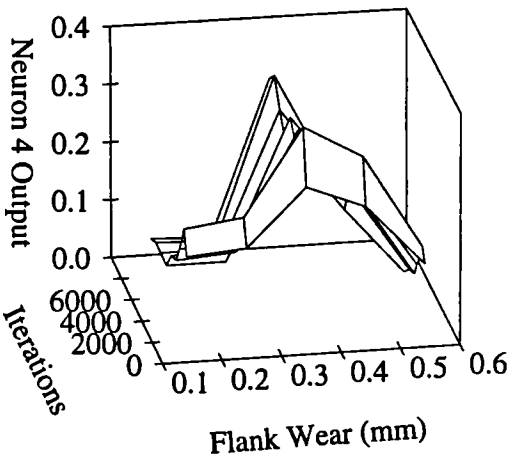

Figure 306: Prediction of 0.45 mm of Flank Wear by Neuron 4 with random AE values

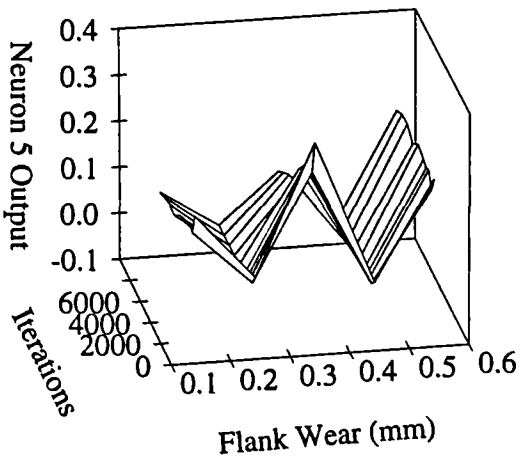

Figure 307: Prediction of a Worn Tool by Neuron 5 with random AE values

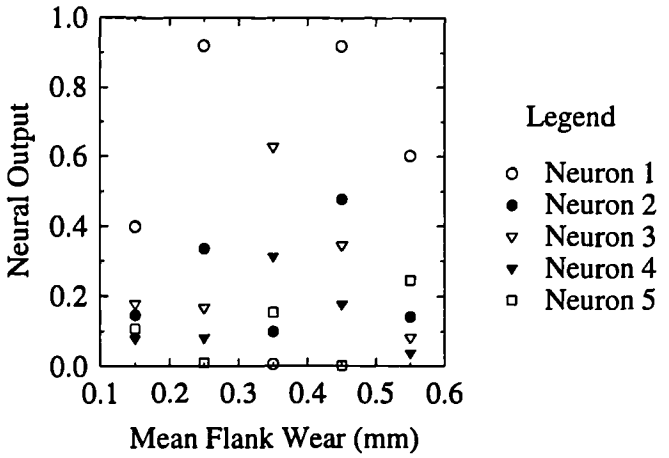

Figure 308: Prediction of Wear by all Neurons for 6000 Iterations, when random AE values are Presented

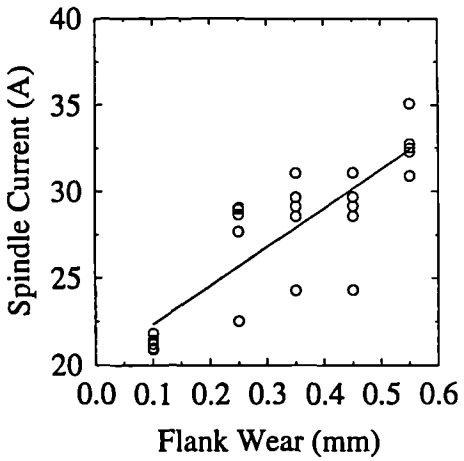

Figure 309: Linear Regression of the Spindle Current Data Set

The linear regressions obtained on the 'training set' of sensorial data from this particular test are shown in Figures 309 to 311. It can be seen that, in general, a good fit to the data was obtained, but the last data set from the force sensor causes a weak correlation to occur.

7.2.1 Results from the Expert System when Presented with all Sensor Outputs

Figure 312 shows the result of combining the predictions made by the Expert System it can be seen that the prediction is consistently high for low values of flank wear (around 0.2 mm) but that when the tool approaches the end of its life the accuracy of the prediction is very good.

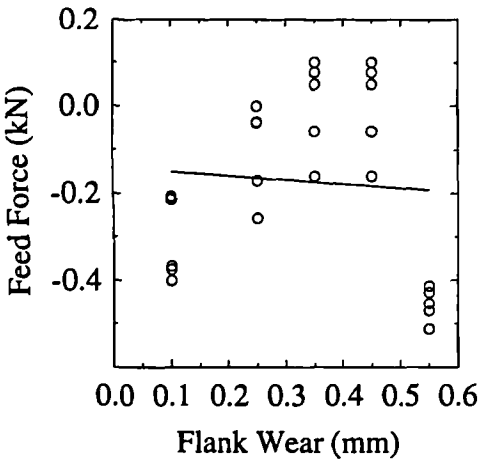

Figure 310: Linear Regression of the Feed Force Data Set

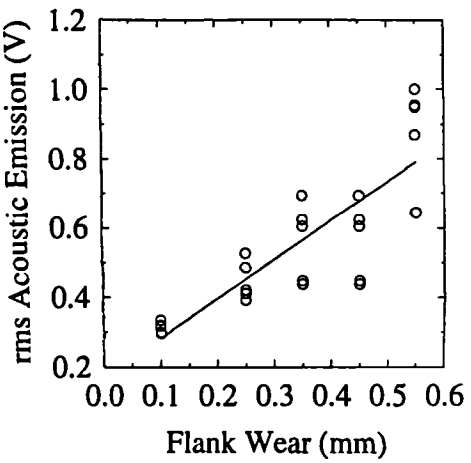

Figure 311: Linear Regression of the rms AE Data Set

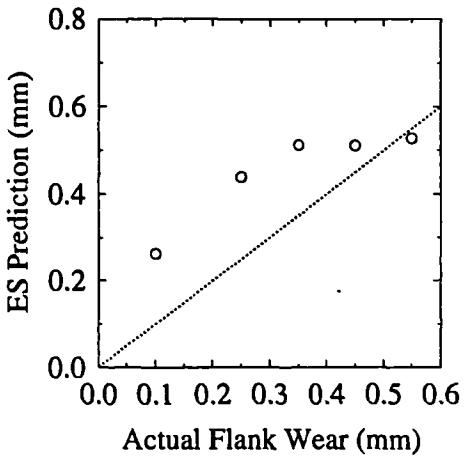

Figure 312: Flank Wear Prediction made by the Expert System when using all Sensors

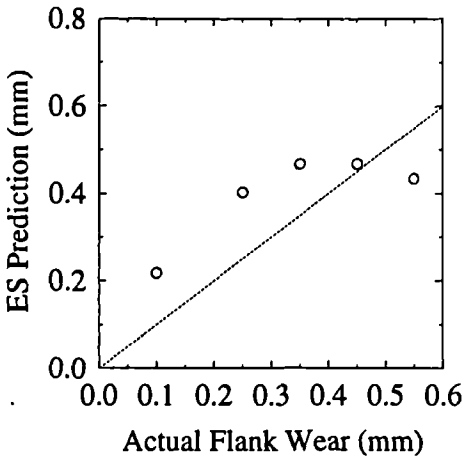

Figure 313: Flank Wear Prediction made by the Expert System when using Feed Force and rms AE

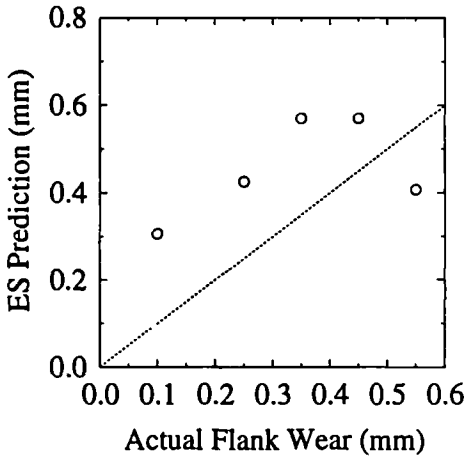

Figure 314: Flank Wear Prediction made by the Expert System when using Spindle Current and Feed Force

7.2.2 Results from the Expert System when only Two out of the Three Sensors are used in the Calculation Process

In an approach similar to that used with the neural network, the Expert System has been tested on the various combinations of the three sensors. The Expert System does perform reasonably for each of the sensor combinations. If all three combinations are observed (Figures 313, 314 and 315) it can be seen that the error is reasonably consistent for each combination.

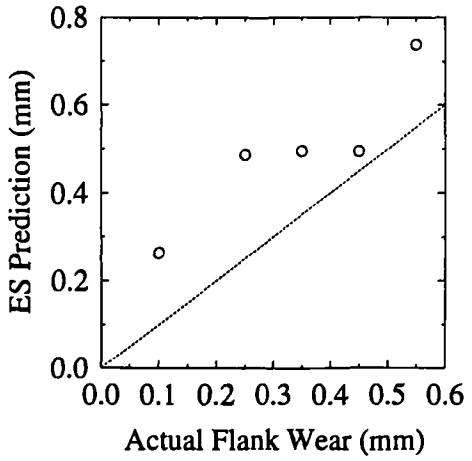

Figure 315: Flank Wear Prediction made by the Expert System when using Spindle Current and rms AE

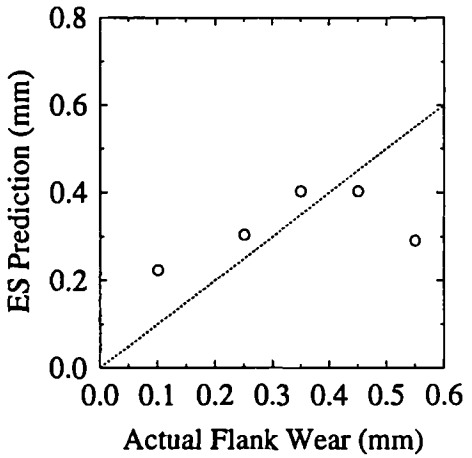

Figure 316: Flank Wear Prediction made by the Expert System when using no rms AE

7.2.3 Robustness of the Expert System Knowledge Base

A robustness test, similar to that used for the neural network, was applied to the ES simulation and again the AE sensor was the one chosen to withdraw from the system. Figures 316 and 317 show the results of the Expert System processing the sensorial data when there is zero and random AE input respectively. From Figure 316 it can be seen that, in contrast to the neural network, the Expert System does make a reasonable prediction at some values of VB_B when the AE sensor suffers a passive malfunction but, for the case of random AE values the Expert System is not much better than the Neural Network. The predicted values of flank wear again following the randomness of the AE values.

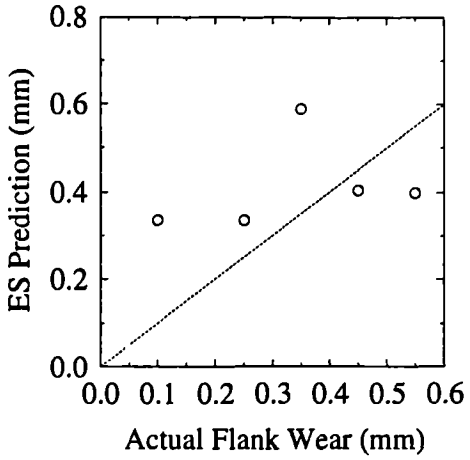

Figure 317: Flank Wear Prediction made by the Expert System when using Random AE Input

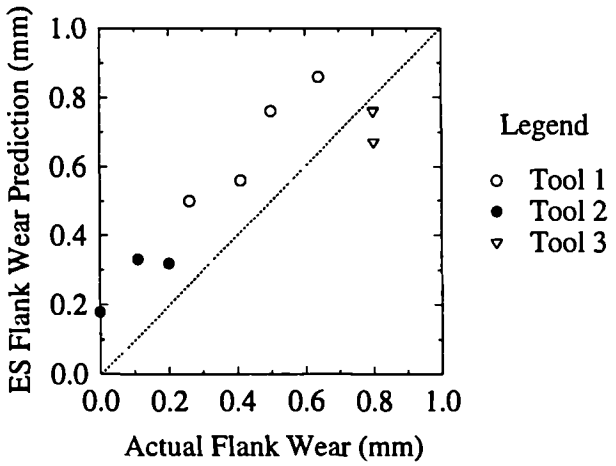

Figure 318: Prediction of VB_B made with a Full ES

7.3 Summary

This experiment has been a rather confined one, in that only the results from one wear test have been analysed. If all of the data had been used a rather better performance would have been expected for both systems. In fact, a complete ES has been developed, using, in part, the data presented in Section 5.3, with rules in the ES being developed in a very similar manner to that presented in this Chapter. This work was performed as part of a large CEC research programme into tool wear monitoring and, as can be seen from Figure 318, a rather better performance did ensue.

In summary it can be seen that, for the particular data set examined, the two methods have contrasting advantages and disadvantages. The neural network is very good at predicting new and worn tools, often even with only two of the three sensors. However, the ANN has little power to interpolate and would not

be able to inform the user of the remaining time the tool had left to cut. The Expert System simulation, as set up here, interpolates rather better as long as all three sensors are used and such a facility would allow the ES to inform the operator of the remaining time the tool could be used for cutting provided that the conditions remained the same, although prediction under different conditions could probably be made provided the ES contained relevant knowledge.

In the face of an absent sensor the Expert System copes rather better than the neural network, it still being possible to make some sort of prediction based on the remaining two good sensors. In the case of an active malfunction, neither system is capable of making a prediction and, to avoid this situation, the sensors would have to undergo some sort of error checking at start up and perhaps at periodic intervals throughout the working day. It so happens that the AE is the strongest sensor in this set of data, therefore random inputs caused random predictions in both the ANN and ES although the weighting method is different in each case.

7.4 Neural Network Application to Short Timescale Events

As has already been mentioned, only a neural network simulation has been applied to the sensorial data from the short-timescale events. It has been found that it is possible for the neural network to recognise the different events presented in Section 5.5 in a time that would probably be very difficult to match with an Expert System running in a workstation-type environment.

7.4.1 Neural Network Simulation

The type of neural network simulation that has been employed is a feed forward multi-layered network trained using a back propagation algorithm similar to the one used for progressive wear detection and described in Chapter 3. Two layouts have been employed, one with four outputs (an output for each of the events) and one with only one output (a likelihood of breakage being given by this output). The general layout of the network is shown in Figure 319 the differences being shown by dashed lines.

In Chapter 6 it was suggested that the AE sensor has the most potential as a breakage monitor. This sensor was selected because the time series seemed to display some predictive capabilities, or at least give an earlier detection of many of the events recorded, than does its nearest competitor, force. In addition, AE sensors would be easier to apply in an industrial milling environment than would a force transducer.

In view of the complexities of the changes in the AE signal, it was felt that a simple threshold detection system would not be capable of providing complete cover

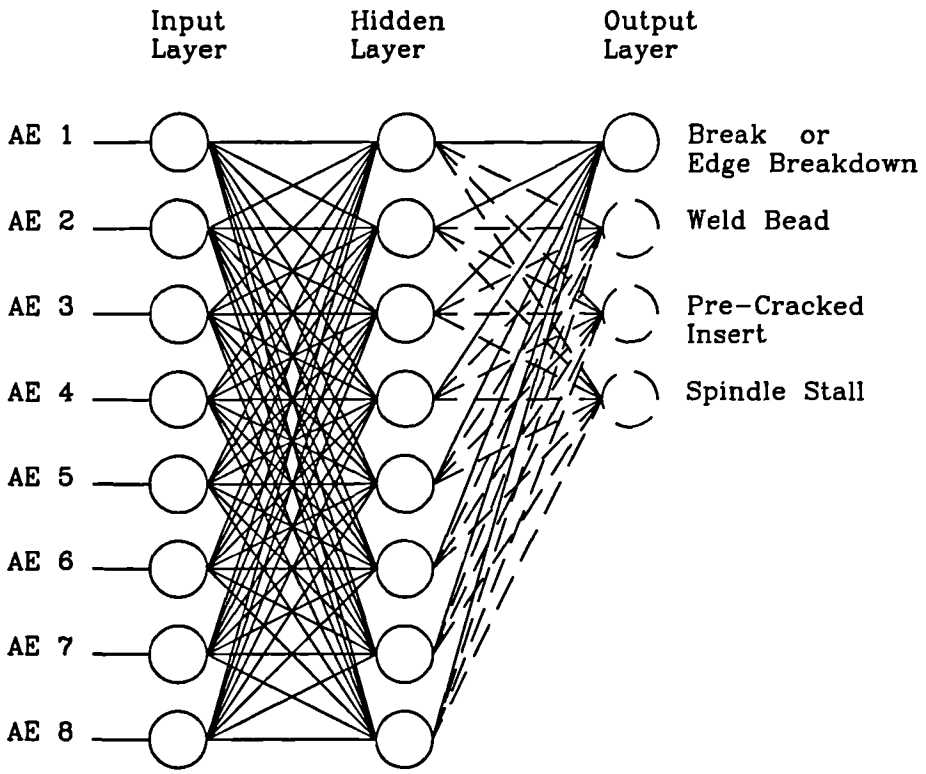

Figure 319: Multi-Layered Neural Network Simulation for Breakage Detection

for all cutting operations and for this reason a neural network simulation has been used to provide a detector that informs the user of situations that could potentially cause a breakage. Further, a similar network has been used to discriminate between the different events recorded with a high degree of confidence.

Each of the eight input neurons takes the peak height of rms AE from each insert pass over the workpiece for one or two tool rotations (depending on the number of inserts in the tool holder). These neurons are then fully connected to one hidden layer of eight neurons which is in turn fully connected to either one or four output neurons depending on the application.

In order to input the rms AE peak height per tooth pass into the network, a small amount of signal processing has been necessary. This consisted of obtaining the peak height and normalising it so that the network input was not saturated. Table 44 shows the values of rms AE peak height that were used as a training set from each of the short timescale events. In general three sets of eight tooth passes from each event were used along with three sets of eight tooth passes from normal cutting. The exception to this is the pre-cracked insert event, where there was only one data record. It was thus necessary to randomise the position of the signal corresponding to the breakage of the insert through the eight peaks of the tool rotation.

Figure 320 shows the performance of the breakage detecting network with varying numbers of iterations (an iteration being defined in exactly the same manner as the previous Section) when presented with data from a traverse through a weld

Short Timescale Event	rms AE Vector
Spindle Stall	0.70 0.84 0.81 0.87 0.86 0.76 0.95 0.94 1.00 1.00 0.84 0.96 0.84 0.85 1.00 1.00 1.00 0.95 0.96 0.89 0.88 0.80 0.88 0.75
Normal Cutting	0.10 0.08 0.09 0.04 0.15 0.10 0.08 0.08 0.17 0.15 0.07 0.05 0.02 0.09 0.08 0.10 0.10 0.10 0.18 0.17 0.08 0.09 0.07 0.01
Weld Bead Traverse	0.50 0.20 0.20 0.20 0.60 0.80 0.20 0.20 0.64 0.68 0.30 0.24 0.80 0.60 0.20 0.20 0.80 0.70 0.20 0.46 0.70 0.65 0.22 0.24
Normal Cutting	0.15 0.10 0.12 0.20 0.10 0.10 0.08 0.09 0.10 0.10 0.11 0.14 0.10 0.08 0.09 0.20 0.18 0.17 0.10 0.08 0.07 0.09 0.10 0.10
Pre-cracked Insert	0.05 0.10 0.08 0.25 0.10 0.07 0.09 0.10 0.25 0.07 0.09 0.10 0.05 0.10 0.08 0.10 0.07 0.09 0.10 0.05 0.10 0.08 0.25 0.10
Normal Cutting	0.07 0.09 0.10 0.05 0.10 0.08 0.11 0.10 0.12 0.07 0.09 0.10 0.08 0.05 0.08 0.09 0.06 0.11 0.10 0.09 0.07 0.09 0.10 0.12
Edge Breakdown	0.09 0.08 0.12 0.14 0.10 0.10 0.09 0.02 0.03 0.04 0.02 0.09 0.07 0.10 0.10 0.05 0.08 0.07 0.02 0.10 0.11 0.10 0.05 0.04
Normal Cutting	0.08 0.06 0.11 0.05 0.12 0.08 0.07 0.10 0.11 0.07 0.07 0.10 0.02 0.10 0.09 0.10 0.06 0.09 0.10 0.08 0.09 0.09 0.05 0.11

Table 44: Training Set

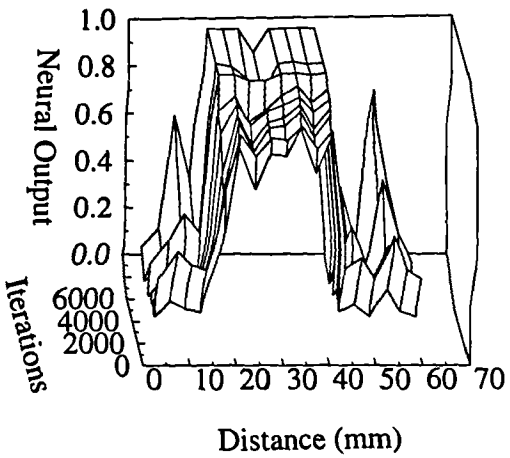

Figure 320: Performance of the Potential Breakage Detecting Neural Network

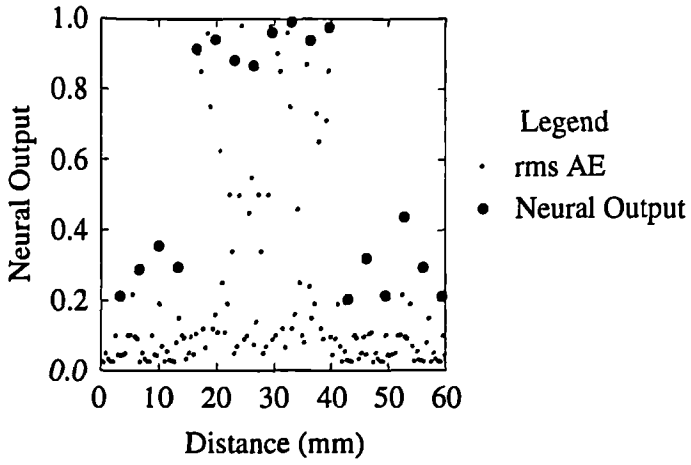

Figure 321: Breakage Detecting Neural Network with 3000 Iterations

bead that it had not been shown previously. It can be seen that there is an optimum training time for this network configuration and that this occurs at around 3000 iterations. As learning time is increased the performance of the network actually decreases as the error in the area of cutting in the base material increases, this means that the network, if over-trained, could incorrectly flag normal cutting operations as a potential breakage situation. Figure 321 shows the variation in the rms AE signal as the tool traverses the weld bead, with the output of the network being displayed after every eight tooth passes. It can be seen that the network easily classifies the event as a potential breakage situation, even though the rms AE is far from constant in amplitude in the weld area. This shows that the network is operating as more than a simple threshold detector.

It would also be useful to the operator of the machine to know what kind of event is occurring in the cutting operation, and if the machine tool can cope with it. In order to do this, a slightly modified network has been used, this time with four output neurons, one for each of the events observed. It was not necessary to change the training set, only the way in which the network was instructed to classify the events. Figures 322 to 325 show the performance of the network for each of the four outputs against training time for a traverse through a weld bead which had again not been presented to the network during training. It can be seen that there is an optimum training time and that this is again around 3000 iterations. There also appears to be a little confusion in the first encounter with the weld bead, as the network has an initial difficulty deciding whether the event is a traverse through a weld bead or an instance of insert breakage. As the tool progresses through the weld bead the network rapidly concludes that it is a weld bead traverse. Figure 326 displays the rms AE as the tool progresses through the weld bead along with the output of the four neurons of the network. It is clear that as the tool enters the weld bead the network 'thinks' that there is a high probability of an insert breaking (probably not an unreasonable assumption) but that, as the tool continues into the weld bead, it can clearly discriminate the event as that of a hard patch in the workpiece material and one with which the tool has coped.

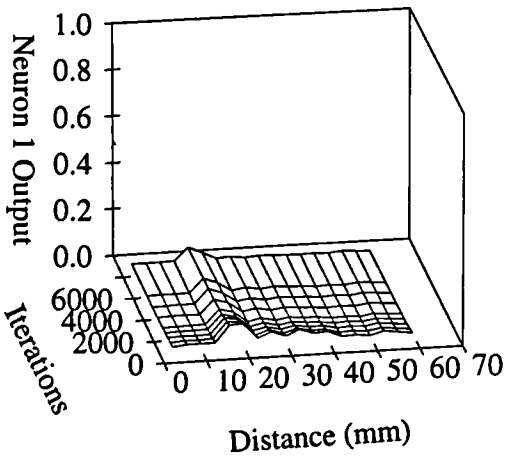

Figure 322: Breakage Detecting Neural Network, Output of Neuron 1 (Edge Breakdown)

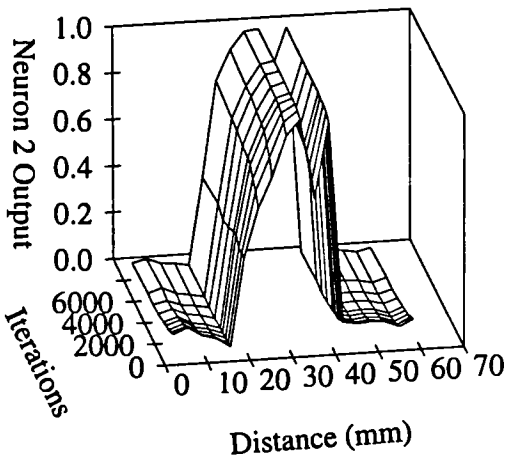

Figure 323: Breakage Detecting Neural Network, Output of Neuron 2 (Weld Bead)

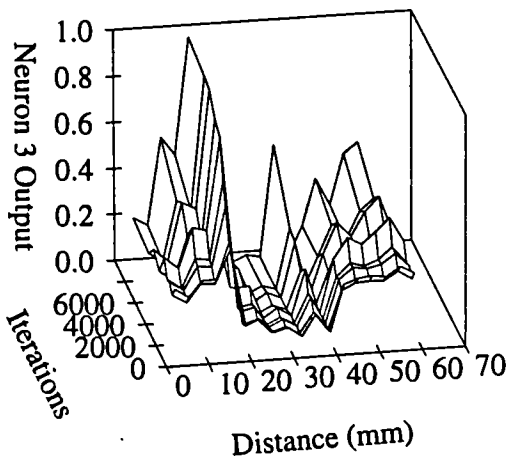

Figure 324: Breakage Detecting Neural Network, Output of Neuron 3 (Pre-Cracked Insert)

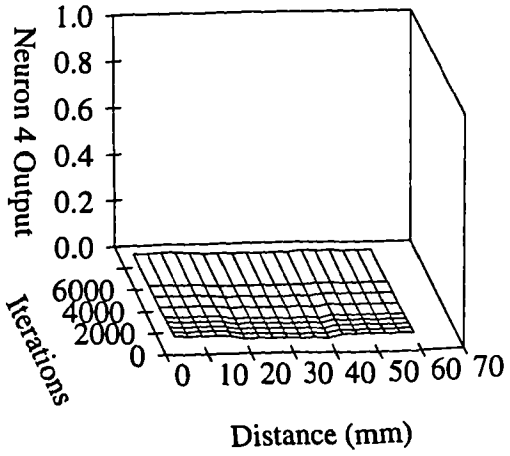

Figure 325: Breakage Detecting Neural Network, Output of Neuron 4 (Spindle Stall)

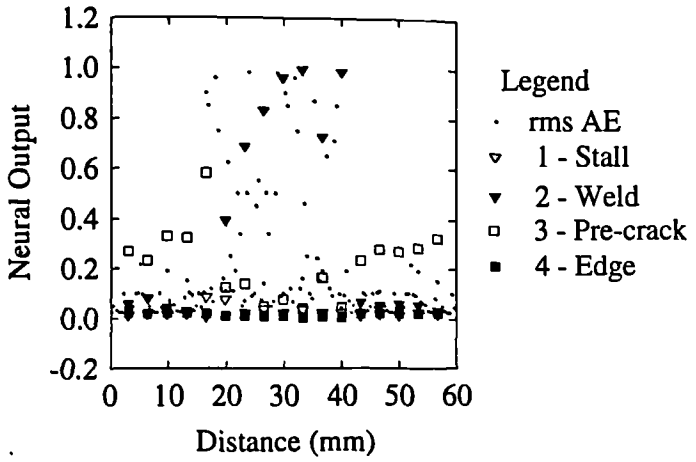

Figure 326: Discriminating Breakage Detecting Neural Network, all Outputs

Summary

In a similar manner to the application of AI to wear monitoring this experiment has been very confined, with attempt to assess the robustness of the network. However, there has been a demonstration of principal in that the neural network approach has been shown to be excellent at detecting the likelihood of the milling cutter to break under a variety of situations and with a small modification it has also been possible for the approach to classify the type of event that is likely to cause cutter failure.

Chapter 8

Conclusions and Recommendations

The conclusions from this work have been sub-divided into those obtained from each of the experiments conducted. In addition, some conclusions pertaining to the AE sensor, the two types of AI that have been employed, and the implications of all the results for tool wear monitoring have been drawn.

8.1 The Influence of the AE Sensor Response Function

From the power spectrum of the AE sensor response to an impulse it is easy to observe the resonances of the crystal. This implies that the sensor will resonate under all impulse functions that are applied to it, as long as the spectral content is high enough. .

It seems that this reasonance dominates the AE recorded from the systematic wear tests, although a small change in spectral content has been found between new and old tools.

It is felt by the author that a sensor that can more accurately reproduce the time evolution of the surface wave will provide more useful information in the frequency domain and hence may reveal more accurate and hopefully more reliable tool wear prediction. It may be that a non-contacting AE sensor is the best approach to take in recording this information as it is completely non-intrusive. However, the cost of such a system would be high in comparison to a PVdF based sensor which, although contacting, does provide for a very high fidelity of AE recording.

8.2 Influence of Machine/Fixture Stiffness on AE and Workpiece Vibration.

Variation in the effective stiffness has been shown to cause considerable distortion of the acceleration power spectrum recorded during milling, particularly in the region of the natural frequency of the secondary table used to vary the effective stiffness.

On the other hand, the power spectrum and the amplitude distribution of the rms acoustic emission were found to be independent of machine/fixture stiffness even in the range of the natural frequency and furthermore no changes in the amplitude distribution of the rms acoustic emission with stiffness could be discerned.

8.3 Influence of Insert Geometry on Sensorial Data

The effect of flank wear has been relatively easy to monitor with all the sensors employed except AE, but some synthesis of the sensorial information is required.

For discontinuities on the rake face the results indicate that the detailed geometry is relatively unimportant. It appears that the fact that the chip flow over the rake face has been disrupted is enough to produce the changes observed.

No sensor exhibits a very systematic change with local rake angle.

8.4 Systematic Wear Tests

8.4.1 Flank Wear vs Cutting Time

In all the systematic wear tests conducted the evolution of wear with time has been fairly linear. This result has also proved to be quite repeatable.

8.4.2 Spindle Current vs Flank Wear

This sensor appears to exhibit the best correlation with flank wear and remains fairly linear for all the cutting conditions investigated. It does not increase at the same rate for different materials or different cutting conditions, but this is something that the Monitoring System should be able to take into account. This sensor is also very repeatable between tests under the same cutting conditions.

8.4.3 Cutting Force vs Flank Wear

In general force measurements show quite a good linear trend with increases in flank wear and results are reasonably repeatable between tests under the same cutting conditions. However, in some tests this sensor followed an inconsistent trend with wear questioning its reliability.

8.4.4 AE vs Flank Wear

The rms AE parameter is very variable in its trend with flank wear. For some of the tests the sensor signal increases quite linearly and reasonably repeatably with flank wear but for others its behaviour is inconsistent and occasionaly shows poor repeatability.

Cumulated rms AE displays a more monotonic variation with flank wear than does the rms AE but it is uncertain whether such evolutions are doing anything more than measuring time.

The mean AE frequency has not been found to vary with wear, but quite a consistent increase in the energy contained within the 100 to 200 kHz band has been found with increasing wear. Also, as wear increases, the higher bands undergo a (smaller) reduction in energy level.

8.4.5 Surface Finish, R_a vs Wear

This parameter exhibits a general tendency for lower values at medium values of flank wear, when compared to new and worn tools. However, the variability in the parameter over the workpiece is such that it is not felt that the surface finish as described by the R_a value is of use in wear monitoring.

8.4.6 Chip Temperature

For the one test where this parameter was measured it has been found that the temperature increased in a linear fashion though the experiment was quite a subjective one. Chip temperatures from a new and worn tool (defined only by crater wear) have also been calculated to increase by roughly the same amount as measured.

8.5 Short Timescale Events

In general it has been shown that short timescale events can be detected and in some cases, predicted.

For breakage events, either caused artificially or by cutting with inappropriate cutting conditions, the rms AE provides a degree of prediction of the event and could therefore be utilised to prevent possible damage occurring to the milling machine. The available prediction time is, however, fairly short at around 300 ms and there would have to be very prompt signal processing in order to stop the milling machine before damage occurred.

8.6 Influence of Cutting Conditions on Sensorial Data

8.6.1 Spindle Current

The effect of cutting conditions on spindle current is quite predictable, and can be explained by traditional empirical knowledge within the limitations of the drive motor, as discussed in Chapter 3.

8.6.2 Cutting Force

Cutting force is similar to spindle current in that it is a very well known technology, and the variation with cutting conditions can almost completely be explained by reference to a machining handbook. However, particularly for the feed component, there appears to be contamination of the signal by resonances in the force transducer.

8.6.3 Acoustic Emission

The variation of the rms AE sensor with cutting conditions appears to be more related to the volume of material removed than to the strain rate. This is not a result that was expected as it is quite well documented that the rms AE signal varies with the strain rate, at least for orthogonal and semi-orthogonal turning.

8.7 Influence of Cutting Conditions on Wear and Sensorial Output

8.7.1 Spindle Current

Spindle current has been shown to be a very acceptable sensor to use to monitor tool wear for the entire range of cutting conditions investigated. This provides for a sensor that, although machine specific, would allow a very complete and

versatile monitoring system for progressive degradation provided that the appropriate knowledge as to how current varies with cutting conditions and material type was availiable.

8.7.2 Cutting Force

For the extremes of cutting conditions tested, it was found that the cutting force did not provide a very good correlation with tool wear. In fact, for some of the cutting conditions there was no variation with tool wear, the response presumably again being contaminated by resonances.

8.7.3 Acoustic Emission

For this particular test the rms AE signal was a very useful sensor for monitoring tool wear. However, no repeat wear test was conducted and so the variable repeatability exhibited in the systematic wear tests could not be addressed, although several cuts were performed at the central point in cutting condition space, which showed only a small variation between different cuts.

8.8 Performance of two Artificial Intelligence Techniques at Predicting Tool Degradation, both Progressive and Catastrophic

8.8.1 Progressive Wear Detection

Artificial Neural Network

For one of the data sets, it has been found that the ANN is very good at diagnosing either a worn or a new tool although performance at intermediate levels of wear was not as good. The ANN was also adaptable to the absence of one of the sensors as long as this was not the strongest one. For malfunction of the strongest sensor, the ANN performed poorly as might be expected.

Expert System

The Expert System simulation was similarly good at predicting new and worn tool but was also reasonably accurate at intermediate wear levels. This would enable the operator to decide whether enough tool life remained in order to finish the workpiece, or whether a new tool was required. This way of predicting wear appeared to be more dependent on having all sensors present as the wear

prediction was a little less accurate when one of the sensors was removed from the calculation. As with the ANN, malfunction of one of the sensors has a serious effect on system performance.

8.8.2 Breakage Detection

The scheme for breakage detection using a neural network which monitors the peak height from the rms AE has been shown to be a very good way of detecting such events.

The network acts as more than a simple threshold detector as the rms AE varies quite considerably during the breakage inducing events monitored. If a neural simulation had not been used other, more time consuming processing would have been necessary.

8.9 General Conclusions on Tool Condition Monitoring

It has been found throughout this work that the spindle current sensor shows the best overall performance as a tool wear monitor. If such a monitoring system were to be constructed, it would be necessary to calibrate the monitoring system for each machine as the sensor output will be partly dependent on motor type and also on machine type. The other important sensors, feed force and AE, both provide a reasonable way of monitoring tool wear, albeit with a lower confidence level. The problem of repeatability with the AE sensor is a matter still to be resolved but it is suspected that the reproducibility of mounting and clamping arrangements is only part of the cause.

It is felt that the best way of providing a wear monitoring system would be to combine the Neural Network and Expert System and to include a degree of adaptability. The incorporation of the Neural Network allows for automatic learning when in new situations, whereas the incorporation of the Expert System allows not only for knowledge of sensor output with wear, but would also for conventional machining knowledge regarding the estimation of the tool life based on the cutting parameters and workpiece material.

For breakage detection, the AE sensor showed best performance, providing a high degree of detection capability. The processing of this sensor output with a neural network provided for a system that can learn and also provide a better degree of protection than could a threshold detection system, which would require manual recalibration in every new situation.

8.10 Recommendations and Future Directions

Following from this work several key areas of more fundamental research and applied research can be identified that would merit attention. This would help to complete or further the fundamental understanding of the various phenomena identified in the thesis or to develop the possibilities of applying incomplete knowledge such as that presented here into other areas of cutting tool or even machine tool condition monitoring.

Work that falls into the more fundamental category can be covered in the following four areas:

(a) *Acoustic Emission*
Further experimentation is required to determine the precise mechanism(s) for the generation of AE in the cutting of steels. This would require an investigation of the effect of chip temperature and strain rate, which could be achieved by varying the carbon content of the workpiece material and the cutting conditions. Further investigation of the power spectrum of the AE signal, probably with a sensor that possesses a flatter frequency response will help to quantify some of these fundamental issues.

(b) *Effect of Wear Geometry on Sensorial Information*
As a tool wears there are many aspects of the evolving geometry that may compete in the effect that they have on chip flow. Further experimentation and modelling of the different wear geometries, and their effect on cutting forces, temperature and strain rate would greatly aid the identification of appropriate sensor(s) and hence prediction of wear.

(c) *The Milling Process*
Milling is probably the most complicated of the metal removal processes. This is partly because, for many of the different milling processes, the chip thickness in non-constant with usually more than one insert in contact with the workpiece at any one time. Detailed modelling of the milling process, in particular the variation of force, temperature and strain rate as a milling cutter rotates from insert entry into the workpiece to exit would be of particular interest. Experimental verification, which could be achieved, for example, by utilising fly cutting operations would, with the knowledge generated in (b), possibly lead to more accurate tool wear prediction.

(d) *Wear Mechanisms*
Since wear is one of the objectives of the monitoring task, it is important to be able to isolate, knowing the cutting conditions, those mechanisms which might affect sensor output. Since it appears that there are different wear regimes then experiments that utilised different cutting conditions to place the tool into each of these areas would lead to a greater understanding of the parameters on which the wear rate depends.

In all probability the metal cutting problem is large enough to require many more years of more fundamental research before the mechanisms, as indicated in (a) to (d) above, are completely understood. In addition, the matrix of possible machining conditions and materials is extremely large necessitating the development of means to handle qualitative or incomplete data. In order to achieve this, a system is needed that can function with a reasonable performance given the current state of knowledge and furthermore be able to learn. This is probably more realisable with the Neural Network approach than with an Expert System. However, there is a vast body of empirical knowledge that has been accumulated over the last few decades that would be ideal for use in an Expert System and could be reasonably quickly used to allow a system to predict wear and manage the maintenance program of tools and machine in an integrated environment. In fact it might be possible to combine both approaches, with the wear prediction of the ANN being one of the inputs of the ES.

Details of AI that would be worthy of investigation include:

(a) Investigation of the different types of ANN that are currently available. In particular the varying accuracy of decisions made, along with the time to make a decision and the efficiency of the network in making those decisions would be valuable information.

(b) Use of parallel processing techniques to improve the speed and efficiency of the data processing and wear prediction software.

(c) Investigation of various AI techniques such as fuzzy knowledge techniques and their usefulness in the condition monitoring of milling tools.

In addition to this work there are some interesting details of behaviour exhibited by some sensors, in particular that associated with the cutting force, that have not been pursued in this work but may require further attention. In particular, it appears that there is a greater tendency for sensor output to exhibit more complex variations with tool wear for more severe cutting conditions. Work is required to establish whether this tendency is a genuine result of the controlled variables. Further analysis might include a frequency domain analysis of the force information, along with a dynamic calibration of the current machine tool and maybe even other machine tools.

Similarly, the surface finish variation with tool wear requires further investigation as there will be a relationship between the surface and wear profile. If this could be isolated (with a parameter more sophisticated than R_a on simpler processes such as fly cutting) then a useful wear indicator that is also relatively simple to acquire would ensue. This would require a different measurement technique to the R_a meter approach used in this work, and some sort of profile producing instrument would allow for more detailed examination of the surface. Measurements in both the short and long traverses could be made as well as with differing vertical resolutions.

Finally it should be borne in mind that the business of removing metal is constantly being researched in order to find more efficient methods. One such area is that of high speed milling, with rotational speeds in excess of 20,000 RPM, and here there are two points to consider. Firstly, high speed processes may cause different characteristic signals and the best sensor to use may well be different from that for conventional milling. Secondly, the need for high speed condition monitoring is greater as any problems that do occur would tend to be more devastating in effect if not detected and corrected with remedial action.

Appendix A

Mechanical Force Transducer

A mechanical force dynamometer was designed and constructed to provide sensorial output for the three orthogonal components of cutting force for use in this work. This Appendix details the (mechanical and electronic) design of the dynamometer and finally shows the calibration for the three components of force.

A.1 Mechanical Design

The dynamometer consisted of two 40 mm thick plates with four 'slender' pillars clamped between them. These pillars were strain gauged to detect bending in the planes xz, yz and zz. A drawing of the dynamometer can be seen in Figure 327.

A limited theoretical analysis has been conducted on the force transducer and this was used to determine a starting point for the more detailed stress and dynamic analysis conducted using the Finite Element method.

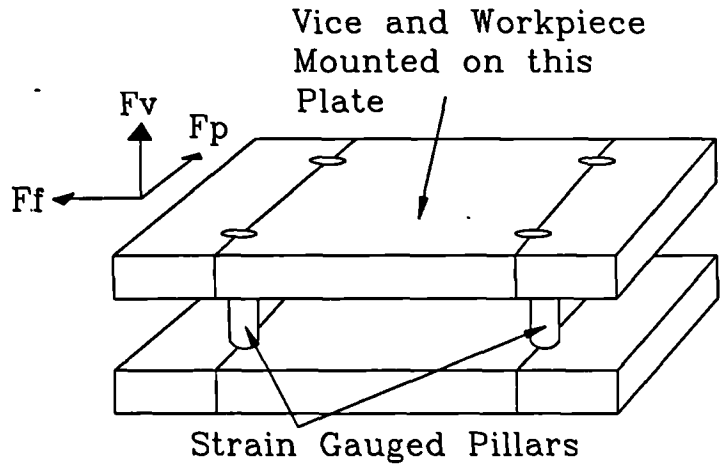

Figure 327: Mechanical, Tri-Axial, Force Dynamometer

A.1.1 Theoretical Analysis

For a unit deflection, the applied load to a pillar of length l and stiffness EI, built-in at both ends in a similar manner to that of the force dynamometer, is;

$$F = 12EI/l^3 \tag{21}$$

with $E = 2.10^{11}\ Pa$, $I = 6.685.10^{-9}\ m^4$ and $l = 0.05\ m$

and utilising the fact that $k = \frac{F}{\delta}$ we find that $k = 156.6.10^6\ Nm^{-}1$

this leads to a natural frequency of 277 Hz when a mass of 400 kg is placed on top of the dynamometer.

A.1.2 Finite Element Analysis

Figure 328 shows the model of a pillar that was used in the finite element analysis. This was constructed inorder to analyse the stress distribution, also shown in Figure 328. As can be seen, with a pillar diameter of 20 mm, the peak Von Mises stress is 81 MPa for a loading on the transducer of 4 kN. This corresponds to an average cutting force quoted by Merchant [7] as the expected value from a roughing cut. The suitability of this design value has been subsequently verified in Chapter 5.

Figures 329 to 333 detail the eigenvalue analysis for the dynamic behaviour of the force transducer. The first natural frequency of 237 Hz in direct bending of the pillars corresponds quite closely to the simple theoretical model applied previously.

A normal roughing cut of 2.5 mm depth of cut, 250 m/min cutting speed and 0.2 mm/insert feed rate was conducted to test the response of the force transducer. The response was determined by placing accelerometers on the side faces of the top plate of the dynamometer. In the frequency range of 0 to 500 Hz it was found that there was an order of magnitude increase in the fixture/workpiece vibration when compared to the frequency response of cutting under the same conditions, but without the force dynamometer in place. The implication being that there will be a dynamic component in the output force transducer.

A.2 Electronic Design

On each pillar 48 strain gauges were positioned so that the three mutually orthogonal components of the cutting force could be measured during cutting. The

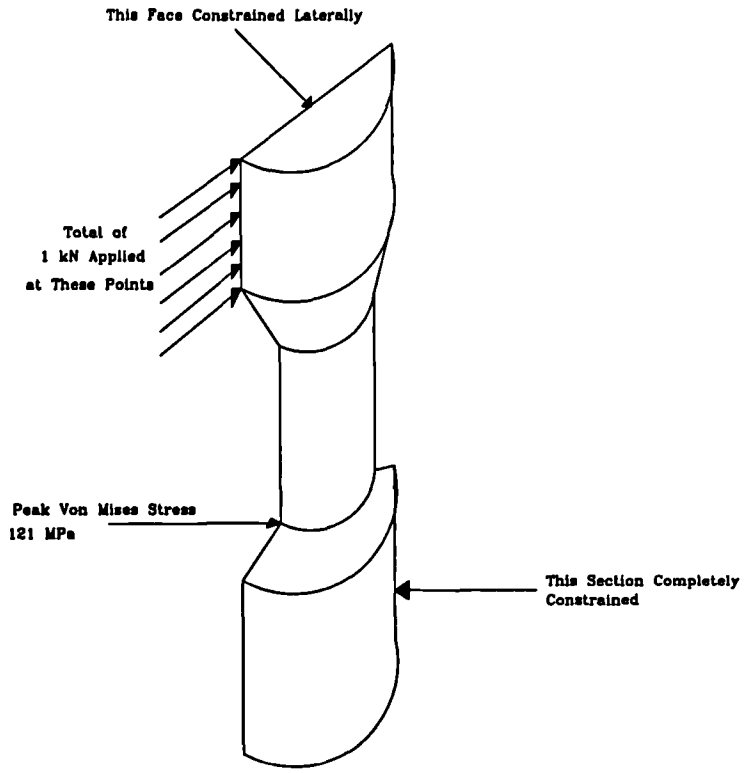

Figure 328: FE Model of Pillar Sensing Element and Results Obtained

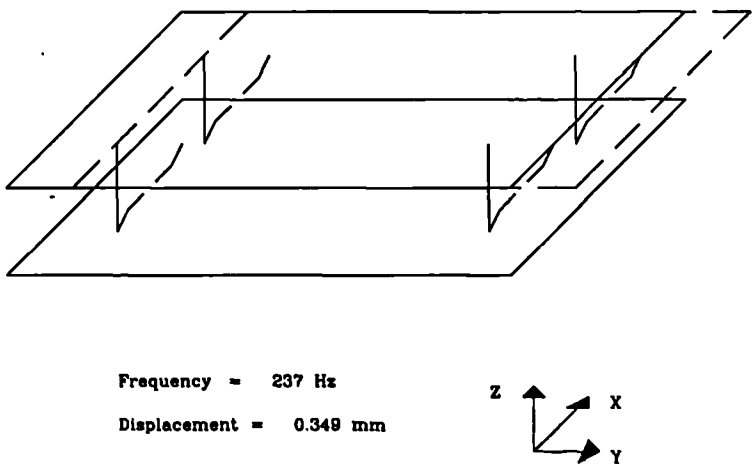

Figure 329: First Natural Frequency, calculated by FE Analysis

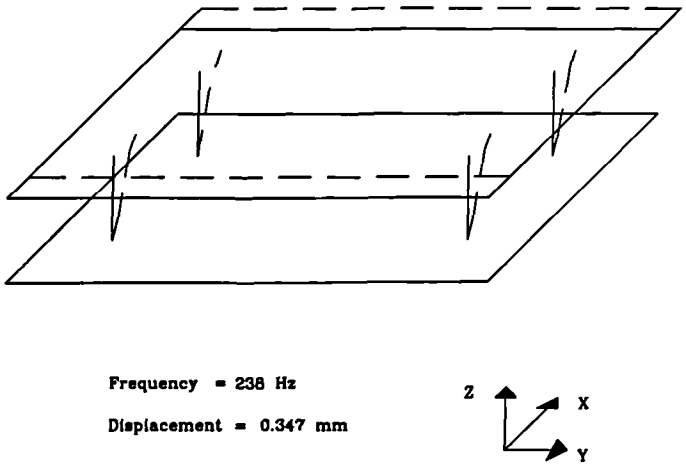

Figure 330: Second Natural Frequency, calculated by FE Analysis

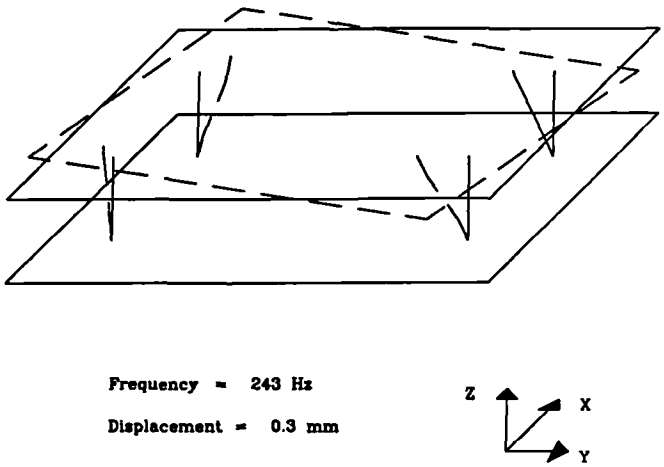

Figure 331: Third Natural Frequency, calculated by FE Analysis

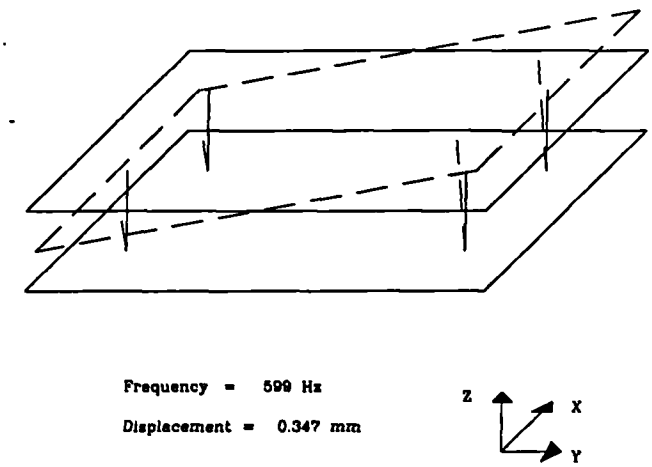

Figure 332: Fourth Natural Frequency, calculated by FE Analysis

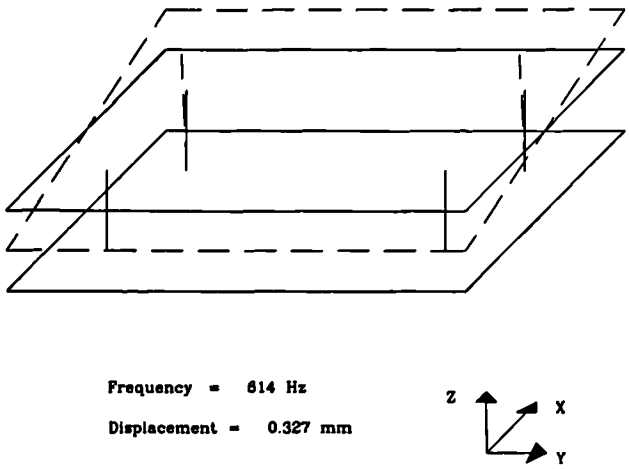

Figure 333: Fifth Natural Frequency, calculated by FE Analysis

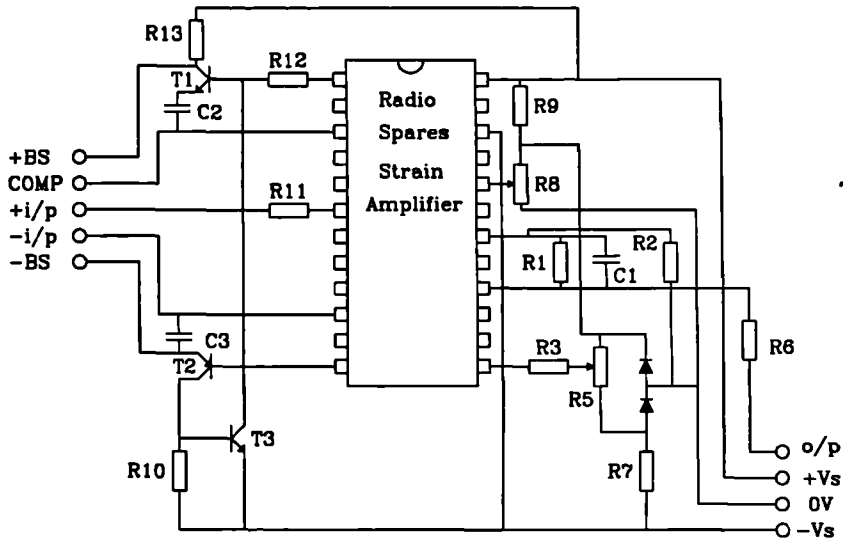

Figure 334: 'Radio Spares' Strain Gauge Ampilfier and Associated Ciruitry

electronic design is based on the 'Radio Spares' instrumentation amplifier 308-815. This dc amplifier is a purpose designed hybrid integrated circuit with low noise and low drift in a 24 pin DIL package. It was chosen because of the high common mode rejection needed to accurately monitor the Wheatstone bridge constructed by the 120 Ω foil gauges attached to the sensing elements. Although it is not impossible to build a circuit to match or better the characteristics of this hybrid, its low cost made this difficult to justify. Figure 334 shows a drawing of this hybrid and its associated circuitry.

A diagram of the one of the three identical summing elements can be seen in Figure 335. The amplifiers were designed to have a bandwidth of 1 kHz which corresponds to a minimum response time of 1 ms.

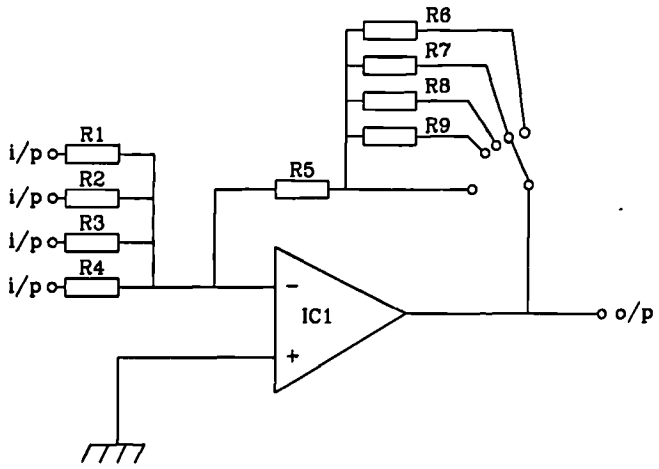

Figure 335: Circuit Diagram of Dynamometer Strain Gauge Amplifier/Summer

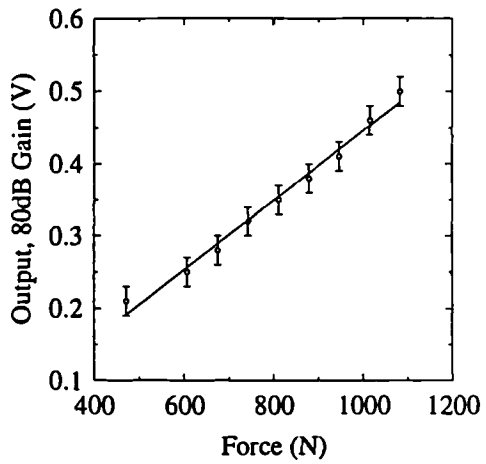

Figure 336: Calibration of the Perpendicular Component of the Force Transducer

A.3 Calibration of Force

The force dynamometer was calibrated by loading the top plate with weights, whilst clamping the bottom plate in a vertical orientation. The results of this can be seen in Figures 336 to 338, for the perpendicular, feed and vertical components respectively. As can be seen, it was not possible to load the transducer to the level of force expected during metal cutting due to the limited number of dead weights that could be applied. However, as the system was not near the yield point, it is reasonable to make a linear extrapolation. There are some points of the feed component of force that do not lie on the regression line. However, the main error occurs for the first point, i.e. for zero force and as this is really a measure of the electrical noise of the force transducer amplifiers it will be ignored. A similar effect can be observed for the other two component of force except that in the other two cases the regression line touches the error bar.

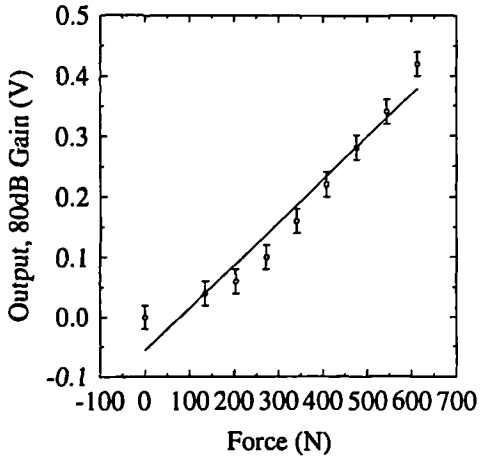

Figure 337: Calibration of the Feed Component of the Force Transducer

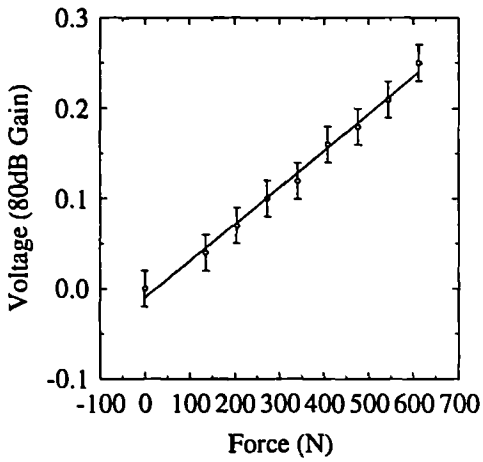

Figure 338: Calibration of the Vertical Component of the Force Transducer

Appendix B

Optical Shaft Encoder

B.1 Introduction

Whilst performing some early experiments, it became clear that it would be useful to be able to correlate the sensorial data with the cutting tool rotational position. In order to do this it was decided to build a shaft encoder.

An optical design was chosen in preference to the more traditional capacitive probe for a number of reasons;

(a) the probe can be made smaller

(b) the object only needs simple preparation in order to facilitate the operation

B.2 Design

The design was based on the detection of the return signal from a reflecting surface placed in the beam path. The source was a Helium Neon (HeNe) laser chosen only for its availability since any other light source, coherent or not, could be used.

Figure 339 shows an optical diagram for the shaft encoder. Light leaves the source, passes through a 50 % beam splitter and is launched into an optical fibre by a small ball lens. At the probe end of the system the light leaves the probe and is focussed onto the object by another ball lens, with a focal length of 15mm. If the object is reflective a return beam is picked up by the probe and passes back to the beam splitter where 50 % of the return signal is sensed with a photodetector, which converts the optical signal into a voltage which is in turn amplified and sampled by the data acquisition computer.

Figure 340 shows the electronic amplifier for the photodetector and Figure 341

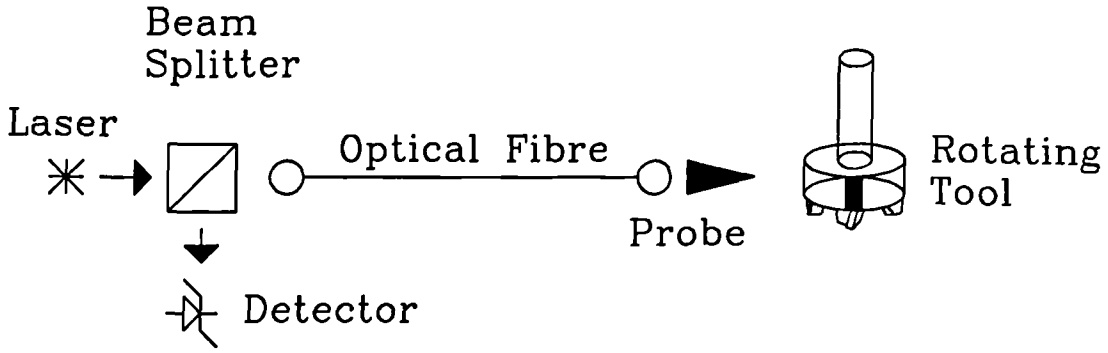

Figure 339: Optical Layout for the Shaft Encoder

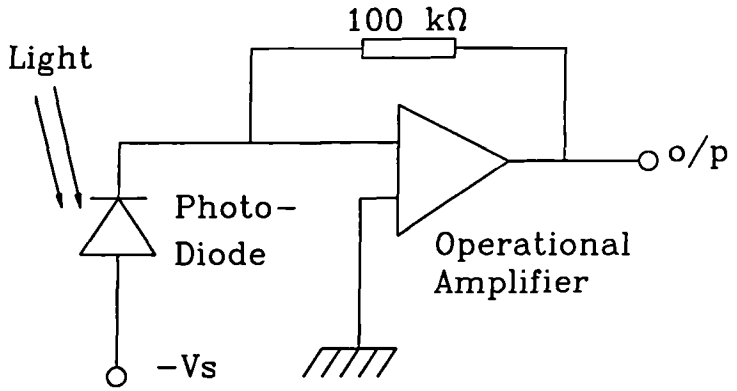

Figure 340: Amplifier for the Optical Shaft Encoder

shows a typical output from the amplifier when the complete system is mounted on to the machine tool.

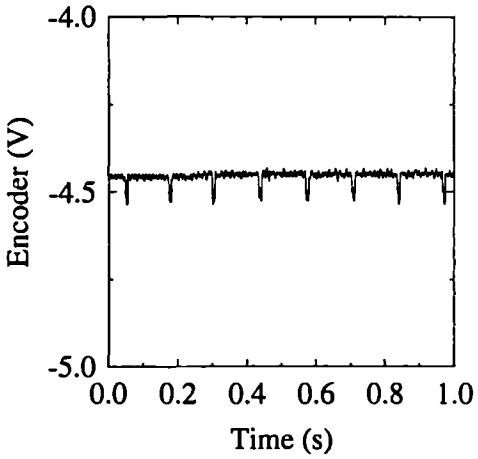

Figure 341: Typical Output of the Sensor

Appendix C

Modification of a Video Cassette Recorder

The principal problem encountered when attempting to record an Acoustic Emission signal is the large bandwidth of the recording medium required to satisfactorily reproduce the signal. High bandwidth analogue tape recorders do exist but are expensive so that it was decided to set about modifying a recording medium that does possess the necessary bandwidth. Some Video Cassette Recorders (VCR) have the necesssary quality of reproduction.

Two video formats are generally available, 'VHS' and 'Umatic', the former being considerably cheaper than the latter but of a lower quality.

A commercial VCR has to have a bandwidth of just over 3 MHz in order to record video information which is sufficient to record AE of bandwidth around 1 MHz. However, all video recorders have some inherent problems associated with their use as general instrumentation recorders:

(a) There is a nonlinear input circuit that normalises the input gain so that there is no possibility of saturating or damaging the circuitry of the VCR when very bright video images are input to the recorder. This circuit is known as the automatic gain control (AGC). A schematic of a typical AGC is shown in Figure 342.

(b) There is a dead period of recording time during which it is impossible to store any data. The dead period is due to the recording head switching process whereby one head disengages the tape before the other engages. This head switching delay lasts between 60 and 250 μs, approximately 1 to 4 lines of picture information. The exact amount of recording that is lost is dependent on the quality of the tape transport system.

(c) A synchronisation pulse is introduced for the tape stepper motor controllers. This takes the form a negative going pulse of around 0.5 ms duration. If the incoming signal to the VCR does not provide this signal then the VCR will

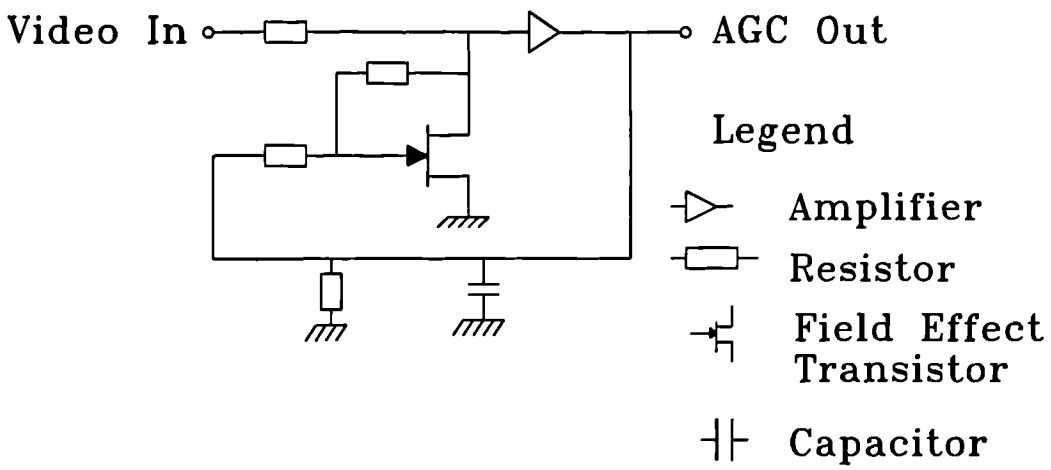

Figure 342: A schematic of a standard AGC

superimpose it onto the recording that is made, so that the motors remain synchronised.

Generally a 'Umatic' VCR is designed with a much higher chip count than the more common VHS VCR. This is because the mechanical parts of the recorder define the box size, and there is therefore a large amount of space available for the electronics. This allows more ready access to the various parts of the signal conditioning. After the non-linear circuitry has been linearised, as shown in Figure 343, the peak-to-peak voltage that can be recorded is 1 Volt.

With careful attention to the tape transport system the recurrent dead period could be reduced to 60 μs in approximately every 25000 μs. This has not been necessary in the current application, but it could be attempted if required. It is also probable that a commercial instrumentation recorder will have similar head switching times.

To avoid the last difficulty it was necessary to construct a circuit that is capable of blanking out the signal at the location of the end of frame pulse. As mentioned in point (c), there are internal timing signals which are used to synchronise the tape transport system and video controller. These circuits were utilised to provide the timing for a blanking pulse and, in this way, a 'Signal Gating Unit' was constructed. Figure 344 shows a schematic of such a circuit, with Figure 345 showing the detailed design of the gating unit.

This method of recording AE has been used thoughout the systematic wear tests in parallel with digital recording using rms AE.

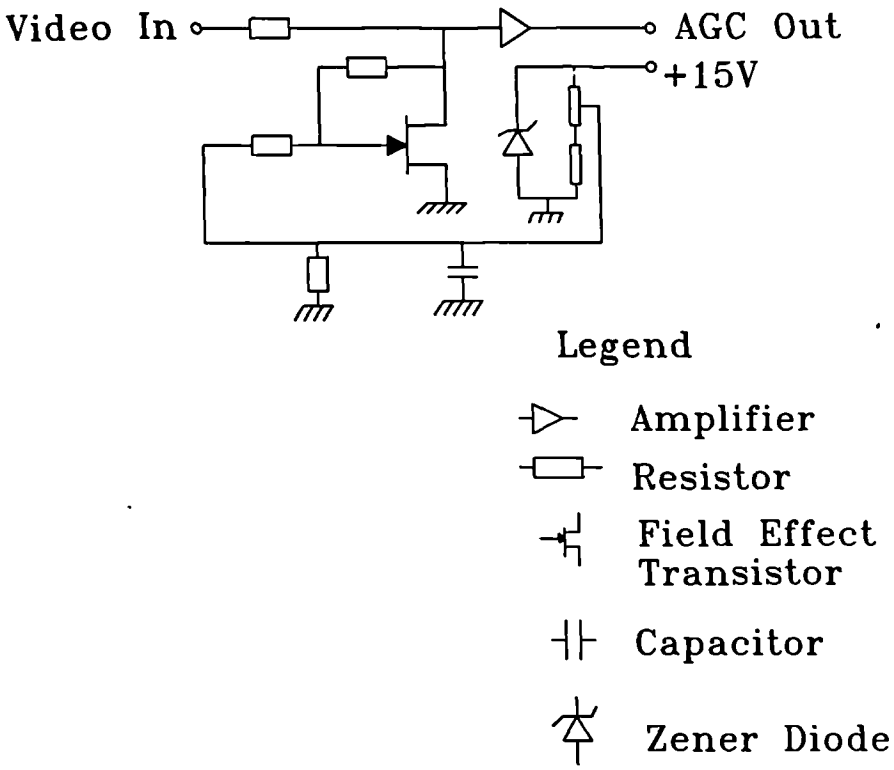

Figure 343: A Schematic of the Modified AGC

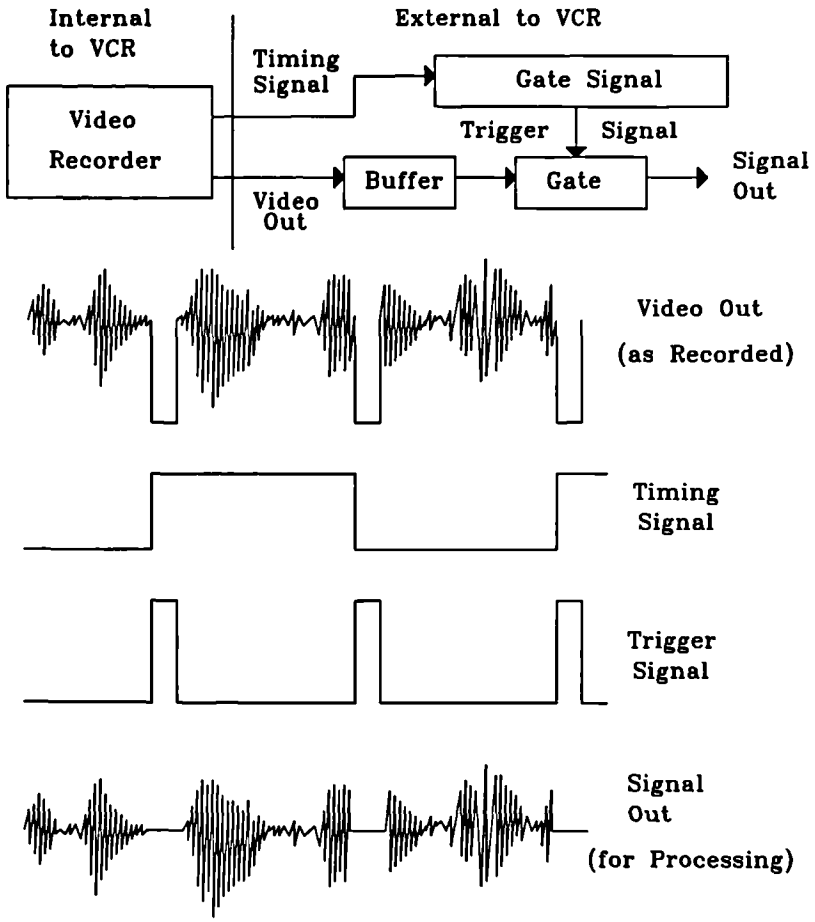

Figure 344: A Schematic of a Custom Signal Gating Unit

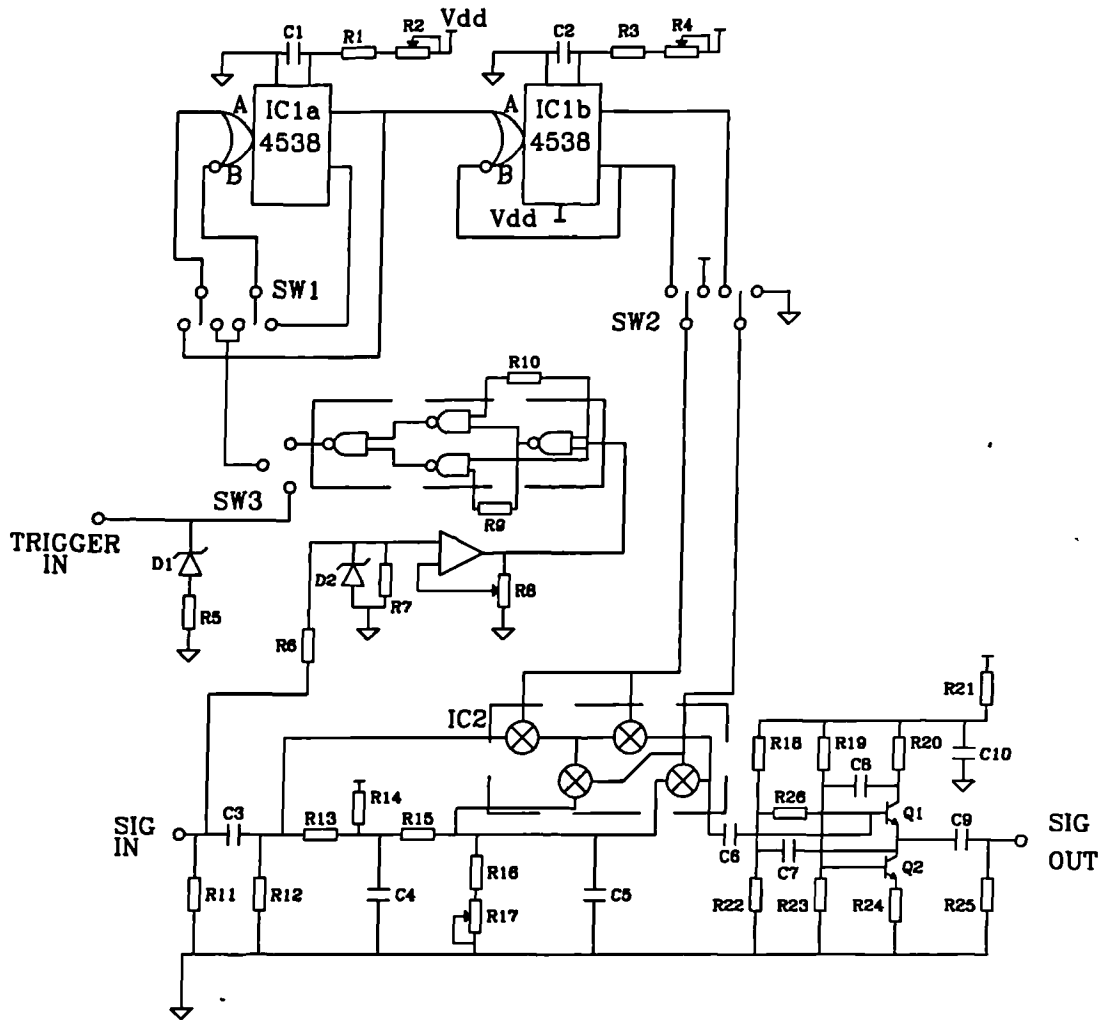

Figure 345: Full Circuit Details of the Signal Gating Unit

Appendix D

Neural Network Code

The following code contains all that is necessary to implement the feed forward ANN used in this work, with a back-propagation training algorithm. The only piece of code that changes between applications is the input routine that gets data to present to the network and the variables that define the size of the network, i.e. the number of input and output neurons and how many hidden layers that the network contains.

The input routine presented here generates data to train the network on the exclusive-or problem as a demonstration of the capabilities of the system. It is an easy matter to change this to input data from a file, or even directly from a data acquisition board.

```
"Standard ANSI C headers"
#include <stdio.h>
#include <stdlib.h>
#include <math.h>

"Define the size of the network"
int nout=1;
int size=2;
int layer=2;

"Define variables used in network"
int count=0;
double average_error=0.0F;
double nerr=0.0F;
double eta=0.7F;

"Declare arrays for netwok, (would operate faster
if redefined as pointers)"
static double output[2][2];
```

```
static double weights[2][3][2];
static double d[2][2];
static double in[2];
static double residule[2];
static double target[2];

"Declare network routines"
void run_network(void);
void get_input(void);
void network_setup(void);
void show_results(void);
void train_network(void);

"Main processing routine for ANN"
void main(void)
{
 int n;
 network_setup();
 for(n=0; n<2000; n++){
  get_input();
  run_network();
  train_network();
  show_results();
  count++;
 } /* end for n */
}

"Routine that calculates output of network
for a given input"
void run_network(void)
{
 int i,j,k;
 double expected;
 for(i=0;i<size;i++){
  expected=weights[i][size+1][0];
  for(j=0;j<size;j++){
   expected=expected+weights[i][j][0]*in[j];
  } /* end for j */
  output[i][0]=1/(1+exp(-expected));
 } /* end for i */

 if(layer>1) {
  for(k=1;k<layer;k++){
   for(i=0;i<size;i++){
    expected=weights[i][size][k];
    for(j=0;j<size;j++){
```

```
      expected=expected+weights[i][j][k]*output[j][k-1];
     } /* end for j */
     output[j][k]=1/(1+exp(-expected));
    } /* end for i */
   } /* end for k */
   for(i=0;i<nout;i++)
    residule[i]=output[i][layer];
   } /* end if */
} /* end of run_network */

"Routine to change to obtain training features
for any specific application, random number
generation could be improved if it was felt necessary"
void get_input(void)
{
 int i;
 int decision;
 for (i=0;i<size;i++){
  decision = rand();
  if(decision>16384)
   in[i]=0.0F;
  else
   in[i]=1.0F;
  } /* end for i */
  if(size>1){

"Change targets to realisable values, for
excitation function"
   target[0]=in[0];
   target[i]=0.0F;
  } /* endif */
  if(target[0]=1.0F)
   target[0]=0.9F;
  else
   target[0]=0.1F;
} /* end of get_input */

"Routine to define network topology"
void network_setup(void)
{
 int k,i,j;
 for(k=0;k<layer;k++) {
  for(i=0;i<size;i++) {
   for (j=0;j<size+1;j++) {
    weights[i][j][k] = (double) rand()/32768.0F;
   }
```

```
  }
 }
} /* end of network_setup */

"Print out results"
void show_results(void)
{
 int i;
 for(i=0;i<size;i++){
  printf("input[%d]=%f\n",i,in[i]);
  if(i<nout){
   printf("Target[%d]= %f -- Residule[%d]=%f\n"
   ,i,target[i],i,residule[i]);
  } /* end if i */
 } /* end for i */
 printf("Number of iterations %d\n",count);
 printf("Error this iteration %f\n",nerr);
 average_error=0.2*nerr + 0.8*average_error;
 printf("Average Error %f\n",average_error);
} /* endof show_results */

"Back-propagation training algorithm"
void train_network(void)
{
 int i,k,j;
 double deltasum=0.0F;
 for(i=0;i<size;i++)
 {
  if(i<nout)
  {
   d[i][layer]=(target[i]-residule[i])*residule[i]*
   (1-residule[i]);
   nerr=pow((pow((target[i]-residule[i]),2)),0.5);
  }
  else
   d[i][layer]=0.0F;
  }

 for(k=layer-1;k>=0;k--){
  for(i=0;i<size;i++){
   for(j=0;j<size;j++){
    deltasum=deltasum+d[j][k+1]*weights[j][i][k+1];
   } /* end for j */
   d[i][k]=output[i][k]*(1-output[i][k])*deltasum;
  } /* end for i */
 } /* end for k */
```

```
for(i=0;i<size;i++){
 for(j=0;j<size;j++){
  weights[i][j][0]=weights[i][j][0]+eta*d[i][0]*in[j];
 } /* end for j */
 weights[i][size+1][0]=weights[i][size+1][0]+
 eta*d[i][0];
} /* end for i */

for(k=1;k<layer;k++){
 for(i=0;i<size;i++){
  for(j=0;j<size;j++){
   weights[i][j][k]=(weights[i][j][k]+(eta*
   d[i][k]*output[i][k-1]));
  }
  weights[i][size+1][k]=weights[i][size+1][k]+
  (eta*d[i][k]);
 }
}
} /* endof train network */
```

Appendix E

Prototype Monitoring Station

Figure 346 shows how the author feels that it would be possible to link data acquisition, signal processing, AI, and milling machine to provide an automatic wear and breakage monitoring system.

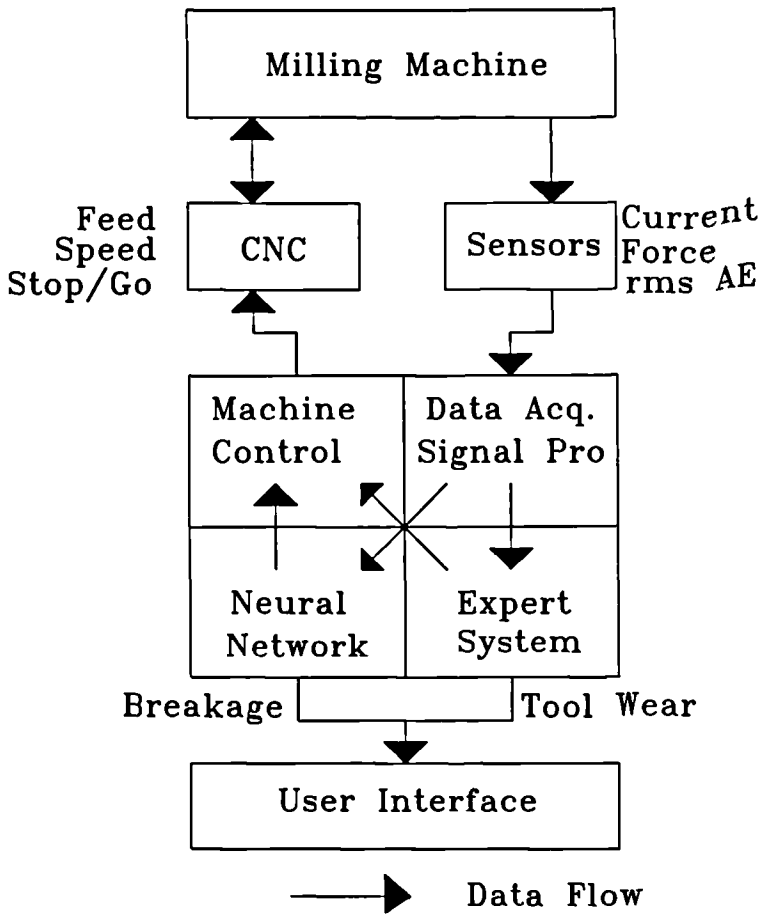

Figure-346: Proposed Organisation of the Monitoring System

Appendix F

Metal Cutting Theory after Oxley et al

The theory that follows is a resume of that developed and presented by Oxley et al [11,12,13,14,15,77].

Oxley and his colleagues, in developing their metal cutting theory, used experimental results from work performed by Oyane et al [76] for the variation in material flow stress with strain, strain rate and temperature. These latter authors have carried out high speed compression tests for plain carbon steels with carbon content in the range 0.16 % to 0.55 %. During these tests the maximum strain was unity, the strain rate was constant at 450 s^{-1} and the temperature was in the range of 300 K to 1500 K. Since the strain rate during most machining is much larger than 450 s^{-1} extrapolation was necessary and this was performed by using the concept of velocity modified temperature, first suggested by McGregor and Fisher [152]:

$$T_{mod} = T[1 - \nu log(\frac{\dot{\gamma}}{\dot{\gamma}_0})] \tag{22}$$

Where:

T is the actual temperature in degrees Kelvin

$\dot{\gamma}$ is the direct strain rate

ν is a constant, set at 0.09

$\dot{\gamma}_0$ is a constant, set at 1 s^{-1}

For each of the plain carbon steels considered, the results of Oyane et al show that, for a given temperature and strain rate the stress-strain relationship, given by:

$$\sigma = \sigma_1 \gamma^n \tag{23}$$

Where:

σ_1 is the flow stress

n is the strain hardening index

gives a good fit to the experimental results, and hence σ_1 and n can be obtained and plotted against T_{mod}.

To find the flow stress for given values of strain, strain rate and temperature T_{mod} is calculated and this in turn gives values of σ_1 and n which are used together with the strain to find the flow stress.

A summary of the processes involved in calculating the strain rate using the Oxley model is shown below:

The basis of the theory is to analyse the stress distribution along the plane near the centre of the primary deformation zone and the chip-tool interface in terms of the shear angle, ϕ, work material properties and cutting conditions and then to select as the solution for ϕ the value for which the resultant force transmitted by the plane AB and the interface are in equilibrium. Once ϕ is known then the various components of force can be determined from the following relations:

$$F_C = Rcos(\lambda - \alpha) \tag{24}$$

$$F_T = Rsin(\lambda - \alpha) \tag{25}$$

$$F = Rsin\lambda \tag{26}$$

$$N = Rcos\theta \tag{27}$$

$$R = \frac{F_s}{cos\theta} = \frac{k_{AB} t_1 w}{sin\phi cos\theta} \tag{28}$$

Where:

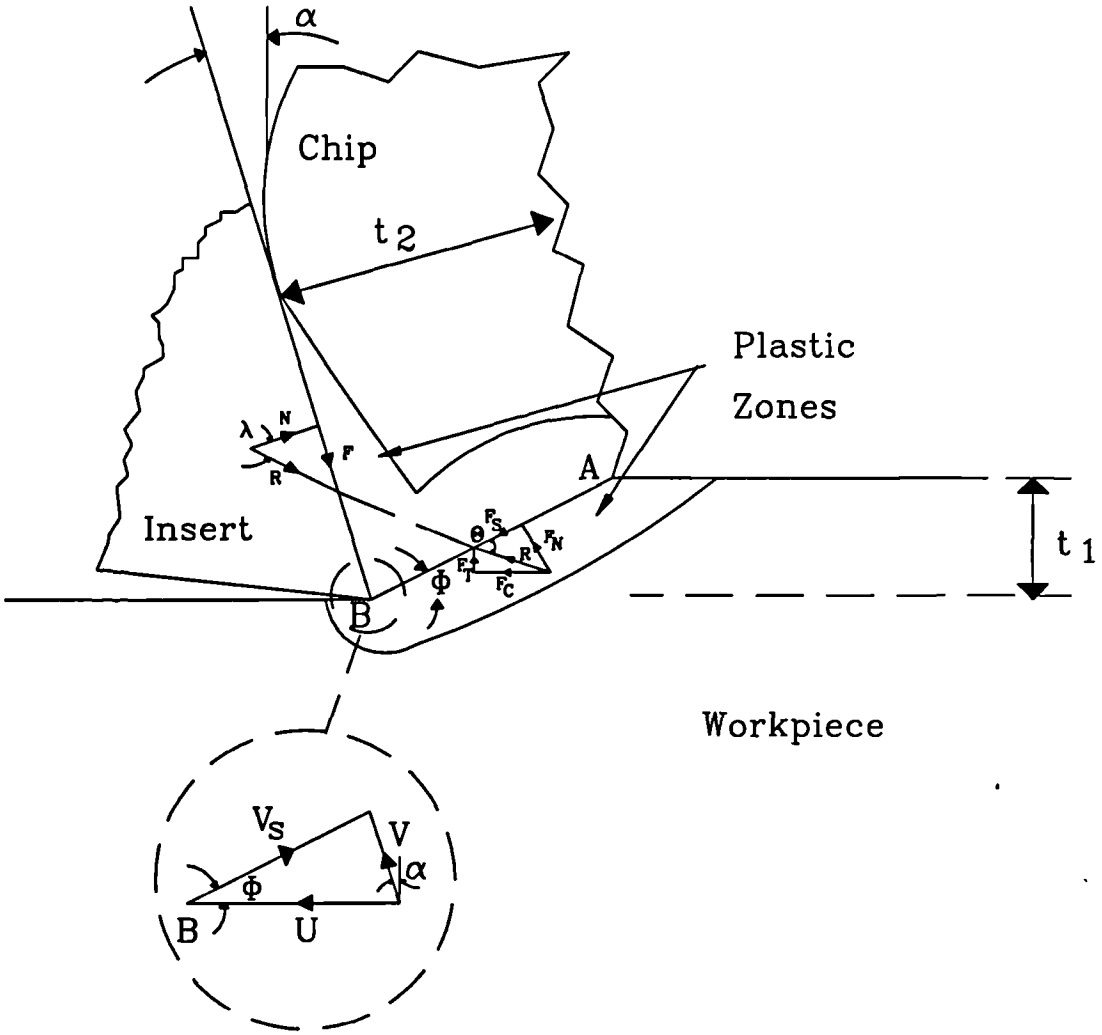

Figure 347: Diagram of the Cutting Process for Orthogonal Cutting after Oxley et al

t_1 is the undeformed chip thickness

w is the width of the cut

k_{AB} is the shear flow stress along the plane AB, Figure 347

$F_s, N, R, \phi, \lambda, \theta, F_C, F_T, F$ are the forces and angles as shown in Figure 347

The shear flow stress k_{AB} is found from:

$$k_{AB} = (\frac{\sigma_1}{\sqrt{3}})\gamma^n \tag{29}$$

using values of σ_1 and n appropriate to the work material properties considered and the value of T_{mod} at the plane AB. Oxley et al by including the prior cold working ϵ_w of the workpiece, found that the effective strain ϵ_{AB} at the plane AB, is given by:

$$\epsilon_{AB} = \epsilon_w + \frac{\Delta\gamma_{AB}}{\sqrt{3}} \tag{30}$$

Here the shear strain rise $\Delta\gamma_{AB}$ in the shear zone up to the plane AB is assumed, on the basis of experimental data, to be equal to half the total shear strain occurring in the primary shear zone, that is:

$$\Delta\gamma_{AB} = \frac{1}{2}.\frac{\cos\alpha}{\sin\phi\cos(\phi-\alpha)} \tag{31}$$

where the tool rake angle α is shown in Figure 347.

There are two zones of intense plastic deformation and these are treated separately below:

For the plane AB

It can be shown that the angle of inclination of the resultant cutting force, R to AB is given by:

$$tan\theta = 1 + 2(\frac{\pi}{4} - \phi) - Cn \tag{32}$$

Where:

C is the constant in the strain rate equation

From the geometry of Figure 347, the angle θ can also be expressed in terms of other angles by the equation:

$$\theta = \phi - \alpha + \lambda \tag{33}$$

The maximum shear strain rate $\dot{\gamma}_{AB}$ along AB is given by the empirical relation:

$$\dot{\gamma}_{AB} = C(\frac{V_s}{l}) \tag{34}$$

Where:

V_s is the shear velocity along AB

l is the length of AB

The temperature rise in the primary shear zone ΔT_{sz} is found from the power dissipated in this zone and is given by:

$$\Delta T_{sz} = \frac{1-\beta}{\rho S t_1 w} \cdot \frac{F_s cos\alpha}{cos(\phi - \alpha)} \tag{35}$$

where β is the proportion of heat conducted into the workpiece. The value of β ($0 < \beta \leq 1$) can be estimated using the following empirical equations:

$$\beta = 0.5 - 0.35 log(R_T tan\phi) \; for \; 0.04 < R_T tan\phi < 10 \tag{36}$$

$$\beta = 0.3 - 0.15 log(R_T tan\phi) \; for \; R_T tan\phi > 10 \tag{37}$$

where R_T is a non-dimensional thermal number defined as:

$$R_T = \frac{\rho S U t_1}{K} \tag{38}$$

The above equations for β are based on experimental data compiled by Boothroyd [153], with specific heat S and thermal conductivity K being given by:

$$S(Jkg^{-1}K) = 420 + 0.504T(K) \tag{39}$$

$$K(Wm^{-1}K) = 57.9 - 0.0345T(K) \tag{40}$$

and U is shown in Figure 347.

The average temperature along AB is taken as:

$$T_{AB} = \eta T_{SZ} + T_W \tag{41}$$

where the factor $\eta(0< \eta \leq 1)$ allows for the fact that not all of the plastic work of chip formation has occurred at AB and the suffices SZ and W denote shear zone and workpiece respectively. The normal stress $\sigma_N^{'}$ is found from the boundary condition at B for the normal stress distribution along AB. It is given by:

$$\frac{\sigma_N^{'}}{k_{AB}} = 1 + 2(\frac{\pi}{4} - \alpha - Cn) \tag{42}$$

For the tool-chip interface

The maximum shear strain rate at the tool-chip interface is assumed to be given by:

$$\dot{\gamma}_{int} = \frac{V_c}{\delta t_2} \tag{43}$$

This equation implies that, across the tool-chip interface plastic zone of thickness δt_2, the velocity changes linearly from zero at the tool surface to the chip velocity V_c. However, for most cutting conditions there will be a small component of the chip sliding over the tool surface and equation 43 therefore will overestimate the strain rate, but the error will usually be small. The average temperature at the tool-chip interface is taken as:

$$T_{int} = T_W + \Delta T_{SZ} + \kappa T_M \tag{44}$$

where the factor κ $(0< \kappa \leq 1)$ accounts for the possible variation of the temperature along the tool-chip interface and T_M is the maximum temperature rise at the tool-chip interface. The maximum temperature rise ΔT_M in the chip is calculated from:

$$log[\frac{\Delta T_M}{\Delta T_C}] = 0.06 - 0.195[\frac{R_T t_2}{h}]^{\frac{1}{2}} + 0.5log[\frac{R_T t_2}{h}] \tag{45}$$

where ΔT_C is the average temperature rise in the chip and is given by:

$$\Delta T_C = \frac{Fsin\phi}{\rho S t_1 w cos(\phi - \alpha)} \tag{46}$$

Equation 46 is based on Boothroyd's results [153]. Boothroyd has calculated ΔT_M using numerical methods and assuming a rectangular heat source at the

tool-chip interface. He has shown that his calculated values of ΔT_M are in good agreement with experimentally measured temperatures.

The tool-chip contact length can be calculated from the equation:

$$h = \frac{t_1 sin\theta}{cos\lambda sin\phi}[1 + \frac{Cn}{3[1 + 2(\frac{\pi}{4} - \phi) - Cn]}] \tag{47}$$

It is based on the assumption that the normal stress distribution at the tool-chip interface is uniform, so that R intersects the tool at a distance $\frac{h}{2}$ from B. Equation 47 is derived by taking moments about B for the normal stresses on AB which, for equilibrium, must be equal to the moment $\frac{Nh}{2}$. Lastly, the average normal stress at the tool-chip interface is given by:

$$\sigma_N = \frac{N}{hw} \tag{48}$$

The above equations are now sufficient to determine ϕ and, hence, cutting forces, temperatures etc. for given cutting conditions as long as the flow stress and thermal properties of the workpiece and the values of the strain rate constant C in equations 32, 34, 42 and 47 and δ in equation 43 are known. For simplicity C and δ have been considered invariant with cutting conditions, and take the values of 5.9 and 0.02 respectively. This assumption holds for a large proportion of cutting conditions [11], and only recently have Oxley et al included numerical methods of calculating these parameters.

The method of solution is to determine by an iterative procedure the shear angle ϕ for which the chip formation process is in equilibrium, that is, when:

$$\tau_{int} = k_{chip} \tag{49}$$

Here the resolved shear stress at the tool-chip interface τ_{int} is calculated from the resultant force and is given by:

$$\tau_{int} = \frac{F}{hw} \tag{50}$$

and the shear flow stress k_{chip} in the chip adjacent to the interface is assumed to be given by:

$$k_{chip} = \frac{\sigma_1}{\sqrt{3}} \tag{51}$$

where σ_1 corresponds to the value of T_{mod} at the interface.

This iterative procedure for calculating the strain rates, temperatures and forces in the cutting process is shown in a flow diagram in Chapter 3.

Appendix G

Wave Propagation

This appendix documents the types of wave propogation that is possible is both bounded and un-bounded isotroptic media, along with equations to calculate wave velocities.

G.0.1 Isotropic unbounded elastic medium

The wave velocity will depend on the material properties of the propagating medium and, in an isotropic unbounded medium, there exist two principal means by which AE energy is propagated. The first of these is by means of dilatational compression waves which propagate parallel to the direction of atomic vibration, with a velocity of [154]:

$$c_1 = \sqrt{\frac{\lambda + 2\mu}{\rho}} \tag{52}$$

The other type of wave motion possible is known as a distortional shear wave. This propagates in the direction transverse to the direction of atomic vibration, with a velocity of:

$$c_2 = \sqrt{\frac{\mu}{\rho}} \tag{53}$$

Where:

ρ is the medium density

λ is one of Lame's constants

μ is one of Lame's constants

If there is a free surface in the medium then it is possible for other types of wave propagation to occur, two of these being Rayleigh and Lamb waves. These waves will propagate at a fraction k_1 of the velocity of the distortional wave c_2. The value of k_1 is obtained from the cubic equation in k_1^2:

$$k_1^6 - 8k_1^4 + (24 - 16\alpha_1^2)k_1^2 + 16\alpha_1^2 - 16 = 0 \tag{54}$$

where α_1 is an elastic constant, given by the expression,

$$\alpha_1 = \frac{1 - 2\eta}{2 - 2\eta} \tag{55}$$

where η is Poisson's ratio for the medium

The Rayleigh vibration is in a plane perpendicular to the free surface which is parallel to the direction of propagation. For a sinusoidal Rayleigh wave the vibration has an elliptical trajectory.

G.0.2 Isotropic bounded medium

In a rod, for example, there are three type of wave propagation, longitudinal, torsional and flexural waves and the speed of propagation is partly dependent on the dimensions of the rod. If the wavelength of the wave is long in comparison to the lateral dimensions of the rod then the longitudinal and torsional waves travel at constant velocities.

For longitudinal waves, the speed of propagation is given by:

$$c_l = \sqrt{\frac{E}{\rho}} \tag{56}$$

For torsional waves, the equivalent expression is:

$$c_t = \sqrt{\frac{\mu}{\rho}} \tag{57}$$

where μ is the shear modulus

For flexural waves, the velocity of propagation is directly related to wavelength, and for a long wavelength this is given by:

$$c_f = \frac{2\pi c_l k}{\lambda} \tag{58}$$

Where:

λ is the wavelength

k is the bulk modulus

When the wavelength becomes comparable to the lateral dimensions, both the longitudinal and flexural wave velocities approach that of the Rayleigh velocity. However, the velocity of torsional waves remains independent of wavelength as long as the body vibrates in its fundamental mode.

Waves propagating in a bounded elastic medium are also subject to dispersion. This will lead to multiple amplitude peaks as the original signal propagates along what is essentially a wave guide. Dispersion leads to an increase in the propagation velocity with reductions in the wavelength. The propagation velocity is considered here to be the group velocity.

The group velocity is a function of the average wavelength of the bundle of waves that are propagating and the rate at which points of constant phase progress along a datum line, the phase velocity.

In flexural waves, where dispersion is unavoidable, the phase velocity is given by Kolsky [154] as:

$$c' = c_l[1 + \frac{\lambda^2}{4\pi^2 k^2}]^{-\frac{1}{2}} \tag{59}$$

and the group velocity as:

$$c_g = c'[1 + \frac{1}{1 + 4\pi^2 \frac{k^2}{\lambda^2}}] \tag{60}$$

References

[1] A.Edwin and T.Vlash. A new approach to tool wear monitoring through mini-computers and modern transducers. In *27th Annual Conference and Exhibition of the Instrumentation Society of America, Part 2*, pages 626–629, 1972.

[2] J.Mathew, D.Plummer, and L.Dan. Tool wear monitoring using vibration and force measurements. In *Proceedings of the 2nd International Machinery Monitoring and Diagnostics Conference and Exhibition*, pages 115–120, 1990. Los Angeles, California.

[3] E.M.Trent. *Metal Cutting.* Butterworths & Co., second edition, 1984.

[4] N.H.Cook. Tool wear and tool life. *Transactions of the ASME, Journal of Engineering for Industry*, pages 931–938, November 1973.

[5] S.Rangwala and D.A.Dornfeld. Sensor integration using neural networks for intelligent tool condition monitoring. *Transactions of the ASME, Journal of Engineering for Industry*, 112:219–227, August 1990.

[6] I.Finnie. Review of the metal–cutting analyses of the past hundred years. In *American Society of Mechanical Engineers*, pages 715–721, March 1956.

[7] M.E.Merchant. Mechanics of the metal cutting process. I. orthogonal cutting and a type 2 chip. *Journal of Applied Physics*, 16(5):267–275, May 1945.

[8] M.E.Merchant. Mechanics of the metal cutting process. II. plasticity conditions in orthogonal cutting. *Journal of Applied Physics*, 16(6):318–324, June 1945.

[9] G.V.Stabler. The fundamental geometry of cutting tools. *Institution of Mechanical Engineers*, 1951.

[10] P.Albrecht. Dynamics of the metal–cutting process. *Transactions of the ASME, Journal of Engineering for Industry*, pages 429–441, November 1965.

[11] R.G.Fenton and P.L.B.Oxley. Mechanics of orthogonal machining: Allowing for the effects of strain rate and temperature on tool–chip friction. *Proceedings of the Institution of Mechanical Engineers, Part 1*, 183(22):417–438, 1968.

[12] M.G.Stevenson and P.L.B.Oxley. An experimental investigation of the influence of speed and scale on the strain–rate in a zone of intense plastic deformation. *Proceedings of the Institution of Mechanical Engineers, Part 1*, 184(31):561–576, 1969.

[13] M.G.Stevenson and P.L.B.Oxley. An experimental investigation of the influence of strain–rate and temperature on the flow stress properties of a low carbon steel using a machining test. *Proceedings of the Institution of Mechanical Engineers*, 185(54):741–D303, 1970.

[14] P.L.B.Oxley and W.F.Hastings. Minimum work as a possible criterion for determining the frictional conditions at the tool/chip interface in machining. *Philosophical Transactions of the Royal Society, London*, 282:565–584, 1976.

[15] P.L.B.Oxley and W.F.Hastings. Predicting the strain rate in the zone of intense shear in which the chip is formed in machining from the dynamic flow stress properties of the work material and the cutting conditions. *Proceedings of the Royal Society, London*, pages 395–410, 1977.

[16] V.Phispanen. Theory of formation of metal chips. *Journal of Applied Physics*, 19:876–881, October 1948.

[17] T.H.C.Childs. Elastic effects in metal cutting chip formation. *International Journal of Mechanical Science*, 22:457–466, 1980.

[18] D.Lee. The nature of chip formation in orthogonal machining. *Transactions of the ASME, Journal of Engineering Materials and Technology*, 106:9–15, January 1984.

[19] H.Chandrasekaran. The transient tool stresses and their implications in milling. In *Comptes Rendus Proceedings, 8th Canadian Congress of Applied Mechanics, Universite de Monctron*, June 1981.

[20] V.K.Jain and B.K.Gupta. Effects of accelerated tests on shear flow stress in machining. *Transactions of the ASME, Journal of Engineering for Industry*, 109:206–212, August 1987.

[21] M.Sarwar and P.J.Thompson. Cutting action of blunt tools. In *Proceedings of the 22nd International Machine Tool Design and Research Conference*, September 1981.

[22] D.A.Stevenson and S.M.Wu. Computer models for the mechanics of three–dimensional cutting processes - part 1: Theory and numerical method. *Transactions of the ASME, Journal of Engineering for Industry*, 110:32–37, February 1988.

[23] D.A.Stevenson and S.M.Wu. Computer models for the mechanics of three–dimensional cutting processes – part 2: Results for oblique end turning and drilling. *Transactions of the ASME, Journal of Engineering for Industry*, 110:38–43, February 1988.

[24] E.Usui and H.Takeyama. A photelastic analysis of machining stress. *Transactions of the ASME, Journal of Engineering for Industry*, pages 303–308, Novemeber 1960.

[25] K.Nakayama and M.Arai. On the storage of data on metal cutting forces. *Annals of the CIRP*, 25(1):13–18, 1976.

[26] R.J.Boness, S.L.McBride, and M.Sobczyk. Condition monitoring of wear using acoustic emission techniques. In *Proceedings of COMADEM 90, The Second International Congress on Condition Monitoring and Diagnostic Engineering Management*, pages 38–43, 1990.

[27] R.J.Boness and S.L.McBride. Adhesive and abrasive wear studies using acoustic emission techniques. *Wear*, 149:41–53, 1991.

[28] A.J.Lissaman and S.J.Martin. *Principles of Engineering Production.* Hodder and Stoughton, second edition, 1982.

[29] T.J.Drozda and C.Wick. *Tool and Manufacturing Engineers Handbook. Volume 1 – Machining.* Society of Manufacturing Engineers, Michigan, fourth edition, 1983.

[30] Kennametal, Inc. Kennametal tcs. système d'avant–garde de surveillance des outils de coupe sur tours. Kennametal Promotion Leaflet, 1987, Latrobe, PA 15650, U.S.A.

[31] Sandvik. Multi–channel tool monitor unit. Sandvik Promotion Leaflet.

[32] K.Danai and A.G.Ulsoy. A dynamic state model for on–line tool wear estimation in turning. *Transactions of the ASME, Journal of Engineering for Industry*, 109:396–399, November 1987.

[33] T.Sata, K.Matsushima, T.Nagakura, and E.Kono. Learning and recognition of the cutting states by spectrum analysis. *Annals of the CIRP*, 22(1):41–42, 1973.

[34] W.Konig, K.Langhammer, and H.-U.Schemmel. Correlations between cutting force components and tool wear. *Annals of the CIRP*, 21(1):19–20, 1972.

[35] Y.Kashimura. Study on detection of drill wear and breakage (1st report). *Bulliten of the Japanese Society of Precision Engineering*, 20(3):159–164, September 1986.

[36] K.Taraman, R.Swando, and W.Yamauchi. Relationships between tool forces and flank wear. University of Detroit Internal Report, MR74–704.

[37] R.Nair, K.Danai, and S.Malkin. Turning process identification through force transients. *Transactions of the ASME, Journal of Engineering for Industry*, 114:1–7, February 1992.

[38] M-S.Lan and Y.Naerheim. In–process detection of tool breakage in milling. *Transactions of the ASME, Journal of Engineering for Industry*, 108:191–197, August 1986.

[39] Y.Altintas, I.Yellowley, and Y.Tlusty. The detection of tool breakage in milling operations. *Transactions of the ASME, Journal of Engineering for Industry*, 110:271–277, August 1988.

[40] Y.Altintas and I.Yellowley. In–process detection of tool failure in milling using cutting force models. *Transactions of the ASME, Journal of Engineering for Industry*, 111:149–157, May 1989.

[41] Y.D.Landau. Adaptive control – the model reference approach. Marcel Dekker, New York, 1979.

[42] Y.D.Landau and M.Tomizuka. Theory and practise of adaptive control systems. *Ohm, Tokyo*, 1981.

[43] S.B.Rao. Tool wear monitoring through the dynamics of stable turning. *Transactions of the ASME, Journal of Engineering for Industry*, 108:183–190, August 1986.

[44] A.M.Petrie, T.S.Sihra, and A.Ismail. The development of an automated system for on–line tool wear monitoring. In *1st International Machinery Monitoring Conference*, September 1989. Las Vegas.

[45] B.Lindström and B.Lindberg. Measurements of dynamic cutting forces in the cutting process, a new sensor for in–process measurements. In *Proceedings of the 24th International Machine Tool Design and Research Conference*, pages 137–142, September 1983. Manchester.

[46] M.A.Elbestawi, T.A.Papazafiriou, and R.X.Du. In–process monitoring of tool wear in milling using cutting force signature. *International Journal of Machine Tools and Manufacturing*, 31(1):55–73, 1991.

[47] Y.S.Tarng. Study of milling cutting force pulsation applied to the detection of tool breakage. *International Journal of Machine Tools and Manufacturing*, 30(4):651–660, 1991.

[48] Y.S.Tarng. Measurement of quasi–mean resultant force using the vibrational signal of spindle in milling. *International Journal of Machine Tools and Manufacturing*, 31(3):295–304, 1991.

[49] S.E.Oraby and D.R.Hayhurst. Development of models for tool wear force relationships in metal cutting. *International Journal of Machine Tools and Manufacturing*, 33(2):125–138, 1991.

[50] A.Thangaraj and P.K.Wright. Drill wear sensing and failure prediction for untended machining. *Robotics and Computer–Integrated Manufacturing*, 4(3):429–435, 1988.

[51] K.F.Hale and B.E.Jones. The use of thermography for tool wear monitoring. In *Proceedings of the 29th International Matador Conference*, pages 493–499, April 1992. UMIST, Manchester.

[52] Infrared Monitoring Systems. IR monitors cutting–tool wear. Photonics Spectra, November 1991.

[53] V.Solaja and D.Vukelja. Identification of tool wear rate by temperature variation of a carbide tip. *Annals of the CIRP*, 22(1):5, 1973.

[54] A.H.Redford and S.Akhtar. Temperature–tool life relationships for resulphurised low carbon free machining steels. *Annals of the CIRP*, 25(1):89–91, 1976.

[55] L.V.Colwell. Cutting temperature versus tool wear. *Annals of the CIRP*, 24(1):73–76, 1975.

[56] J.Raja and D.J.Whitehouse. An investigation into the possibility of using surface profiles for machine tool surveillance. *International Journal of Production Research*, 22(3):453–466, 1984.

[57] W.P.Dong and W.Y.Wang. Tool wear monitoring by the analysis of surface roughness. In *Proceedings of COMADEM 90, The Second International Congress on Condition Monitoring and Diagnostic Engineering Management*, pages 56–61, 1990.

[58] European Working Group on Acoustic Emission European. Codes for acoustic emission examination. *NDT International*, 18(4):185–194, 1985.

[59] American Society for Testing and Philadelphia Materials. Standard definitions of terms relating to acoustic emission. American National Standard, ANSI/ASTM E610–77.

[60] J-C.Lenain. General principals of acoustic emission. Dunegan (Paris, France), Report Number DE78–5.

[61] C.A.Tatro. Design criteria of acoustic emission experimentation. Acoustic Emission, ASTM STP 505, American Society for Testing and Materials, 1972.

[62] J-B.Chung and E.Kannatey-Asibu. Acoustic emission from a pure single crystal. In *Proceedings of the 4th World Meeting on Acoustic Emission and the 1st International Conference on Acoustic Emission in Manufacturing*, pages 33–41, September 1991. Boston.

[63] P.P.Gillis. Dislocation motions and acoustic emissions. Acoustic Emission, ASTM STP 505, American Society for Testing and Materials, 1972.

[64] H.L.Dunegan and A.T.Green. Factors affecting acoustic emission response from materials. Acoustic Emission, ASTM STP 505, American Society for Testing and Materials, 1972.

[65] M.Friesel and S.H.Carpenter. Determination of the sources of acoustic emission generated during the deformation of titanium. *Metallurgical Transactions A*, 15A:1849–1853, October 1984.

[66] R.J.Landy and K.Ono. Acoustic emission behaviour of a low alloy steel. *Journal of Acoustic Emission*, 1(1):7–19, 1982.

[67] C.R.Heiple, S.H.Carpenter, and S.S.Christiansen. Fracture of boron particles in 2219 aluminium as a known acoustic emission source. *Acta Metallurgica et Materialia*, 38(4):611–618, 1990.

[68] S.H.Carpenter and Z.Zhu. Correlation of the acoustic emission and the fracture toughness of ductile nodular cast iron. *Journal of Materials Science*, 26:2057–2062, 1991.

[69] Y.Nakamura. Detection and analysis of acoustic emission signals. In *Proceedings of the 1st Conference on Acoustic Emission/Microseismic activity in Geologic Structures*, pages 445–457, 1975.

[70] C.R.Heiple and S.H.Carpenter. Acoustic emission from low temperature phase transformations in plutonium. *Journal of Nuclear Materials*, 149:168–179, 1987.

[71] X.Liu and E.Kannatey-Asibu. Acoustic emission during athermal martensitic transformation in steels. *Transactions of the ASME, Journal of Engineering for Industry*, 112:84–91, February 1990.

[72] D.A.Dornfeld. An investigation of orthogonal cutting via acoustic emission signal analysis. In *7th Proccedings of the North American Metal Working Research Conference*, pages 270–274, 1979.

[73] D.A.Dornfeld. Tool wear sensing via acoustic emission analysis. In *NSF Grantees 8th Conference on Production Research and Technology*, January 1981. Stanford, California.

[74] E.Kannatey-Asibu and D.A.Dornfeld. Quantitative relationships for acoustic emission from orthogonal metal cutting. *Transactions of the ASME, Journal of Engineering for Industry*, 103:330–340, August 1981.

[75] D.A.Dornfeld and E.Kannatey-Asibu. Acoustic emission during orthogonal metal cutting. *International Journal of Mechanical Science*, 22:285–296, 1980.

[76] M.Oyane, F.Takashima, K.Osakada, and H.Tanaka. The behaviour of some steels under dynamic compression. In *Proceedings of the 10th Japan Congress on Testing Materials*, 1967.

[77] W.F.Hastings and P.L.B.Oxley. Predicting tool life from fundamental work material properties and cutting conditions. *Annals of the CIRP*, 25(1):33–38, 1976.

[78] V.Messaritis and W.K.D.Borthwick. Processing acoustic emission signal data for characterising tool wear and chip management. In *Proceedings of the 1st International Conference on Computer Aided Production Engineering*, pages 261–268, 1986.

[79] Z.Yaohui and X.Rongbao. A study on the separation of acoustic emission signals in metal cutting process. *Progress in Acoustic Emission IV, The Japanese Society for NDI*, pages 462–469, 1988.

[80] D.V.Hutton and Q.Yu. On the effects of built–up edge on acoustic emission in metal cutting. *Transactions of the ASME, Journal of Engineering for Industry*, 112:184–189, May 1990.

[81] P.Fleischman, F.Lakestani, J.C.Baboux, and D.Rouby. Analyse spectrale et energétique d'une source ultrasonore en mouvement – application à l'emission acoustique de l'aluminium soumis à déformation plastique. *Materials Science and Engineering*, 29:205–212, 1977.

[82] G.Malaprade, D.Rouby, G.Fantozzi, and P.F.Gobin. Influence de la vitesse de déformation sur le comprtement mécanique d'un acier doux et d'un acier faiblement alliz'e à limite elastique. *Materials Science and Engineering*, 38:1–6, 1979.

[83] S.Rangwala and D.A.Dornfeld. A study of acoustic emission generated during orthogonal metal cutting – 2: Spectral analysis. *International Journal of Mechaincal Science*, 33(6):489–499, 1991.

[84] R.McBride, J.S.Barton, J.D.C.Jones, and W.K.D.Borthwick. Fibre optic interferometry for acoustic emission sensing in machine tool wear monitoring. In *Electro–Optics and Laser International Conference, Birmingham, U.K.*, 1990.

[85] Y.Kakino. In–process detection of tool breakage by monitoring acoustic emission. In *Proceedings of an International Conference, Ft. Mitchel, Kentucky, U.S.A.*, pages 25–39, September 1980.

[86] T.M.Proctor. An improved piezoelectric acoustic emission transducer. *Journal of the Acoustical Society of America*, 71(5):1163–1168, May 1982.

[87] S.C.Kerkyras, S.J.Wilcox, W.K.D.Borthwick, and R.L.Reuben. Acoustic emission monitoring of turning operations using PVdF film and PZT sensors. In *4th World Meeting on Acoustic Emission and 1st International Conference on Acoustic Emission in Manufacturing*, September 1991. Boston, Massachusetts.

[88] C.H.Palmer and R.E.Green. Materials evaluation by optical detection of acoustic emission signals. *Journal of Applied Optics*, 16:23–33, 1977.

[89] A.S.Mardapitas and Y.H.J.Au. Blanking process characterisation using acoustic emission. In *Proceedings of COMADEM 90, The Second International Congress on Condition Monitoring and Diagnostic Engineering Management*, 1990.

[90] B.S.Kim. Punch press monitoring with acoustic emission (AE) part I: Signal characterisation and stock hardness effects. *Transactions of the ASME, Journal of Engineering Materials and Technology*, 105:295–300, October 1983.

[91] S.Y.Liang and D.A.Dornfeld. Characterisation of sheet metal forming using acoustic emission. *Transactions of the ASME, Journal of Engineering Materials and Technology*, 112:44–51, January 1990.

[92] S.Rangwala, S.Liang, and D.A.Dornfeld. Pattern recognition of acoustic emission signals during punch stretching. *Mechanical Systems and Signal Processing*, 1(4):321–332, 1987.

[93] K.Iwata and T.Moriwaki. An application of acoustic emission measurement to in–process sensing of tool wear. *Annals of the CIRP*, 25(1):21–26, 1977.

[94] E.Kannatey-Asibu and D.A.Dornfeld. A study of tool wear using statistical analysis of metal-cutting acoustic emission. *Wear*, 76(2):247–261, 1982.

[95] T.Moriwaki and M.Tobito. A new approach to automatic detection of life of coated tool based on acoustic emission measurement. *Transactions of the ASME, Journal of Engineering for Industry*, 112:212–218, August 1990.

[96] M.Raghunandan and R.Krishnamurthy. Condition monitoring systems for machining applications. In *Proceedings of COMADEM 90, The Second International Congress on Condition Monitoring and Diagnostic Engineering Management*, pages 49–55, 1990.

[97] S.J.Wilcox, W.K.D.Borthwick, and R.L.Reuben. An investigation of the influence of machine/fixture stiffness on ae and workpiece vibration generated during face milling on bright mild steel. In *Proceedings of COMADEM 92, The Fourth International Congress on Condition Monitoring and Diagnostic Engineering Management*, pages 77–82, July 1992.

[98] H.Takeshita and I.Inasaki. Monitoring of end-mill cutter failure with an AE sensor. In *4th World Meeting on Acoustic Emission and 1st International Conference on Acoustic Emission in Manufacturing*, September 1991. Boston, Massachusetts.

[99] R.H.Sturgess. Monitoring milling processes through AE and tool/part geometry. *Transactions of the ASME, Journal of Engineering for Industry*, 114:8–14, February 1992.

[100] V.E.Vainberg. Choice of acoustic emission traits in recognition of the state of cutting tools. *Soviet Journal of Non-Destructive Testing in the USSR*, 25(10):719–723, 1989.

[101] M.S.Lan and D.A.Dornfeld. Experimental studies of tool wear via acoustic emission analysis. In *Proceedings of the 10th NAMRC*, pages 305–311, 1982.

[102] G.S.Choi, Z.Wang, and D.A.Dornfeld. Adaptive optimal control of machining process using neural networks. In *Proceedings of the 1991 IEEE, International Conference on Robotics and Automation*, pages 1567–1572, April 1991. Sacramento, California.

[103] R.H.Osuri, S.Chatterjee, and S.Chandrashekhar. On–line condition monitoring of tool wear in end milling using acoustic emission. *International Journal of Production Research*, 29(7):1339–1353, 1991.

[104] E.N.Diei and D.A.Dornfeld. Acoustic emission sensing of tool wear in face milling. *Transactions of the ASME, Journal of Engineering for Industry*, 109:234–240, August 1987.

[105] T.Blum, I.Suzuki, and I.Inasaki. AE–monitoring systems for the detection of single–point and multi–point cutting tool failures. In *Progress in Acoustic Emission IV, The Japanese Society for NDI*, pages 470–477, 1988.

[106] F.Roethel, M.Dobovšek, and I.Grabec. Acoustic emission of grinding. *Strojniški Vestnik – Mechanical Journal, Ljubliana*, 23(11):1–6, 1977.

[107] D.A.Dornfeld and H.G.Cai. An investigation of grinding and wheel loading using acoustic emission. *Transactions of the ASME, Journal of Engineering for Industry*, 106:28–33, February 1984.

[108] T.Kaneeda and H.Tsuwa. Detecting fracture phenomina in separation process at tool tip in metal cutting by acoustic emission technique. *Bulleten of the Japanese Society of Precision Engineering*, 13(3):159–160, September 1979.

[109] I.Inasaki and S.Yonetsu. In–process detection of cutting tool damage by acoustic emission measurement. In *Proceedings of the 22nd MTDR Conference*, pages 261–268, 1981.

[110] E.N.Diei and D.A.Dornfeld. A model of tool fracture generated acoustic emission during machining. *Transactions of the ASME, Journal of Engineering for Industry*, 109:227–233, August 1987.

[111] S.Vajpayee and A.Sampath. Micro–based AE system for tool monitoring. In *The 29th Meeting of the Acoustic Emission Working Group*, pages S12–S15.

[112] M.S.Lan and D.A.Dornfeld. In–process tool fracture detection. *Journal of Engineering and Materials Technology*, pages 111–118, 1984.

[113] S.J.Wilcox and R.L.Reuben. The detection of short timescale tool degradation during face milling operations using cutting force and acoustic emission. *To be published.*

[114] Y.Kakino, H.Suizu, M.Hashitani, T.Yamada, H.Yoshioka, and A.Fujiwara. In–process detection of thermal crack of cutting tool by making use of acoustic emission. *Bulleten of the Japanese Society of Precision Engineering*, 17(4):241–246, 1983.

[115] T.C.Ramaraj, S.Santhanam, and M.C.Shaw. Tool fracture at the end of a cut – part I: Foot formation. *Transactions of the ASME, Journal of Engineering for Industry*, 110:333–338, November 1988.

[116] D.W.Yen and P.K.Wright. Adaptive control in machining – a new approach based on the physical constraints of tool wear mecahnisms. *Transactions of the ASME, Journal of Engineering for Industry*, 105:31–38, February 1983.

[117] W.S.Sampath, Y.M.Lee, and M.C.Shaw. Tool fracture probability under steady state cutting conditions. *Transactions of the ASME, Journal of Engineering for Industry*, 106:161–167, May 1984.

[118] E.Kannatey-Asibu and E.Emel. Linear discriminant function analysis of acoustic emission signals for cutting tool monitoring. *Mechanical Systems and Signal Processing*, 1(4):333–347, 1987.

[119] E.Emel and E.Kannatey-Asibu. Tool failure monitoring in turning by pattern recognition analysis of AE signals. *Transactions of the ASME, Journal of Engineering for Industry*, 110:137–145, May 1988.

[120] S.J.Wilcox, R.L.Reuben, and W.K.D.Borthwick. AE detection of edge chipping on a multi–point milling tool during a face milling test. In *4th World Meeting on Acoustic Emission and 1st International Conference on Acoustic Emission in Manufacturing*, September 1991. Boston, Massachusetts.

[121] Y.Kakino. Monitoring of metal cuttting and grinding processes by acoustic emission. *Journal of Acoustic Emission*, 5(5):108–116, 1984.

[122] S.Vahaviolos. Ae in the machine tool industry. *Materials Evaluation*, 43:44–45, January 1985.

[123] E.Emel and E.Kannatey-Asibu. Acoustic emission monitoring of the cutting process–negating the influence of varying conditions. *Transactions of the ASME, Journal of Engineering Materials and Technology*, 113:456–464, October 1991.

[124] J.I.El Gomayel and K.D.Bregger. On–line tool wear sensing for turning operations. *Transactions of the ASME, Journal of Engineering for Industry*, 108:44–47, February 1986.

[125] A.J.Pekelharing and J.M.B.Orelio. When does the tool crack? In *8th Proceedings of the North American Metal Working Conference*, pages 8–11, 1980.

[126] J.G.Wager. The use of statistical transformations in assessing the life of cutting tools. *Annals of the CIRP*, 25(1):29–31, 1976.

[127] F.Rosenblatt. *Principles of Neurodynamics: Perceptrons and the Theory of Brain Mechanisms.* Spartan Books, New York, 1962.

[128] M.Minsky and S.Papert. *Perceptrons: an Introduction to Computational Geometry.* MIT Press, 1969. Massachusetts.

[129] D.W.Tank and J.J.Hopfield. Neural computation by concentrating information in time. *Proceedings of the National Academy of Science*, 84:1896–1900, April 1987.

[130] D.Ballard, G.E.Hinton, and T.J.Sejnowski. Parallel visual computation. *Nature*, 306(21):26, 1983.

[131] A.M.Turing. Computing machinery and intelligence. *Mind*, 59:433–460, 1950.

[132] J.Weizenbaum. Eliza – a computer program for the study of natural language communication between man and machine. *Communications of the Association for Computing Machinery*, 9:36–45, 1966.

[133] M.B.V.Roberts. *Biology a functional approach.* Nelson, third edition, 1984.

[134] R.Lindsay, B.Buchanan, E.Feigenbaum, and J.Lederberg. *Applications of Artificial Intelligence for Organic Chemistry.* McGraw–Hill, New York, 1980.

[135] D.Michie. *Studies in Cybernetics: 1 – Introductory Readings in Expert Systems.* Gordon Breach Science Publishers, 1982.

[136] A.Newell and H.A.Simon. *Human Problem Solving.* Prentice–Hall, New Jersey.

[137] R.C.Witcomb, P.J.C.Skitt, and M.J.Down. Automating the collection and organisation of reference spectra for use in vibration monitoring. In *Proceedings of COMADEM 91, The Third International congress on Condition Monitoring and Diagnostic Engineering Management*, 1991.

[138] M.Chow, P.Mangum, and S.Yee. A neural network approach to real–time condition monitoring of induction motors. *IEEE Transactions on Industrial Electronics*, 38:448–453, December 1991.

[139] I.Grabec, W.Sachse, and E.Govekar. Solving AE problems by a neural network. In *Acoustic Emission: Current Practice and Future Directions*, pages 165–182. 1991.

[140] L.A.Burke and S.Rangwala. Tool condition monitoring in metal cutting: a neural network approach. *Journal of Intelligent Manufacturing*, 2:269–280, 1991.

[141] C.Okafor, M.Markus, and R.Tipirneni. Multiple sensor integration via neural networks for estimating surface roughness and bore tolerance in circular end milling – part 1: Time domain. *Journal of Condition Monitoring and Diagnostic Technology*, 2(2):49–57, October 1991.

[142] G.S.Choi, Z.X.Wang, and D.A.Dornfeld. Detection of tool wear using neural networks. In *4th World Meeting on Acoustic Emission and 1st International Conference on Acoustic Emission in Manufacturing*, September 1991. Boston, Massachusetts.

[143] S.Sukvittayawong and I.Inasaki. Identification of chip form in turning process. *JSME International Journal*, 34(4):553–560, 1991.

[144] V.Venkatasubramanian, R.Vaidyanathan, and Y.Yamamoto. Process fault detection and diagnosis using neural networks–I. steady–state processes. *Computers in Chemical Engineering*, 14(7):699–712, 1990.

[145] M.M.Ahmed and R.D.Pringle. Application of syntactic pattern recognition techniques to condition monitoring of machines. In *Proceedings of COMADEM 90, The Second International Congress on Condition Monitoring and Diagnostic Engineering Management*, pages 49–55, 1990.

[146] C.Yuedong and Q.Liangsheng. Forecasting the change of operating condition for machinery via fuzzy classification. In *Proceedings of COMADEM 90, The Second International Congress on Condition Monitoring and Diagnostic Engineering Management*, 1990.

[147] T.Brown, S.M.Alexaander, V.Jagannathan, and R.Kirchner. Demonstration of an expert system for manufacturing process control. In *Proceedings of the AI, Graphics and Simulation (Society of Computer Simulation) USA*, 1985.

[148] R.S.Hu, P.Mathew, P.L.B.Oxley, and H.T.Young. Allowing for end cutting edge effects in predicting forces in bar turning with oblique machining conditions. *Proceedings of the Institution of Mechanical Engineers*, 200(C2):89–99, 1986.

[149] G.E.Dieter. *Mechanical Metallurgy.* McGraw-Hill International Book Company, second edition, 1981.

[150] D.P.Hand, T.Carolan, J.D.C.Jones, J.S.Barton, S.J.Wilcox, P.Wilkinson, and R.L.Reuben. Cutting tool condition monitoring by fibre optic interferometry. In *Proceedings of the I.O.P. Leeds Conference in Applied Optics*, pages 53–55, 1992.

[151] I.Aleksander and H.Morton. *An Introduction to Neural Computing.* Chapman & Hall, 1991.

[152] C.W.McGregor and J.C.Fisher. *Transactions of the ASME, Journal of Applied Mechanics*, 13, 1946. A11.

[153] G.Boothroyd. Temperatures in orthogonal metal cutting. *Proceedings of the Institution of Mechanical Engineers*, 177:789–802, 1963.

[154] H.Kolsky. *Theory of Elastic Waves.* Dover Publications Incorporated, 1963.